Project Title: Reactive Distillation for Esterification of Bio-based Organic Acids
Award Number: DE-FG36-04GO14249

Recipient: National Corn Growers Association
Project Location: Chesterfield, MO, East Lansing, MI

Project Period: 10/1/03 – 9/30/06
Date of Report: 5/6/2007
Written by: Nathan Fields (Subcontractors, Dennis Miller *et. al.*)
Program Manager: Nathan Fields
Principle Investigators: Nathan Fields, Richard Glass, Dennis Miller

Subcontractors: Michigan State University
**Cost-Sharing Partners: National Corn Growers Association, Michigan State
University**

DOE Project Team
DOE-HQ contact: Mark Decot   202-586-6501 mark.decot@ee.doe.gov
DOE Field Project Officer: Fred Gerdeman fred.gerdeman@go.doe.gov
DOE Contract Specialist: Nanette Ortiz   303-275-4748   nanette.ortiz@go.doe.gov
DOE Project Engineer: Nicholas Frasier 303-275-4772   nicholas.frasier@go.doe.gov

The following is the final report of the three year research program to convert organic acids to their ethyl esters using reactive distillation. This report details the complete technical activities of research completed at Michigan State University for the period of October 1, 2003 to September 30, 2006, covering both reactive distillation research and development and the underlying thermodynamic and kinetic data required for successful and rigorous design of reactive distillation esterification processes. Specifically, this project has led to the development of economical, technically viable processes for ethyl lactate, triethyl citrate and diethyl succinate production, and on a larger scale has added to the overall body of knowledge on applying fermentation based organic acids as platform chemicals in the emerging biorefinery. Organic acid esters constitute an attractive class of biorenewable chemicals that are made from corn or other renewable biomass carbohydrate feedstocks and replace analogous petroleum-based compounds, thus lessening U.S. dependence on foreign petroleum and enhancing overall biorefinery viability through production of value-added chemicals in parallel with biofuels production. Further, many of these ester products are candidates for fuel (particularly biodiesel) components, and thus will serve dual roles as both industrial chemicals and fuel enhancers in the emerging bioeconomy.

The technical report from MSU is organized around the ethyl esters of four important biorenewables-based acids: lactic acid, citric acid, succinic acid, and propionic acid. Literature background on esterification and reactive distillation has been provided in Section One. Work on lactic acid is covered in Sections Two through Five, citric acid esterification in Sections Six and Seven, succinic acid in Section Eight, and propionic acid in Section Nine. Section Ten covers modeling of ester and organic acid vapor pressure properties using the SPEAD (Step Potential Equilibrium and Dynamics) method.

Reactive Separations for Producing Bio-Based Organic Acid Esters
DOE PROJECT No. DE-FG36-04GO14249
Final Report
10/1/03 – 09/30/06
National Corn Growers Association

Navinchandra S. Asthana, Aspi K. Kolah, Dung Vu, Carl T. Lira, Dennis J. Miller (PI)
Department of Chemical Engineering and Materials Science
Michigan State University
East Lansing, Michigan 48824
(517) 353-3928
millerd@egr.msu.edu

Executive Summary

The chemistry of lactic acid is quite complex because it contains both a hydroxyl (alcohol) and a carboxylic acid group; its molecular characteristics are also highly dependent on the quantity of water present in solution. Efficient conversion of lactic acid to ethyl lactate requires proper treatment of lactic acid oligomers at low water concentrations. For this reason, much of the kinetic and thermodynamic data developed over the past three years focus on the behavior of acid and oligomer esters. The rigorous analysis of reactions and thermodynamic properties of lactate oligomers has not been reported previously in the literature, so we have substantially forwarded the understanding of lactic acid in general and lactate esters in particular. Specifically, we have developed 1) practical descriptions of reaction kinetics and equilibria of monomer and oligomer lactic acid esterification, including development of a kinetic model (Section Two); 2) a new mathematical model describing the reaction equilibrium of lactic acid oligomerization (Section Three) and 3) a rigorous characterization of the vapor-liquid equilibrium data for the lactic acid − ethyl lactate − ethanol − water system (Section Four). We have also characterized the breakdown of the desired product, ethyl lactate, at process conditions (Section Two). Together, these data constitute a body of knowledge that provides our project team the unique capability of properly designing a reactive distillation process for ethyl lactate production.

We conducted extensive experimental studies of the formation of ethyl lactate via reactive distillation in our pilot-scale (4.5 m height) reactive distillation column (Section Five). In the pilot-scale unit, we have conducted extensive parametric evaluation over a wide variety of conditions for ethyl lactate formation. We routinely achieve lactic acid conversion of 90% in the pilot-scale column, with ethyl lactate yield as high as 86%. In all cases, we find that the best column operation occurs at reflux ratios at or near zero. Refluxing distillate, which contains water as well as ethanol, tends to lower conversion and reduce the yield of ethyl lactate. The column thus operates best as a reactive stripper with lactic acid fed at or very near the top of the column. It was also found that preheating the feed streams, particularly ethanol, reduces the quantity of water and ethanol present in the bottoms (product) stream. The elimination of water and ethanol from the product stream facilitates more efficient recovery of high purity ethyl lactate.

Other parametric studies include the effect of boilup ratio, the use of azeotropic versus absolute ethanol feed, ethanol feed location and temperature, and the ethanol:lactic acid molar feed ratio. Beside experiments, we have conducted extensive process simulation of ethyl lactate formation at both the pilot scale and the commercial scale using AspenPlus process simulation software. We have investigated several reaction models ranging from simple equilibrium reaction of monomer lactic acid esterification to a rate-based kinetic model involving lactic acid and ester oligomers up to tetramer acid and trimer ester. The pilot-scale simulations aid in understanding reactive distillation behavior and in directing the course of the experimental studies. The commercial-scale simulations indicate that complete lactic acid conversion and essentially quantitative ethyl lactate yields can be obtained with moderate-sized columns of approximately 40 equilibrium stages. Hydrolysis and alcoholysis reactions of the monomer and oligomer lactate esters were studied in order to better develop an efficient process flowsheet. These results indicate that we can convert oligomer acids and esters efficiently, thus facilitating an attractive process for ethyl lactate formation that we believe will compete effectively with existing solvent production systems. We have conducted a rigorous economic analysis of the process in collaboration with NCGA and our industrial partner MECS, Inc. The economic analyses indicate that ethyl lactate produced by the technology developed from this research project can be sold at lower prices ($0.60 - $1.00/lb) than ethyl lactate produced by conventional routes ($1.20 – 1.60/lb).

Triethyl citrate can be used as a biorenewable plasticizer in place of di-octyl phthalates, but its application is limited because of the lack of large-scale production capability. Via studies analogous to those conducted for lactate ester formation, we have shown that reactive distillation can be utilized for cost-effective large scale synthesis of triethyl citrate from citric acid. These results are discussed in Section Six, where we present a kinetic/thermodynamic model for citric acid esterification, and in Section Seven, where we present several process scenarios for commercial triethyl citrate production. Economic analysis of the process gives an estimated triethyl citrate selling price of $1.00 - $1.30/lb, much lower than current values of $2.00 – 3.00 /lb.

The production of diethyl succinate from succinic acid is presented in Section Eight. Diethyl succinate has very good solvent characteristics, serves as an interesting platform intermediate for a variety of chemicals and monomers, and is perceived as a possible diesel fuel additive. A detailed kinetic analysis and development of a process model for large-scale production of succinic acid has been carried out. Finally, Section Nine contains the details of synthesis of ethyl propionate.

For the most part, the physical properties database that is used in the design and analysis of chemical processes in today's world has been built upon the study of hydrocarbons. Very limited information is available in the open literature which can be successfully extended for the study of biobased fuels and chemicals, including organic acids and their esters. For example, prediction of vapor pressures and heats of vaporization, physical properties that are very important for design of our continuous reactive distillation processes, are simply not available. Therefore, in collaboration with our outside partners we have developed a new model to accurately predict the vapor

pressure and heats of vaporization of biobased organic acids and their esters. This model is known as SPEAD (Step Potential Equilibrium and Dynamics); its application to predicting vapor pressures of organic acids and their esters has been detailed in Section Ten.

TABLE OF CONTENTS

LIST OF FIGURES

SECTION TWO

SECTION THREE

SECTION FOUR

SECTION FIVE

SECTION EIGHT

SECTION NINE

SECTION TEN

LIST OF TABLES

SECTION ONE
INTRODUCTION AND LITERATURE BACKGROUND ON ESTERIFICATION AND REACTIVE DISTILLATION

1.1. Introduction

Organic esters are gaining increased importance in a number of industrial applications, primarily as solvents to replace petroleum-derived materials, and thus hold promise as a major class of bio-based commodity products. The application of reactive distillation to esterification holds great promise for efficient production, yet is relatively unexplored as a commercial process. The aim of the proposed project was to implement a full complement of scientific and technical tools ranging from fundamental thermodynamic data collection to detailed process economic and market analyses in order to demonstrate the viability of reactive distillation for esters production. The project was conducted by a multi-faceted team with combined expertise in scientific area necessary for the successful outcome of this project.

Reactive distillation has gained substantial attention recently in the research and industrial communities,[1-2] because it offers clear advantages over traditional approaches for carrying out equilibrium-limited chemical reactions. Candidate reactions for reactive distillation are characterized by a substantial difference in volatility between reaction products, such that removal of one product by distillation drives the reaction to completion. Reactions are often catalyzed, either by solid catalysts packed within the distillation column or by addition of homogeneous catalysts (acids, bases, metal complexes, etc.) added to the column feed.

Esterification of organic acids satisfies the above criterion for consideration as a reaction amenable to reactive distillation. In particular, the formation of alkyl esters, typically formed by reaction of simple alcohols such as methanol, ethanol, etc. with the acid, is attractive, as the ester and water produced as reaction products can usually be separated by distillation. Although this principle is well understood, reactive distillation has not been broadly exploited for esterification because of the typical complexity of the thermodynamics of these systems. An application of reactive distillation which has been demonstrated commercially is Tennessee Eastman's methyl acetate process[3]. Upon its implementation; the single reactive distillation column replaced thirteen individual unit operations and now meets the company's entire demand for methyl acetate. Although representative of the kind of success possible with reactive distillation, it must be noted that the methyl acetate process is not without the above-mentioned thermodynamic complexity and subsequent specificity of design. In the process, water and methyl acetate form a minimum-boiling azeotrope that, in theory, prevents their separation and thus the application of reactive distillation. Fortunately, engineers at Eastman determined that the azeotrope is broken by addition of acetic acid near the top of the column, thus allowing methyl acetate to be produced as a pure distillate product.

Challenges involving azeotrope formation arise frequently in reactive distillation, because both reaction and separation occur simultaneously. Other potential difficulties of

applying reactive distillation have been described by Feng and Huang[4]. These include the requirement of using excess reactant to drive the reaction, the necessity that reaction occurs at the same temperature as the reactants and products vaporize, and high energy costs. These challenges have led to reluctance on the part of industry to consider the broader applications of reactive distillation. Overcoming these challenges requires a thorough understanding of thermodynamics of reaction equilibrium and vapor-liquid phase equilibrium, distillation column design, and processing strategies. Indeed, we have already addressed many of these potential difficulties in reactive distillation for esterification. We have designed into our process the recycle of excess alcohol required to drive the reaction, such that only a stoichiometric quantity is actually consumed in the process. We circumvent the requirement that reaction and vaporization occur at the same temperature by controlling the reactive distillation column pressure, which in turn controls column temperature. This further allows us to conduct reactions on species with normal boiling points above the maximum operating temperature of the ion exchange resin catalyst. Finally, energy costs for reactive distillation are no greater than those for conventional distillation to purify reaction products. Thus, having already established a firm, cohesive concept for ester formation via reactive distillation, and already having addressed many of the key challenges therein, we believe that our project team of academic and corporate participants has the expertise and experience to successfully design and demonstrate economically viable, commercial-scale reactive distillation for organic acid ester formation.

1.2. Building National Bio-Based Products capability

Through this project, we have tried to address several key areas identified in the Biomass Research Development Act of 2000. First, production of esters provides a route to chemical co-products from biomass refining that will enhance the economic viability of the biorefinery for fuel ethanol production. Organic esters have significant potential as large volume commodity replacements for current petroleum-based solvents; there is impending political pressure for manufacturers to use "non-hazardous" chemicals for national security and other reasons, and organic esters will be prime candidates as substituents for even mildly hazardous solvents. Indeed, this is happening already: organic ester use is expanding by 6-7% annually, a sign that entry into the market will not have serious barriers.

Second, this research has added a significant new component to the overall capability of the U.S. to produce and purify products from bio-based resources. Our initial studies show that organic acid esters can be formed and purified in near-theoretical yields within a single reactive distillation column. Reactive distillation thus provides a highly efficient approach to co-product manufacture at greatly reduced capital cost and with essentially no waste generation. When integrated with ethanol manufacturing, combined esterification and transesterification facilitates production of entire families of esters from a single unit operation.

1.3. Technical Literature and Technical Barriers

Recent literature has included an ever-increasing number of studies on reactive distillation, including new work concerning formation of acetate esters by reactive distillation. Methyl acetate is the ester of choice for many such studies[5-6]. Peng *et al*[6]. compare the equilibrium stage models and the rate based packed column models, and shows that there are no major differences in the column profiles, conversions, or optimum column locations for the two methods. Popken *et al*[5]. report that intermediate reflux ratios give the best balance between conversion and separation. Low column reflux is insufficient to separate the products from the reaction mixture. At high reflux, reactants are separated too effectively and conversion also drops. Studies of n-butyl acetate are reported by Hanika, *et al*[7] and Steinigeweg and Gmehling[8]. The column conditions were accurately modeled using a kinetic model together with an equilibrium stage model. The workers found that a prereactor was helpful because the reactants have similar boiling points. In cases where the reactants have dissimilar boiling points, the feed locations should be separated. The butyl acetate process uses an overhead decanter to recycle unreacted butanaol, permitting high butanol conversion.

Currently, use of membranes with reaction via pervaporation is under development for production of ethyl lactate[9-11], but there are technical challenges with membrane fouling, energy requirements, and the necessity to distill the product once it is formed. (*Note: Prior to commencement of this project in 2003, no open literature reference was found for reactive distillation of lactates. Recently, we came across the only patent literature from Dow-Halterman Chemicals on ethyl lactate using reactive distillation but their strategy is completely different from ours.*)

Azeotropes limit the separation that can be achieved in single distillation columns, and non-reactive azeotropes occur at maxima or minima in temperature for a given pressure. Therefore, in a distillation column, frequently one end of a column with an azeotropic system approaches an azeotropic composition. Separations of azeotropic systems are often performed by adding additional components to alter the relative volatility of the azeotropic pair. Another strategy is to use liquid-liquid equilibria to decant phases of different compositions which are on either side of the azeotrope, such as the technique of Font *et al*[12] who add isooctane to separate ethanol and water. Design tools such as residue curve maps and design heuristics are now available to help in the design of non-reactive distillations. However, reactive systems have more complicated behavior and the techniques are not directly applicable[13].

The phase behavior of systems exhibiting reactive behavior has been discussed by Barbosa and Doherty.[14] In their work they demonstrate that systems showing ideal solution behavior in a ternary, A + B → C, or quaternary, A + B → C + D mixture can be azeotropic if the reaction equilibrium constant is sufficiently large and the volatility of both reactants is either higher or lower than the volatility of the products. However, unlike non-reactive azeotropes, the azeotropic behavior is not at a maximum or minimum in temperature and the impact of this condition on column design is not explored in the

publication. Also, the cited work does not consider the behavior in reactive distillation where the temperature of each stage is different and the material balance of column flows affects the compositions on the stages.

1.4. Project Objectives

The global goal of the research program was to develop commercial-scale processes for organic acid ester (solvents and plasticizer) production. These ester production processes were targeted as additions to existing corn and other biomass processing facilities, with the objective of adding value to the corn-refining industry, which is currently based primarily on ethanol production. We have examined esters of four different organic acids produced from corn-derived feedstocks, namely lactic acid and propionic acid (mono-carboxylic), succinic acid (di-carboxylic), and citric (tri-carboxylic).

SECTION TWO

A KINETIC MODEL FOR ESTERIFICATION OF LACTIC ACID AND ITS OLIGOMERS

2.1. Background

At concentrations above 20 wt% in water, lactic acid undergoes oligomerization reactions to form linear oligomer acids. The extent of oligomerization is inversely related to water content of the solution.[16-17] These oligomer acids react with ethanol to yield oligomer esters. In reactive distillation or any other lactic acid esterification scheme, oligomer formation and esterification adversely affect ethyl lactate yield and pose a considerable challenge in predicting process behavior. For accurate design, therefore, it is critical to include and to characterize oligomer reactions in the process model.

Many reactive distillation models only consider reaction equilibrium.[2,5] These reaction equilibrium models are useful in cases where reaction kinetics are very fast; e.g., where equilibrium is achieved in short reaction time, but systematically predict higher conversions than are obtained experimentally in cases where reaction kinetics are slow. In those cases, it has been shown that kinetics-based simulations give more accurate and reliable predictions.[17,18] In lactic acid esterification, where a series of relatively slow reactions take place, a reliable knowledge of kinetics is thus essential to effectively simulate the process.

There have been several reports describing the kinetics of lactic acid esterification with different alcohols.[9,19-26] Most of them involve dilute aqueous solutions of lactic acid ($\leq$ 20 wt%),[18-21] thus obviating the need to account for oligomers in solution. Others have examined esterification kinetics at high lactic acid concentrations, but have not explicitly included the role of oligomers. Engin et al.[25] studied the esterification of 92 wt% lactic acid solutions with ethanol, accounting for hydrolysis of oligomer acids but ignoring esterification reactions. Zhang et. al[26] made no mention of oligomers in their study of esterification kinetics of 80 wt% lactic acid. The esterification kinetics developed by Tanaka et. al[24] represent the only prior work that considers higher oligomer acids and their esters. Although they modeled reaction kinetics and generated rate constants, they did not clearly describe the catalyst quantity used in reaction and thus their results have limited utility. Further, the limited parametric studies they conducted hinder the applicability of their rate constants to predicting composition profiles over a wide range of reaction conditions.

Because prior kinetic models do not reliably or completely predict the behavior of lactic acid oligomers and their esters, we have conducted and report here a kinetic study describing rate expressions and rate constants for formation, esterification, and hydrolysis of oligomer acids and esters over a wide range of lactic acid concentrations, alcohol contents, temperatures, and catalyst loadings. The kinetic model presented is useful in both batch and continuous process designs for lactic acid esterification.

2.2. Reaction procedure

Kinetics of esterification involving 88 and 50 wt% lactic acid solutions with ethanol were measured in a stirred glass batch reactor (85 cm^3). This reactor was equipped with an outer circulating heating jacket (to maintain constant temperature inside the reactor) with silicon oil as the circulating fluid. The reactor was also equipped with a condenser, thermocouple, and sampling port.

At the start of reaction, the reactor was filled with the desired amount of lactic acid and ethanol and heated to reaction temperature. Catalyst was added to the reactor thorough one of the reactor ports. The point of catalyst addition was considered as time zero for the reaction. The extent of reaction was followed by sample withdrawal and analysis at regular intervals.

All reactions involving 20 wt% lactic acid, as well as reactions conducted at temperatures higher than 80°C for 88 wt% and 50 wt% lactic acid, were carried out in a stirred 300 mL Parr batch reactor (Model 4561, Parr Instr. Co.). For each experiment, reagents and catalyst were charged into the reactor and heated to reaction temperature. Stirring was commenced once the temperature was reached; this was noted as zero reaction time. Samples were withdrawn periodically over the course of reaction and analyzed. For all reactions, total concentration of lactic acid is reported on a monomer equivalent basis. The 88 wt% lactic acid solution consists of monomer acid (L_1) and linear oligomer dimer acid (L_2), trimer acid (L_3), and tetramer acid (L_4); concentrations of L_2, L_3 and L_4 were therefore multiplied by 2, 3, and 4, respectively, and added to L_1 concentration to give the monomer equivalent concentration.

2.3. Analysis

All samples were analyzed for water (W) and ethanol (EtOH) using a Varian 3700 gas chromatograph equipped with thermal conductivity detector (TCD) and a stainless steel column (4 m x 3.25 mm) packed with a liquid stationary phase of Porapak Q. The column oven was subject to a temperature program involving heating from 413 K (after a 2-min hold) to 493 K (and held for 6 min) at a rate of 20 K min^{-1}. High purity helium (99.999 % pure) was used as carrier gas at a flow rate of 20 ml/min. The injector and detectors were maintained at 493 K.

Lactic acid monomer (L_1) and its linear oligomer acids (L_2, L_3 & L_4), ethyl lactate (L_1E), and ethyl esters of oligomer acids (L_2E, L_3E and L_4E) were analyzed using high performance liquid chromatography (HPLC). L_1 monomer and $L_2 - L_4$ oligomers and their esters were quantitatively analyzed on a Hewlett-Packard 1090 HPLC using a reverse phase C18 column (Novapak, 3.9 mm x 150 mm) held at 40°C. Water/acetonitrile (ACN) mixtures, buffered at pH=1.3, were used as mobile phase (1.0 ml/min) in a gradient mode (0% ACN (t=0) to 60% ACN (t=20 min) to 90% ACN (t=25 min) to 0% ACN (t=28 min)), and species were quantified by UV detection (Hitachi L400H) at a wavelength of 210 nm. Lactic acid (L_1) was identified and quantified by comparing HPLC retention time and peak area with a calibration standard prepared by diluting 20 wt% lactic acid feed to 7-8% and then titrating to determine exact monomer concentration. Standards for L_2-L_4 acid oligomers and their esters could not be obtained commercially; however, since 50 wt% lactic acid feed solution contains only L_1 and L_2,

the response factor for L_2 was obtained from the combination of titration and HPLC of 50 wt% lactic acid solution. This L_2 response factor (area/g) was found to be 12% larger, on a mass basis, than the L_1 monomer response factor. Based on this result, the response factor (area/g) for L_3 was assigned a value 12% larger than that of L_2 and the response factor for L_4 assigned a value 12% larger than that of L_3. These response factors were verified as suitable based on the combination of HPLC and titrations of the 88 wt% lactic acid feedstock: oligomer concentrations determined from HPLC peak using the calculated L_3 and L_4 response factors matched to within ±1% with those determined by titration and use of L_1 and L_2 response factors determined above.

The oligomer esters L_2E, L_3E, and L_4E, were quantified by HPLC. The response factor for L_2E was determined by injection of pure L_2E isolated from an experimental product stream by fractional vacuum distillation, and found to be the same value as that for the L_2 acid. The L_3E and L_4E oligomer esters were thus assigned the same response factors on a mass basis as their corresponding acid oligomers; again this was verified to be a reasonable assumption based on comparison of oligomer concentrations of an esterified 88 wt% lactic acid mixture with corresponding results from titration, HPLC, and GC.

A total acid content was determined by titration with a standard 0.1 N NaOH solution, using phenolphthalein as indicator, as a check of HPLC results. Results obtained for acid content from HPLC were comparable to those from titration.

2.4. Results

The "base case" conditions for reaction included 88 wt% lactic acid feed and ethanol with feed quantities of 0.30 mol of lactic acid (L_1 equivalent), 0.2 mol of water (present in 88 wt% lactic acid solution), and 0.97 mol of ethanol, a catalyst loading of 3 wt% of total reactant weight, a temperature of $80^{o}C$, and an agitation speed of 740 rpm. To cover a broad range of conditions, esterification reactions were also performed on solutions containing 20 wt%, 50 wt%, or 88 wt% lactic acid (compositions provided in Table 2.1) using ethanol:lactic acid molar feed ratios from 1:1 to 4:1, catalyst loadings from 0 to 5 wt%, and reaction temperature from $60^{o}C$ to $90^{o}C$. The results of these experiments were used in the regression analysis of the kinetic model (described below) to determine an optimum set of rate constants describing esterification. Representative results from experiments and from the kinetic model are represented in Figures 2.1-2.6 by data points and dotted lines, respectively. Because the 88 wt% lactic acid solution contains the highest concentrations of oligomers (Table 2.1) and thus represents the most complex reaction mixture, results from its esterification are presented in detail here.

2.4.1. Effect of Reactant Molar Ratio. The effect of ethanol:lactic molar feed ratio was studied over the range of 1:1 to 4:1. An increase in overall acid conversion was observed with increasing molar ratios (Fig. 2.1) up to 3:1. Little enhancement in acid conversion was seen when the feed molar ratio was increased from 3:1 to 4:1; therefore, most reactions were carried out at a feed molar ratio of approximately 3:1.

Table 2.1 Composition of Lactic Acid Feedstocks

Feed component	Feed designation (nominal)		
	20 wt%	50 wt%	88 wt%
L_1 wt% (mol%)	23 (5.6)	46 (15.2)	58 (43.5)
L_2	-	3 (0.5)	22 (9.2)
L_3	-	-	6 (1.8)
L_4	-	-	2 (0.4)
H_2O	77 (94.4)	51 (84.3)	12 (45.1)
Monomer equivalent concentration (M)	2.6	5.9	10.8

        2.4.2. Effect of Catalyst Loading. The effect of resin catalyst loading on esterification rate over the range of 0 to 5 wt% of total solution mass was studied. The absolute initial rate of acid conversion was found to increase linearly with catalyst loading (Fig. 2.2). From this result, a turnover frequency (TOF) of $0.06s^{-1}$ was determined for Amberlyst 15 resin at 80^oC. Because lactic acid esterification is auto-catalytic, a non-zero intercept was observed in Figure 2.2. For 88 wt% lactic acid solution, this uncatalyzed esterification rate contributed about 20% of the rate observed for 1% catalyst loading, a contribution thus equivalent to ~0.2 wt% resin catalyst. This contribution is smaller for lower acid concentrations and is relatively unimportant for higher catalyst loadings, and is thus omitted from the kinetic model described below. The effect of catalyst loading was also observed on reactions of oligomers such as L_2E: when loading was increased from 0 to 5 wt%, as rates of formation and hydrolysis of L_2E were found to increase proportionally. Most reactions were carried out with a catalyst loading of 3 wt%.
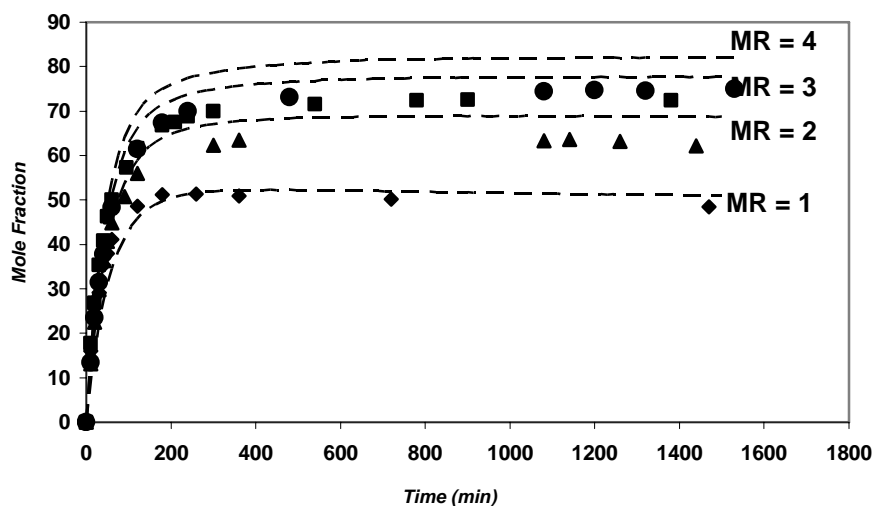
Figure 2.1 Effect of ethanol to lactic acid initial molar ratio (MR) on conversion. Reaction conditions: 88 wt% Lactic acid solution; Catalyst loading = 3 wt%; Agitation rate = 740 rpm; Reaction temperature = 80^oC. Dotted lines are model fit. Experimental: (◆) - MR=1; (▲) - MR=2; (■) - MR=3; (●) - MR=4

2.4.3. Effect of Reaction Temperature. The influence of reaction temperature on esterification rate was studied over the range of 62°C to 90°C. An Arrhenius plot for initial rate of Reactions 2.1-2.3 is given in Figure 2.3. The activation energy for esterifcation reactions (Reactions 2.1-2.3) based on initial rate increased with the degree of oligomerization of lactic acids; from 48000 kJ/kmol for esterification of monomer lactic acid (L_1) to 74100 kJ/kmol for esterification of trimer lactic acid (L_3). These values are consistent with kinetically controlled reactions. Further reactions were carried out at 80°C, the normal boiling point of ethanol.

2.4.4. Effect of Lactic acid Feed Composition. Component profiles for esterification of 88, 50 and 20 wt% lactic acid feed solutions at typical conditions are given in Figures 2.4 - 2.6. Because of the presence of oligomers, it is apparent that predicting the behavior of 88 wt% lactic acid solution requires a more complex model than that required for 50 wt% and 20 wt% feed solutions.
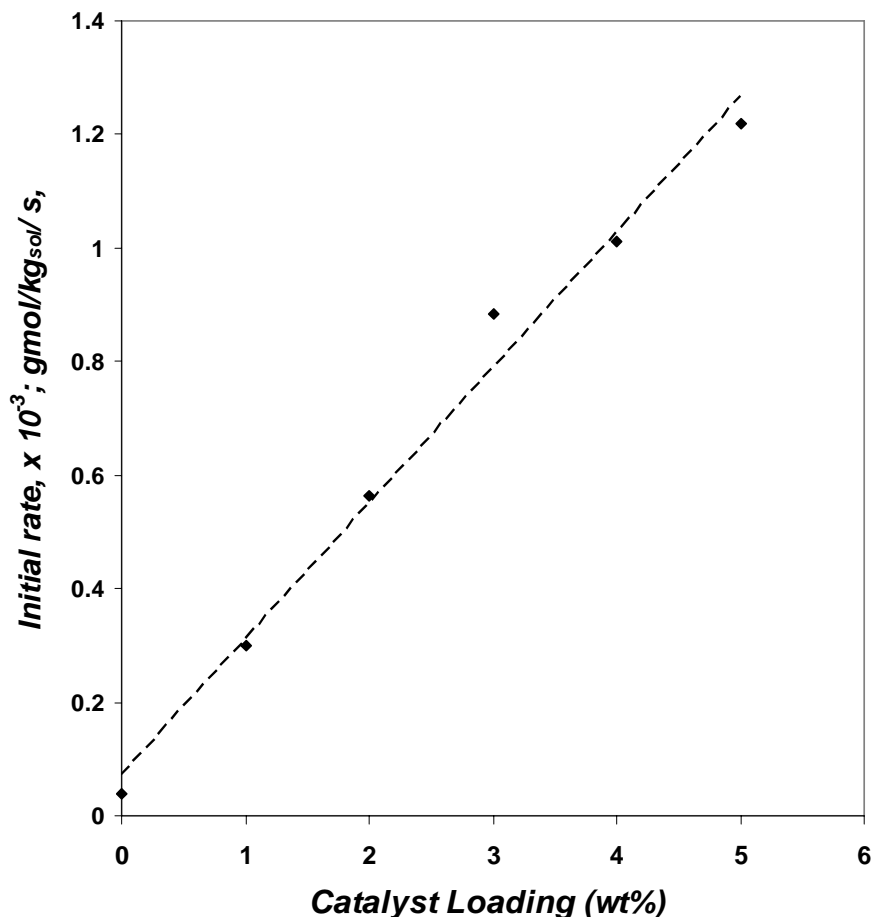
Figure 2.2 Initial rate of acid conversion vs. catalyst loading. Reaction conditions: 88 wt% Lactic acid solution; Mole ratio of ethanol to lactic acid = 3; Agitation rate = 740 rpm; Reaction temperature = 80°C.

2.5. Kinetic Model

2.5.1. Reaction Pathways. Based on reactant and product composition profiles during esterification of 88 wt% lactic acid solution, a set of reaction pathways have been defined for the kinetic model. The set of reactions, given in Equations 2.1-2.5 below, describes lactic acid monomer esterification as well as oligomer formation and esterification. All oligomers larger than dimers (L_2 and L_2E) are lumped as L_3 and L_3E; the quantities of larger oligomers are small enough that they do not significantly influence the reaction, either kinetically or with regard to overall acid concentration and mass balances. A similar set of reaction pathways was proposed by Tanaka et al.[24] Esterification of 50 wt% and 20 wt% lactic acid is completely described by Eq. 2.1, 2.2 and 2.4 respectively.

$$L_1 \ + \ EtOH \ \underset{k_1/K_1}{\overset{k_1}{\rightleftharpoons}} \ L_1E \ + \ H_2O \tag{2.1}$$

$$L_2 \ + \ EtOH \ \underset{k_2/K_2}{\overset{k_2}{\rightleftharpoons}} \ L_2E \ + \ H_2O \tag{2.2}$$

$$L_3 \ + \ EtOH \ \underset{k_3/K_3}{\overset{k_3}{\rightleftharpoons}} \ L_3E \ + \ H_2O \tag{2.3}$$

$$L_2 \ + \ H_2O \ \underset{k_4/K_4}{\overset{k_4}{\rightleftharpoons}} \ 2 \ L_1 \tag{2.4}$$

$$L_3 \ + \ H_2O \ \underset{k_5/K_5}{\overset{k_5}{\rightleftharpoons}} \ L_1 \ + \ L_2 \tag{2.5}$$
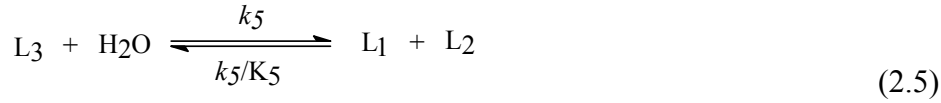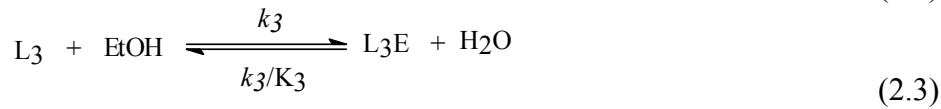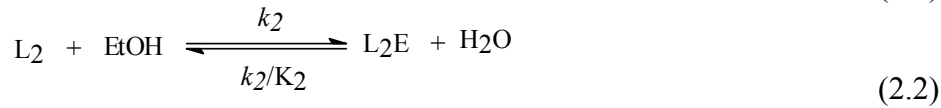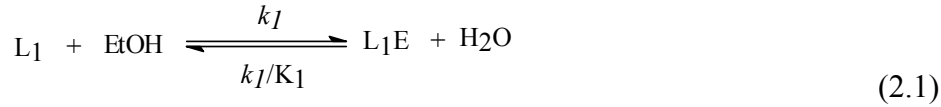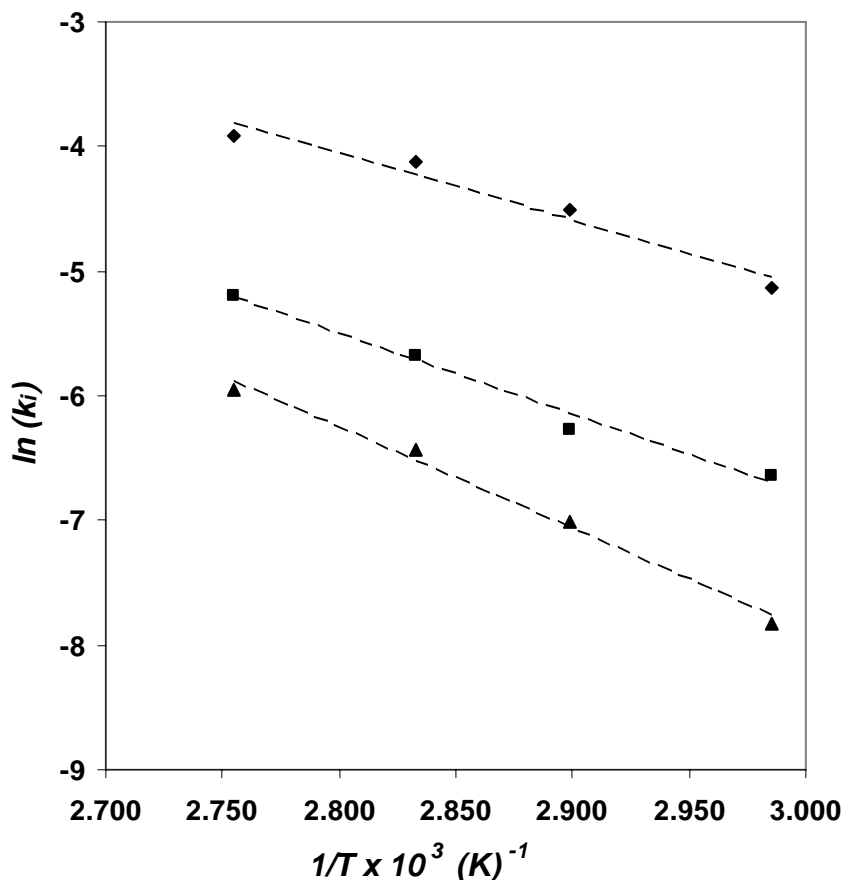
Figure 2.3 Arrhenius plot of initial rate constants for esterification of lactic acid. Reaction conditions: 88 wt% Lactic acid solution; Mole ratio of ethanol to lactic acid = 3; Catalyst loading = 3 wt%; Agitation rate = 740 rpm. ($\blacklozenge$) - k_1; ($\blacksquare$) - k_2; ($\blacktriangle$) - k_3.

2.5.2. Evaluation of Mass Transfer Limitations. Two possible modes of mass-transfer limitations are associated with heterogeneously catalyzed reactions, one across the solid-liquid interface (external mass transfer) and other within the catalyst particle (intra-particle diffusion). In the evaluations below, liquid-phase diffusivities were calculated using the Wilke-Chang equation.[27]

Chakrabarti and Sharma[28] suggest that external mass-transfer limitations for ion-exchange resin catalyzed reactions can be eliminated by carrying out experiments at stirring rates above 500 rpm. To check their assumption, a theoretical calculation was done to ascertain the magnitude of external mass transfer rate. Solid-liquid mass transfer coefficients were calculated using a Sherwood number of 2.0, the theoretical minimum value. The observed reaction rates of L_1, L_2 and (L_3+L_4) were calculated from their concentration vs. time profiles. (Oligomers L_3 and L_4 were lumped together because of uncertainty in the response factor for L_4 and because of its low concentration.) For each component, the maximum mass transfer rate ($k_{SLj} \times C_j$) was found to be at least an order of magnitude greater than the observed reaction rate, indicating that there are no significant solid-liquid mass transfer limitations. Resin particles physically disintegrate above 800 rpm stirring rate; therefore all reactions were carried out at a speed of ~740 rpm.

The possible presence of intraparticle mass transfer resistances was examined by determining the observable modulus ($\eta\varphi^2 = (-r_{Lj,obs})L_t^2/C_{Lj,b}/D_{eLA}$) and applying the Weisz-Prater criterion; the maximum value of $\eta\varphi^2$ observed was 0.15, which is sufficiently small to indicate that intraparticle mass transport resistances are unimportant. This is consistent with previous reports that intra-particle diffusion limitations in reactions with Amberlyst-15 at similar conditions could be considered negligible.[19,20,29]

2.5.3. Kinetic Model Equations. A simple nth-order, reversible reaction model has been chosen to describe lactic acid esterification catalyzed by Amberlyst-15 ion exchange resin. The rate of formation for each component in the reaction system described in Eq. 2.1 – 2.5 above is given in Equations 2.6 - 2.13 below.

$$-\frac{dx_{L_1}}{dt} = w_{cat}.C_T.\left[k_1^0\exp(-\frac{E_{A_1}}{RT})(x_{L_1}.x_{EtOH} - \frac{x_{L_1E}.x_W}{K_1})\right] \tag{2.6}$$

$$+ w_{cat}.C_T\left[k_4^0.\exp(-\frac{E_{A_4}}{RT})\left(\frac{x_{L_1}^2}{K_4} - x_{L_2}.x_W\right) + k_5^0.\exp(-\frac{E_{A_5}}{RT})\left(\frac{x_{L_1}.x_{L_2}}{K_5} - x_{L_3}.x_W\right)\right]$$

$$-\frac{dx_{L_2}}{dt} = w_{cat}.C_T\left[k_2^0\exp(-\frac{E_{A_2}}{RT})(x_{L_2}.x_{EtOH} - \frac{x_{L_2E}.x_W}{K_2})\right] \tag{2.7}$$

$$+ w_{cat}.C_T\left[k_4^0.\exp(-\frac{E_{A_4}}{RT})\left(x_{L_2}.x_W - \frac{x_{L_1}^2}{K_4}\right) + k_5^0.\exp(-\frac{E_{A_5}}{RT})\left(\frac{x_{L_1}.x_{L_2}}{K_5} - x_{L_3}.x_W\right)\right]$$

$$-\frac{dx_{L_3}}{dt} = w_{cat}.C_T\left[k_3^0\exp(-\frac{E_{A_3}}{RT})(x_{L_3}.x_{EtOH} - \frac{x_{L_3E}.x_W}{K_3})\right] \tag{2.8}$$

$$+ w_{cat}.C_T\left[k_5^0.\exp(-\frac{E_{A_5}}{RT})\left(x_{L_3}.x_W - \frac{x_{L_1}.x_{L_2}}{K_5}\right)\right]$$

$$-\frac{dx_{L_1E}}{dt} = w_{cat}.C_T\left[k_1^0\exp(-\frac{E_{A_1}}{RT})(x_{L_1}.x_{EtOH} - \frac{x_{L_1E}.x_W}{K_1})\right] \tag{2.9}$$

$$-\frac{dx_{L_2E}}{dt} = w_{cat}.C_T\left[k_2^0\exp(-\frac{E_{A_2}}{RT})(x_{L_2}.x_{EtOH} - \frac{x_{L_2E}.x_W}{K_2})\right] \tag{2.10}$$

$$-\frac{dx_{L_3E}}{dt} = w_{cat}.C_T\left[k_3^0\exp(-\frac{E_{A_3}}{RT})(x_{L_3}.x_{EtOH} - \frac{x_{L_3E}.x_W}{K_3})\right] \tag{2.11}$$

$$-\frac{dx_{EtOH}}{dt} = w_{cat}.C_T\left[k_1^0\exp(-\frac{E_{A_1}}{RT})(x_{L_1}.x_{EtOH} - \frac{x_{L_1E}.x_W}{K_1})\right] \tag{2.12}$$

$$+ w_{cat}.C_T \left[k_2^0 . \exp(-\frac{E_{A_2}}{RT}) \left(x_{L_2} . x_{EtOH} - \frac{x_{L_2E} . x_W}{K_2} \right) + k_3^0 . \exp(-\frac{E_{A_3}}{RT}) \left(x_{L_3} . x_{EtOH} - \frac{x_{L_3E} . x_W}{K_3} \right) \right]$$

$$-\frac{dx_W}{dt} = w_{cat}.C_T \left[k_1^0 \exp(-\frac{E_{A_1}}{RT}) (\frac{x_{L_1E} . x_W}{K_1} - x_{L_1} . x_{EtOH}) \right] \tag{2.13}$$

$$+ w_{cat}.C_T \left[k_2^0 . \exp(-\frac{E_{A_2}}{RT}) \left(\frac{x_{L_2E} . x_W}{K_2} - x_{L_2} . x_{EtOH} \right) + k_3^0 . \exp(-\frac{E_{A_3}}{RT}) \left(\frac{x_{L_3E} . x_W}{K_3} - x_{L_3} . x_{EtOH} \right) \right]$$

$$+ w_{cat}.C_T \left[k_4^0 . \exp(-\frac{E_{A_4}}{RT}) \left(x_{L_2} . x_W - \frac{x_{L1}^2}{K_4} \right) + k_5^0 . \exp(-\frac{E_{A_5}}{RT}) \left(x_{L_3} . x_W + \frac{x_{L_1} . x_{L_2}}{K_5} \right) \right]$$

The equilibrium constant for L_1E formation (K_1) was obtained by reaction of 20 wt% solution of lactic acid with ethanol in the presence of Amberlyst-15. Complete chemical equilibrium was achieved after 72 h of reaction. The value for K_1 was found to be 2.4. The equilibrium constants for hydrolysis of all linear acid oligomers were taken as 5.0 based on our earlier work[30]. The equilibrium constants for L_2E and L_3E formation via esterification of L_2 and L_3 were treated as adjustable parameters in the model.

The pre-exponential factors (k_i^o) and activation energies (E_{Ai}) in the kinetic model were fit to the experimental data. To minimize the number of degrees of freedom, the activation energies for Reactions 2.1-2.3 were fixed at the values obtained from Figure 2.2 for initial reaction rates. Values for the five pre-exponential factors and E_{A4} and E_{A5} were then generated by nonlinear regression analysis using MATLAB 7.0 to minimize the sum of the mean square differences (Eq. 2.14) between experimental and predicted liquid phase mole fractions for all species over the course of reaction. The resulting pre-exponential factors, activation energies, and equilibrium constants for all reactions are given in Table 2.2.

$$F_{min}{}^2 = \frac{\sum\limits_{samples} (x_{i,cal} - x_{i,expt})^2}{n_{samples}} \tag{2.14}$$

2.6. Discussion

To illustrate the validity of the kinetic model, composition profiles were generated from Eq. 2.6-2.13 for the entire range of experimental conditions examined. Representative results of the model are shown in Figures 2.1-2.6 (additional esterification results are given in **Annexure I**). For 50 and 88 wt% lactic acid, predictions for component profiles were in reasonably good agreement with experimental values; for 20 wt% lactic acid, predictions were in excellent agreement with experiments. Error values or deviations (%) between experimental and model predictions for each component are provided in Table 2.3. For experiments with 88 wt% feed solution, errors were small during the initial 180 minutes of reaction but became larger as the reaction approached equilibrium. Errors were larger for L_2E and L_3E on a percentage basis, but those species were present in small quantities and thus do not significantly affect major component

concentrations. For 88 wt% lactic acid, over-prediction of L_2E formation at equilibrium resulted in over-prediction of acid conversion relative to experiment (Fig. 2.3).

Table 2.2 Rate Constants of the Kinetic Model

Parameters	Unit	Values
k_1^o	$kg^2_{sol}/kg_{cat}/s$	1.91×10^6
k_2^o	$kg^2_{sol}/kg_{cat}/s$	2.66×10^5
k_3^o	$kg^2_{sol}/kg_{cat}/s$	1.24×10^8
k_4^o	$kg^2_{sol}/kg_{cat}/s$	1.62×10^5
k_5^o	$kg^2_{sol}/kg_{cat}/s$	6.67×10^4
E_{A1}	kJ/kmol	48000
E_{A2}	kJ/kmol	54500
E_{A3}	kJ/kmol	74100
E_{A4}	kJ/kmol	52000
E_{A5}	kJ/kmol	50800
K_1		2.4
K_2		0.6
K_3		0.3
K_4		5.0
K_5		5.0

The kinetic model described here is based on the concentration of species (e.g. mole fraction) in solution. We recognize that species activity is a fundamentally more appropriate variable for kinetic modeling, but for this system there is little or no experimental data available on liquid-phase activity coefficients of lactic acid, its oligomers, and their esters in ethanol-water solutions. Prediction of such activity coefficients, which is possible using UNIFAC or other group contribution methods, is subject to substantial uncertainties, particularly for the high concentrations examined here. In fact, we did prepare an activity-based kinetic model for the lactate esterification system that included application of UNIFAC for activity coefficient prediction. The optimized activity-based model gave errors larger than those obtained with the mole fraction-based model – thus we do not believe there is any advantage to application of such a model at this time.

The choice of simple n^{th} order kinetic expressions for esterification, as opposed to a more mechanistically-based approach such as a Langmuir-Hinshelwood model, was made in part because of uncertainty in the liquid phase environment within the Amberlyst-15 cation exchange resin. When placed into aqueous solutions containing ethanol and organic acid, Amberlyst-15 swells due to selective absorption of water.[31] We observe the same behavior with dilute solutions of lactic acid (20 wt% and 50 wt%) in esterification, where water is present in large excess relative to lactic acid (20-fold excess for 20 wt% and 6-fold excess for 50 wt%) and thus free water can absorb.

Table 2.3 Comparison of Experimental Values and Model Prediction for Esterification of 20 wt%, 50 wt%, and 88 wt% Lactic acid aqueous solutions with Ethanol

Lactic acid Solution (wt %)	EtOH: LA Mole Ratio*	Catalyst Loading (wt%)	Temp. of Reaction (°C)	% Error (Eq. 2.14)							
				L_1	L_2	L_3	L_1E	L_2E	L_3E	EtOH	W
88	1	3	80	8.7	19.9	24	20.5	37.1	25.1	10.9	5.2
	2	3	80	8.9	17.2	15.5	10.1	15.9	28	4.4	2.3
	3	3	80	13.9	15.8	11.2	7.7	12.2	20.5	2	2.1
	4	3	80	22.2	21	12.8	2.7	16.9	25	1.1	0.9
	3	1	80	11.3	9.8	9.3	11.2	16	31.2	1.6	2.1
	3	2	80	7.4	10.1	7.6	7	9	29.8	1.4	1.6
	3	4	80	15.7	7	4.8	3.6	5.7	29.1	1.4	1
	3	5	80	11.5	33.4	27.9	2.6	6.6	16	1.2	0.6
	3	3	62	8.3	1.2	1.8	2.5	9.6	31.5	0.8	0.8
	3	3	72	5.5	3.5	3.2	0.6	3.6	13.1	0.6	0.2
	3	3	90	9.5	41.8	25.9	6.6	14.5	29.6	3	4.2
50	1	3	80	2.6	6.9	-	20.2	49	-	6.2	0.4
	2	3	80	2.2	5.1	-	11.2	29.2	-	2.9	0.04
	3	3	80	5.1	10.3	-	4.8	37.1	-	1.1	0.4
	4	3	80	8.4	20.4	-	5	25.9	-	0.5	0.6
	3	1	80	4.2	1.8	-	13	14.7	-	2.0	0.2
	3	2	80	5.6	6	-	4	24.4	-	1	0.4
	3	4	80	6.3	14	-	3.5	24.7	-	1.4	0.4
	3	3	61	6.6	3.2	-	14.2	39.1	-	0.4	0.8
	3	3	71	7.1	8.4	-	5.2	14.8	-	1.2	0.6
	3	3	90	1	20.8	-	4.1	34.8	-	1.2	0.5
20	1	3	80	1.5	-	-	9.2	-	-	0.8	0.06
	2	3	80	1.4	-	-	3.5	-	-	0.3	0.05
	3	3	80	1.8	-	-	4.2	-	-	0.2	0.07
	4	3	80	4.4	-	-	17	-	-	0.1	0.2
	3	1	80	5.8	-	-	9.7	-	-	1.3	0.4
	3	2	80	1	-	-	5.8	-	-	0.2	0.03
	3	4	80	2	-	-	14.1	-	-	0.7	0.2
	3	3	60	1.2	-	-	2.8	-	-	0.2	0.08
	3	3	70	2.5	-	-	5.6	-	-	0.5	0.2
	3	3	90	1.2	-	-	4.6	-	-	0.2	0.05

When concentrated (88 wt%) lactic acid, where the water to lactic acid molar ratio is 0.7, is subject to esterification, ethanol and not water is preferentially absorbed into Amberlyst-15. We attribute this behavior to the association of free water with lactic acid, such that very little or no free water is available for absorption onto resin particles at high lactic acid concentration. This hypothesis was further verified by an experiment in which a known composition of 88 wt% lactic acid and ethanol were brought in contact with resin at room temperature, equilibrated for 30 minutes, and analyzed. At this

temperature, no reaction was observed and ethanol was found to be preferentially adsorbed.
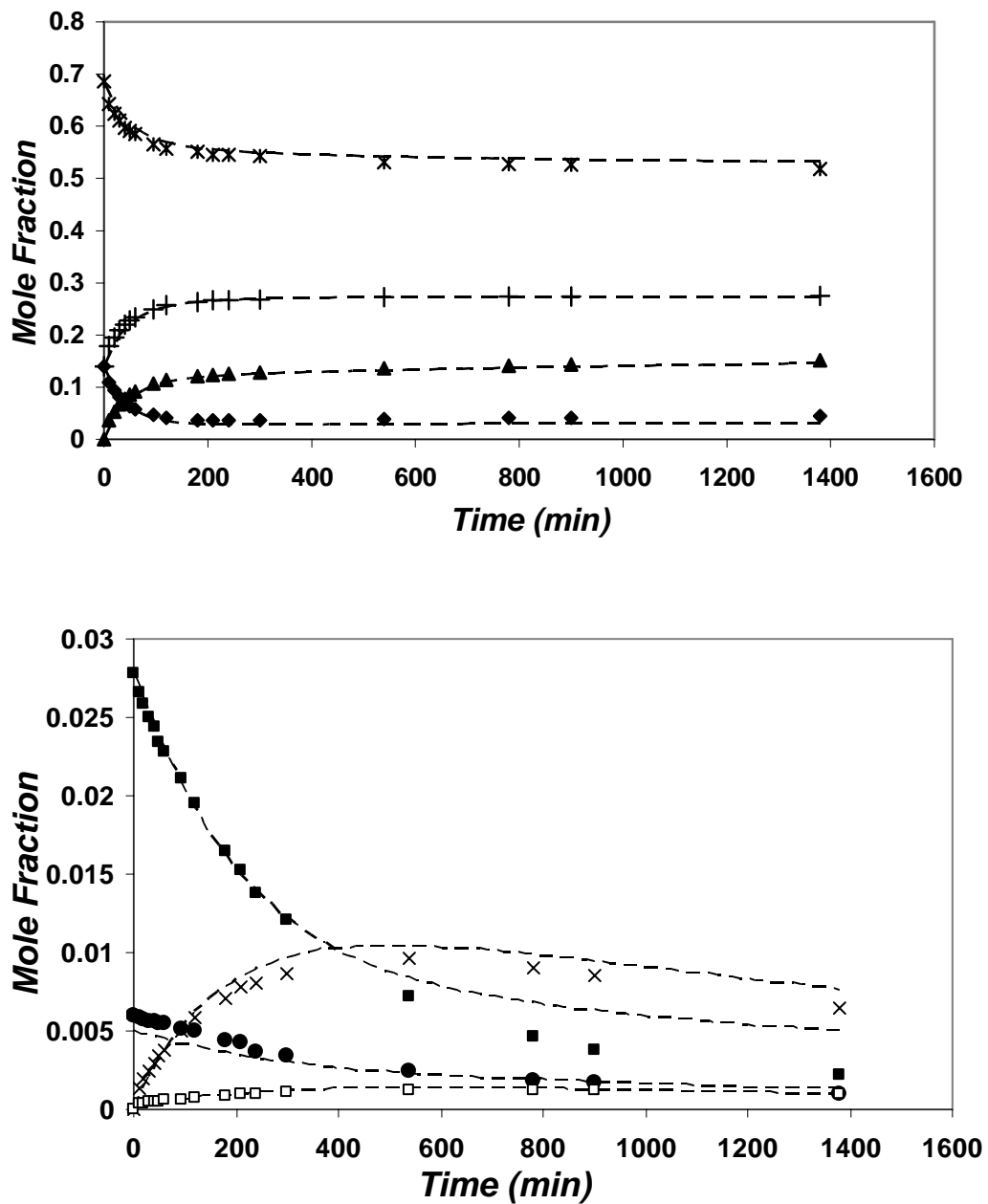
Figure 2.4 Esterification of 88 wt% lactic acid solution. Reaction conditions: Mole ratio of ethanol to lactic acid = 3; Catalyst loading = 3 wt%; Agitation rate = 740 rpm; Reaction temperature = 80°C. (◆) - L_1; (▲) - L_1E; (+) - Water; (✱) - Ethanol; (■) - L_2; (×) - L_2E; (●) - L_3; (□) - L_3E.
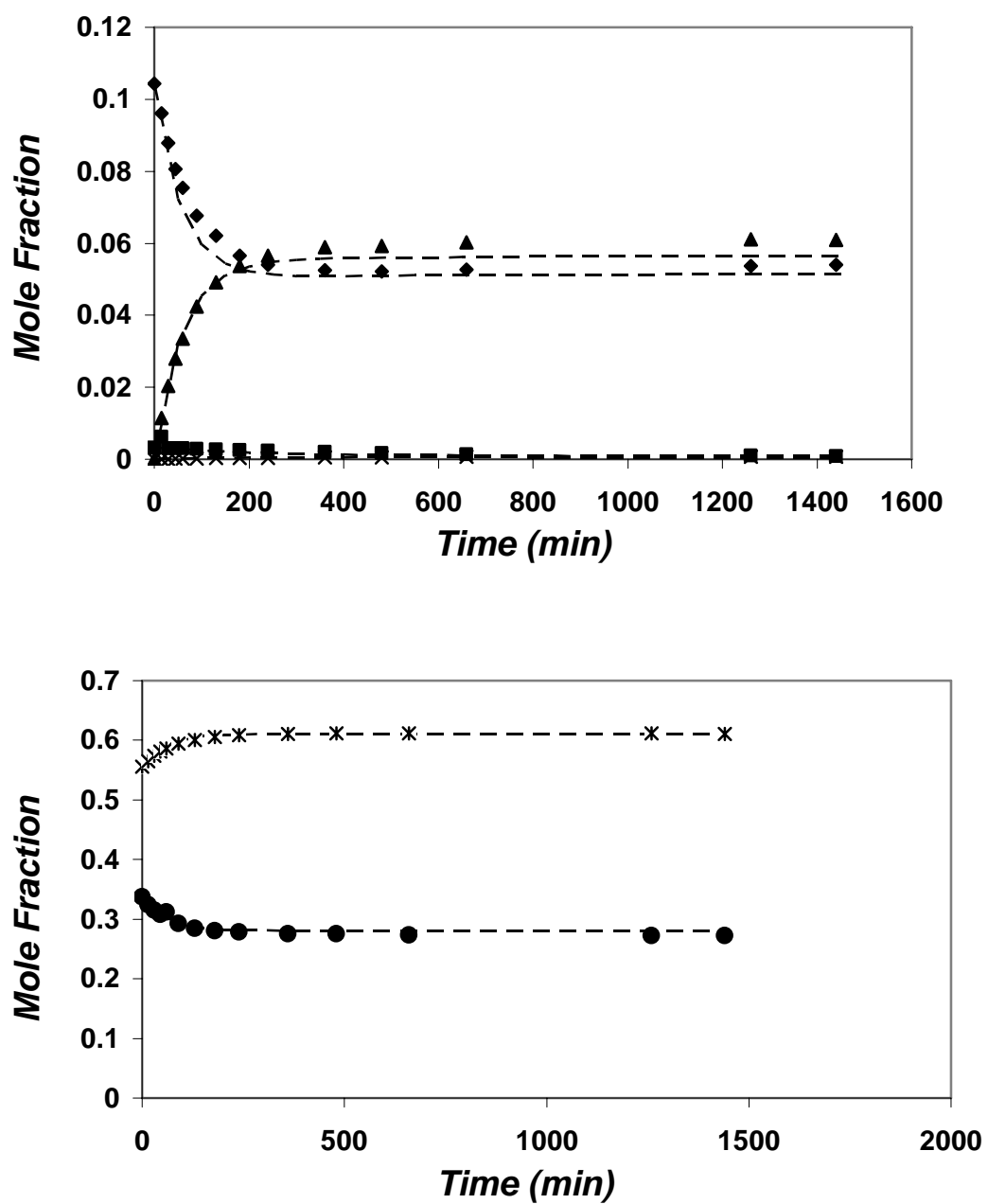
Figure 2.5 Esterification of 50 wt% lactic acid solution. Reaction conditions: Mole ratio of ethanol to lactic acid = 3; Catalyst loading = 3 wt%; Agitation rate = 740 rpm; Reaction temperature = 80°C. (◆) - L_1; (▲) - L_1E; (■) - L_2; (✕) - L_2E; (✳) - Water; (●) – Ethanol
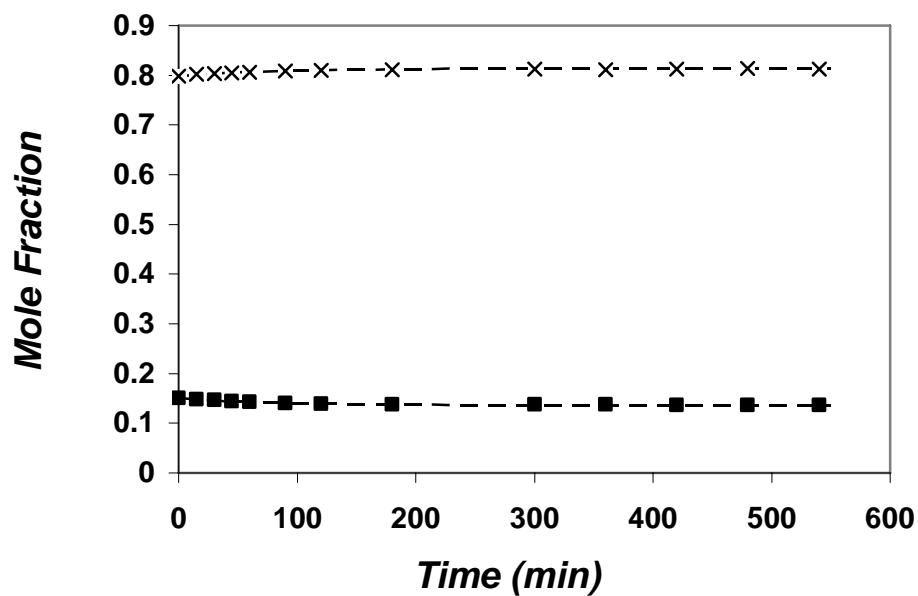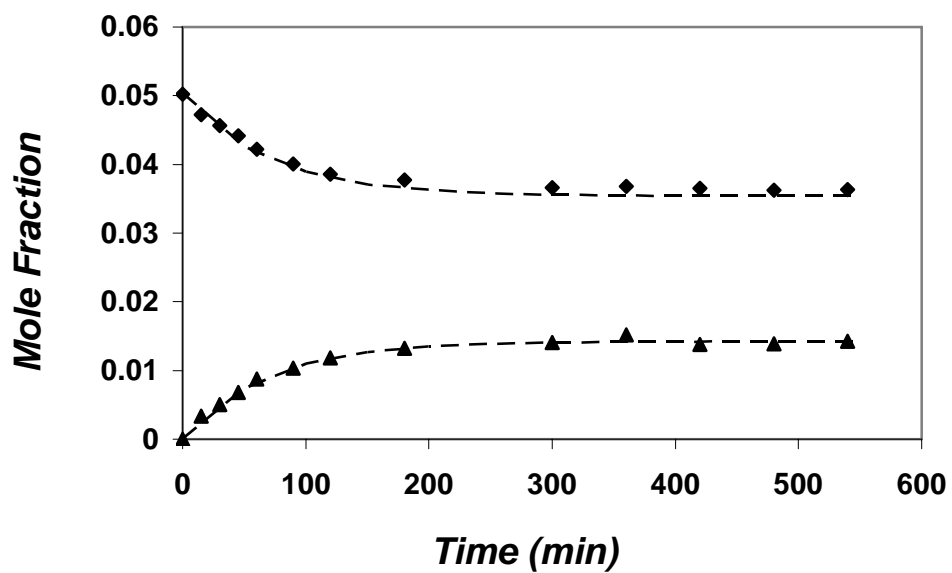
Figure 2.6 Esterification of 20 wt% lactic acid solution. Reaction conditions: Mole ratio of ethanol to lactic acid = 3; Catalyst loading = 3 wt%; Agitation rate = 740 rpm; Reaction temperature = 80°C. ($\blacklozenge$) - L_1; ($\blacktriangle$) - L_1E; ($\blacksquare$) - Ethanol; ($\times$) – Water

2.7. Conclusions

Kinetics of esterification of lactic acid and its linear oligomers with ethanol have been described using simple n^{th}-order reversible rate expressions. Pre-exponential factors, activation energies, and equilibrium constants were either fit to the experimental data using nonlinear regression analysis or, in some cases, were calculated directly or taken from other work. Activation energy values between 48000 and 74100 kJ/kmol and analysis of mass transport resistances indicate that the reaction is kinetically controlled. The predicted time-dependent species profiles in esterification were in good agreement with experimental results over a wide range of reaction conditions.

EQUILIBRIUM MODEL FOR LACTIC ACID OLIGOMERIZATION

3.1. Introduction

In recent years there is increasing emphasis on using biorenewable materials as substitutes for petroleum-based feedstocks. This paradigm shift is attributable to rising crude oil prices and the increasing desire to reduce dependence on petroleum. A major building block for the biorenewable economy is lactic acid (2-hydroxypropionic acid), an α-hydroxy acid containing both a hydroxyl and carboxylic acid functional group. For an excellent review on lactic acid the reader is referred to Holten.[16] Lactic acid was first isolated by the Swedish scientist Scheele in 1780[32], and first produced commercially in 1881.[33] Applications for lactic acid are found in the food (additive and preservative), pharmaceutical, cosmetic, textile, and leather industries. Lactic acid can be formed either via fermentation of carbohydrate monomers or via a chemical route, but since about 1990 only the fermentation route is practiced commercially. The recent completion of the NatureWorks lactic acid facility for polylactic acid production, with an annual capacity of 140,000 metric tons of polylactic acid[34], has greatly enhanced the stature of lactic acid as a key biorenewable platform.

Polylactic acid (PLA)[35] is a versatile thermoplastic polymer that has useful mechanical properties including high strength and high modulus. Applications of PLA include household commodity products, polymers used in food contact, biomedical materials like surgical sutures, absorbable bone plates for internal bone fixation, artificial skin, tissue scaffolds, and controlled release drugs. PLA is one of the few polymers whose structure and properties can be modified by polymerizing a controlled composition of the L- and D-isomers to give high molecular weight amorphous or crystalline polymers. PLA has a degradation time of 6 months to 2 years in the environment. For more details on PLA the reader is referred to Garlotta [36].

Esters of lactic acid, formed via combination with alcohols like methanol and ethanol, are finding increased use as environmentally benign solvents. Lactic acid esters are biodegradable, non-toxic, and have excellent solvent properties, which make them attractive candidates to replace halogenated solvents for a wide spectrum of uses. Esterification of lactic acid with alcohol can also be used as a highly efficient method for purification of lactic acid from fermentation broths, especially when lactic acid is desired in concentrated solutions.

It has been observed experimentally that dilute (<20 wt%) lactic acid solutions contain only lactic acid monomer (LA_1),[37] an observation that has been verified in this paper. However, many processes involving lactic acid, including polymerization and esterification, require concentrated lactic acid solutions, and lactic acid in these solutions undergoes intermolecular self-esterification to form higher oligomers. This oligomerization occurs to an increasing degree at high acid concentration, low water concentration, and high temperature.

In oligomerization, two molecules of lactic acid first react to form a linear dimer, commonly called lactoyllactic acid (LA_2), along with a mole of water.

$$2 \ \underset{\text{Lactic Acid (LA}_1)}{CH_3\overset{HO}{\underset{}{C}}H\overset{O}{\overset{\|}{C}}OH} \ \rightleftharpoons \ \underset{\text{Lactoyllactic acid (LA}_2)}{CH_3\overset{HO}{\underset{}{C}}H\overset{O}{\overset{\|}{C}}-O\overset{O}{\overset{\|}{\underset{CH_3\overset{}{C}H\overset{}{C}OH}{C}}}} \ + \ H_2O \tag{3.1}$$
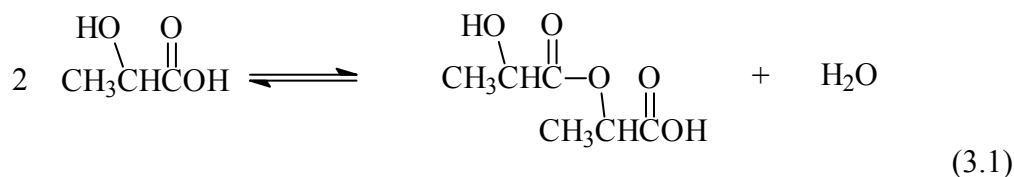
Lactic acid also forms a cyclic dimer noted as lactide, but this compound is known to be unstable in water[16] and thus is not a concern in this work. Lactoyllactic acid (LA$_2$) can further esterify with LA$_1$ to form the trimer lactoyl-lactoyllactic acid (LA$_3$); this process can further continue to give higher chain intermolecular polyesters LA$_4$, LA$_5$ and so on.

$$CH_3\overset{HO}{\underset{}{C}}H\overset{O}{\overset{\|}{C}}OH \ + \ CH_3\overset{HO}{\underset{}{C}}H\overset{O}{\overset{\|}{C}}-O\overset{O}{\overset{\|}{\underset{CH_3CHCOH}{C}}} \ \rightleftharpoons \ \underset{\text{Lactoyl-lactoyllactic acid (LA}_3)}{CH_3\overset{HO}{\underset{}{C}}H\overset{O}{\overset{\|}{C}}-O\overset{O}{\overset{\|}{\underset{CH_3\overset{}{C}H\overset{}{C}-O\overset{O}{\overset{\|}{\underset{CH_3CHCOH}{C}}}}{C}}}} \ + \ H_2O \tag{3.2}$$
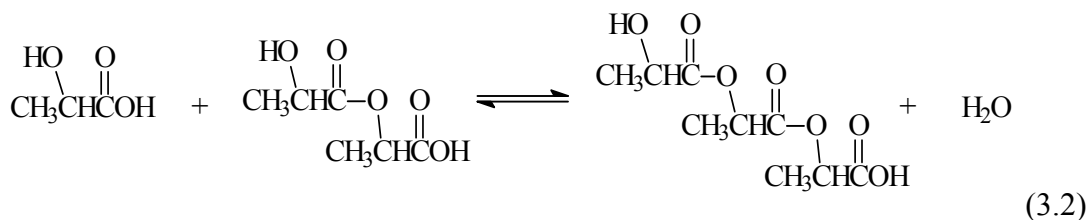
The inherent tendency of aqueous lactic acid to form intermolecular esters in solution poses a formidable obstacle in the modeling of its liquid-phase behavior and vapor-liquid phase equilibria. For design of reaction and separation processes involving concentrated lactic acid solutions, a model to predict thermodynamic properties of these complex chemically reactive mixtures is an indispensable tool. This paper presents such a model that requires only one parameter to adequately represent lactic acid solution behavior over the full range of concentration.

3.1.1. Definition of concentrations. Experimental work on quantifying concentrations of lactic acid oligomers in aqueous solution has been previously reported by Montgomery[37], Ueda and Terashima[38], and Watson[39], but the methods used in reporting these concentrations and the definitions of concentrations are not always clearly presented. Therefore, we clearly define here the quantities used to describe the concentration of lactic acid and its oligomers in solution.

3.1.1.1. Equivalent monomer lactic acid. In the literature, it has been found convenient to express the concentration of lactic acid oligomers as a percent of equivalent monomer lactic acid on a water-free basis. We abbreviate such a description with the acronym %EMLA$_j$. To illustrate the concept, consider a solution consisting of 50 mol water, 9.20 mol LA$_1$, 0.343 mol LA$_2$, and 0.0128 mol LA$_3$. Upon hydrolysis of the oligomers, 9.20 + 2*0.343 + 3*0.0128 = 9.924 mol lactic acid monomer would be present. The amount of water present would be 50 – 0.343 – 2*0.0128 = 49.63 mol H$_2$O. The lactic acid in the original solution is reported as 9.20/9.924 = 92.7 %EMLA LA$_1$, 2*0.343/9.924 = 6.9 %EMLA LA$_2$, and 3*0.0128/9.924 = 0.38 %EMLA LA$_3$. Introducing the molecular weight of water and oligomers, the solution has a total mass of 50*18.02 + 9.20*90.08 + 0.343*162.14 + 0.0128*234.21= 1788.3 g.

3.1.1.2. Superficial weight percent. The superficial weight percent of lactic acid is expressed as the weight of total monomer with the corresponding water of hydrolysis

divided by total solution weight. For the example above, the superficial wt% is (9.924 mol LA*90.08/1788.3 = 0.500) 50.0 wt% lactic acid, and (49.63*18.02/1788.3 = 0.500) 50.0 wt% water. When lactic acid is purchased, the concentrations expressed in wt% should be interpreted as superficial wt%. In this manuscript, we explicitly label such concentrations superficial wt% to avoid confusion.

When solutions are very concentrated, the superficial concentration of lactic acid can exceed 100 wt%. The concept of 125 superficial wt% lactic acid arises from the fact that 100 g of a polymer $(C_3H_4O_2)_n$ upon hydrolysis gives rise to 100*90.08/72.06 = 125 g of lactic acid, where 90.08 is the molecular weight of lactic acid monomer, and 72.06 is the molecular weight of the ester repeat unit in the polymer. When an aqueous solution has a lactic acid content exceeding 100 superficial wt%, the water of esterification (oligomerization) has been removed from the solution, and the solution is thus characterized by a negative superficial wt% of water.

3.1.1.3. True weight percent. True weight percent utilizes the mass of a particular sample and the total mass of the individual species within the solution. Using the same example again, the true wt% values are 46.3 true wt% LA_1 (9.20*90.08/1788.3 = 0.463), 3.1 true wt% LA_2 (0.343*162.14/1788.3 = 0.031), 0.17 true wt% LA_3 (0.0128*234.21/1788.3 = 0.0017), and 50.4 true wt% H_2O (50*18.02/1788.3 = 0.504).

3.2. Experimental.

3.2.1. Chemicals. Analytical grade aqueous lactic acid solutions were used in experiments: 85 superficial wt% was purchased from J.T. Baker, Inc. and 50 superficial wt% was purchased from Purac, Inc. HPLC grade water was purchased from J.T. Baker, Inc. HPLC grade acetonitrile was purchased from EMD Chemicals. An aqueous solution of 85 wt% phosphoric acid was purchased from J. T. Baker, Inc.

3.2.2. Preparation of oligomer solutions. Solutions of lactic acid below 50 superficial wt% were prepared by adding water to 50 superficial wt% lactic acid, whereas solutions between 50 superficial wt% and 85 superficial wt% were prepared by mixing the 50% and 85% solutions. After mixing, the solutions were heated at 80°C for one week to ensure that equilibrium between the various oligomers of lactic acid was reached. To concentrate lactic acid above 85 wt%, water was removed from 85 wt% lactic acid at 45 mmHg using a vacuum distillation apparatus. At that pressure, the boiling point temperature started at 30°C for 90 superficial wt% solution and rose to 135°C for solutions of 120 superficial wt%. Following evaporation, the solutions were equilibrated by refluxing at 100°C for 30 hours.

3.2.3. Analytical methods. The composition of lactic acid and its oligomers in solution was characterized using a combination of three analytical techniques.

3.2.3.1. Titration. The composition of dilute solutions containing less than 20 superficial wt% lactic acid corresponds to >98 %EMLA LA_1 and water.[16] Titration with standardized 0.1 N NaOH (Sigma-Aldrich) gave an accurate analysis of LA_1 in solution.[16,24]

For solutions containing more than 20 but less than 85 superficial wt% lactic acid, the total free acidity of the solution was determined from titration with standard 0.1 N NaOH In solutions above 85 superficial wt%, titration with 0.1 N NaOH occurred with too little base to accurate determine the endpoint. More reproducible results were found when using 0.01N NaOH. In addition, titrating the lactic solution in ice yielded more reproducible results due to decreased probability of hydrolysis. After titration of free acidity, excess NaOH was added and the solution was heated to about $80^{\circ}C$ to hydrolyze the oligomers to monomeric sodium lactate. Hydrolysis was carried out for two hours for solutions below 100 superficial wt% and for four hours for solutions above 100 superficial wt%. The quantity of unreacted NaOH was determined by back titration of the resultant solution with standardized 0.1 N H_2SO_4 solution (Sigma-Aldrich). For concentrations where only monomer and dimer exist, the quantity of LA_1 in solution was calculated by the difference between NaOH consumed for neutralization of total acid and the quantity of NaOH consumed for the hydrolysis of ester linkage present in oligomers.[25,40]

3.2.3.2. GC Analysis and GC/MS Analysis. Water concentrations in lactic acid standard solutions were verified using a Varian 3600 gas chromatograph (GC) equipped with a thermal conductivity detector (TCD). The GC column was 3.25mm OD x 4m long and was packed with 80/100 mesh Porapak-Q. The oven temperature was held constant at 353 K for 2 min, ramped at $20^{\circ}C$/min to 493 K, and held at 493 K for six minutes. The injector temperature was maintained at 493 K and the TCD block temperature was held at 503 K. Helium was used as the carrier gas. HPLC grade acetonitrile was used as an internal standard.

Qualitative analysis of LA_1 and its higher oligomers LA_2, LA_3 LA_4, etc. by GC-MS was carried out on a JEOL AX-505H double-focusing mass spectrometer coupled to a Hewlett-Packard 5890J gas chromatograph via a heated interface. GC separation employed a J&W DB-23 fused-silica capillary column (30 m length × 0.25 m I.D. with a 0.25 μm film coating). Splitless injection was used. Helium gas flow was maintained at 1 mL/min. The GC temperature program was initiated at 323 K and was ramped at $10^{\circ}C$/min to 533 K. MS conditions were as follows: interface temperature 523 K, ion source temperature 523 K, electron energy 70 eV, and scan frequency was 1Hz over the m/z range of 45-750. Prior to its injection for analysis by GC-MS, LA_1, LA_2, LA_3, and LA_4 were derivatized with TMS {Propanoic acid,2-[(trimethylsilyl)oxy]-trimethyl silyl ester} to enhance their volatility.

3.2.3.3. HPLC Analysis. The concentration of LA_1 and oligomers in concentrated lactic acid solutions were quantified using a Hewlett Packard 1090 Liquid Chromatograph equipped with an auto sampler, gradient flow pump, oven and a Hitachi-L400H UV detector set at 210 nm. Lactic acid samples below 85 superficial wt% were analyzed using a mobile phase of water + acetonitrile in gradient concentration at a flow rate 1 mL/min on a Novapak C_{18} column (3.9 × 150 mm). Both water and acetonitrile were acidified using 2 ml of 85% (w/v) phosphoric acid in 1L of solvent. The water was analyzed to be pH 1.3. The column oven temperature was maintained at $40^{\circ}C$. Beginning with a mobile phase of 100% acidified water, the acetonitrile concentration was ramped

linearly to 60 vol% from zero to 20 min and then ramped linearly up to 90% from 20 min to 25 min. The mobile phase composition was maintained constant at 90% to 28 min and then returned to 100% water.

For analysis of solution concentrations above 85 superficial wt% lactic acid, the total flow rate and column temperature were maintained as above, but the gradient was modified. The mobile phase was ramped linearly from 10% to 100% acetonitrile from 0 to 25 min. Acetonitrile concentration of mobile phase was brought back to 10% at 35 min.

3.2.3.3.1. Response factor for LA1. Dilute solutions of lactic acid (<20 superficial wt%) contain >98 %EMLA LA_1; their concentrations can be accurately determined by titration as described in Section 3.2.3.1. To prepare a standard containing only LA_1, a dilute solution containing 7-8 superficial wt% total lactic acid in water was prepared and heated for 6 h in presence of Amberlyst-15 cation exchange resin to facilitate hydrolysis of any LA_2 or higher oligomers present. Titration of this solution with 0.1 N NaOH showed a value of 7.3 true wt% LA_1. This solution was used to create HPLC calibration standards for LA_1 that spanned the range of LA_1 concentrations (0.1 to 1 true wt%) used in HPLC analysis. A linear UV response was observed from the calibration curve obtained by sample dilution. The response factor for LA_1 obtained from this calibration was used for quantitative determination of LA_1 in concentrated lactic acid solutions.

3.2.3.3.2. Response factor for LA2. A 50 superficial wt% lactic acid solution, containing LA_1 and LA_2, was titrated/hydrolyzed/back-titrated with standardized 0.1 N NaOH solution as described in Section 3.2.3.1. By this method the composition of LA_1 and LA_2 were quantified as 46 and 3 true wt%, respectively. HPLC analysis was performed on the sample and LA_1 was quantified using the response factor from calibration described in Section 3.2.3.3.1. GC analysis of the sample showed the presence of 51 true wt % water, and closed the material balance. This standardized solution was diluted in water to provide a series of calibration standards that spanned the pertinent range of true wt% of LA_1 (0.1 to 1 wt% by appropriate dilution with water) and LA_2. A linear UV response with concentration was observed for LA_2 following prompt analysis. The response factor from this calibration curve for LA_2 was used for quantitative determination of the superficial LA_2 concentration in lactic acid solutions. The ratio of response factors for superficial wt% was found to be $LA_2/LA_1 = 1.43$ in all HPLC analyses.

3.2.3.3.3. Response factors for LA3 and LA4. In a solution with approximately 93 superficial wt% aqueous lactic acid solution, the linear oligomers LA_3 and LA_4 are observed in significant quantities in addition to LA_2. HPLC analyses of the solution showed compositions of 58 and 22 true wt% for LA_1 and LA_2, respectively, with the remaining lactic acid in the form of higher oligomers. GC analysis of the solution showed the presence of 12 true wt% water. The presence of lactic acid oligomers up to LA_4 was also verified by GC-MS analysis. The assignment of response factors for higher oligomers was based on the following premises: 1) the difference in successively higher oligomers of lactic acid is the presence of an additional ester group; 2) the UV detector response is related to the presence of carbonyl groups in the ester functionality; and 3) the

ratio of LA_2/LA_1 response factors was 1.43. Therefore, the same ratio of response factors was assigned to each of the successively higher oligomers of lactic acid for superficial wt% ($LA_j/LA_1 = 1.43$). Using these response factors, the concentrations of LA_3 and LA_4 were determined from HPLC to be 6 and 2 true wt% respectively. Using these values, the material balance closed ($58 + 22 + 6 + 2 + 12 = 100$).

To further test the calibration, a series of dilutions where prepared from a solution that was determined by titration to be 73.8 superficial wt% lactic acid. The dilutions spanned the range of various wt% of LA_1, LA_2, LA_3, and LA_4 acids (0.1 to 1 wt% by appropriate dilution with water), and the HPLC analysis showed a linear concentration response. Using the response factors determined above, the total superficial concentration was determined to be 74%, in excellent agreement with titration and thus verifying the reliability of the oligomer HPLC response factors.

3.2.3.3.4. Analysis of higher (>LA_4) lactic acid oligomers. High oligomers of lactic acid are insoluble in water, but they are miscible in acetonitrile. Mixtures of acetonitrile + water have intermediate solvent strength. To dilute a sample of 115 superficial wt% lactic acid to an overall concentration of 2 wt% in a homogeneous phase, a solution of at least 50 wt% acetonitrile was needed. However, this composition was not suitable for injection because HPLC could not provide reliable resolution between LA_1 and LA_2 if more than 20 wt% acetonitrile was present in an injected sample containing large quantities of LA_1 and LA_2. The difficulties did not arise when the quantities of LA_1 and LA_2 were small. To provide reliable results, lactic acid solutions greater than 105 superficial wt% were analyzed in two fractions. Approximately 0.1g lactic acid solution was transferred to a microcentrifuge tube and weighed. Approximately 1 mL of water was added, the solution was shaken, and then centrifuged at 4000 rpm in a desktop microcentrifuge for 4 min. The water phase was carefully removed using a pipet. The water extraction was repeated four to five times. This water soluble fraction was weighed and held for analysis. Next, the water-insoluble high oligomers were recovered in 100% acetonitrile and this acetonitrile phase was weighed. All steps were done at room temperature. The oligomer contents in both water and acetonitrile were combined in calculation of superficial wt% oligomer distribution in the two fractions, and then combined to calculate the superficial wt% of the original sample and %$EMLA_j$. The response factors for the higher oligomers where assumed to be the same as the values for LA_3 and LA_4. The HPLC results for total lactic acid content determined by adding the superficial wt% of the individual oligomers is in good agreement with the results from titration as shown in Table 3.1.

3.3. Mathematical model

We present here a model of infinite oligomer formation using chemical theory. There are a few examples in the literature of compounds whose phase equilibria properties have been described with the help of chemical theory or chemical theory along with physical intermolecular forces. The most strikingly related example is that of formaldehyde in aqueous and/or methanolic solutions, which reveals extreme deviations from ideality caused mainly by chemical reactions. Formaldehyde in the presence of

water gives methylene glycol and polyoxomethylenes; in the presence of methanol it gives hemiformal and higher hemiformals.[41]

VLE for formaldehyde-containing systems has been described using chemical theory by Kogan[42], Kogan and Ogorodnikov[43,44], Brandani et al.[45] and Masamoto and Matsuzaki.[46] Maurer[41] presented for the first time a model in which chemical reactions together with physical intermolecular forces were used successfully to describe the VLE and enthalpy for formaldehyde-containing systems containing both reactive and inert components such as trioxane. Maurer's model was subsequently extended and tested using new data; for an update on the model up to 1992 the reader is referred to Hahnenstein et al.[47] This approach has also been used by Brandani et al.[48-50]

For the system formaldehyde-water, the mole fraction of compounds in the liquid phase is calculated by modeling the oligomerization as two equilibrium constants – one for methylene glycol formation from formaldehyde and water and the second for subsequent higher methylene glycol oligomer formation.

$$K_1 = [x_{MG}/(x_w x_{FA})][\gamma_{MG}/(\gamma_w \gamma_{FA})] \qquad (3.3)$$

$$K_n = [x_n x_w/(x_{n-1} x_{MG})][\gamma_n \gamma_w/(\gamma_{n-1} \gamma_{MG})] \qquad 2 \leq n \qquad (3.4)$$

These assumptions are reasonable since methylene glycol is a chemically different structure than formaldehyde, while the higher oligomers of methylene glycol are chemically similar to each other. The formaldehyde-methanol system is treated in a similar way.

3.3.1. Literature models for lactic acid based on chemical theory. Prior modeling work to determine the distribution of lactic acid oligomers in solutions above 20 wt% concentration has been performed by Bezzi et al.[51] and reported by Holten.[16] In the first modeling approach, only the dimers of lactic acid (LA$_2$) were considered. This approach, however, becomes inaccurate at higher concentrations of lactic acid (>50 wt%), where significant oligomerization occurs. In a second modeling approach, polylactic acids were taken into account, giving a more realistic representation at high concentrations. However, this model was limited in that solutions were characterized only by concentration of free lactic acid (LA) and total oligomer species; no distributions of oligomers was generated. This polylactic model works poorly at low concentrations, and is interpretative rather than predictive in its application.

We are unaware of published mathematical models, apart from the ones described above, which attempt to represent the liquid phase distribution of lactic acid and its oligomers in solution. Therefore, we propose here a model that is based on chemical theory and incorporates an infinite series of oligomer components. The model accurately predicts liquid phase compositions of lactic acid in a method similar to Maurer's for formaldehyde systems, and represents a clear advancement of the characterization of concentrated lactic acid solutions. In order to compare the present model to those in the literature, this work utilizes the terminology used by Montgomery[37] and Ueda and Terashima[38] as clarified in Section 3.1.1.

3.3.2. Infinite Series Polymer Model. From a thermodynamic standpoint, the formation of oligomeric intermolecular esters of lactic acid can be described as the set of successive reactions shown below, where W denotes water

$$2 \text{ LA}_1 \quad \square \quad \text{LA}_2 + \text{W} \qquad (3.5)$$

$$LA_2 \ + \ LA_1 \ \square \quad LA_3 \ + \ W \tag{3.6}$$

$$LA_3 \ + \ LA_1 \ \square \quad LA_4 \ + \ W \tag{3.7}$$

Generally, oligomer formation can be written as

$$LA_{(j-1)} \ + \ LA_1 \ \square \quad LA_j \quad + \ W \tag{3.8}$$
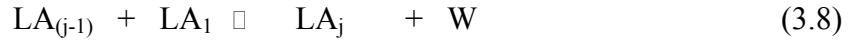
The chemical reaction equilibrium constants for the above reactions in a generalized form by

$$K_j \ = \ n_{LAj} n_W / (n_{LA(j-1)} n_{LA1}) \quad j > 2 \tag{3.9}$$

Note that since the number of moles of products and reactants is equivalent regardless of the degree of oligomerization, the equilibrium constant written in eq (3.9) is equivalent to an equilibrium constant written in mole fractions.

Since lactic acid oligomers (LA_2, LA_3, etc.) are all formed via identical reaction pathways and are themselves chemically similar, it is reasonable to assume that the esterification reactions (eq 3.5-3.8 above) have the same value of equilibrium constant.

$$K \ = \ K_1 \ = \ K_2 \ = \ K_3 \ = \ K_4 \ = \ ..... \ = \ K_j \tag{3.10}$$

This reasoning is analogous to the treatment of the formaldehyde model, where all polyoxomethylenes have the same equilibrium constant since they are chemically very similar but the formaldehyde to methylene glycol reaction involves different chemical structures and therefore has a different equilibrium constant.[41]

Eq (3.9) can be rearranged to the following form

$$n_{LAj} = n_{LA(j-1)} \cdot r \tag{3.11}$$

where

$$r = n_{LA1} \ K / n_W \tag{3.12}$$

and it is recognized that n_{LA1} and n_W are properties of the solution, identical for all oligomers at a specific superficial concentration. Because of the recursion, it is possible to write

$$n_{LAj} = n_{LA1} \cdot r^{(j-1)} \tag{3.13}$$

A total lactic acid superficial mole balance is given by

$$n_{LA}^i = \sum j \times n_{LAj} = n_{LA1}(1 + 2r + 3r^2 + 4r^3 + ...) = n_{LA1} / (1 - r)^2 \tag{3.14}$$

where the left hand side is the superficial number of moles of lactate in solution, the second and third expressions represent the infinite converging series obtained by inserting eq (3.13), and the final term represents the closed form solution. The water superficial mole balance is given by taking the difference between the true moles present, and those consumed by hydrolysis of oligomers

$$n_W^i = n_W - \sum (j-1) n_{LAj} = n_W - n_{LA1} r(1 + 2r + 3r^2 + 4r^3 + ...) = n_W - n_{LA1} r / (1 - r)^2 \tag{3.15}$$

where eq (3.13) is substituted into the summation between the second expression and the third, and the right hand side is the closed form solution. The left-most variable in eq (3.15) is the superficial number of moles of water. Eq (3.14) can be inserted into (3.15) to give

$$n_W = n_W^i + n_{LA}^i . r \tag{3.16}$$

Inserting eq (3.14) and (3.16) into eq (3.12) provides a relation between K and r in terms of the superficial concentrations of lactic acid and water

$$K = r(n_W^i + n_{LA}^i r) / [(n_{LA}^i (1 - r)^2] \tag{3.17}$$

Free acid and all oligomers contribute to titratable acidity that can be calculated by

$$\sum n_{LAj} = n_{LA1}(1 + r + r^2 + r^3 + ...) = n_{LA1}/(1-r) \qquad (3.18)$$

3.3.3. Application. To apply the model, an overall superficial number of moles n^i_W, n^i_{LA} and K are specified. Eq (3.17) is rearranged as a cubic in r and solved explicitly for the value of r. The value of r is then used to calculate n_{LA1} from eq (3.14), and subsequently the distribution of oligomers from eq (3.13) as well as the remaining balances.

The equations can be manipulated to express the various oligomer concentrations in terms of the overall superficial wt% lactic acid. The %EMLA for LA_j is

$$\%EMLA_j = j \cdot r^{(j-1)}(1-r)^2 \qquad \qquad ... \qquad (3.19)$$

The superficial wt% of LA_j is

(Superficial wt% of LA_j) = (%EMLA$_j$)(overall superficial wt% LA).. $\qquad$ (3.20)

The true wt% of water is

(True wt% water) = 100 + (overall superficial wt% LA)(0.2r − 1) .. $\qquad$ (3.21)

The true wt% of an LA_j is

(True wt% LA_j) = (0.8j + 0.2)(overall superficial wt% LA) $r^{(j-1)}(1-r)^2$ $\qquad$ (3.22)

3.4. Results and Discussion

Aqueous solutions of lactic acid were prepared and analyzed for oligomer concentrations up to 120 superficial wt% lactic acid. Table 3.1 gives a summary of the HPLC results and a comparison with total acidity of the solution determined by titration. The HPLC results for overall superficial wt% were calculated by summing the peak areas for the individual oligomers. As a check of the HPLC method, the total acid content by the HPLC and titration agreed within ±3 wt% for solutions up to 105 wt% lactic acid.

The value of the equilibrium constant K = 0.2023 was obtained by least squares regression of %EMLA for species LA_1 through LA_4 simultaneously. Using this value, the titratable acidity is modeled with an average deviation of ±0.12% of the reported %EMLA. For each composition from Table1, calculated %EMLA of the oligomers is presented in Table 3.2. From the HPLC results, the material balance provided the superficial number of moles of lactic acid and water. Using the value of K and the superficial moles, the value of r was determined for each overall composition, and then eq. (3.19) was applied.

Figure 3.1 shows a GC/MS result for an 85 superficial wt% lactic acid solution, demonstrating by molecular weights that only linear oligomers of lactic acid are present. All four components, namely LA_1, LA_2, LA_3 and LA_4, were identified and verified by their respective mass fragmentation data obtained from GC/MS.
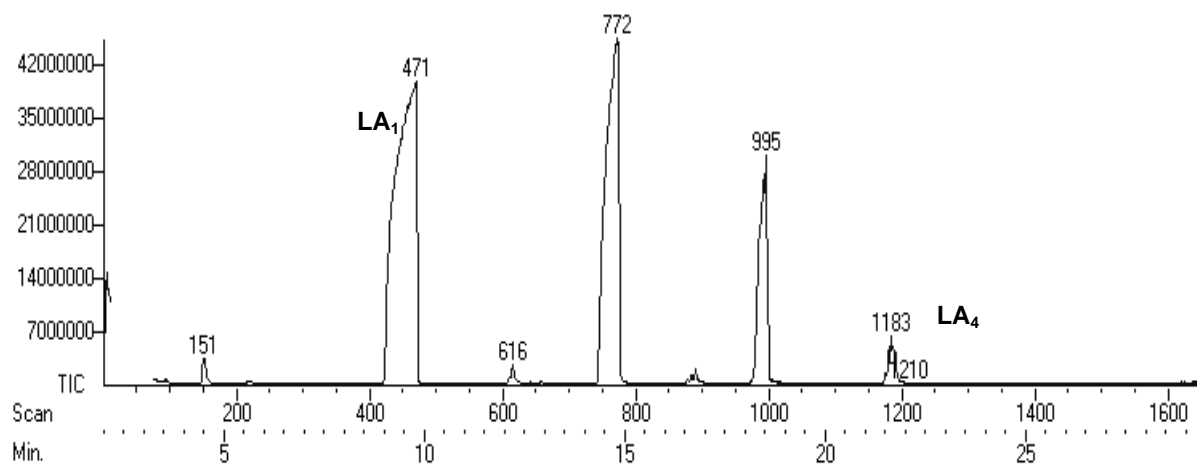
Figure 3.1 GC/MS of 85 wt% LA. The mass fragments (not shown) were used to verify that linear oligomers of LA are present. No lactide was observed
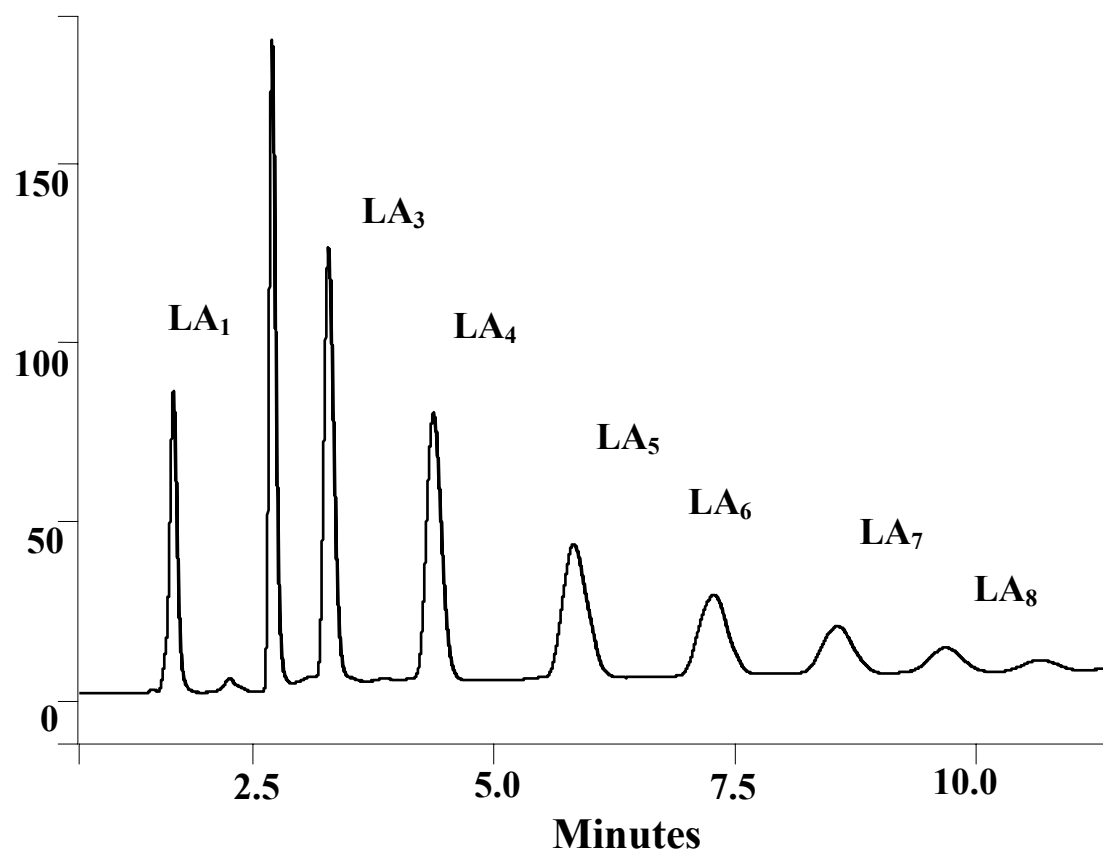
Figure 3.2 HPLC chromatograph of the water soluble fraction from 115 superficial wt% lactic acid demonstrating the separation of oligomers

Figure 3.2 shows an example HPLC chromatograph of a 115 superficial wt% solution of lactic acid. Figure 3.3 shows total titratable acidity as a function of lactic acid concentration as summarized by Holten[16] from various sources and from this work. The titratable acidity reflects a balance between increasing total acid content and increasing degree of oligomerization that eliminates free acid groups. The titratable acidity goes through a maximum at about 90 wt% lactic acid. The model represents the experimental data with an average deviation of ±2% of titratable acidity.
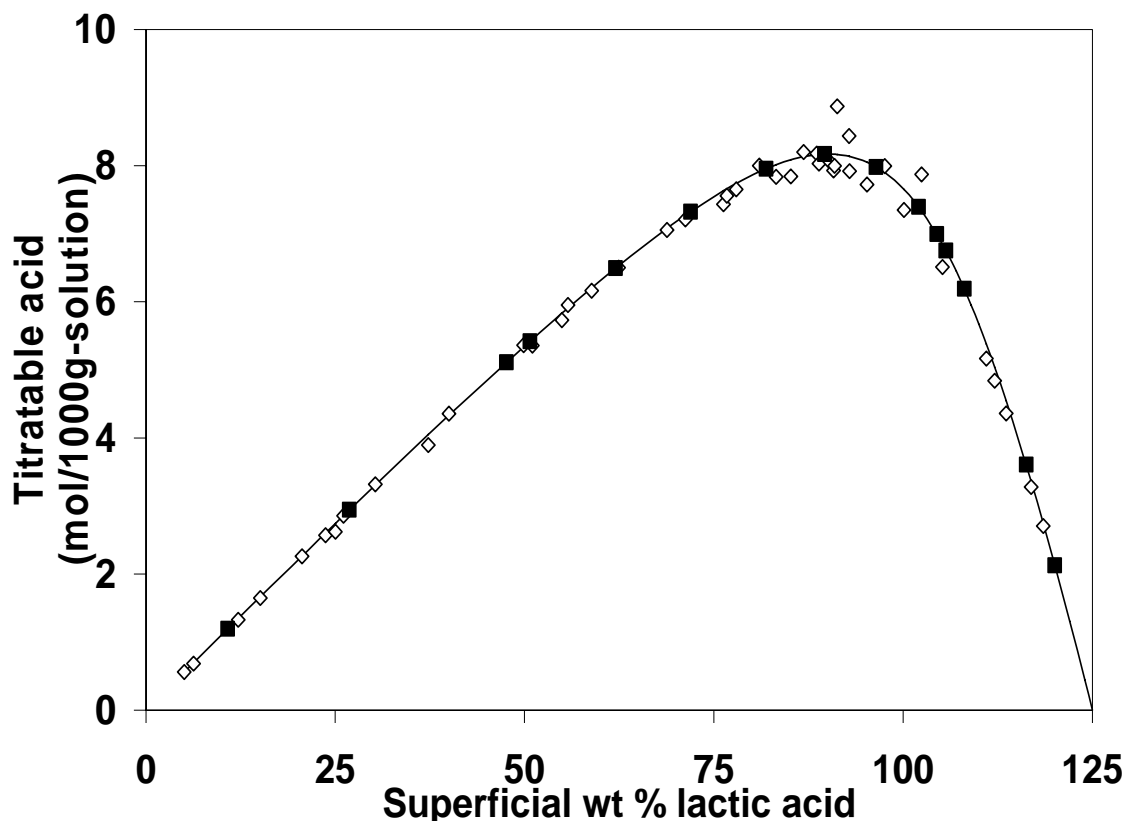
Figure 3.3 Total titratable acidity tabulated from various workers by Holten and measured in this work compared with the model proposed in this work. □ data compiled by Holten, ■ this work

Figure 3.4 shows the experimental distribution of LA_1, LA_2, LA_3 and higher oligomers collected in this work and compared to data from Ueda and Terashima[38] and Montgomery.[37] Higher oligomers are denoted by LA_{4+}, i.e. sum of tetramers and higher oligomers. The abscissa of Figure 3.4 denotes the superficial lactic acid concentration; note that it runs through 125% as explained in the introduction. The ordinate of Figure 3.4 denotes the %EMLA distribution of lactic acid between monomer and its oligomers on a water-free basis. The percentages are calculated as described in the introduction. The lines shown in Figure 3.4 are the calculated values of LA_1, LA_2, LA_3. LA_4 and LA_{4+} from the model. Excellent agreement is seen between the experimental values of this work and the values calculated from the model.

It can be seen from the experimental data of this work and also from Montgomery[37], that there is a maximum value of approximately 15 %EMLA LA_3

occurring at 114 superficial wt% and a maximum value of 29 %EMLA LA_2 occurring at 105 superficial wt%. Experimental data from Ueda and Terashima[38] are also presented; this set of experimental data runs up to 87% total acidity. Watson's[39] experimental data are not plotted because he reports the presence of lactide, which is known to be unstable in aqueous solutions.
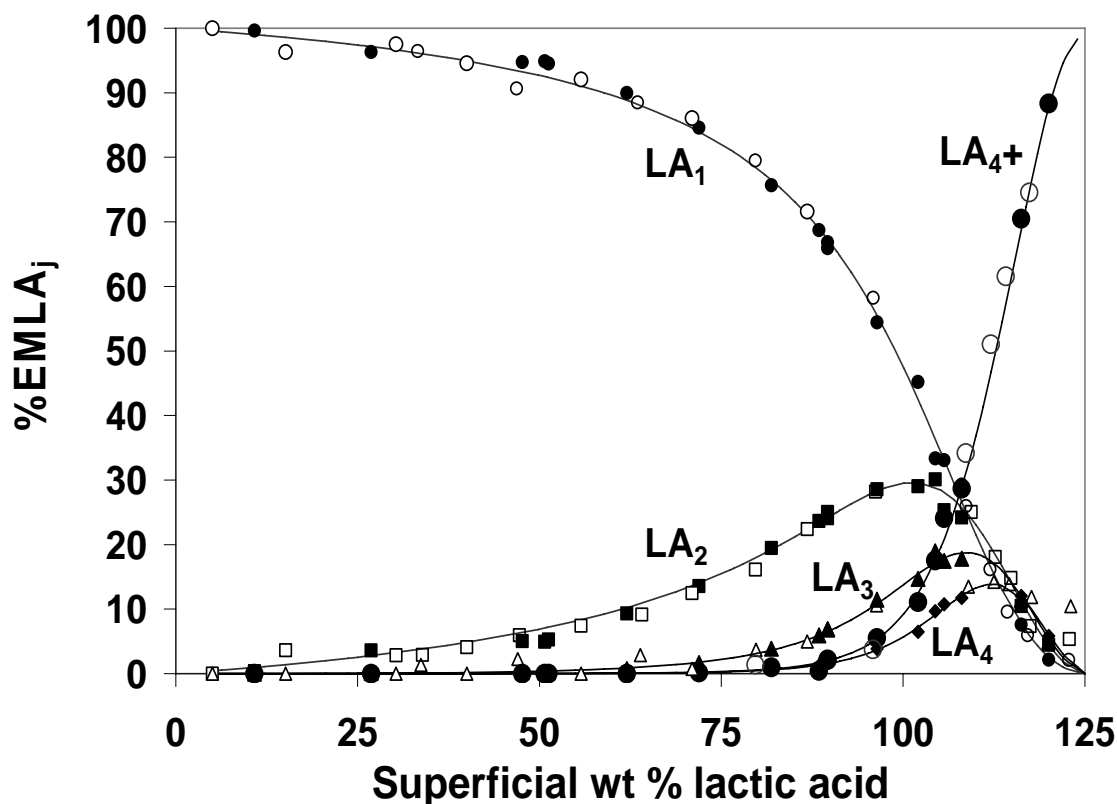
Figure 3.4 Experimental oligomer distribution compared with the model expressed as %EMLA. Solid lines represent the model, solid symbols are measured in this work and open symbols are from literature as reported by [7] and [16]. The curve labeled LA4+ indicates the sum of all oligomers LA_j where $j \geq 4$

Figure 3.5 compares the experimental analysis and model concentrations of LA_5 through LA_{10} for solutions with superficial lactic acid content of 80 to 125 wt%. The agreement is excellent for analyzed solutions up to 108 superficial wt% of acid. The agreement is not as good for the solutions with superficial concentrations of 116 wt% and 120 wt%. These samples were analyzed in two fractions as discussed above. Since the total acid content is in good agreement by HPLC and titration (Table 3.1), we believe that the disagreement between the model and HPLC results is due to the incomplete separation of oligomers in the HPLC, even though distinct peaks appear on the HPLC chromatogram. Attempts to refine the HPLC method further for these very high molecular weight solutions have not been successful.

Concentrated solutions of lactic acid (>105 superficial wt%) are fluid at 120°C, but are very viscous at room temperature. The solutions had a very slight amber tint, but none of the dark coloration indicated by Montgomery[37]. Our results are in good agreement with those of Montgomery[37] except at the highest concentration. Montgomery

reported incomplete separation of LA_3 and higher oligomers -- a problem that we experienced only for higher oligomers ($>LA_5$). To test for hydrolysis under analysis conditions in this work, ethyl lactate was analyzed using the same HPLC method as for the lactic acid oligomers and was found to be stable. Also, our results are also consistent with those of Montgomery, who tested extensively for hydrolysis.
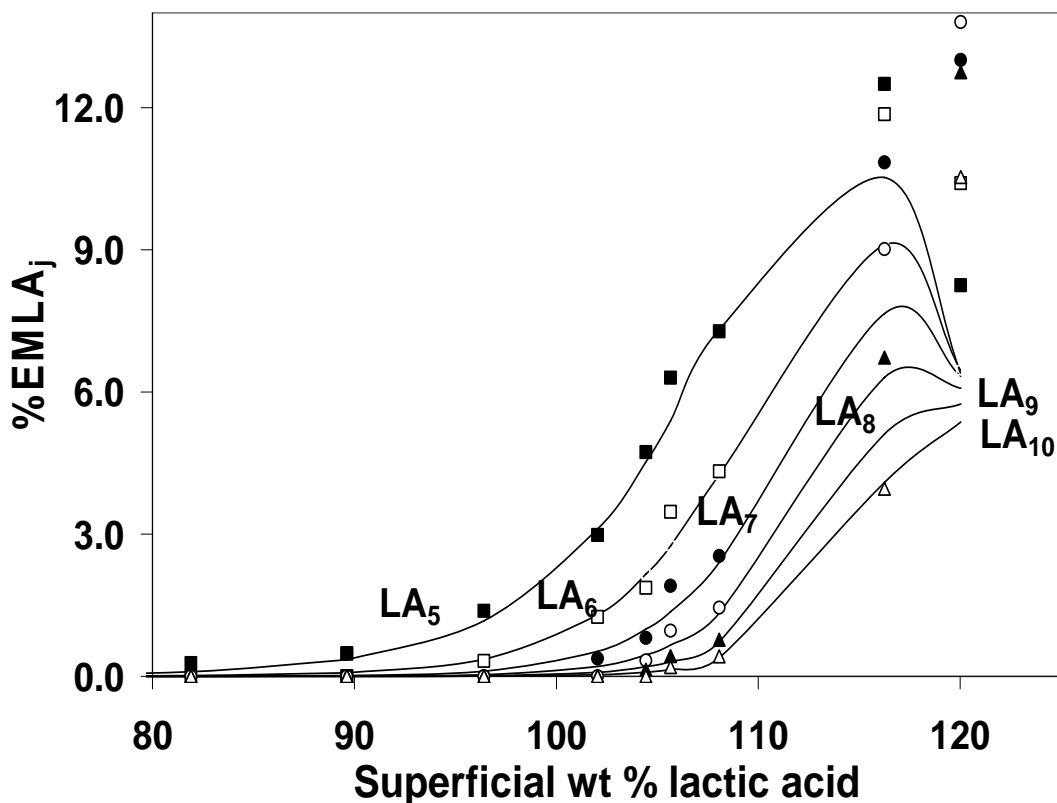
Figure 3.5 Experimental oligomer distribution compared with the model expressed as %EMLA. Experimental difficulties in analyzing the two highest concentrations are discussed in the text

In discussion of the distribution of weight percentages in lactic acid solutions, it is appropriate to express the concentrations in terms of superficial wt%. The superficial wt% for oligomers can be quickly calculated from the values in Table 3.1 by multiplying the total acid superficial wt% by the %EMLA. A summary of true weight percentages calculated by the oligomer model is shown in Table 3.3.

3.4.1. Implementation of lactic acid model into ASPEN Plus. Implementation of the model is extended to ASPEN Plus, which is the most widely used simulation software in the chemical process industry.

The proposed model could be incorporated into the process simulator via a user-written subroutine. As an alternative, we assume that oligomerization is adequately approximated by a truncated series. Figure 3.4 implies that solutions up to 85 wt% can be represented by monomer lactic acid and the first four oligomers ($LA_2 - LA_5$). We have used this assumption to simulate a distillation column for the purpose of evaluating its suitability for process simulation.

Table 3.1 Summary of HPLC results and comparison with total superficial acid by titration. Percentages by HPLC analysis are calculated as explained in the introduction and are also plotted on Figure 3.4. (*: commercial LA 50%, $^{+}$: commercial LA 85 %)

Overall superficial wt LA%		HPLC analysis (%EMLA$_j$)										
Titration	HPLC	LA$_1$	LA$_2$	LA$_3$	LA$_4$	LA$_5$	LA$_6$	LA$_7$	LA$_8$	LA$_9$	LA$_{10}$	LA$_4$+
12.24	10.81	99.63	0.37	0.00	0.00	0.00	0.00	0.00	0.00	0.00	0.00	0.00
24.36	26.88	96.31	3.59	0.10	0.00	0.00	0.00	0.00	0.00	0.00	0.00	0.00
44.47	47.62	94.74	5.06	0.20	0.00	0.00	0.00	0.00	0.00	0.00	0.00	0.00
53.43*	51.25*	94.53*	5.28*	0.19*	0.00	0.00	0.00	0.00	0.00	0.00	0.00	0.00
59.59	62.02	89.95	9.33	0.72	0.00	0.00	0.00	0.00	0.00	0.00	0.00	0.00
70.60	71.93	84.61	13.58	1.65	0.16	0.00	0.00	0.00	0.00	0.00	0.00	0.16
81.46	81.90	75.66	19.49	3.88	0.69	0.28	0.00	0.00	0.00	0.00	0.00	0.97
87.13^{+}	89.62^{+}	65.92^{+}	25.05^{+}	6.90^{+}	1.63^{+}	0.49^{+}	0.00	0.00	0.00	0.00	0.00	2.12
88.06	89.63	66.85	24.09	6.87	1.72	0.48	0.00	0.00	0.00	0.00	0.00	2.20
96.75	96.42	54.42	28.56	11.48	3.84	1.38	0.32	0.00	0.00	0.00	0.00	5.55
100.18	102.05	45.19	29.03	14.69	6.49	2.98	1.25	0.37	0.00	0.00	0.00	11.10
103.27	104.43	33.36	30.11	18.97	9.68	4.73	1.87	0.81	0.33	0.14	0.00	17.56
106.41	105.65	33.10	25.33	17.46	10.76	6.30	3.47	1.91	0.96	0.43	0.19	24.11
113.61	108.07	29.29	24.20	17.83	11.74	7.28	4.32	2.54	1.45	0.77	0.42	28.69
115.47	116.25	7.62	10.47	11.44	12.06	12.50	11.86	10.84	9.01	6.72	3.96	70.47
119.57	120.02	2.18	4.49	5.02	5.83	8.25	10.40	13.00	13.81	12.75	10.54	88.31

Table 3.2 Summary of calculated %ELMA for oligomers at each of the experimental compositions from Table 3.1. The first four columns are from experimental results, and the remaining columns are calculated based on the model using K = 0.2023.

sample (g)	acid wt%	n^i_w (mmol)	n^i_{LA} (mmol)	r	Calculated ($\%EMLA_j$)										
					LA_1	LA_2	LA_3	LA_4	LA_5	LA_6	LA_7	LA_8	LA_9	LA_{10}	LA_4+
0.081	10.8	3.99	0.097	0.005	99.0	0.96	0.007	0.000	0.000	0.000	0.000	0.000	0.000	0.000	0.000
0.293	26.9	11.9	0.876	0.014	97.1	2.80	0.061	0.001	0.000	0.000	0.000	0.000	0.000	0.000	0.001
0.213	47.6	6.21	1.13	0.034	93.3	6.36	0.326	0.015	0.001	0.000	0.000	0.000	0.000	0.000	0.015
0.112	50.7	3.06	0.631	0.038	92.5	7.07	0.405	0.021	0.001	0.000	0.000	0.000	0.000	0.000	0.022
0.111	62.0	2.34	0.763	0.058	88.8	10.2	0.884	0.068	0.005	0.000	0.000	0.000	0.000	0.000	0.073
0.115	71.9	1.80	0.922	0.084	84.0	14.0	1.76	0.196	0.020	0.002	0.000	0.000	0.000	0.000	0.218
0.107	81.9	1.08	0.977	0.126	76.4	19.2	3.62	0.607	0.095	0.014	0.002	0.000	0.000	0.000	0.719
0.093	89.6	0.533	0.921	0.180	67.3	24.2	6.51	1.56	0.350	0.075	0.016	0.003	0.001	0.000	2.00
0.086	96.4	0.171	0.920	0.255	55.5	28.3	10.8	3.68	1.17	0.358	0.107	0.031	0.009	0.003	5.36
0.081	102.0	-0.093	0.923	0.348	42.5	29.6	15.4	7.16	3.11	1.30	0.527	0.209	0.082	0.032	12.4
0.093	104.4	-0.228	1.07	0.397	36.3	28.9	17.2	9.11	4.52	2.16	1.00	0.454	0.203	0.090	17.6
0.079	105.7	-0.249	0.931	0.425	33.1	28.1	17.9	10.1	5.39	2.75	1.36	0.662	0.316	0.149	20.9
0.054	108.1	-0.240	0.642	0.484	26.6	25.8	18.7	12.1	7.32	4.25	2.40	1.33	0.725	0.390	28.9
0.111	116.2	-1.01.	1.44	0.721	7.80	11.2	12.2	11.7	10.5	9.10	7.65	6.30	5.11	4.09	68.8
0.198	120.0	-2.20	2.64	0.840	2.57	4.32	5.440	6.095	6.402	6.456	6.329	6.078	5.746	5.365	87.7

Table 3.3 Model calculations of true wt% of water and lactic acid oligomers for various superficial compositions.

superficial wt % LA	superficial wt% water	True Weight Percent Compositions											
		water	LA_1	LA_2	LA_3	LA_4	LA_5	LA_6	LA_7	LA_8	LA_9	LA_{10}	LA_{11+}
5	95	95.0	4.98	0.019	0.000	0.000	0.000	0.000	0.000	0.000	0.000	0.000	0.000
10	90	90.0	9.91	0.079	0.001	0.000	0.000	0.000	0.000	0.000	0.000	0.000	0.000
15	85	85.0	14.8	0.187	0.002	0.000	0.000	0.000	0.000	0.000	0.000	0.000	0.000
20	80	80.0	19.6	0.350	0.005	0.000	0.000	0.000	0.000	0.000	0.000	0.000	0.000
25	75	75.1	24.3	0.575	0.011	0.000	0.000	0.000	0.000	0.000	0.000	0.000	0.000
30	70	70.1	29.0	0.874	0.021	0.000	0.000	0.000	0.000	0.000	0.000	0.000	0.000
35	65	65.1	33.6	1.26	0.038	0.001	0.000	0.000	0.000	0.000	0.000	0.000	0.000
40	60	60.2	38.0	1.75	0.064	0.002	0.000	0.000	0.000	0.000	0.000	0.000	0.000
45	55	55.3	42.3	2.35	0.105	0.004	0.000	0.000	0.000	0.000	0.000	0.000	0.000
50	50	50.4	46.3	3.11	0.167	0.008	0.000	0.000	0.000	0.000	0.000	0.000	0.000
55	45	45.5	50.2	4.03	0.260	0.015	0.001	0.000	0.000	0.000	0.000	0.000	0.000
60	40	40.6	53.8	5.18	0.400	0.028	0.002	0.000	0.000	0.000	0.000	0.000	0.000
65	35	35.8	56.9	6.58	0.611	0.051	0.004	0.000	0.000	0.000	0.000	0.000	0.000
70	30	31.1	59.6	8.31	0.931	0.094	0.009	0.001	0.000	0.000	0.000	0.000	0.000
75	25	26.4	61.5	10.4	1.42	0.175	0.020	0.002	0.000	0.000	0.000	0.000	0.000
80	20	21.9	62.5	13.0	2.18	0.330	0.047	0.007	0.001	0.000	0.000	0.000	0.000
85	15	17.5	62.2	16.2	3.37	0.636	0.113	0.019	0.003	0.001	0.000	0.000	0.000
90	10	13.3	60.1	19.8	5.23	1.25	0.282	0.061	0.013	0.003	0.001	0.000	0.000
95	5	9.49	55.4	23.6	8.04	2.48	0.725	0.204	0.056	0.015	0.004	0.001	0.000
100	0	6.20	47.6	26.6	11.9	4.83	1.85	0.684	0.246	0.087	0.030	0.010	0.005
105	-5	3.61	36.6	27.0	16.0	8.56	4.34	2.12	1.01	0.469	0.216	0.098	0.079
110	-10	1.79	23.7	22.9	17.7	12.4	8.21	5.24	3.25	1.98	1.19	0.708	0.989
115	-15	0.689	11.6	14.3	14.1	12.5	10.6	8.58	6.79	5.27	4.03	3.05	8.55
120	-20	0.149	3.09	4.67	5.66	6.22	6.45	6.44	6.27	5.99	5.64	5.25	44.2
123	-23	0.0219	0.506	0.853	1.15	1.41	1.63	1.82	1.97	2.10	2.20	2.29	84.1

Figure 3.6 shows the ASPEN Plus simulation to remove water from a 22 superficial wt% lactic acid solution and form an 85 superficial wt% solution.   The reactive distillation column is assumed to operate with equilibrium stages, so the bottoms product contains an equilibrium mixture of lactic acid oligomers at an overall concentration of 85 superficial wt%. The oligomer concentrations obtained from the ASPEN Plus simulation with the truncated model compare well with those from the non-truncated oligomer model and the experimental values.

Stream 1 – 22 wt% (superficial) Lactic Acid
Flow 100 kg/s

	Wt %
LA	22.0
Water	78.0

Stream 2
Flow 76.27 kg/s

	Wt %
LA	0.00
LA2	0.00
LA3	0.00
LA4	0.00
LA5	0.00
Water	100.00

Reflux ratio :   0.5
Boilup ratio : 19.2

Stream 3 – Concentrated Lactic Acid
Flow   23.73 kg/s

	Aspen true wt %	Full model true wt %
LA	58.15	57.90
LA2	21.86	21.85
LA3	6.59	6.62
LA4	1.80	1.82
LA5	0.46	0.47
Water	11.13	11.17
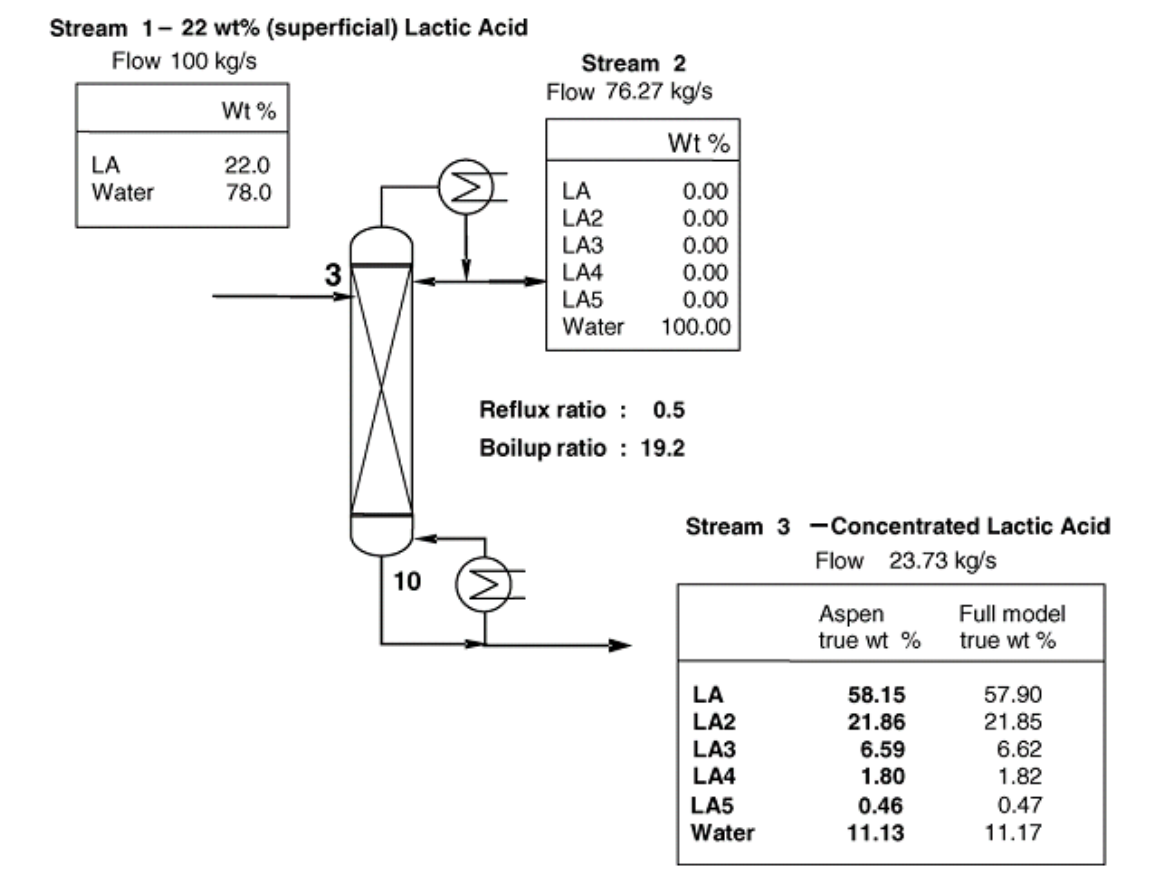
Fig. 3.6 Process flow diagram and results for the truncated ASPEN simulation compared to the complete oligomer model. The comparisons of composition are for a superficial composition of 92.72 wt% lactic acid

3.5. Conclusions

In this work, we provide new data to complement and extend literature data for oligomerization of lactic acid in aqueous solutions. We present a model based on chemical theory that consists of an infinite sequence of equilibrium homo-esterification reactions between successive oligomers of lactic acid. We show that a single value of the equilibrium constant (K=0.2023) applied to all oligomerization reactions accurately predicts titratable acidity and oligomer concentrations for solution concentrations ranging from very dilute to greater than 100 superficial wt% lactic acid. We demonstrate that

inclusion of oligomers only up to LA_5 is suitable for process modeling of lactic acid solutions less than 85 wt%.

3.6. List of Symbols

K_j chemical reaction equilibrium constant for j order oligomer
LA_1 monomeric lactic acid
LA_2 dimer lactic acid, lactoyllactic acid
LA_3 trimer lactic acid, lactoyl-lactoyllactic acid
LA_j polymeric lactic acid consisting on j units of lactic acid
n_j molar concentration of component j
r   defined by Equation 12
x_j mole fraction of component j
γ_j activity coefficient of component j

Superscripts
i   initial (used for superficial number of moles)
Subscripts
FA   formaldehyde
j   component
LA_j polymeric lactic acid consisting of j units of lactic acid
MG   methylene glycol
MG_n higher polyoxomethylene glycols
n   order of oligomer
W   water

SECTION FOUR

PHASE EQUILIBRIUM STUDIES OF BINARY MIXTURES OF ETHYL LACTATE-WATER, WATER-ETHANOL, ETHANOL-ETHYL LACTATE

4.1. Introduction

Despite their numerous attractive advantages, the production volume of lactate esters used has been small in industry. Traditional batch processing is expensive compared to the potential for continuous processing. New technologies have been developed to yield lactate esters from carbohydrate feedstocks via esterification using reactive distillation (as discussed later in Section 5.1) or pervaporation membranes.[9]

Esterification usually requires distillation to purify the esters. For column designs and process simulation, thermodynamic properties such as reliable vapor-liquid equilibrium (VLE) data of the related components are valuable. Recently, phase equilibrium of the methyl lactate system has been studied and VLE of some lactate esters with their associated alcohols at 101.33 KPa were made available.[52,53] However, no information for the ethyl lactate + water system has been found in the existing literature. This work presents the equilibrium P-x-y data of the ethyl lactate + ethanol and ethyl lactate + water systems. We have chosen to collect P-x-y data isothermally because the temperature can be kept low where the reactive system ethyl lactate + water is kinetically more stable.

4.2. Experimental Details

4.2.1. Chemicals. Ethyl (S) – (-) lactate 98% and ethyl alcohol (200 proof) were purchased from Sigma Aldrich. Water (HPLC grade) was obtained from J.T. Baker, Inc. Water and ethyl alcohol were used as received. Ethyl lactate was further purified by vacuum distillation. Only 85-90% of the pre-distilled volume was collected for the VLE experiments. Both the first overhead fraction (5-10%) and reboiler residue (5%) were discarded. No detectable water or ethanol remained in the ethyl lactate after distillation as determined using gas chromatography (GC). The GC procedure will be described in the analytical method section.

4.2.2. Apparatus. A P-x-y apparatus was constructed for VLE measurements of binary systems from ambient temperature to 353 K (Figure 4.1). The apparatus is based on the design of similar equipment described in the literature.[54] The apparatus has three main sections: an equilibration section, a feed section, and a sampling section.
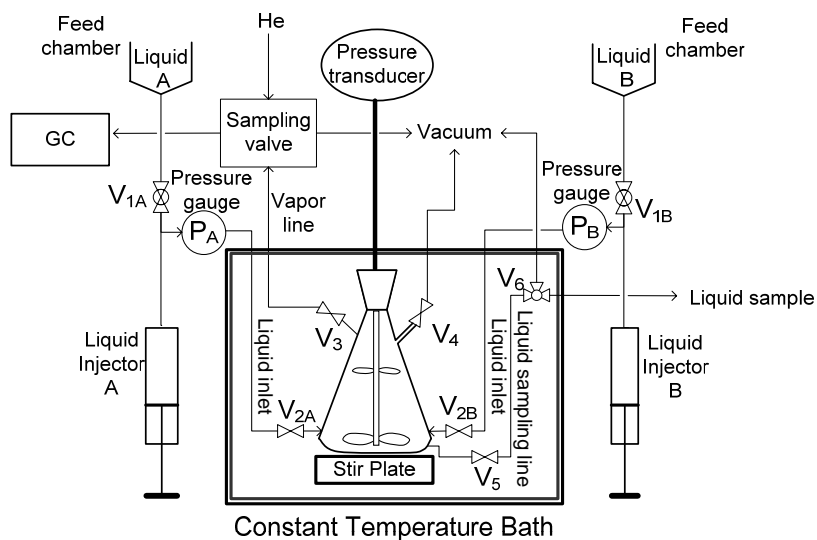
Figure 4.1 Schematic of the apparatus

4.2.2.1. Equilibrium Chamber and Isothermal Bath. A modified 125 ml Erlenmeyer flask was used as an equilibrium cell. The cell was placed on a submersible stir plate immersed in the isothermal water bath. Temperature was maintained by a PolyScience Series 730 circulator. To minimize water bath evaporation, approximately one inch of mineral oil was added to the bath to cover the water's surface when conducting experiments at 80 ^{o}C. The bath had fluctuations less than $\pm$ 0.01 ^{o}C at 40 ^{o}C and below, but the variation was $\pm$ 0.05 ^{o}C at 60 ^{o}C and 80 ^{o}C. Temperature was measured using a thermometer calibrated against a NIST traceable thermometer, the accuracy was better than $\pm$ 0.001 ^{o}C. Pressure inside the cell was measured using a MKS Baratron Model PDR 2000 dual capacitance diaphragm absolute pressure gauge. The pressure gauge provides reliable values between 1 and 999 torr with the resolution of 0.1 torr and an accuracy of 0.25% of the reported reading.

The cell was connected to the feed and gas sampling systems using 1/16" OD 316 stainless steel tubing sealed to the chamber using ACE glass Teflon adapters (CAT. 5801-07) and connectors (CAT. 5854-07, 5824-24). The Baratron gauge was attached to the top of the cell using a length of glass tubing with a tapered ground glass joint to provide a vacuum tight connection. The Baratron and glass were joined using a Cajon union (SS-4-UT-6).

The liquid and vapor phases were both stirred. Two different vapor phase stirrer configurations were used in the course of this work. In the first configuration, a vertical length of 1/8" stainless steel rod was used to support the vapor phase agitator. The rod was placed vertically in the center of the equilibrium cell; the bottom end was soldered to a small clip mounted onto a magnetic stir bar. At the middle of the vertical rod, two small arms were created by soldering a wire to the rod. Teflon$^{®}$ plumbing tape (1/2" x 1''x 0.04") was wrapped around the arms to create the agitator. The bar and Teflon$^{®}$ tape provided means of mixing for the liquid and vapor phases simultaneously. However, when the apparatus was modified by adding a liquid phase sampling section, the equilibrium chamber had to be placed 3/4" above the submersible stir plate. Consequently, the magnetic field was considerably reduced, the bottom of the flask was

no longer flat, and the vapor stirrer did not work reliably. Thin polypropylene strips (0.06" x 3" x 0.04") where wrapped around the center of the magnetic stir bar, and small supports were fabricated from Teflon sheet.

4.2.2.2. Feed Section. Two 125ml flasks and two liquid injectors were connected using ¼"OD polypropylene and 316 stainless steel tubing and Swagelok adapters. Polypropylene tubing provided flexibility for the connection between glass (feed chambers) and stainless steel valves (V_{1A}, V_{1B}), and permitted observation of the liquid level in the feed section. The length of polypropylene tubing was minimized to limit permeability of air from the environment. The flasks were mounted three feet above the injectors, providing a hydrostatic head to load the injectors with liquids from the flasks when valves V_{1A} and V_{1B} were opened (Figure 4.1). The liquid injectors were 30 ml calibrated pumps (High Pressure Equipment Company 62-6-10), used to meter liquids to the equilibrium cell with the accuracy of ± 0.003 ml of the injected volume. Pressure of the liquids inside the injectors was monitored using inexpensive pressure gauges.

4.2.2.3. Liquid Phase Sampling. Degassing of the liquids in the feed section (flasks and injectors) was tedious. However, we found that the liquids could be degassed reliably within the equilibration chamber. Complete degassing was easy to identify by a reliable stable pressure in the chamber after repeatedly pulling the pressure down several torr. Because of the expected minor shift in composition during degassing after liquids were charged to the equilibrium chamber, a liquid sampling section was added to the apparatus. This modification was done for the ethyl lactate + water system, reducing considerably the experimental time. High vacuum needle valves, purchased from Chemglass (CG 553-02, CG-534-02) were connected by a four inch length of ¼" OD glass tubing. To take a liquid sample, valve V_6 was first opened to permit evacuation of the sample region. Then valve V_6 was closed before valve V_5 was cracked opened for ten seconds to collect approximately 0.2 ml of liquid from the equilibrium cell. No fluctuation in pressure of the equilibration cell was noted when valve V_5 was opened. After sample collection, valve V_5 was closed entirely and valve V_6 was opened fully to permit a narrow Teflon® tube connected to a syringe to be inserted for withdrawal of most of the liquid sample.   To remove all residual traces of liquid, acetone was added through V_6 and then removed via the syringe apparatus. Any remaining acetone was evaporated under vacuum while the cell was undergoing the next equilibration.

4.2.2.4. Vapor Phase Sampling. The vapor sample system was based on a Valco six-port switching valve (00V-1375V) positioned immediately above the water bath, approximately 8" from the equilibrium cell A high temperature rotor (SSAC6WE, 225°C) and preload nut (PLAW30) were chosen as part of the valve assembly. The vapor line was 1/16" stainless steel with a 1/16" stainless steel valve. The vacuum line was a 6" length of 1/16" stainless steel connected to a 1/16" valve and adapted to vacuum tubing. He carrier gas entered through 1/16" stainless tubing connected to the outlet of the gas chromatography (GC) injector, and 1/16" stainless tubing was used to return the sample to the GC oven where it was fed onto to the column. The GC was placed as close as practical to the apparatus, using about 24" of tubing between the GC and sample valve. A 1.8 ml sample loop was created by adapting a coiled length of ¼" tubing to the Valco

ports. Each vapor sample was equivalent to about 0.3 µL of the related liquid mixture directly injected into the GC. To avoid condensation of the high boiling components, the vapor line was heat-traced and maintained 15-20 $^{\circ}$C above the temperature of the equilibrium cell. To collect a vapor phase sample, the sample loop was evacuated by placing the valve in the 'load' position with the vapor line valve V_3 closed and the vacuum valve V_{vc} opened; then the valve V_{vc} was closed, and the vapor line valve was opened. The loading was done within a minute, and then the valve V_3 was closed and the sampling valve was switched quickly to the 'inject' position. No pressure drop in the equilibrium cell was observed during the course of vapor sampling, since the volume of vapor sample was small compared to the volume of the chamber. Additional details on the vapor and liquid sampling configurations are available from the corresponding author.

4.3. Experimental Procedure and Analysis

4.3.1. Experimental Procedure. A Sargent-Welch two-stage vacuum pump (model 1400) was used to evacuate the apparatus and sample sections and to provide degassing of liquids. Prior to the experiment, the entire system was evacuated and checked for the leaks. A stable base pressure of 0.5-0.7 torr for 3-4 hours indicated that the chamber was leak tight. Liquids were degassed before they were loaded into the injectors. During the degassing process, fluids in the flasks were shaken and a tested using the click test for degassing as described by Van Ness and Campbell.[55,56]
When performing experiments where the liquid composition was determined from the quantities of liquids injected, the following tests supplemented the click test to verify complete degassing in the feed lines and injectors, and to verify a leak-tight feed section: 1) Pressure of fully loaded injectors with degassed liquids observed from gauges P_A and P_B had to be steady and equal to the vapor pressure of liquids. If the pump A (or B) was operated while V_{1A} (or V_{1B}) was opened and V_{2A} (or V_{2B}) was closed, the displacement of liquid level in the polypropylene feed line had to be proportional to the displacement inside the injector. 2) If the V_{1A} (or V_{1B}) and V_{2A} (or V_{2B}) were closed, the pressure of the injector A (or B) had to increase instantaneously when the pump started to compress the liquid inside that injector.
To inject liquid A (or B) to the equilibrium cell, pressure P_A (or P_B) was raised to approximately 0.3MPa before valve V_{2A} (or V_{2B}) was opened. After the pressure of the injector dropped, the valve was closed and the injector pressure was restored and the injected volume was recorded.
To carry out the experiment, 10-20 ml of component 1 of the studied binary system was charged to the equilibrium cell. After the vapor pressure of this pure liquid was measured, a predetermined quantity of the component 2 was added to the cell. After equilibration, vapor and liquid samples were collected. These steps were continued until the liquid mole fraction of component 1 approached 0.1. Afterward, the equilibrium chamber was emptied; the entire system was cleaned and degassed thoroughly. Then, the process was reversed, charging the equilibrium cell first with component 2 and then adding component 1.
The volume of the initial charge in the experiments with the ethyl lactate + ethanol system was selected to ensure that error in calculation of liquid compositions from the injected volume would be negligible. For the ethyl lactate + water system, 5 ml

of liquid inside the equilibrium chamber was found to be sufficiently large to ensure accurate composition measurements, because the volumes of liquid injections were not critical with the liquid sampling section in place. Both liquid and vapor of the studied binary mixture were well-mixed and were allowed to reach equilibrium before any measurement was performed. Equilibration was identified by the consistency of the equilibrium pressure reading from the Baratron following vapor withdrawals using vacuum, and by the reproducibility of the equilibrium vapor phase composition.

4.3.2. Analytical Methods. Liquid compositions in the ethanol + water and ethyl lactate + ethanol mixtures were calculated from the known volume of each component charged to the cell. For ethyl lactate + water, samples of the liquid phase were taken via the liquid sampling section and the compositions were determined from GC analysis. Vapor samples of the studied binary mixtures were injected to the gas chromatograph using the vapor sample valve.

The GOW-MAC 350 gas chromatograph was operated under isothermal conditions using a carrier stream of helium at 35ml/min. The column temperature was $220\,^{o}C$ in experiments involving ethyl lactate, but it was reduced to $150\,^{o}C$ for the ethanol + water system. A thermal-conductivity detector was set at $290\,^{o}C$ and 110 mA filament current. The column packing used was Poropak Q 50/80, packed in 6' long x 1/8" OD x 0.085" wall stainless steel tubing. To ensure that all vapor samples were analyzed in the column without loss via condensation, one foot of 1/16" OD 316 stainless steel tubing was added to the column and used as a pre-column heater within the GC oven.

Calibrations of known compositions of mixtures were done for each binary system to obtain the correlation between the ratio of GC peak areas and the mixture compositions.   From the calibration, the unknown compositions of the injected samples were determined. The amounts of each component in the calibrated mixtures were weighed using an electronic balance with its readability of 0.1mg. The standard mixtures were prepared gravimetrically in an approximate size of 1.0g ± 0.3mg; therefore the deviation in calculation of molar compositions was negligible. To reduce the error due to the possible evaporation of the more volatile component, two duplicate mixtures were prepared for each calibration point. Three GC injections were done for every data point, in both calibration and sample analyses. The difference in the ratio of peak areas of the triplicate GC injections was less than ± 0.05% of the calculated value.

4.4. Results and Discussion

Ethanol + water system: Isothermal VLE data for the ethanol + water system at $40.0\,^{o}C$ were collected and compared to literature data for validation of reliability of the constructed VLE apparatus (Table 4.1). The ethanol + water system was chosen to study because its components are in the system of interest, and $40.0\,^{o}C$ isothermal literature data are available from two independent sources. Both literature and experimental data were regressed using the Britt-Luecke algorithm, maximum-likelihood principle, provided by ASPEN PLUS 12.1. The area test of Redlich-Kister and point-to-point test of Van Ness and Fredenslund were used to check for data reliability.[57-59] The data are considered to pass the area test if the difference between the positive and negative areas is less than

10%. However, in order to pass the point-to-point test, the absolute mean deviation between the calculated and experimental vapor compositions should be ≤ 0.01.

Table 4.1 VLE data for ethanol (1) + water (2) at $40.0^{\circ}C$

$P^{40.0}$(torr)	$x_1^{40.0}$	$Y_1^{40.0}$	$P^{40.0}$(torr)	$x_1^{40.0}$	$y_1^{40.0}$
55.6	0	0	106.9	0.158	0.541
58.7	0.005	0.036	112	0.201	0.573
60.6	0.007	0.069	116.3	0.256	0.598
62.0	0.010	0.096	118.4	0.319	0.612
64.1	0.014	0.133	122.8	0.418	0.655
67.3	0.020	0.181	124.3	0.448	0.66
69.9	0.026	0.221	127.2	0.518	0.697
73.9	0.035	0.269	129.1	0.583	0.730
79.8	0.050	0.332	131.3	0.682	0.767
87.9	0.075	0.407	132.8	0.748	0.805
91.3	0.085	0.421	133.6	0.828	0.841
97.6	0.108	0.478	134.6	0.892	0.893
98.4	0.111	0.474	135.0	0.943	0.960
103.3	0.136	0.519	135.0	1.000	1.000

UNIQUAC with the Hayden and O'Connell (HOC) virial coefficient correlation were used to evaluate thermodynamic consistency. The point-to-point test value was 0.011, significantly smaller than that of 0.063 from Udovenko's[60] and 0.248 from Mertl's.[61] In the available literature, these are the only isothermal VLE data that can be found for the ethanol + water system at $40.0^{\circ}C$. Neither data from Udovenko's nor this work passed the area test, but the value of 10.40%, which is obtained from this work, is smaller than Udovenko's and close to the accepted value. The smoothness of the P-x-y curve in Figure 4.2 and results from the thermodynamic consistency tests show that the VLE data of ethanol + water from this work are very reliable and more consistent than existing literature data at $40^{\circ}C$.

Ethyl lactate + ethanol system: VLE were measured at $40.0^{\circ}C$, $60.1^{\circ}C$, and $80.2^{\circ}C$ for this system (Table 4.2). To minimize the the effects of any systematic errors in particular runs; the VLE experiments were performed at least five times using different increments and decrements of each component molar fraction at the reported temperature. All the activity coefficient models listed on Table 4.3 provide similar correlation of experimental data. The value of α used in the NRTL-HOC equation is 0.3. Figure 4.3 shows the representation of the UNIQUAC with the Hayden and O'Connell (HOC) correlation. The same non-linear regression method and consistency tests were used as described. For the Hayden-O'Connell method, the   values were assumed to be 1.3 for ethyl lactate + ethanol and 0.53 for ethyl lactate with itself. These values were based on the assumption that solvation of ethyl lactate would be similar to that of ethyl acetate in ethyl acetate + ethanol mixture and that ethyl lactate pure self-interactions would be

similar to ethyl acetate pure self-interactions. It should be noted that the calculated vapor fugacity coefficient of ethyl lactate is in the range of 0.990 to 0.998, and for ethanol is from 0.993 to 0.999 at the system pressure.
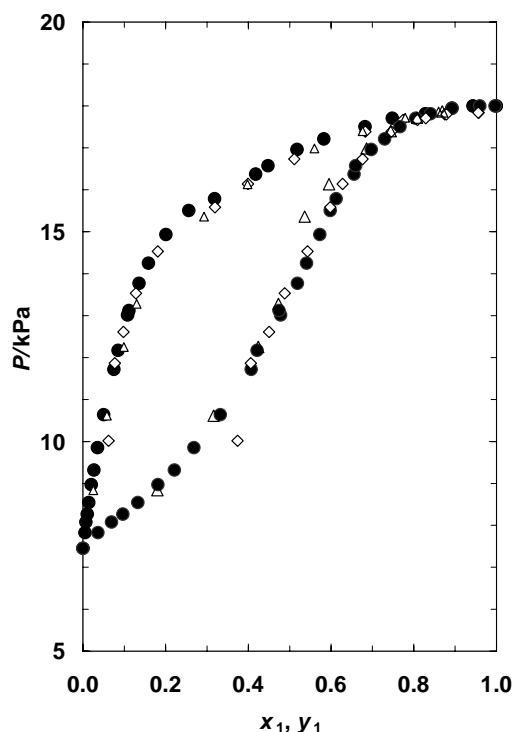
Figure 4.2 P-x-y of ethanol (1) + water (2) at 40.0°C: ●-this work, Δ-Udovenko[60], and ◊-Mertl[61]

      Data are combined from at least five different runs for each reported temperature as described. All P-x-y diagrams are smooth and do not exhibit any trends of systematic error within specific runs. All experimental data satisfied the point-to-point test but only data at 40.0°C passed the area test. The area test results were 31% and 19% for data at 60.1°C and 80.2°C respectively. The inconsistency could be due to the error in measuring the vapor phase at low concentration of ethyl lactate where the GC detection was limited. Another potential source of error could be minor decomposition of the ethyl lactate in the GC detector during vapor phase analysis. It was noted during runs that the outlet lines of the thermal conductivity detector gradually became restricted due to deposits over a period of several hours. The lines were kept clear using a syringe cleaning wire, but this method did not allow determination of the extent of decomposition. Plugging of lines was not noted on the GC used to analyze the liquid samples. Additional experimental runs were consistent with each other, as compiled in the Tables and Figures, and did not improve the results of the consistency tests.

      The prediction of isobaric VLE data of ethyl lactate + ethanol at 101.33 KPa using the binary parameters obtained from the reported data is in good agreement with Peña-Tejedor et al.[62] For the ethyl lactate + water at 40.0°C, with Peña-Tejedor's binary parameters, the activity coefficients at infinite dilution of ethanol and ethyl lactate are predicted to be 1.38 and 1.35 respectively using UNIQUAC-HOC model. From this

Table 4.2 VLE data for ethyl lactate (1) + ethanol (2) systems at 40.0°C, 60.1 °C, and 80.2°C.

$P^{40.0}$(torr)	$x_1^{40.0}$	$y_1^{40.0}$	$P^{60.1}$(torr)	$x_1^{60.1}$	$y_1^{60.1}$	$P^{80.2}$(torr)	$x_1^{80.2}$	$y_1^{80.2}$
8.4	1.000	1.000						
19.3	0.951	0.433	22.7	1.000	1.000			
26.9	0.893	0.271	44.8	0.946	0.482			
32.1	0.862	0.219	64.1	0.897	0.306			
40.9	0.814	0.160	85.6	0.836	0.205			
49.1	0.754	0.125	108.8	0.774	0.148	57.2	1.000	1.000
59.3	0.689	0.093	132.3	0.722	0.101	105.6	0.935	0.488
69.1	0.608	0.074	144.3	0.675	0.095	165.6	0.863	0.283
74.4	0.554	0.061	156.5	0.641	0.073	231.2	0.775	0.184
88.2	0.430	0.042	187.9	0.559	0.060	289.1	0.705	0.133
99.8	0.329	0.029	191.4	0.532	0.052	359.6	0.620	0.101
106.7	0.283	0.015	220.4	0.448	0.039	432.5	0.534	0.075
110.7	0.239	0.024	240.8	0.386	0.034	509.6	0.443	0.059
118.6	0.172	0.008	249.5	0.354	0.027	609.8	0.316	0.032
126.1	0.102	0.012	277.3	0.266	0.022	610.3	0.316	0.036
127.4	0.097	0.004	278.8	0.259	0.019	690.4	0.203	0.020
129.8	0.073	0.003	298.6	0.195	0.011	752.4	0.121	0.013
122.8	0.120	0.006	318.5	0.128	0.012	760.7	0.106	0.007
135.1	0.000	0.000	354.1	0.000	0.000	818.5	0.000	0.000

work, these values are 1.25 and 1.67 respectively. Similar results were obtained for the data at 60.1 °C and 80.2 °C.

The P-x bubble line is nearly linear, and the infinite dilution activity coefficients are not large. The ethyl lactate + ethanol system, thus, can be considered slightly non-ideal. This is due to the presence of the hydroxyl group in ethyl lactate, such that the interaction between ethyl lactate molecules is similar to their interaction with the ethanol molecule.

Ethyl lactate + water system: VLE at 40.0°C and 60.0°C were measured for the ethyl lactate + water binary system (Tables 4.4). Ethyl lactate was hydrolyzed significantly at 80 °C, as verified by the presence of ethanol in GC analyses. Hydrolysis was not detected in the experiments performed at 40.0°C and 60.0°C. The VLE experiments at each listed temperature were performed five times; the same methods as described for the ethyl lactate + ethanol system were used. Figure 4.4 shows that the system has a minimum boiling azeotrope, occurring at 5-7 mol% ethyl lactate. Due to the narrow phase envelope at high water concentrations, it was not possible to determine the exact azeotrope composition using gas chromatography, even though the analysis was very reproducible.

The data are fitted with several thermodynamic models, and the binary parameters determined are listed in Table 4.5. All of the selected activity models fit the data equally well; the deviations are given in table 4.5. The Hayden-O'Connell   value of 1.3 was used for ethyl lactate with water (based on the literature value for ethyl acetate + water) and same method as described above was applied for data regression. The azeotrope composition is predicted to be at 6.5-6.7 mol% ethyl lactate, based on the UNIQUAC-HOC fit.

Table 4.3 The binary parameters of ethyl lactate (1) + ethanol (2) system and average absolute percent deviation (%) for equilibrium pressure (P) and vapor phase mole fractions (y_1), (y_2). The vapor phase Hayden-O'Connell parameters are given in the text.

Equation	Binary Parameters		Average Absolute Percent Deviation		
	b_{12} (K)	B_{21}(K)	P (%)	y_1 (%)	y_2 (%)
UNIQUAC – IG $\tau_{ij} = \exp(b_{ij}/T)$	-43.00	-23.10	3.3%	23.2%	1.5%
UNIQUAC-HOC $\tau_{ij} = \exp(b_{ij}/T)$	-40.03	-29.40	3.1%	24.7%	1.4%
NRTL-HOC $G_{ij} = \exp(-0.3b_{ij}/T)$	-298.69	585.62	3.8%	24.8%	1.5%
VAN LAAR-HOC $A_{ij} = b_{ij}/T$	169.19	65.21	3.3%	24.7%	1.5%
WILSON-HOC $L_{ij} = \exp(b_{ij}/T),\ V_i/V_j = 1$	-198.48	71.55	3.7%	24.8%	1.5%
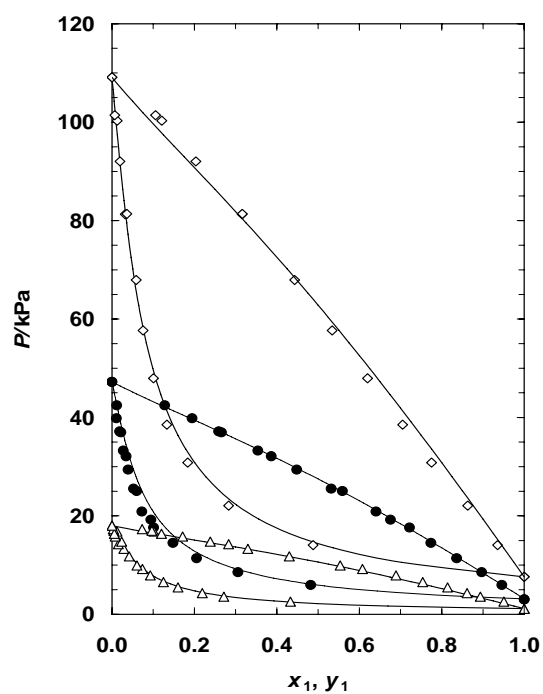
Figure 4.3 P-x-y of ethyl lactate (1) + ethanol (2) system. Δ 40.0°C; $\bullet$60.1°C; $\Diamond$ 80.2°C; solid lines are the representation of UNIQUAC with HOC correlation.
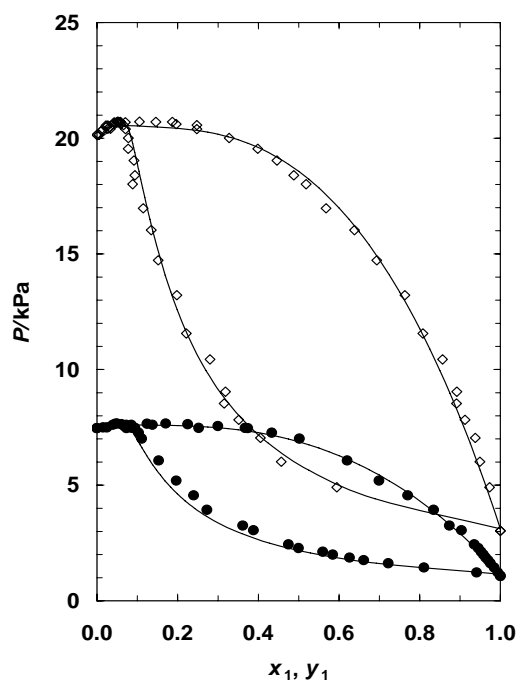
Figure 4.4 P-x-y of ethyl lactate (1) + water (2) system. $\bullet$ 40.0°C; $\Diamond$ 60.0°C; solid lines are the representation of UNIQUAC with HOC correlation.

Table 4.4 VLE data for ethyl lactate (1) + water (2) system at 40.0°C, and 60.0°C

$P^{40.0}$(torr)	$x_1^{40.0}$	$y_1^{40.0}$		$P^{60.0}$(torr)	$x_1^{60.0}$	$y_1^{60.0}$
				22.7	1.000	1.000
				36.8	0.973	0.594
				45.1	0.949	0.457
8.4	1.000	1.000		52.8	0.938	0.405
9.2	0.994	0.941		58.7	0.912	0.351
10.8	0.985	0.811		67.8	0.892	0.319
12.2	0.975	0.722		64.0	0.891	0.315
13.2	0.970	0.661		78.3	0.856	0.280
14.0	0.964	0.626		86.7	0.808	0.222
15.0	0.958	0.584		99.1	0.763	0.198
15.9	0.952	0.560		110.4	0.694	0.152
17.1	0.945	0.500		120.2	0.638	0.135
18.3	0.935	0.474		127.3	0.568	0.115
22.9	0.903	0.388		135.1	0.518	0.089
24.4	0.874	0.361		138.0	0.488	0.094
29.5	0.834	0.272		142.8	0.446	0.092
34.2	0.770	0.240		146.6	0.399	0.078
39.0	0.699	0.197		150.1	0.328	0.078
45.5	0.620	0.153		153.0	0.248	0.071
52.6	0.502	0.111		154.3	0.248	0.066
54.5	0.433	0.103		154.6	0.197	0.059
56.0	0.374	0.073		155.3	0.187	0.059
56.1	0.367	0.094		155.3	0.146	0.055
56.7	0.300	0.068		155.4	0.106	0.052
56.1	0.252	0.087		155.2	0.070	0.049
57.3	0.225	0.061		155.1	0.042	0.044
57.5	0.171	0.050		153.1	0.027	0.033
57.1	0.137	0.085		153.6	0.023	0.032
57.4	0.124	0.046		154.2	0.022	0.027
57.1	0.073	0.039		152.5	0.012	0.012
56.2	0.025	0.015		151.1	0.005	0.005
56.0	0.000	0.000		150.1	0.000	0.000

Table 4.5 The binary parameters of ethyl lactate (1) + water (2) system and average absolute percent deviation (%) for equilibrium pressure (P) and vapor phase mole fractions (y_1), (y_2). The vapor phase Hayden-O'Connell parameters are given in the text.

Equation	Binary Parameters		Average Absolute Percent Deviation		
	b_{12} (K)	b_{21}(K)	P (%)	y_1 (%)	y_2 (%)
UNIQUAC – IG $\tau_{ij} = \exp(b_{ij}/T)$	250.51	-133.02	2.4	22.0	4.1
UNIQUAC-HOC $\tau_{ij} = \exp(b_{ij}/T)$	248.19	-131.44	2.4	22.2	4.1
NRTL-HOC $G_{ij} = \exp(-0.3b_{ij}/T)$	-87.07	967.20	3.4	21.6	3.8
VAN LAAR-HOC $A_{ij} = b_{ij}/T$	895.05	307.06	3.4	21.4	4.2
WILSON-HOC $\mathsf{L}_{ij} = \exp(b_{ij}/T),\ V_i/V_j = 1$	-978.35	-51.56	2.1	22.9	5.0

The data satisfy the area test, but are less satisfactory when analyzed via the point-to-point test. The values of 8.6% and 0.04 for area and point-to-point tests, respectively, were obtained for the VLE data at 40.0°C. Likewise, the values for data at 60.0°C were 4.6% and 0.037. Because the point-to-point test is more significant for isothermal VLE than the area test, the data were carefully re-evaluated, including the regression used to generate the GC calibration curve. It was found that the difference in calculation of phase compositions using different representations of the GC calibration curve is negligible. However, the consistency tests are very sensitive to a small change in vapor phase composition. For example, if data point at P= 9.2 torr in Table 4.4 is omitted, the value of the point-to-point test changes from 0.04 to 0.026. We have also evaluated point-to-point consistency using Legendre polynomials[59] and the Modified Margules[63] to represent the excess Gibbs energy, but the differences between the calculated and measured values in vapor composition are also larger than the target of 0.01. Consistency failure due to inadequacy of the HOC method is unlikely, because the vapor fugacity coefficients are near 0.989 and 0.993 across the composition range for ethyl lactate and water, respectively. Additional experimental runs were consistent with each other as shown in the Tables and Figures and did not improve the consistency test results.

Fitting of the ethyl lactate + water system is challenging because the infinite dilution activity coefficients are large. These coefficients are 17.7 for ethyl lactate and 2.8 for water from UNIQUAC-HOC in ASPEN 12.1. The UNIQUAC-HOC fails to represent the vapor phase accurately at 40.0°C, and fails to represent the pressure maximum accurately at 60.0°C, as shown in Figure 4.4.

The vapor phase analysis in this system may be subject to the same potential decomposition of ethyl lactate as mentioned earlier. Degradation was more noticeable in this system than in the ethyl lactate + ethanol system.

4.5. Summary and Conclusions

This work presents a simple design of an isothermal VLE apparatus that is capable of measuring the vapor pressure of single components down to about 5 torr and the VLE of non-ideal binary systems. The P-x-y apparatus is valuable for collecting data at low temperature, where reactive chemicals are kinetically more stable. With the liquid sampling section and the ability to perform the degassing in situ, the apparatus can be extended to multicomponent systems. Data have been evaluated with standard consistency tests and all data sets passed or nearly passed at least one of the standard tests.

<center>SECTION FIVE</center>

<center>A CONTINUOUS PROCESS FOR ETHYL LACTATE FORMATION</center>

5.1. Background

Reactive distillation has found increasing application over the past several decades for conducting equilibrium-limited reactions. Prominent examples include production of methyl acetate by Tennessee Eastman[3] and production of methyl-tertbutyl ether as a gasoline additive. Excellent reviews detailing the growth of reactive distillation have been prepared by Mahajani et. al[64], Sharma et. al[65] and Hiwale et. al[66]. In our laboratory, we have recently demonstrated the use of reactive distillation to recover propylene glycol and ethylene glycol from aqueous solution via formation of their acetals[17]. Here, we illustrate the use of reactive distillation for efficient production of ethyl lactate.

Ethyl lactate holds promise as an effective, non-toxic replacement for petroleum-based solvents that have long dominated U.S. and world markets. But U.S. ethyl lactate production is low (10-15 million kg/yr) and the selling price of $2.90 - $3.70 /kg reflects processing challenges and high feed costs. The recent advent of large-scale lactic acid production, primarily for production of polylactic acid polymers (PLA), ensures an ample, low-cost supply of the monomer lactic acid (L_1) and thus opens opportunities for expanded production, provided that low manufacturing costs can be achieved.

Prior work on lactate ester formation has been conducted primarily with dilute lactic acid solutions and a large excess of alcohol, mainly to purify fermentation-derived lactic acid for polylactic acid (PLA) formation.[67,68] Because lactic acid must be neutralized as it is formed, the raw fermentation product is typically sodium, calcium, or ammonium lactate. Direct ethyl lactate formation is possible from ammonium lactate via reaction with ethanol,[69,70] but ammonia inhibits lactic acid production and leads to undesired lactamide as a byproduct. Thus, addition of lime (CaO) during fermentation, direct acidulation with H_2SO_4 to precipitate $CaSO_4$, and esterification with excess ethanol is still a preferred route to pure L_1 monomer.[71]

Because of its bifunctional nature, lactic acid undergoes intermolecular esterification in aqueous solutions above ~30 wt% to form linear dimer (L_2) and higher oligomer acids (L_3, L_4, etc.). The extent of homoesterification increases with increasing acid concentration, thus complicating the use of lactic acid as a reactive substrate. When mixed with an alcohol, lactic acid and its oligomers undergo esterification (Figure 5.1). The resultant esters simultaneously undergo hydrolysis and transesterification (alcoholysis), leading to a mixture of acid and ester monomer and oligomers whose distribution depends on water and ethanol content. Ethyl lactate (L_1E), typically the desired product, can be recovered from the mixture, but its yield is reduced from the theoretical maximum by the presence of the oligomeric compounds. The oligomer esters (L_2E, L_3E, etc. in Figure 5.1) have been reported to have use as plasticizers,[72-75] but no commercial market yet exists. Thus, the challenge in achieving high L_1E yields from lactic acid is to either 1) further convert the oligomeric byproducts to the monomer L_1E, or 2) avoid the formation of oligomers altogether by working with dilute lactic acid

solutions. The second option is less desirable, as water limits the extent of esterification and thus large alcohol excess and high energy costs are required.

Lactic acid (L₁)

Ethyl lactate (L₁E)

Lactic acid oligomers (L$_{n+1}$)

Lactic acid oligomer esters (L$_{n+1}$E)
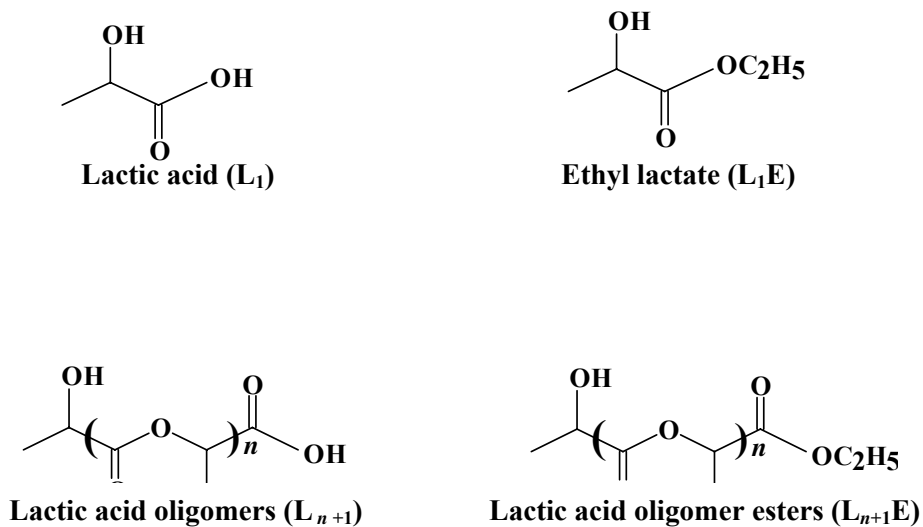
n = 1; Lactoyllactic acid (L₂) and its ethyl ester (L₂E)
n = 2; Lactoyllactoyllactic acid (L₃) and its ethyl ester (L₃E)
n = 3; Lactoyllactoyllactoyllactic acid (L₄) and its ethyl ester (L₄E)

Et = Ethanol; W = Water
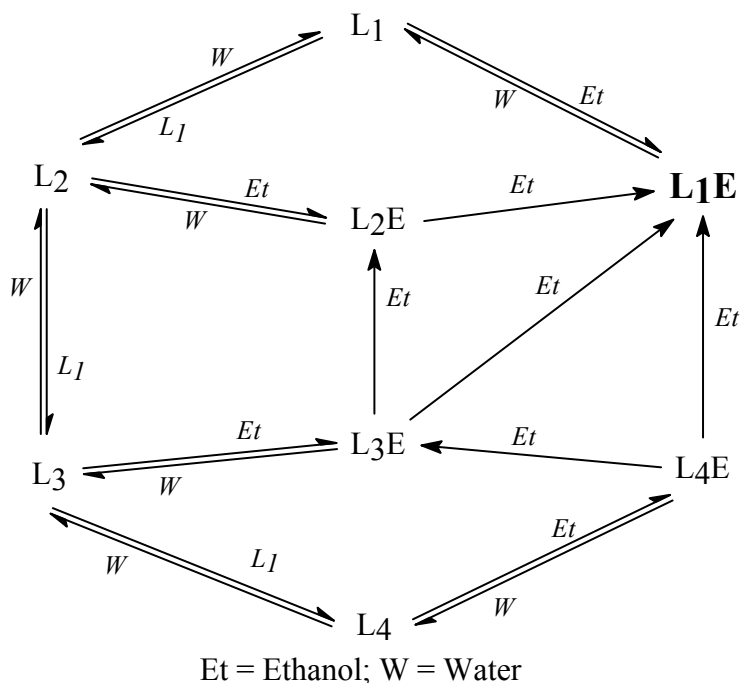
Figure 5.1 Species and reaction pathways for ethyl lactate formation

Concentrated or dehydrated lactic acid has been reacted with alcohol to achieve high L₁E yields and achieve complete esterification,[76-77] but these processes require

multiple unit operations for separation and recovery of the lactate ester. Recently, Tretjak et. al.[78] disclosed a continuous process wherein lactic acid and ethanol are partially converted in a stirred reactor. Reactor effluent is fed to a distillation column, where ethanol, ethyl lactate and water are removed as distillate and unreacted lactic acid and oligomers in the bottoms are recycled to the reactor. High purity ethyl lactate is recovered by distillation in a second column. A simpler, commercially-practiced route to ethyl lactate is direct reaction of ethanol with dilactide, the cyclic dimer of lactic acid and an intermediate in PLA formation. Unfortunately, the high cost of dilactide limits the potential for this pathway.

Datta et. al[79] reported the first membrane-based approach for L_1E production using electrodialysis to recover lactic acid from ammonium lactate salt. The acid was then reacted with alcohol, and water and ammonia produced were removed via pervaporation across a polyvinyl-based hydrophilic membrane. Jafar et al.[10] and Tanaka et al.[24] successfully extended the application of zeolite membranes for lactic acid esterification. Budd et al.[80] employed alternating layers of cationic and anionic polyelectrolytes on a Zeolite A membrane to prevent degradation and to achieve higher fluxes of water.

Although prior approaches to forming ethyl lactate can achieve high yields, either they require multiple unit operations, use high-cost feedstocks, or are prone to process difficulties (e.g. membrane fouling). We present here a reactive separation method for producing ethyl lactate that includes secondary conversion of lactate oligomer esters to L_1E, thus giving near-theoretical yields in a simple, efficient process. We note one prior attempt to produce L_1E using reactive distillation was reported in the early 1920's, but that process involved the use of aromatics to break the ethanol-water azeotrope[81] and thus had a different goal than the present work.

The method presented departs from typical organic acid ester formation via reactive distillation, where the ester has either the highest volatility of the species present (e.g., methyl acetate)[3] or the lowest volatility (n-hexyl acetate)[82], in which case water is usually the most volatile component. In those cases, recovery of 100% pure ester is straightforward via optimization of column operating conditions. For ethyl lactate production, reactive distillation column operation does not fit into either of these categories – products L_1E (b.p. 155°C) and water have volatilities that are lower than ethanol (b.p. 78°C) but higher than lactic acid (b.p. 122°C at 15 mm Hg) and its oligomers. A schematic of the proposed column is given in Figure 5.2; column operation is targeted at complete lactic acid conversion, removal of L_1E along with ester oligomers in a bottoms stream, and recovery of ethanol and water as distillate. We believe it is especially important to avoid the presence of water in the column bottoms stream, as separating product ester from water by distillation leads to undesirable ester hydrolysis.[83,84] With L_1E and oligomer esters as the only bottoms products, pure L_1E recovery is readily achievable by simple distillation. Oligomer esters can be refined for sale or further converted to give near-theoretical L_1E yield for the process.
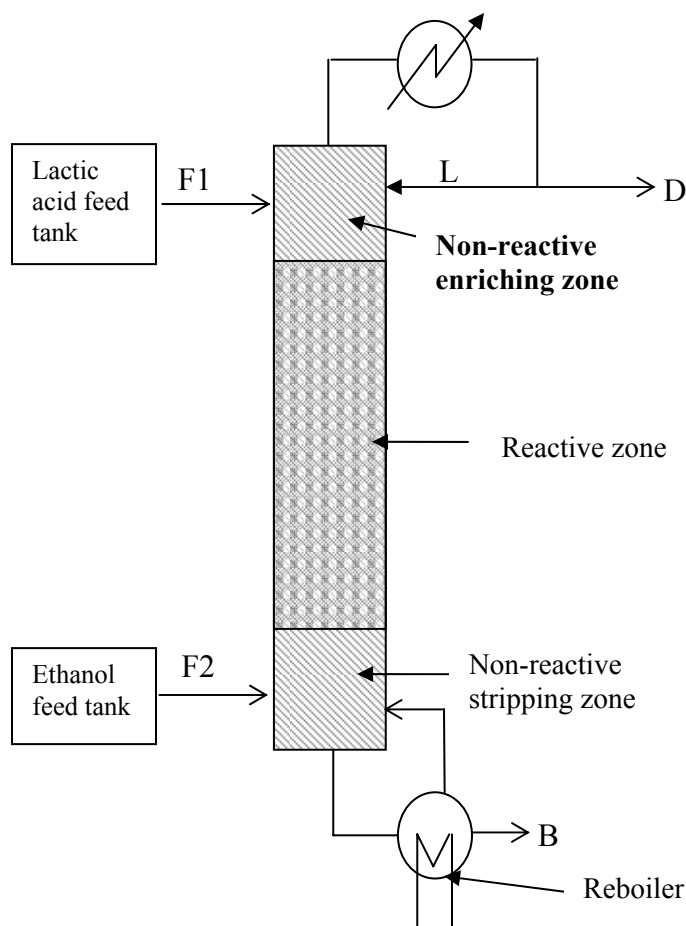
Figure 5.2 Set-up for Reactive Distillation Experiments

5.2. Experimental Methods

5.2.1. Reagents. Three aqueous lactic acid solutions were used in experiments: 88 wt% (J.T. Baker, Inc.), 50 wt% (Purac, Inc.), and 20 wt% (Aldrich). The compositions of these lactic acid feed solutions, including the distribution of acid oligomers as determined by the analytical methods outlined below, are given in Table 2.1. Absolute ethanol (99% purity) and HPLC grade water were procured from J.T. Baker. Ethyl lactate (98% purity) was purchased from Acros Organics. Purities of all chemicals were verified by gas or liquid chromatography.   Water, L_1E, and ethanol used as calibration standards were purified by distillation before use; all other reagents were used as received. Dimer ethyl ester (L_2E) was produced in a reactive distillation experiment and was isolated by vacuum distillation.

5.2.2. Analysis. Analytical methods have been described in detail under sections 2.3 & 3.2.3.

5.2.3. Continuous reactive separation column. Continuous reactive separation experiments were performed in bench-scale and pilot-scale columns[17] according to column set-up shown in Figure 5.2. The columns consist of 50 mm ID Pyrex tubes of height 3.0 m for bench-scale column and 5.5 m for pilot-scale column. Each column is outfitted with an electronic reflux splitter to control reflux ratio, a total condenser with chiller capable of achieving a condenser temperature of -20°C, and a reboiler with an overflow outlet to maintain a constant level and allow product withdrawal. The reboiler solution volume is ~0.5 liter for the bench-scale column and ~1.0 liter for the pilot-scale column. Each column has two feed pumps to dispense feed solutions to the column at a controlled rate. The columns have several ports along their length that allow internal temperature measurement, introduction of feed, and sample withdrawal. The columns are wrapped with electric heating tapes that are controlled by surface thermocouples and Omega controllers to temperature just below the internal column temperature to minimize the heat loss. Heat loss is further minimized by insulating each column with bands of glass wool.

Each column is divided into three sections: a non-reactive stripping section (0.4 m in bench-scale, 1.0 m in pilot-scale), a reactive section, and a non-reactive enriching section (0.4 m in bench-scale, 0.8 m in pilot-scale). The reactive section, 1.7 m in height for the bench-scale column and 2.6 m in height for the pilot-scale column, is packed with Katapak-S structured packing[84] elements (Sulzer Chemtech Ltd.) filled with 0.25 mm Amberlyst-15 cationic exchange resin as the esterification catalyst. The Amberlyst 15, a robust, strongly acidic cationic exchange resin known to catalyze esterification reactions, has an acid site density of 4.6 meq/g dry resin. Structured packings such as the Katapak-S are widely used in industry because they facilitate high catalyst loadings (~75 g resin per meter of column height in our 5 cm diameter column) and excellent interphase mass transfer. The packing has a height of an equivalent theoretical plate (HETP) of 0.6 m. Empty Katamax structured packing (Koch-Glitsch, Ltd.) is used to fill non-reactive column sections.

5.2.4. Procedures for Column Operation. Following a series of initial experiments, the columns were configured such that aqueous lactic acid solution (F1 in Fig. 5.2) was fed near the top of rectification zone, while ethanol (F2 in Figure 5.2) was fed either 0.09 m above the reboiler or one meter above the reboiler, exactly at the bottom of the reactive zone. The molar feed ratio of ethanol to lactic acid ranged from 1.4:1 to 10.3:1. In certain cases, both lactic acid and ethanol feeds were preheated, with ethanol fed either as a liquid near its bubble point or in partially vaporized form. The reflux ratio (L/D) ranged from 0.0 to 2.3. The reboiler duty was held constant for all experiments in both bench- and pilot-scale columns, so that comparisons in column performance could be made on a constant energy consumption basis.

The column was started by turning on the external heating tapes and reboiler heater, and setting the feed pumps to specified feed rates. Steady state was generally achieved after about 6 hr of operation. Several samples were collected from distillate and bottoms streams to ensure time invariant stream compositions, column temperatures were recorded, and steady state feed, bottoms, and distillate flow rates were measured by timed filling of graduated cylinders. The feeds, bottoms, and distillate compositions and flow

rates were then entered into a spreadsheet to determine product yields and species and overall material balance closure for the experiment.

5.2.5. Hydrolysis and transesterification of oligomer acids and esters. To demonstrate the further conversion of unreacted $L_1 - L_4$ acids and $L_2E - L_4E$ esters formed in esterification to the desired L_1E product, bottoms product from several pilot-scale reactive separation experiments was collected and vacuum distilled to remove water, ethanol, and most of the L_1E. The residue, containing $L_1 - L_4$ acids and $L_1E - L_4E$ esters, was then subjected to hydrolysis and transesterification to determine the extent to which additional L_1E could be formed.

Reactions were performed in either a closed batch mode with reflux or in a semi-batch reactive distillation mode in which vapor produced during reaction was withdrawn from the reaction flask. A schematic of the reaction set-up is provided in Figure 5.3. Amberlyst 15 cation exchange resin was used as the catalyst in these batch reactions at a loading of 2.5-3 g resin per 100 ml solution. Typically, reactants were mixed and brought to the desired reaction temperature and then catalyst was added. Samples were then collected periodically to follow the concentrations of reactive species over the course of reaction.
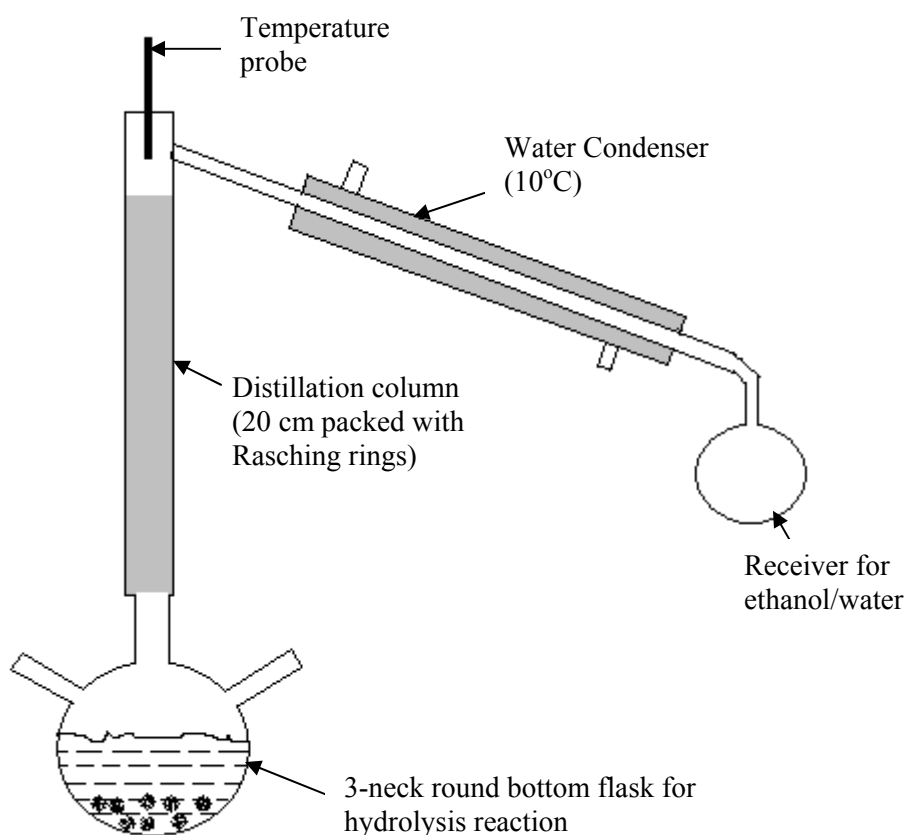
Figure 5.3 Batch reactor for hydrolysis and transesterification

5.3. Results and Discussion

Lactic acid conversion is based on total L_1 equivalent fed. Yield of L_1E is defined as mol L_1E formed per mol of total L_1 equivalent fed – thus, 100% yield signifies that all $L_1 - L_4$ acids are converted to L_1E.

5.3.1. Esterification in bench-scale column. Preliminary experiments were performed in the bench-scale reactive distillation column to verify feasibility of the ethyl lactate formation and identify operating conditions for achieving high lactic acid conversion, eliminating water from the bottoms stream, and obtaining high purity L_1E. No HPLC analyses were conducted for these experiments, only GC to determine ethyl lactate, water, and ethanol concentrations and titration to determine acid concentrations. Parameters varied in these initial experiments were ethanol:lactic acid feed ratio, ethanol feed temperature, and reflux ratio. The best results were obtained when vaporized ethanol (at 85°C) and lactic acid solution (88 wt%) at 25°C were fed in a 3:1 molar ratio to the column operating at a reflux ratio of zero (e.g. as a reactive stripping column). A lactic acid conversion of 85% with an L_1E yield of 66% was achieved, with water and ethanol concentrations in the bottoms stream at 2 and 4 mol%, respectively (on an oligomer-free basis).

In addition to experiments directed at L_1E formation, we operated the bench-scale reactive distillation column at similar conditions to produce methyl lactate from methanol and 88 wt% lactic acid in a yield of 87%. We also demonstrated transesterification of methyl lactate to L_1E in a yield of 94% using a 3:1 ethanol: methyl lactate feed ratio.

5.3.2. Esterification in pilot-scale column.
5.3.2.1. 88 wt% lactic acid feed. The results of esterifying lactic acid as an 88 wt% solution in water in the pilot-scale column are described in Tables 5.1a and 5.1b. For these experiments, lactic acid was fed ~0.14 m below the condenser and ethanol was fed either 0.09 m or 1.0 m above the reboiler. In all runs in Table 5.1, the reboiler duty was held constant. In pilot-scale runs, species material balances closed to within ±7% in all cases, with many runs having smaller errors.

For many of the pilot-scale runs, the objective of eliminating water from the bottoms stream of the distillation column was achieved. Removal of water from the reboiler was aided by its formation of a minimum-boiling azeotrope with ethanol, by the presence of excess ethanol, and by the high boiling point of L_1E which keeps reboiler temperature high. Further optimization via reduction of ethanol feed rate or preheating the ethanol feed stream (Runs E3 and E5) led to elimination of both water and ethanol from the bottoms stream. In both of these runs, L_1E was the predominant species in the bottoms stream. Although other runs give higher conversion of lactic acid (95% in E4) and higher L_1E yield (73% in E6), conditions in E3 and E5 that eliminate water and ethanol from the bottoms stream are the most attractive from a processing viewpoint (as discussed below).

Runs E1, E2, and E3 illustrate the effect of decreasing ethanol:lactic acid molar feed ratio from 3.56:1 to 1.4:1. Reducing ethanol feed rate lowered lactic acid conversion slightly, but significantly decreased ethanol content in the bottoms stream. The decline in ethanol concentration in the bottoms is a manifestation of maintaining a constant reboiler

Table 5.1a. Esterification of 88 wt% lactic acid in pilot-scale Reactive distillation column

Run	EtOH feed rate (mol/min)	Molar feed ratio EtOH: LA	EtOH feed temperature (^{o}C)	Reflux ratio (L/D)	Lactic acid conversion (%)	L_1E yield (%)
E1	0.34	3.6:1	25	0	94	69
E2	0.24	2.5:1	25	0	93	70
E3	0.14	1.4:1	25	0	90	58
E4	0.34	3.6:1	78 (sat. liq)	0	95	65
E5	0.34	3.6:1	85 (vap)	0	95	59
E6	0.34	3.6:1	25	0.2	91	73
E7	0.34	3.6:1	25	0.5	85	69
E8	0.34	3.6:1	25	1	80	64
E9	0.34	3.6:1	25	0	94	68
E10[a]	0.34	3.6:1	25	0	83	66
E11[a]	0.34	3.6:1	85 (vap)	0	85	45
E12[b]	0.34	3.6:1	25	0	96	68

Conditions: Lactic acid feed compostion = 88 wt% (aqueous); Lactic acid monomer equivalent feed rate = 0.097 mol/min; Water feed rate = 0.06 mol/min; Lactic acid feed temp. = 25°C. Runs E1-E8, ethanol feed position = 0.09 meter above reboiler; Runs E9-E12, ethanol feed position 1 meter above reboiler. [a]Runs E10,E11 carried out with azeotropic water:ethanol mixture (water feed rate = 0.108 mol/min). [b]Run E12, 3 wt% Amberlyst 15 cationic exchange resin catalyst added to reboiler.

Table 5.1b Product stream properties from esterification of 88 wt% lactic acid in pilot-scale reactive distillation column

Run	Bottom composition (mol%)										Distillate composition (mol%)			Reboiler temp. (°C)	Bottom flow rate Mol/min	Distillate flow rate Mol/min
	H_2O	EtOH	L_1	L_2	L_3	L_4	L_1E	L_2E	L_3E	L_4E	H_2O	EtOH	L_1E			
E1	0.0	46	1.4	1.2	0.4	0.1	45	4.6	0.6	0.2	45	54	0.8	99	0.15	0.34
E2	0.0	16	2.8	1.8	0.6	0.2	71	7.1	0.8	0.2	50	49	0.8	126	0.10	0.30
E3	0.0	1.4	6.5	2.4	0.9	0.2	77	9.5	1.6	0.4	65	34	0.9	159	0.070	0.21
E4	0.0	15	1.6	1.8	0.7	0.1	71	8.2	1.1	0.2	37	62	0.9	128	0.089	0.40
E5	0.0	1.9	2.4	2.1	0.9	0.2	79	11	1.6	0.4	34	65	1.2	159	0.072	0.45
E6	0.2	57	1.5	1.4	0.4	0.1	36	2.9	0.3	0.1	49	50	0.5	95	0.20	0.28
E7	0.8	64	3.2	1.3	0.3	0.1	28	1.8	0.2	0.0	53	47	0.4	91	0.24	0.21
E8	2.4	67	4.3	1.2	0.2	0.0	23	1.2	0.2	0.0	51	48	0.3	88	0.27	0.17
E9	0.1	49	1.2	1.2	0.4	0.1	43	4.3	0.5	0.1	41	58	0.8	98	0.15	0.32
E10	15.4	53	3.8	0.8	0.2	0.0	24	1.8	0.2	0.0	57	42	0.6	90	0.26	0.31
E11	1.6	1.2	12	2.9	1.2	0.4	65	12	2.2	0.5	45	54	0.8	162	0.068	0.53
E12	3.2	42	1.1	0.6	0.3	0.1	46	5.2	0.6	0.1	43	56	1.3	97	0.14	0.36

duty in operating the column (ethanol can be eliminated from the bottoms stream at any ethanol feed flow rate by increasing reboiler duty) – nevertheless, any conditions that eliminate water and ethanol from the bottoms stream are desirable because L_1E can easily be recovered from the bottoms stream in a single column and the oligomer acids and esters can be further converted or recycled. Also, the oligomer ester (L_2E, L_3E, L_4E) yield increased about 10% as ethanol feed rate was lowered, as there was less alcohol present in the column for transesterification (alcoholysis) of the oligomer esters to L_1E.

Runs E1, E4, and E5 show the effect of preheating the ethanol feed stream on column performance with excess ethanol. Overall, the effect of preheating ethanol feed is similar to that of reducing ethanol feed rate. Preheating ethanol to near its bubble point (E4) and then partially vaporizing it (E5) had surprisingly little effect on lactic acid conversion. The ethanol content of the column bottoms stream was strongly affected, with very little ethanol present with vaporized ethanol feed. This is because preheating feed ethanol is equivalent to providing additional reboiler duty. The L_2E - L_4E yield increased by about 20% when vaporized ethanol was fed, again a consequence of less ethanol in the column reboiler for transesterification of the oligomer esters to L_1E. The concentration of L_1E in the distillate was found to increase from 0.8 mol% to 1.1 mol% in distillate; the higher reboiler temperature was responsible for producing more L_1E vapor at the bottom of the column.

Experiments E1 to E4 were run with no reflux to the column, thus essentially making it a reactive stripping column. The presence of a small quantity of L_1E in the distillate stream of these runs, along with the bench-scale result that showed reduced L_1E in the distillate with reflux, prompted us to further explore column operation with modest reflux ratios in order to reduce L_1E in the distillate without adversely affecting acid conversion and L_1E yield. Runs E1 and E6 - E8 delineate the effect of reflux ratio on overall column performance. As the reflux ratio increased, a decrease in overall lactic acid conversion from 94% to 79% was observed. In addition, substantial water and ethanol appeared in the bottoms stream, with a corresponding decrease in reboiler temperature from 99°C in E9 to 88°C in E8. L_1E yield at first increased and then only dropped slightly as reflux ratio was increased from zero to one. Unfortunately, increasing reflux ratio did not eliminate L_1E from the distillate (it declined from 0.8 mol% in E1 to 0.3 mol% in E8). The L_1E in the distillate arises because of two prominent reasons: (1) the rectifying section in the pilot-scale column is too short to facilitate separation, and (2) L_1E forms a minimum-boiling azeotrope with water (Described in Section 3). Adding reflux therefore does not lead to any positive outcome for L_1E production, and we conclude that the continuous column is best operated without reflux as a reactive stripper.

Runs E1-E8 were run with ethanol fed 0.09 m above the bottom of the stripping section. In an effort to reduce ethanol content in the bottoms stream, the ethanol feed location in Run E9 was moved to 1.0 m above the reboiler. The results obtained are virtually identical to those of Run E1, indicating that the ethanol feed location is unimportant at the conditions used. It is possible that further optimization involving a change in reboiler duty would lead to a dependence of column performance on ethanol feed location, but with the excess ethanol used there is little fractionation taking place at the bottom of the column.

The use of an azeotropic ethanol-water mixture as the feed for L_1E formation was examined in Runs E10 and E11. There would certainly be economic advantages of using such an azeotropic mixture in an ethyl lactate process, as the mixture could be isolated and directly recycled from the distillate stream. In E10, the ethanol-water mixture was fed at 25°C and in E11 the feed mixture was partially vaporized. The use of the azeotropic feed at room temperature resulted in a decrease in lactic acid conversion from 94% to 83% and an increase in water concentration in the reboiler from essentially zero to 15 mol%. The concentrations of water and ethanol in the bottoms were both reduced substantially by vaporizing the azeotropic feed mixture, but lower acid conversion and lower L_1E yields were observed relative to the corresponding experiment with absolute ethanol (E5). Based on these results, a commercial-scale column for L_1E production using an azeotropic ethanol-water feed stream could be designed and operated that would avoid the presence of water and ethanol in the bottoms stream. The ultimate decision regarding ethanol feed composition for L_1E production would thus depend on process economics.

In an effort to increase lactic acid conversion and L_1E yields, approximately 30 g of Amberlyst 15 cation exchange resin were added to the reboiler flask in Run E12. The net result of this addition was an increase in lactic acid conversion from 94 to 96%, but L_1E yield was not affected. The additional reaction taking place in the reboiler resulted in an increase in water content of the bottoms stream. It is seen in comparing E9 with E12 that $L_2 - L_4$ concentrations are lower upon addition of the resin, indicating that they were hydrolyzed to some extent. The concept of adding catalyst to the reboiler does not appear to have a positive effect on column performance.

5.3.2.2. 50 wt% Lactic acid feed. The low water content of 88 wt% lactic acid solution makes it relatively straightforward to achieve high acid conversion and L_1E yield without a large excess of ethanol. However, the presence of oligomeric species in the concentrated lactic acid feed reduces per-pass ethyl lactate yield and complicates column operation. We therefore explored the use of commercially available 50 wt% lactic acid feed, which contains only a small amount of L_2 (3 wt%) along with 46 wt% L_1, in order to increase overall yield of L_1E. For these runs, the total mass feed rates of lactic acid solution and ethanol were kept the same as in E1-E12 with 88 wt% lactic acid, resulting in lower lactic acid throughput and higher ethanol:lactic acid feed ratios. Lactic acid was fed near the top of the rectification section (0.14 m below the condenser) and ethanol was fed 1 m above the reboiler. All runs were conducted without reflux to the column.

Results of esterification of 50 wt% lactic acid with ethanol under various operating conditions are tabulated in Table 5.2a and 5.2b. The effects of both ethanol:lactic acid feed ratio and feed temperatures on column performance have been examined. For both feeds at room temperature (E13), a lactic acid conversion of 79 % was achieved with an L_1E yield of 78%. The bottoms product contains very little ester oligomers; thus all lactic acid converted goes to L_1E. Unfortunately, with room temperature feeds there are large quantities of water and ethanol in the bottoms streams – an undesirable outcome. This is a direct result of the additional water content of the 50 wt% lactic acid feed.

The effect of raising lactic acid feed temperature to 100°C was examined in Run E14. A slight increase in lactic acid conversion and corresponding increase in L_1E yield

Table 5.2a Esterification of 50 wt% lactic acid in pilot-scale
Reactive distillation column

Run	EtOH feed rate (mol/min)	Molar feed ratio EtOH:LA	Lactic acid feed temp. (^{o}C)	EtOH feed temperature (^{o}C)	Lactic acid conversion (%)	L$_1$E yield (%)
E13	0.35	7.1:1	25	25	79	79
E14	0.35	7.1:1	100	25	82	86
E15	0.5	10.3:1	100	25	83	86
E16	0.5	10.3:1	100	85 (vap)	94	80
E17	0.35	7.1:1	100	85 (vap)	91	66
E18	0.26	5.4: 1	25	85 (vap)	87	72
E19	0.36	7.4:1	25	85 (vap)	88	70
E20	0.52	10.5:1	25	85 (vap)	93	82
E21	0.26	5.4:1	25	78 (sat. liq)	83	78

Conditions: Lactic acid feed compostion = 50 wt % (aqueous); Lactic acid monomer equivalent feed rate = 0.049 mol/min; Water feed rate = 0.25 mol/min; Ethanol feed position = 1 meter above reboiler; Reflux ratio = 0

Table 5.2b Product stream properties from esterification of 50 wt% lactic acid in pilot-scale reactive distillation column

Run	Bottom composition (mol%)										Distillate composition (mol%)			Reboiler temp. (^{o}C)	Bottom flow rate (mol/min)	Distillate flow rate (mol/min)
	H_2O	$EtOH$	L_1	L_2	L_3	L_4	L_1E	L_2E	L_3E	L_4E	H_2O	$EtOH$	L_1E			
E13	9.5	73	3	0.4	0.0	0.0	14	0.2	0.0	0.0	68	32	0.3	83	0.28	0.36
E14	3.8	76	2.7	0.4	0.0	0.0	17	0.4	0.0	0.0	69	31	0.5	83	0.25	0.39
E15	3.3	81	2	0.3	0.0	0.0	13	0.2	0.0	0.0	68	32	0.5	82	0.33	0.37
E16	0.0	38	2.4	1.1	0.2	0.0	57	2	0.1	0.0	48	52	0.2	120	0.069	0.68
E17	0.0	0.0	8.4	2.1	0.3	0.0	84	5.1	0.4	0.0	50	50	0	159	0.038	0.56
E18	0.1	0.1	11	1.8	0.4	0.0	78	7.5	1.2	0.2	55	45	0.2	163	0.045	0.47
E19	0.1	7.9	9.8	1.6	0.2	0.0	75	4.7	0.4	0.0	49	51	0.2	139	0.046	0.57
E20	0.0	51	2.6	0.7	0.0	0.0	45	1.1	0.0	0.0	44	56	0.2	95	0.089	0.63
E21	0.2	35	9.2	1.1	0.1	0.0	52	2.2	0.2	0.0	61	39	0.2	105	0.073	0.44

was observed, and water content in the bottoms stream declined substantially. In E15, ethanol molar feed ratio was increased from 7.10 to 10.30; very little change was observed other than an increase in alcohol content in the bottoms stream. Feeding ethanol as a vapor (E16, E17) led to a marked increase in lactic acid conversion with a corresponding elimination of water from the bottoms stream and, for E17, elimination of ethanol from the bottoms stream as well. A lower L_1E yield was observed with E17, but an increase in $L_2E - L_4E$ was seen. This is expected, as removal of water from the liquid phase as it travels down the column will concentrate unreacted lactic acid and lead to oligomer formation. The results of E17 are important, as they illustrate the potential for more dilute lactic acid streams to be converted to L_1E while avoiding undesired water and ethanol in the bottoms stream. The results of E17 are similar to those in E3 and E5 with 88 wt% lactic acid feed.

  The effect of ethanol molar feed ratio on column performance was studied in experiments E18 - E20, where lactic acid solution was fed at 25^oC and vapor ethanol was fed at 85^oC. Increasing ethanol feed rate increased lactic acid conversion and increased L_1E yield, but unfortunately also forced ethanol into the bottoms stream. Again, increasing reboiler duty may alleviate this problem, but varying reboiler duty was not a part of this study. Increasing ethanol rate also decreased the formation of $L_2E - L_4E$ and $L_2 - L_4$, the former via transesterification to form L_1E and the latter by enhanced conversion of lactic acid.

  Finally, Run E21 illustrates the outcome of feeding ethanol as a liquid near its bubble point. Lower lactic acid conversion and lower L_1E yield were obtained relative to E15 (vapor ethanol feed), and significantly higher ethanol content in the bottoms stream was observed.

  5.3.3. Discussion. Results of lactic acid esterification in the bench and pilot-scale columns show that L_1E can be produced in high yield in a single-pass operation. This is in contrast to prior methods such at Tretjak et al.,[78] where multiple operations are required. Given the equilibrium constant of ~2.4 for monomer lactic acid esterification to L_1E[24], the conversion of lactic acid and the ethyl lactate yield achieved significantly exceed the conversion that would be obtained by simple mixing of the feed streams. We did not expect to achieve complete conversion of lactic acid to L_1E in the relatively short column, but the conversions that were achieved, in the mid 90% range, are a promising sign that complete conversion can be achieved in a larger column with water and ethanol appearing only in the column distillate stream.

  Column operation without reflux is possible in part because the vapor pressures of lactic acid and all oligomeric products in the range of ethanol and water boiling points are negligible. Thus, the rectifying section only functions to separate L_1E from ethanol and water; the incomplete separation achieved in this study indicates that either the pilot-scale rectifying section is too short to separate out L_1E or an azeotrope is formed that precludes L_1E separation.

  The composition of the product streams, particularly the distribution of ethanol between distillate and bottoms streams, is heavily dependent on three factors: ethanol feed rate, ethanol feed temperature, and reboiler duty. In this study, the reboiler duty (energy/time) was kept constant by choice and because the reboiler heater has a limited capacity of about 750 W. Total energy input to the column was varied by preheating

ethanol and lactic acid feed streams; in essence, this preheating is equivalent to adding reboiler duty as it provides more vapor flow in the column. The results show that the reboiler duty is sufficiently high to give excellent column performance for low ethanol:lactic acid feed ratios and for vaporized ethanol feed streams.

Reaction conditions giving good column performance for feeds containing either 50 wt% lactic acid or 88 wt% lactic acid have been identified. The 88 wt% feed gives a greater throughput of lactic acid and requires as little as 40% excess ethanol to achieve high conversion. The drawback of the concentrated feed is the existence of oligomer acids and esters – these will require additional unit operations for conversion or separation from L_1E. High conversions are achievable with the 50 wt% lactic acid feed, but higher ethanol:lactic acid feed ratios are required. Unfortunately, under operating conditions where ethanol and water are excluded from the bottoms stream, oligomer acids and esters form with 50 wt% acid in quantities similar to those for the 88 wt% acid. Thus, the advantage of using 50 wt% acid as a feed is lost, and 88 wt% acid is preferred because it has a lower alcohol requirement and contains less water to be evaporated in the column.

Formation of L_1E in a reactive separation column is thus both feasible and straightforward, complicated only by the presence of the lactate oligomers and their esters. In order to further increase the yield of L_1E, these oligomeric compounds can be either hydrolyzed to L_1 and recycled or further transesterified with ethanol to form additional L_1E. In the following section, we describe experiments that demonstrate the viability of these two routes for ultimately converting the oligomeric compounds to additional L_1E.

5.3.4. Conversion of lactate oligomer acids and esters to ethyl lactate. The column bottoms stream from Run E9 was vacuum distilled to remove water, ethanol, and most of the ethyl lactate, leaving an oligomeric residue consisting of $L_1 - L_4$ acids and $L_1E - L_4E$ esters. The composition of this residue is L_1 (10.0 wt%), L_2 (6.2 wt%), L_3+L_4 (0.7 wt%), L_1E (8.7 wt%), L_2E (67.0 wt%), L_3E (6.5 wt%), and L_4E (1.6 wt%). This oligomeric residue was used as the starting material in the reactions described below to further convert oligomers to desired L_1E.

5.3.4.1. Hydrolysis via batch reactive distillation. Hydrolysis of the oligomer residue was conducted at 80°C (ethanol-water azeotrope temperature) in the stirred glass batch reactor equipped with a condenser and sampling port (Figure 5.3). A 37 g sample of oligomeric residue along with 37 g of water was added to the reactor, giving a water to L_2E molar ratio of 16. To these reactants, 2.3 g (dry basis) of Amberlyst 15 cation exchange resin was added as a catalyst. The reactor was heated to reflux temperature and ethanol, the volatile product of hydrolysis, was removed as the ethanol-water azeotrope and collected as a distillate product over the course of reaction. Samples of the liquid phase were collected to follow the concentrations of reactants and products during reaction.

After seven hours of reaction, all L_2E, L_3E, and L_4E were consumed along with L_3 and L_4. The concentrations of L_1 and L_2 in the final solution were determined by direct titration with NaOH and by HPLC analysis to be 52 wt% L_1 and 6 wt% L_2. Water was determined by gas chromatograph to be 41 wt%. There was no L_1E in the reaction

solution. The L_1 and L_2 concentrations are consistent with equilibrium concentrations of L_1 and L_2 in water as reported in the literature for this concentration range of lactic acid.[27] Thus, complete hydrolysis of the oligomer acids and esters to a mixture of L_1 and L_2 is possible.

5.3.4.2. Hydrolysis in closed batch reactor. A second experiment was conducted with a 28.5 g sample of the oligomeric residue described above along with 54 g of water and 2.0 g of Amberlyst 15 resin (dry basis), giving a water:L_2E molar ratio of 28. Reaction products were not withdrawn from the reactor (except for analysis) during the six hours of heating at the reflux temperature of 78°C. The concentrations of key species over time are given in Figure 5.4. Substantial hydrolysis takes place as indicated by the decline in L_2E concentration over the course of reaction and the increase in lactic acid concentration. Some L_1E is formed during reaction as part of the product mixture. Even after six hours, the hydrolysis reaction mixture was not at equilibrium, indicating that multiple reaction pathways are in effect and kinetics are relatively slow.
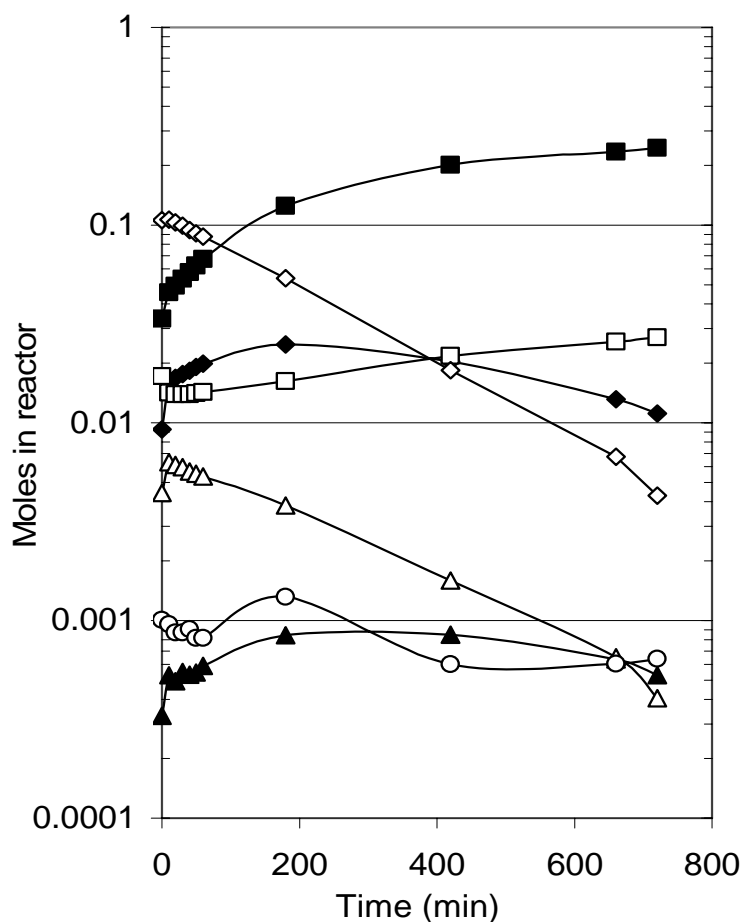
Figure 5.4 Hydrolysis of byproduct acid and ester oligomer mixture. ■ – L_1; ♦ - L_2; ▲ - L_3; □ – L_1E; ◊ - L_2E; △ - L_3E; ○ – L_4E. Initial mixture composition: L_1 = 0.03 mol; L_2 = 0.01 mol; L_3 = 0.0005 mol; L_4 = 0.00005 mol; L_1E = 0.02 mol; L_2E = 0.1 mol; L_3E = 0.01 mol; L_4E = 0.001 mol; Water = 0.3 mol; Temperature = 80°C; Catalyst = Amberlyst 15; Catalyst loading = 2 g (2.5 wt% of total mass of reactant)

5.3.4.3. Transesterification in closed batch reactor. As an alternative to hydrolysis to recover acid, we conducted transesterification of the oligomer mixture with ethanol to directly produce L_1E. Transesterification was performed at $80^{\circ}C$ in the stirred batch reactor by adding 38 g of the oligomeric residue and 27.6 g of ethanol along with 1.7 g (dry basis) Amberlyst 15 cation exchange resin, giving a molar ratio of ethanol to L_2E of 2.6. Samples were collected during reaction to follow the concentrations of reactants and products.

The concentrations of species in the batch reactor over the course of 24 hr experiment are given in Figure 5.5.
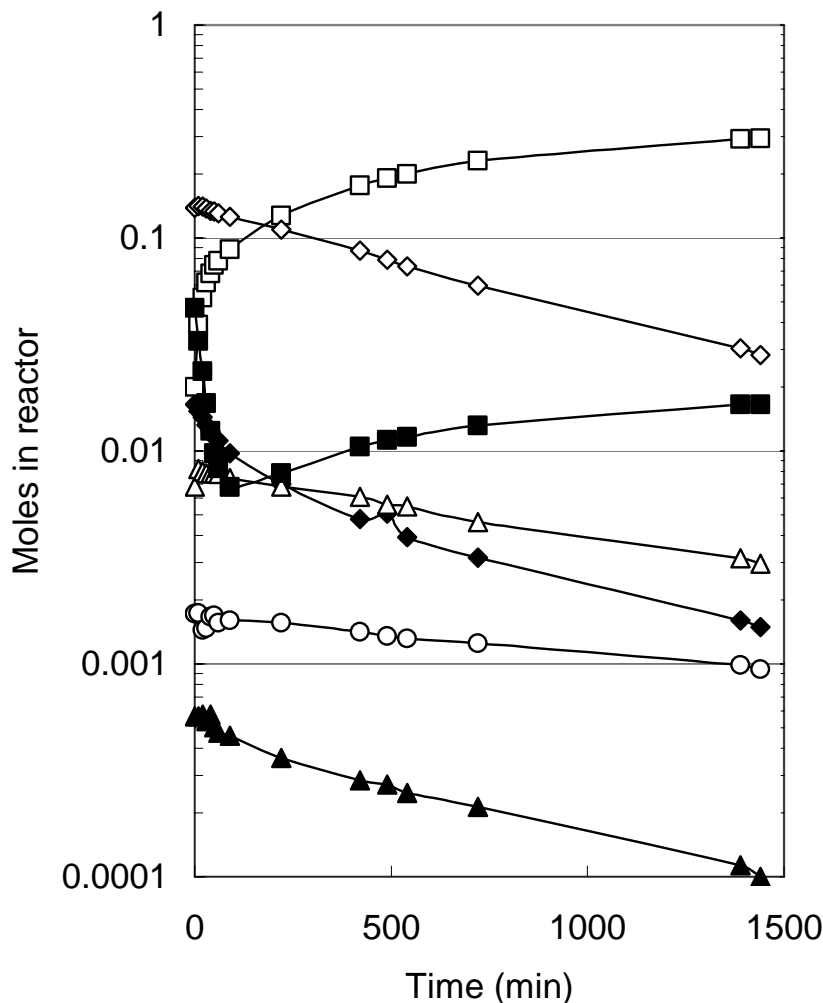
Figure 5.5 Transesterification of byproduct acid and ester oligomer mixture. ■ – L_1; ♦ - L_2; ▲- L_3; □ – L_1E; ◊ - L_2E; △ - L_3E; ○ – L_4E. Initial mixture composition: $L_1 = 0.04$ mol; $L_2 = 0.01$ mol; $L_3 = 0.006$ mol; $L_4 = 0.0003$ mol; $L_1E = 0.02$ mol; $L_2E = 0.134$ mol; $L_3E = 0.009$ mol; $L_4E = 0.002$ mol; Ethanol = 0.6 mol; Temperature = $78^{0}C$; Catalyst = Amberlyst 15; Catalyst loading = 1.7 g (2.5 wt% of total mass of reactants)

The predominant product of reaction is L_1E; concentrations of all other species decline or remain constant over the course of reaction. The acid oligomers undergo transesterification to form L_1E and $L_1 - L_3$; L_1 also undergoes esterification to L_1E with

liberation of water. $L_2E - L_4E$ transesterify directly to L_1E. Based on the concentrations of all monomer and oligomeric species in the residual starting mixture, the overall conversion of lactate to L_1E in this experiment is 76%. It is interesting to note that the transesterification reactions are thermodynamically more favorable than the hydrolysis reactions presented above, but kinetically they are significantly slower. Even after 24 hr of reaction, it is clear that concentrations of $L_2E - L_4E$ continue to decline and L_1E concentration increases – thus the reaction is not close to equilibrium. Based on this result in a single stage batch reactor, it is apparent that a continuous, multistage reactive separation column for transesterification would lead directly to secondary conversion of the residual oligomer stream to desired L_1E.

5.4. Process for Ethyl Lactate Formation
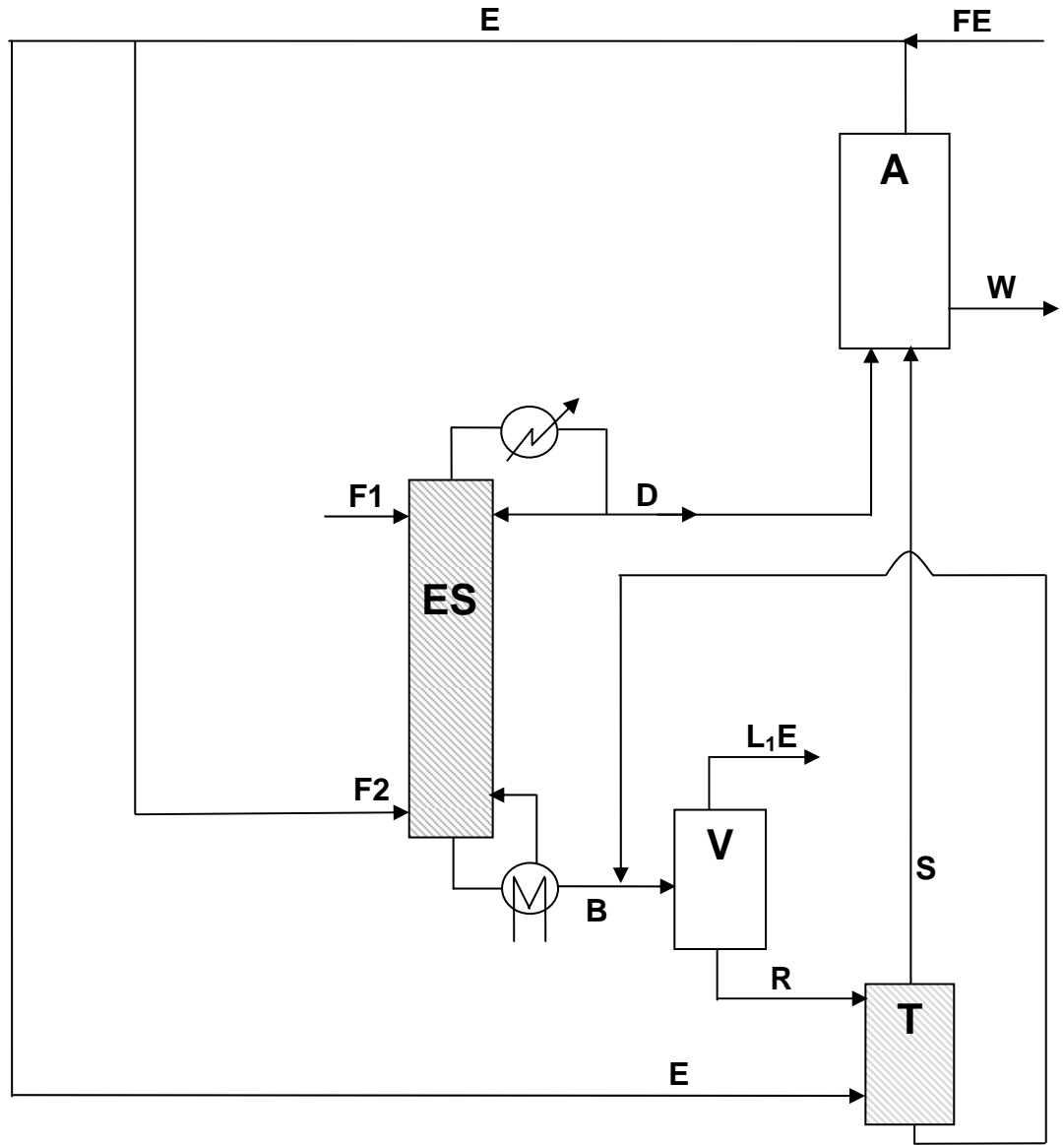
Figure 5.6 Process concept for ethyl lactate production. **F1**: Lactic acid feed; **F2**: Ethanol feed to column; **FE**: Ethanol process feed; **ES:** Primary esterification column**; B:** Bottom stream from **ES; V:** Vacuum distillation column for L_1E recovery**; L_1E:** Ethyl lactate product**; R:** Oligomer residue from **V; T:** Transesterification column; **S & D:** Mixture of ethanol and water; **A***:* Absolute ethanol recovery unit; **E***:* Ethanol stream; **W**: Water

A process concept for producing L_1E continuously is given in Figure 5.6. The process contains three major columns: the primary reactive separation column for L_1E and oligomers production, a vacuum distillation column to separate product L_1E from the oligomers, and a second reactive separation column in which transesterification of the

oligomeric mixture is carried out. A fourth separation unit (A in Fig. 5.6) is required for recycling ethanol; this unit may be dedicated to the proposed esterification process or it may be part of a fuel ethanol production facility with which the esterification process is associated. Ethanol recycle is very simple if azeotropic ethanol is used for esterification, and somewhat more complex if absolute ethanol is required.

5.5. Conclusions

Ethyl lactate (L_1E) can be synthesized from aqueous lactic acid solution using a continuous reactive separation column. Although L_1E yield in reactive distillation column per pass is comparable to that obtained at equilibrium in simple batch reaction but complete lactic acid conversion is possible to L_1E and a mixture of oligomer acids and esters. Concentrated (88 wt%) lactic acid is the preferred feedstock for the reaction because it contains relatively little water; efficient conversion is achieved with as little as 40% excess ethanol fed to the column along with the acid. We have also shown by experimental method of verification that (i) diluted lactic solution of lactic acid (50 wt% lactic acid solution in water (containing only 4 wt% of oligomeric acid products) can also be used efficiently, although more alcohol and preheating of feed streams are required and (ii) azeotropic composition of ethanol-water can be used in place of absolute alcohol as feed. This process is much simpler and straightforward than the process reported by Tretjak et.al[78]. By our process 99.9% pure ethyl lactate is obtained by simple vaccum distillation of bottom product stream because it is the most volatile component present in bottom product stream. The oligomeric byproduct mixture of esterification can be either hydrolyzed to monomer acid or transesterified to form L_1E in near-theoretical yields. The process thus has potential advantages over current methods for L_1E production from biorenewable feedstocks.

SECTION SIX
REACTION KINETICS OF ESTERIFICATION OF CITRIC ACID

6.1. Background

Citric acid (2-hydroxy-1,2,3-propanetricarboxylic acid) is produced commercially via fungal fermentation of glucose. Citric acid can be esterified with alcohols such as ethanol and n-butanol through a series of reactions to yield tri-ethyl citrate (TEC) and tri-n-butyl citrate (Figure 6.1). Tri-ethyl citrate and tri-butyl citrate are used as non-toxic plasticizers in toys, medical products (e.g. as enteric coatings for controlled release drug delivery systems), printing ink coatings, cosmetics, and other applications. These plasticizers are also suitable as food additives such as whipping agents for dried egg whites, food flavorings, or food packaging materials. Citrate esters rapidly metabolize in the body via liver and blood serum enzymes to liberate the citrate ion, which is disposed of through the usual biochemical pathways. The global plasticizers market has been estimated at around 11 billion pounds per year; according to 2003 statistical data, the U.S. share of this market is 2.4 billion pounds[1].
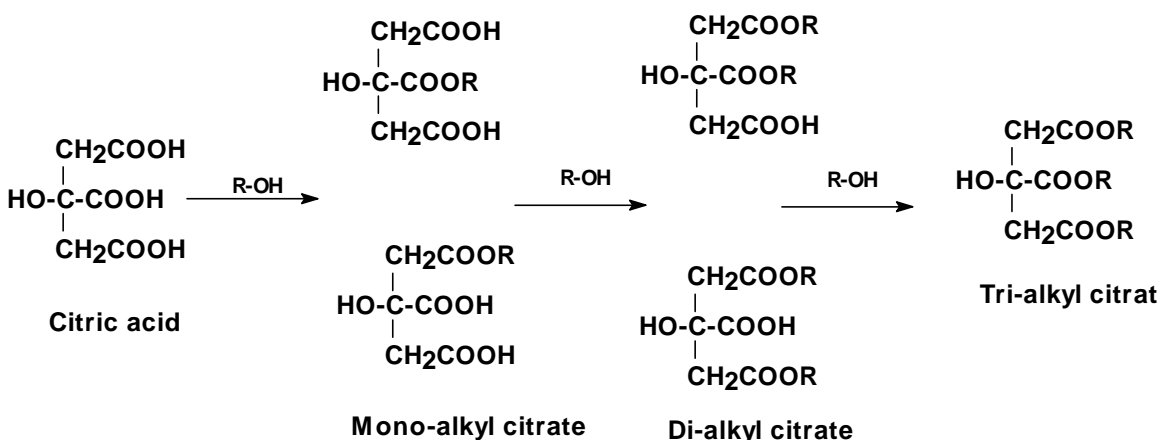
Figure 6.1 Esterification of citric acid

In a conventional process to synthesize TEC, citric acid and ethanol are combined in a batch or continuous stirred reactor using a homogeneous catalyst such as sulfuric acid. Use of heterogeneous solid catalysts can eliminate many of the disadvantages involved with use of homogeneous catalysts; heterogeneous catalysts allow easy separation of the catalyst from reaction media by decantation or filtration, reduce or eliminate corrosion problems, and facilitate continuous process operation.

Prior studies on the esterification of citric acid with ethanol or n-butanol are found mainly in the Chinese and German patent literature. Schröter et al.[85] describe a process for synthesis of TEC via a three stage batch process using methanesulfonic acid as catalyst. Tao[86] discusses the synthesis of TEC in the presence of p-toluenesulfonic acid as catalyst and continuous removal of the formed water. Frappier et al.[87] discuss a process for synthesis of TEC from fermentation broths containing citric acid. Some recent attempts to synthesize tri-butyl citrate have been described by Nong[88] using an aluminum phosphotungstate supported catalyst, Shi et al.[89] using a solid super acid

catalyst, Zheng et al.[90] using tetra-butyl titanate, Deng et al.[91] using sodium hydrogen sulfate, Song et al.[92] using a aluminophosphate solid acid catalyst, Liu et al.[93] using a dealuminated USY Zeolite, Meng et al.[94] using a nanosolid super acid SO_4^{2-}/Fe_2O_3, Zhao et al.[95] using a WO_3-TiO_2-SO_4^{2-} super acid catalyst, Meng et al.[96] using p-toluenesulfonic acid catalyst, and Fu et al.[97] using SO_4^{2-} modified zirconium crosslinked clay catalyst.

The esterification of citric acid is an equilibrium-limited reaction. In order to overcome the equilibrium limitation, it is necessary either to carry out esterification in multiple stages or use a process such as reactive distillation, in which chemical reaction and distillation occur in a single vessel. Design of reactive distillation processes often uses equilibrium-based models in which both phase and chemical equilibrium are achieved on each stage. Such equilibrium models suffice when reaction kinetics are very fast, but for slow chemical reactions such as citric acid esterification the kinetics must be taken into account in order to achieve a reasonable design.[2,98]

Because no information is available in the open literature describing kinetics of citric acid esterification over ion exchange resin catalysts, we have undertaken a study of citric acid esterification kinetics in order to develop a rate model that will be useful in designing reactive distillation processes for tri-alkyl citrate formation. Both resin-catalyzed and citric acid-catalyzed ("self-catalyzed") reactions are included, and ethanol dehydration to form di-ethyl ether (DEE) is included as part of the reaction system. Experimental vapor-liquid equilibrium studies were performed on the citric acid-ethanol and citric acid-water binary pairs in order to obtain the UNIQUAC activity coefficients. A pseudo-homogeneous activity based kinetic model is presented for correlation of the experimental data.

6.2. Experimental

6.2.1. Materials. Anhydrous citric acid crystals were obtained from Aldrich Chemical Company. Absolute ethanol (99% purity) and HPLC grade water were obtained from J. T. Baker, Inc. The strong acid cation exchange resin catalyst Amberlyst-15 (Rohm and Haas, Philadelphia, PA) was obtained in H^+ form and was used without modification. Purity of all chemicals was checked by gas chromatography or HPLC.

For the VLE experiments, water (HPLC grade) was obtained from J.T. Baker, Inc. Ethanol (200 proof) and TEC (99% purity) were purchased from Sigma-Aldrich. Chemicals were used as received.

6.2.2. Analysis. The presence of citric acid, mono-ethyl citrate (MEC), di-ethyl citrate (DEC) and TEC was first confirmed by GC-MS analysis of their trimethylsilyl (TMS) derivatives. For reaction samples, citric acid and its ethyl esters (MEC, DEC and TEC) were quantitatively analyzed on a Hewlett-Packard 1090 HPLC using a reversed phase C18 column (Novapak, 3.9 mm x 150 mm) held at 40°C. Water/acetonitrile (ACN) mixtures, buffered at pH=1.3, were used as mobile phase (1.0 ml/min) in a gradient mode (0% ACN (t=0) to 60% ACN (t=20 min) to 90% ACN (t=25 min) to 0% ACN (t=28 min)), and species were quantified by UV detection (Hitachi L400H) at a wavelength of 210 nm. Citric acid and TEC were identified and quantified by comparing HPLC retention time and peak area with their respective calibration standards. Standards

for MEC and DEC could not be obtained commercially. On a mass basis, the response factors for citric acid and TEC were found to be same; therefore MEC and DEC were each assigned the same response factor as TEC and citric acid. Using this response factor, the carbon balance for each reaction sample, based on citric acid and its esters, was in the range of ±10%.

Reaction samples were analyzed for water content using a Varian 3700 gas chromatograph equipped with thermal conductivity detector (TCD) and a Stainless Steel column (4 m x 3.25 mm) packed with a liquid stationary phase of Porapak Q. The column oven was subject to a temperature program involving heating from 413 K (after a 2-min hold) to 493 K (and held for 6 min) at a rate of 20 K min^{-1}. n-Butanol was used as an internal standard. High purity helium (99.999 % pure) was used as carrier gas at a flow rate of 20 ml/min. The injector and detectors were maintained at 493 K.

Samples were analyzed for ethanol and DEE using a Perkin-Elmer Sigma-2000 gas chromatograph equipped with flame ionization detector (FID) and a bonded-phase fused-silica capillary column (SPB-5, 30 m x 0.53 mm). The column oven was subject to a temperature program involving heating from 313 K (after a 7-min hold) to 473 K (and held for 5 min) at a rate of 2 K min^{-1}. Anhydrous toluene was used as an internal standard. High purity helium (99.999 % pure) was used as carrier gas at a flow rate of 10 ml/min. The injector and detectors were maintained at 493 K.

Analysis of samples from VLE experiments was performed a Varian 3400 gas chromatograph with both FID and TCD detectors. Column packing was 10% OV-101 on Chromosorb W-HP 80/100 with a helium flow rate at 20 ml/min.

6.2.3. Batch Kinetic Experiments. Esterification reactions at 78$^{\text{o}}$C were performed in a 2 x 10^{-4} m^3 jacketed glass reactor equipped with a recirculating constant temperature oil bath. The reaction volume was maintained between 100 and 110 ml. A spiral coil condenser, open to the atmosphere, was placed on top of the reactor. The glass reactor was equipped with temperature and stirrer speed monitoring devices and a sampling port. In operation, measured quantities of ethanol and citric acid were added to the reactor, and heating and stirring were started simultaneously. Once the desired temperature was achieved, usually in about 15 minutes, catalyst (Amberlyst 15 ion exchange resin) was added for the case of resin catalyzed reactions and stirring speed was increased to 800 rpm. This point in time was considered as the zero reaction time. Samples were withdrawn at specific time intervals and immediately transferred to an ice bath (prior to analysis) in order to ensure that no further reaction took place.

For reaction temperatures of 90$^{\text{o}}$C and above, esterification was performed in a 1 x 10^{-4} m^3 stainless steel autoclave (5000 Multi-reactor System, Parr Instrument Co.) equipped with temperature and stirrer speed monitors and a sampling port. In operation, measured quantities of ethanol, citric acid and catalyst for the resin catalyzed reaction cases were added to the reactor and heating was started with slow stirring. The total reaction volume was maintained between 55 and 60 ml. The desired temperature was achieved in about 15 minutes, at which time the stirring rate was increased to 740 rpm. This time was considered as the zero reaction time. Samples were withdrawn at specific time intervals through a cooled metal tube and immediately transferred to an ice bath in order to ensure no further reaction took place before analysis. All samples were analyzed using the method described in Section 6.2.2.

6.2.4. Vapor-Liquid Equilibrium Experiments. The primary volatile species in this reaction system are ethanol and water, so the vapor-liquid equilibria behavior of these components with TEC was characterized in order to obtain TEC-ethanol and TEC-water binary pair thermodynamic parameters for reliable process design. A P-x-y apparatus, described in detail in the section 4.2, was used in the investigation.

6.3. Results and Discussion

Several batch kinetic experiments were carried out to study the effects of reaction temperature, catalyst loading, and initial reactant molar ratio on the heterogeneously catalyzed esterification of citric acid with ethanol. Table 6.1 shows the reaction conditions and summarized results for all of the experimental studies performed in this work. We observed from initial experiments and comparison with prior work that external mass-transfer resistances were negligible at stirring speeds above 500 rpm. Hence all kinetic experiments were performed at 800 rpm. The influence of internal mass transfer resistances were neglected for reactions catalyzed by Amberlyst 15 (Gangadwala et al.[22], Asthana et al.[23]).

6.3.1. Effect of Reaction Temperature. Effect of increasing reaction temperature from 78° to 120^oC on the esterification of citric acid with ethanol at a catalyst loading of 5 wt% and an initial mole ratio of ethanol:citric acid of 15:1 was studied in the present work. Figures 6.2, 6.3 and 6.4 give a full description of product evolution at 78^oC, 100^oC and 120^oC, respectively. The full set of graphs is located in **Annexure II** (Figures 6.S1 through 6.S5). It can be observed from Figures 6.2-6.4 that the rate of conversion of citric acid, MEC, and DEC increases with increasing reaction temperature. Experimental quantification of DEE formation was carried out at reaction temperatures of 100, 110 and 120^oC. At lower temperatures, negligible quantities of DEE were formed.

Table 6.1 Summary of kinetic experiments and average prediction errors

Run No.	Figure No.	Mole Ratio EtOH:CA	Resin Catalyst Loading (wt%)	Temp (^{o}C)	Average relative error (F_{rel}) (Equation 3)						Average absolute error (F_{abs}) (Equation 4)					
					CA	MEC	DEC	TEC	EtOH	Water	CA	MEC	DEC	TEC	EtOH	Water
1	2 / S1	15 : 1	5	78	8.3	10.6	34.8	27.9	1.8	19.0	0.16	0.17	0.29	0.08	1.55	0.92
2	S2	15 : 1	5	90	13.5	10.7	37.4	57.5	2.5	24.4	0.35	0.21	0.40	0.16	1.41	0.77
3	3 / S3	15 : 1	5	100	13.2	8.9	24.2	44.6	2.8	19.2	0.26	0.16	0.43	0.34	2.55	1.80
4	S4	15 : 1	5	110	9.3	20.9	19.7	39.8	2.2	13.4	0.11	0.28	0.35	0.32	1.75	1.35
5	4 / S5	15 : 1	5	120	12.8	14.1	12.5	27.5	2.7	8.8	0.06	0.18	0.30	0.33	2.06	1.13
6	S6	15 : 1	3	120	12.1	16.8	6.1	27.9	0.9	3.8	0.08	0.23	0.15	0.26	0.70	0.41
7	5 / S7	15 : 1	2	120	12.6	13.1	11.9	38.6	1.0	17.8	0.09	0.20	0.16	0.23	0.86	1.00
8	S8	15 : 1	1	120	13.4	10.1	26.4	48.7	5.6	23.6	0.18	0.20	0.50	0.49	4.34	2.67
9	S9	15 : 1	3	78	19.5	7.6	14.2	43.4	1.3	8.3	0.24	0.17	0.08	0.06	1.10	0.31
10	6 / S10	15 : 1	2	78	21.4	8.4	13.6	40.0	0.8	4.7	0.37	0.21	0.06	0.05	0.67	0.15
11	S11	15 : 1	1	78	13.9	6.0	16.4	13.2	1.4	6.1	0.35	0.15	0.09	0.01	1.20	0.32
12	S12	20 : 1	5	120	25.8	12.9	13.5	16.9	0.5	3.1	0.08	0.09	0.22	0.16	0.43	0.30
13	S13	10 : 1	5	120	11.9	15.3	6.6	28.7	2.3	6.8	0.19	0.25	0.20	0.48	1.60	1.18

14	7 / S14	5 : 1	5	120	12.5	27.1	7.4	35.7	9.2	10.1	0.34	0.98	0.43	1.14	4.02	3.31
15	S15	20 : 1	0	120	14.8	6.7	11.1	30.2	0.5	6.9	0.12	0.09	0.15	0.16	0.40	0.37
16	8 / S16	15 : 1	0	120	14.6	14.3	13.2	17.1	3.1	10.3	0.18	0.37	0.46	0.10	2.51	1.28
17	S17	10 : 1	0	120	15.2	2.1	10.6	9.1	1.7	5.6	0.11	0.05	0.39	0.05	1.23	0.84
18	S18	5 : 1	0	120	6.9	4.4	11.1	6.0	4.2	5.2	0.09	0.18	0.82	0.12	2.12	1.51
19	S19	15 : 1	0	78	4.1	15.3	40.1	22.6	1.0	20.5	0.18	0.22	0.10	0.00	0.88	0.30
20	S20	15 : 1	0	90	5.7	6.1	22.8	37.3	0.9	11.1	0.15	0.11	0.12	0.02	0.76	0.33
21	S21	15 : 1	0	100	2.9	6.0	22.1	29.2	2.0	13.8	0.05	0.15	0.32	0.06	1.68	0.92
22	S22	15 : 1	0	110	8.0	4.5	15.4	19.7	1.2	8.2	0.08	0.10	0.25	0.05	1.06	0.52
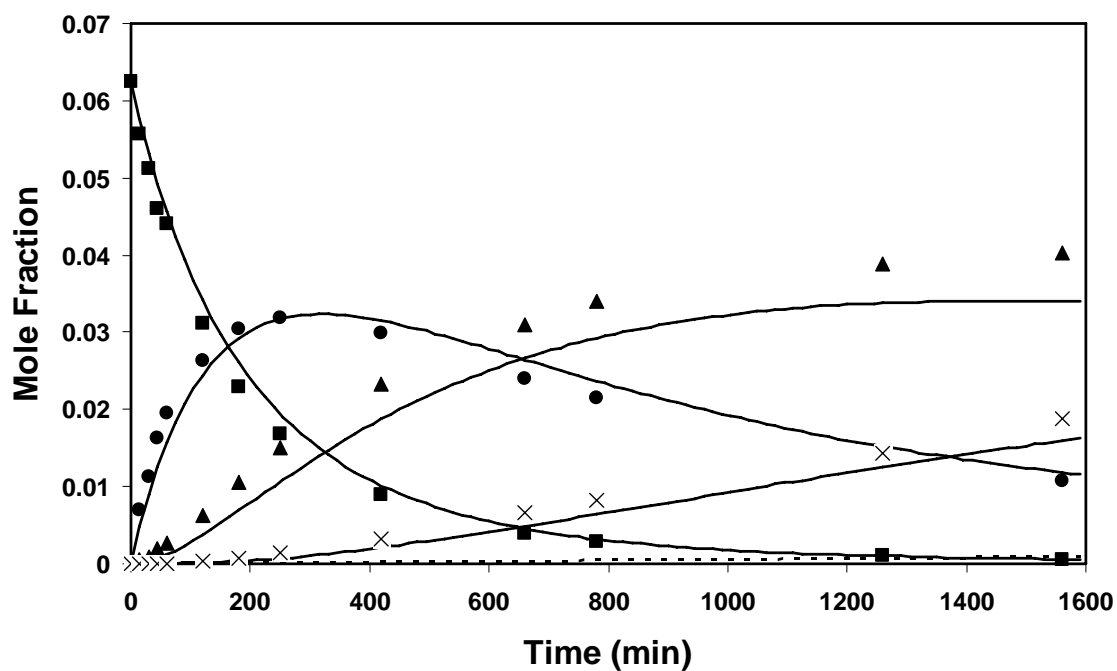
Figure 6.2 Esterification of citric acid catalyzed by ion exchange resin. Reaction Conditions: Mole Ratio Ethanol:Citric acid, 15:1; Catalyst Loading, 5 wt%; Reaction Temperature, 78°C. (■ , CA; ● , MEC; ▲ , DEC; × , TEC; Δ , DEE)
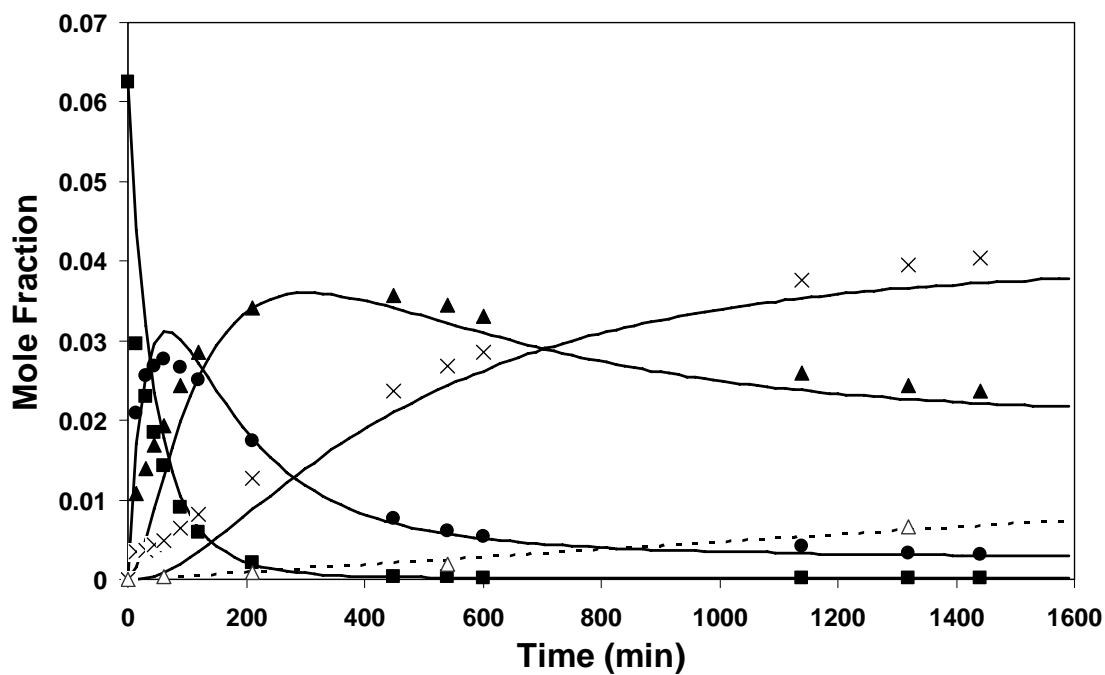
Figure 6.3 Esterification of citric acid catalyzed by ion exchange resin. Reaction Conditions: Mole Ratio Ethanol:Citric acid, 15:1; Catalyst Loading, 5 wt%; Reaction Temperature, 100°C. (■ , CA; ● , MEC; ▲ , DEC; × , TEC; Δ ,DEE)
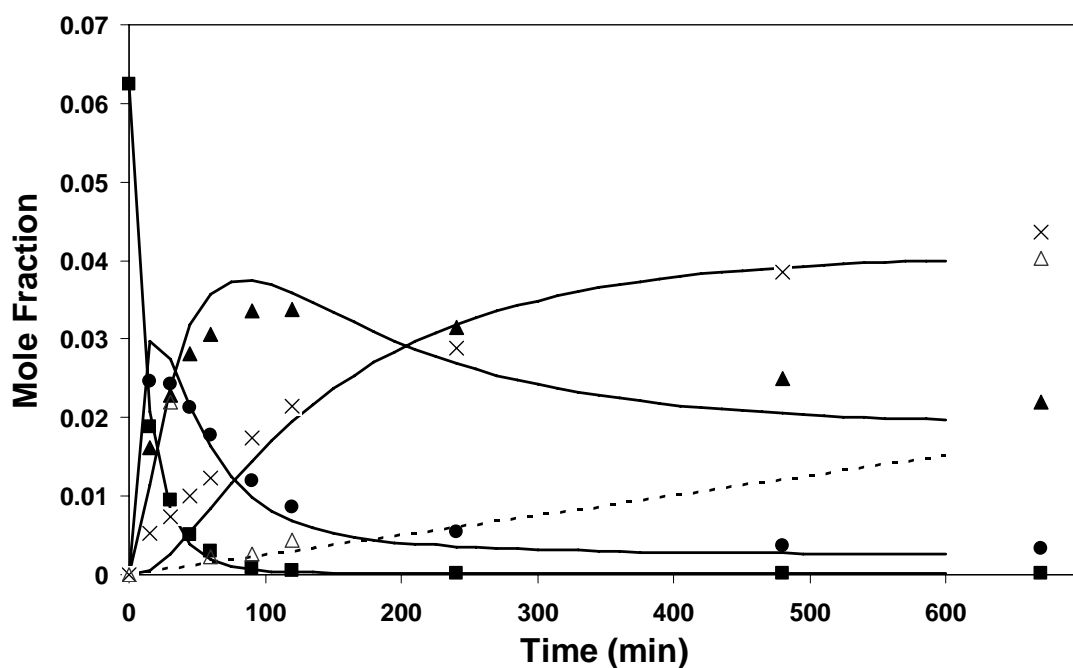
Figure 6.4 Esterification of citric acid catalyzed by ion exchange resin. Data at right edge of graph represent liquid phase composition at end of reaction (t =1600 minutes). Reaction Conditions: Mole Ratio Ethanol:Citric acid, 15:1; Catalyst Loading, 5 wt%; Reaction Temperature, 120°C. (■, CA; ●, MEC; ▲, DEC; ×, TEC; Δ, DEE)
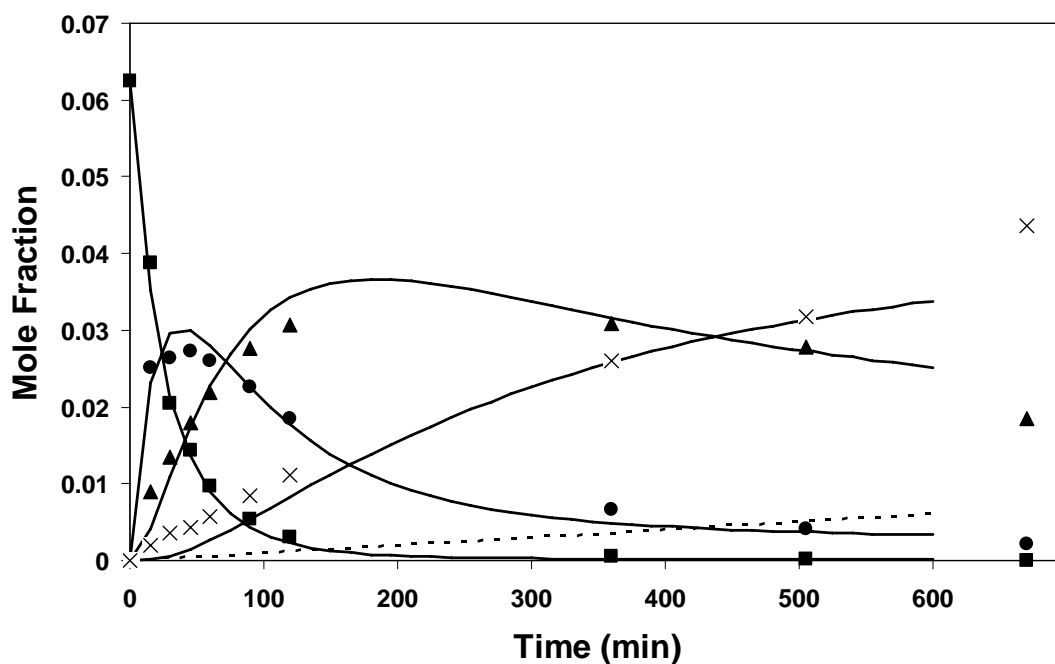
Figure 6.5 Esterification of citric acid catalyzed by ion exchange resin. Data at right edge of graph represent liquid phase composition at end of reaction (t = 1600 minutes). Reaction Conditions: Mole Ratio Ethanol:Citric acid, 15:1; Catalyst Loading, 2 wt%; Reaction Temperature, 120°C. (■, CA; ●, MEC; ▲, DEC; ×, TEC; Δ, DEE)

6.3.2. Effect of Catalyst Loading. The effect of varying catalyst loading from 1 to 5 wt% (of reaction solution) on citric acid esterification with ethanol and an initial mole ratio of ethanol:citric acid of 15:1 was examined. Figures 6.4 and 6.5 give results for 5 wt% and 2 wt% catalyst loading, respectively, at 120°C; Figures 6.2 and 6.6 show results for the same loadings at 78°C. The full set of graphs is available in the supplementary material (Figures 6.S5 to 6.S8 for 120 °C and Figures 6.S1 and 6.S9 – 6.S11 at 78°C). Analysis of the initial reaction rate shows that esterification rate is linearly dependent on catalyst loading.
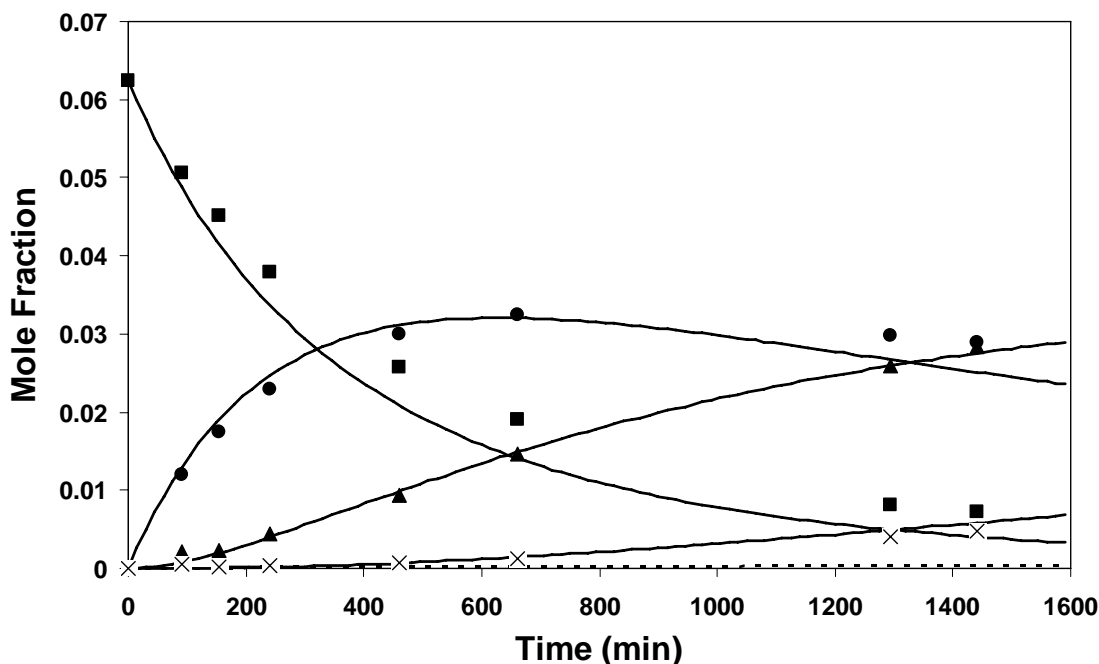
Figure 6.6. Esterification of citric acid catalyzed by ion exchange resin. Reaction Conditions: Mole Ratio Ethanol:Citric acid, 15:1; Catalyst Loading, 2 wt%; Reaction Temperature, 78°C. (■, CA; ●, MEC; ▲, DEC; ✕, TEC; Δ, DEE)

6.3.3. Effect of Initial Reactant Mole Ratio. The effect of varying initial ethanol:citric acid mole ratio is shown in Figures 6.4 and 6.7 for an initial ethanol:citric acid mole ratio of 15:1 and 5:1, respectively. All reactions were conducted with 5 wt% catalyst loading at 120°C. Complete results are given in the supplementary material (Figures 6.S5 and 6.S12 – 6.S14). The equilibrium extent of conversion to TEC increases with increasing initial ethanol to citric acid molar ratio.

6.3.4. Self-catalyzed Reactions. The self-catalyzed reaction of citric with ethanol at 120°C and an initial mole ratio of ethanol:citric acid from 5:1 to 20:1 was examined; a representative graph is shown in Figure 6.8 with full results available in the supplementary material (Figures 6.S15 – 6.S22). Comparing the self-catalyzed rate with that of the ion exchange resin-catalyzed reactions, it is evident that the self-catalyzed rate contributes significantly to esterification at low catalyst loadings, especially at higher reaction temperature of 120°C.
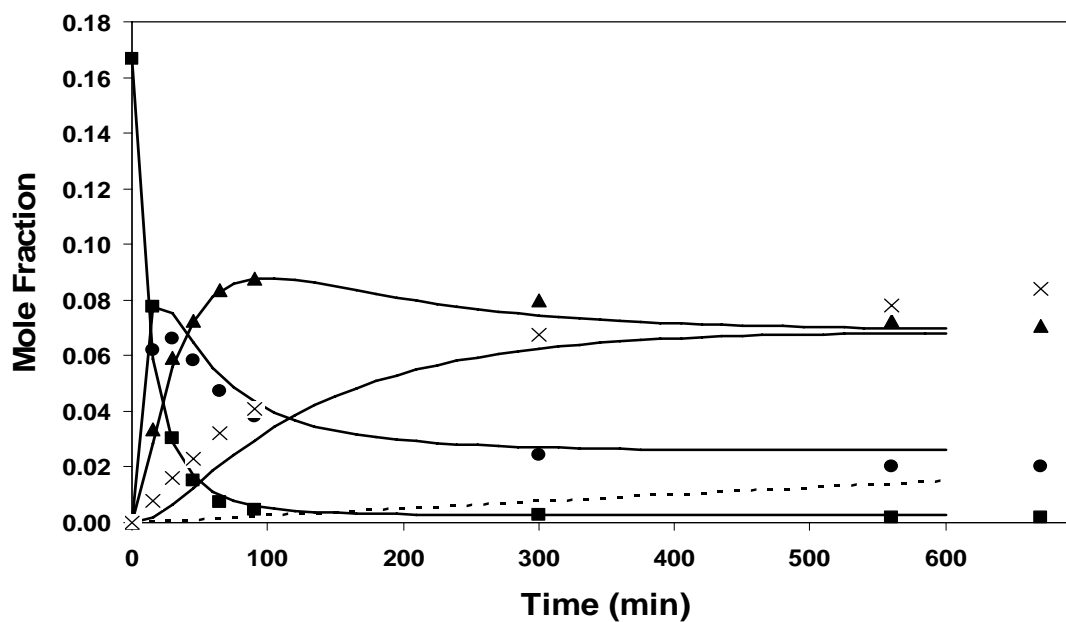
Figure 6.7. Esterification of citric acid catalyzed by ion exchange resin. Data at right edge of graph represent liquid phase composition at end of reaction (t = 1600 minutes). Reaction Conditions: Mole Ratio Ethanol:Citric acid, 5:1; Catalyst Loading, 5 wt%; Reaction Temperature, 120°C. (■, CA; ●, MEC; ▲, DEC; ✕, TEC; Δ, DEE)
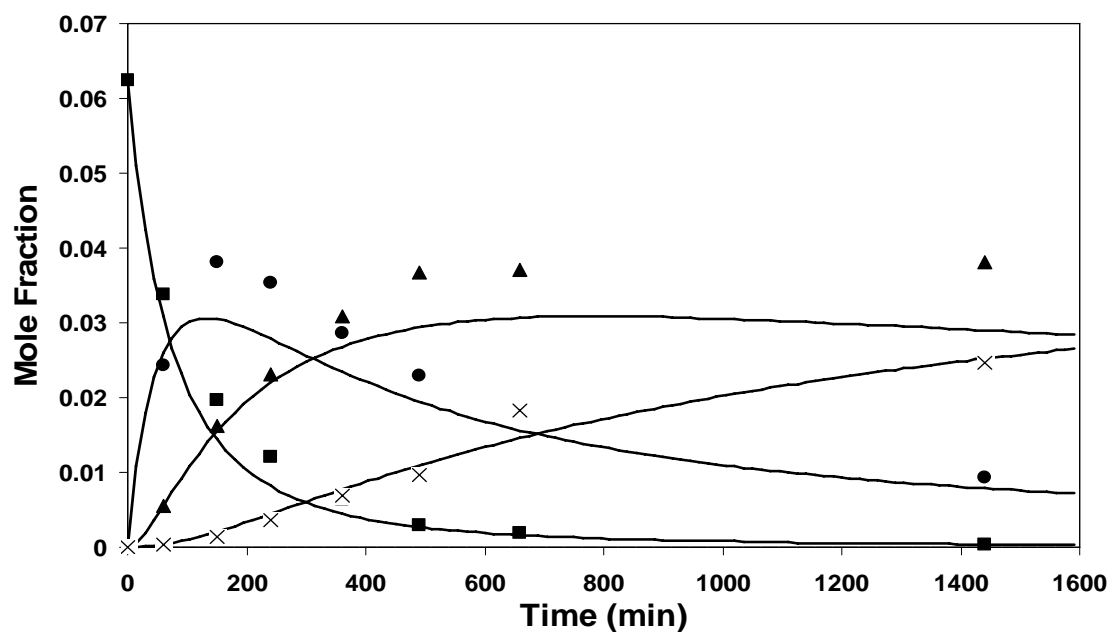
Figure 6.8. Self-catalyzed esterification of citric acid. Reaction Conditions: Mole Ratio Ethanol:Citric acid, 15:1; Reaction Temperature, 120°C. (■, CA; ●, MEC; ▲, DEC; ✕, TEC)

6.3.5. Vapor-Liquid Equilibria. Experimental P-x data for TEC (1) + ethanol (2) were collected at 40°C as shown in Figure 6.9 and fit (solid line in Figure 6.9) using the UNIQUAC model to obtain binary interaction parameters.
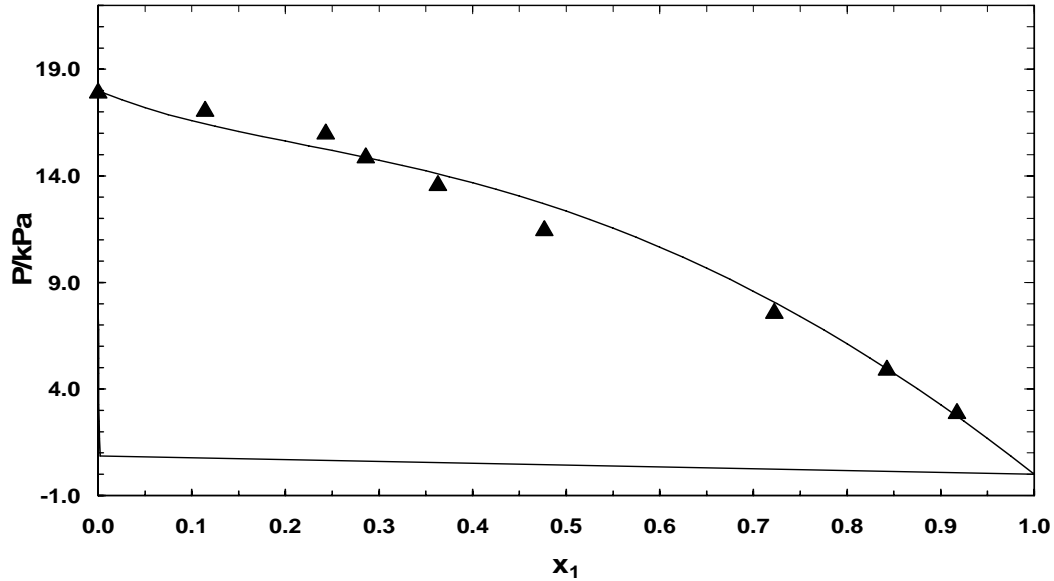
Figure 6.9. P-x data for TEC(1) – Ethanol(2) at 40°C compared with the UNIQUAC fit. The lower line represents the calculated vapor phase composition.
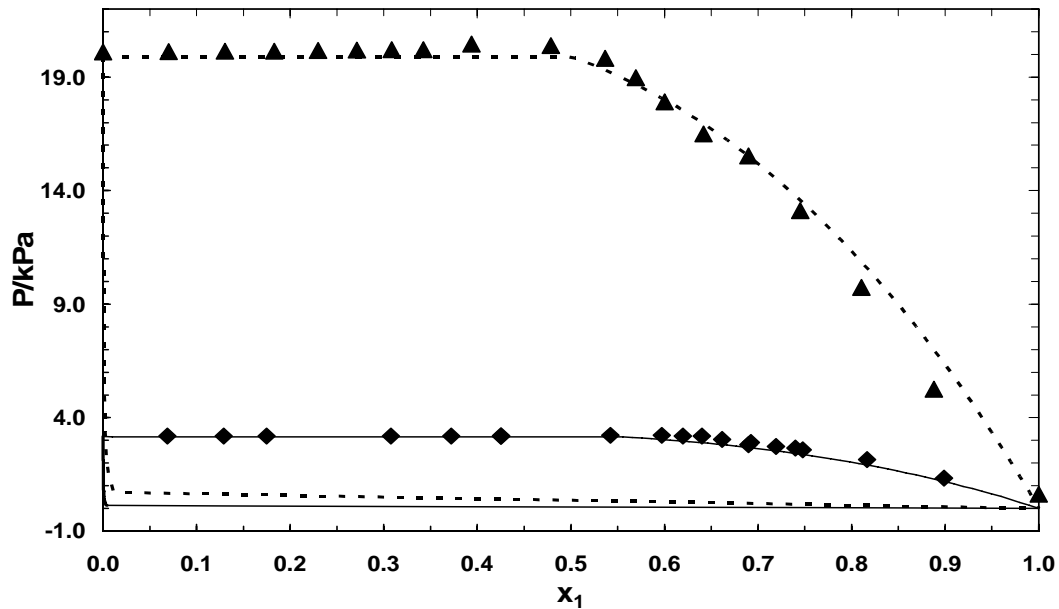
Figure 6.10. P-x data for TEC(1) – Water(2) at 25°C and 60°C compared with the UNIQUAC fit. (◆, 25°C; ▲, 60°C). The lower lines represent the calculated vapor phase compositions.

Experimental P-x data for TEC (1) + water(2) at 25°C and 60°C are shown in Figure 6.10 and are similarly fit. Calculated vapor phase compositions are also included in the Figures. The r and q values used in the UNIQUAC model are 5.9585 and 4.808 for CA, 7.1912 and 6.380 for MEC, 8.4674 and 7.424 for DEC, 9.7436 and 8.468 for TEC, 2.1055 and 1.972 for ethanol, 0.92 and 1.4 for water, and 3.3949 and 3.016 for DEE. The TEC-water binary system exhibits liquid-liquid immiscibility (horizontal line in Figure 6.10) with one phase nearly pure in water, and the other phase approximately equimolar in water and TEC. ASPEN Plus (Ver 12.0) was unable to converge on an improved parameter set. The vapor-liquid behavior of the system near the pure water side is not possible to discern from the measurements, because the solubility of TEC in water is very low. The UNIQUAC parameters used in fitting of the experimental VLE data sets are shown in Table 6.2. VLE data for MEC and DEC were not collected because they are not available commercially and were not isolated experimentally.

6.4. Kinetic Model

6.4.1. Kinetic Pathways. Reactions (6.1) to (6.4) below describe the esterification of citric acid with ethanol and the formation of side product diethyl ether.

$$CA + EtOH \underset{k_1/Keq_{a,1}}{\overset{k_1}{\rightleftarrows}} MEC + W \qquad …(6.1)$$

$$MEC + EtOH \underset{k_2/Keq_{a,2}}{\overset{k_2}{\rightleftarrows}} DEC + W \qquad …(6.2)$$

$$DEC + EtOH \underset{k_3/Keq_{a,3}}{\overset{k_3}{\rightleftarrows}} TEC + W \qquad …(6.3)$$

$$2\ EtOH \overset{k_4}{\longrightarrow} DEE + W \qquad …(6.4)$$
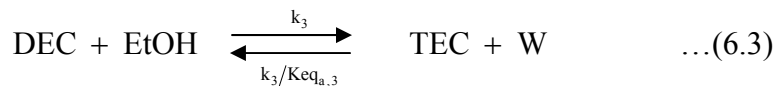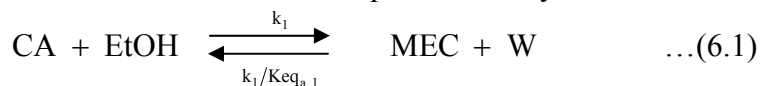
The formation of DEE (Equation 6.4) via dehydration of two molecules of ethanol is significant at relatively high temperatures and high catalyst loadings. Dehydration of ethanol to DEE is considered irreversible, since the equilibrium constants for such reactions are known to be very high (Song et al.[24]). Formation of DEE was considered only in the presence of ion exchange resin.

Based on the above reactions, a pseudo-homogeneous, activity-based kinetic model has been developed. The model used is based on the law of mass action as first order with respect to catalytic acid concentration, reacting acid concentration and ethanol concentration. An activity-based model is preferred over the conventional concentration-based model, since water and ethanol are highly polar in comparison to other components of the system and thus strong non-ideal behavior exists. Moreover, kinetic models used in process simulation and design using programs such as Aspen Plus are best written in terms of activities (Rehfinger and Hoffmann[99], Sundmacher and Hoffmann[100], Venimadhavan et al.[101], Song et al.[102], Gangadwala et al.[29]).

The UNIQUAC model was used to determine activity coefficients in the liquid phase. The UNIQUAC parameters for the TEC-ethanol and TEC-water pair were determined using the experimental VLE data presented in Section 6.3.5. The UNIQUAC parameters for the ethanol-water, DEE-ethanol and DEE-water pairs were obtained from literature data reported in the ASPEN Plus databank. The rest of the UNIQUAC

parameters were obtained by fitting the UNIQUAC model to the UNIFAC predictions. Table 6.2 shows the UNIQUAC parameters used in the present modeling work.

Table 6.2 UNIQUAC interaction parameters for binary component pairs in the form $\tau_{ij} = \exp(A_{ij} + B_{ij}/T)$.

Component pairs	A_{ij}	A_{ji}	B_{ij} (K)	B_{ji} (K)
Ethanol – Water	2.0046	-2.4936	-728.971	756.948
Ethanol – TEC			70.5	-301.6
TEC – Water			-501.8	82.56
CA – Ethanol			-139.839	54.177
CA – TEC			90.604	-172.585
CA – Water			92.644	53.676
CA – MEC			28.751	-33.13
CA – DEC			-19.605	-0.897
Ethanol – MEC			-79.836	17.574
Ethanol – DEC			-135.446	60.371
TEC – MEC			-154.776	107.843
TEC – DEC			-95.921	77.814
Water – MEC			-447.773	263.187
Water – DEC			-336.304	178.184
MEC – DEC			28.784	-34.376
Ethanol – DEE	-3.7063	5.3512	1175.781	-1893.535
Water – DEE			-50.888	-611.06
CA – DEE			47.749	-457.830
TEC – DEE			103.507	-171.685
MEC – DEE			84.542	-315.967
DEC - DEE			105.529	-244.055

6.4.2. Reaction equilibrium constants. Chemical reaction equilibrium constants are given by

$$K_{a,i} = \prod a_i^{\nu_i} = K_{x,i}.K_{\gamma,i} = \prod x_i^{\nu_i}.\prod \gamma_i^{\nu_i} \qquad ...(6.5)$$

The values of the equilibrium constants $K_{a,i}$ for esterification reactions were determined by analysis of the experimental data at long reaction times (e.g. approaching equilibrium) and were found to be 6.35, 2.72 and 3.78 for the formation of MEC, DEC and TEC, respectively. These constants were taken to be independent of temperature. The values of $K_{x,i}$ are technically not constant, but over the range of typical reaction conditions were found to be approximately 6.35, 1.82 and 0.54 for the formation of MEC, DEC, and TEC, respectively. The values of $K_{\gamma,i}$, also not constant, were averaged from γ_i determined from UNIQUAC at the extrapolated equilibrium concentrations and were found to be approximately 1.0, 1.5 and 7.0 for the formation of MEC, DEC and TEC, respectively.

6.4.3. Kinetic Model for Self-Catalyzed Esterification. The rate of self-catalyzed esterification is a significant fraction of the ion exchange resin-catalyzed rate at low catalyst loadings and high temperatures. The self-catalyzed reactions are thus modeled using a pseudo-homogeneous model based on the law of mass action as first order with respect to reactants and to catalytic acid concentration, denoted as x_{acid} in the equation below. The reaction rate for the self-catalyzed esterification is written in generalized form as

$$r_{self,i} = k_{self,i}\ x_{acid}\left(a_{Reacting\,acid}\ a_{Alcohol} - \frac{a_{Ester}\ a_{Water}}{K_{a,i}}\right) \qquad ...(6.6)$$

The catalytic acid concentration x_{acid} is taken to be proportional to the hydrogen ion (proton) activity, which can arise not only from citric acid but from MEC and DEC as well. Because pK_a values for the partial esters are not available in the literature, we assume that hydrogen ion activity is proportional to the summed weighted mole fractions of acidic species. This is equivalent to assuming that the acid strength of all –COOH groups in citric acid and in the partial esters are the same, and that the mean ionic activity coefficient is equal for all species in the range of concentrations studied. The constants that quantify these assumptions are lumped into the pre-exponential factors for the self-catalyzed reactions. The catalytic acid concentration in Equation (6.6) can thus be written as

$$x_{Acid} = \left(x_{CA} + \frac{2}{3}x_{MEC} + \frac{1}{3}x_{DEC}\right) \qquad ...(6.7)$$

The rate of formation of each species in the reaction mixture is described by Equations (6.8) to (6.13) given below:

$$-\frac{dx_{CA}}{dt} = k_{self,1}\ x_{acid}\left(a_{CA}.a_{EtOH} - \frac{a_{MEC}.a_W}{K_{a,1}}\right) \qquad ...(6.8)$$

$$-\frac{dx_{MEC}}{dt} = k_{self,2}x_{acid}\left(a_{MEC}.a_{EtOH} - \frac{a_{DEC}.a_W}{K_{a,2}}\right) + k_{self,1}x_{acid}\left(\frac{a_{MEC}.a_W}{K_{a,1}} - a_{CA}.a_{EtOH}\right) \qquad ...(6.9)$$

$$-\frac{dx_{DEC}}{dt} = k_{self,3} x_{acid}\left(a_{DEC}.a_{EtOH} - \frac{a_{TEC}.a_W}{K_{a,3}}\right) + k_{self,2} x_{acid}\left(\frac{a_{DEC}.a_W}{K_{a,2}} - a_{MEC}.a_{EtOH}\right) ..(6.10)$$

$$-\frac{dx_{TEC}}{dt} = k_{self,3} x_{acid}\left(\frac{a_{TEC}.a_W}{K_{a,3}} - a_{DEC}.a_{EtOH}\right) \qquad ...(6.11)$$

$$-\frac{dx_{EtOH}}{dt} = k_{self,1} x_{acid}\left(a_{CA}.a_{EtOH} - \frac{a_{MEC}.a_W}{K_{a,1}}\right) + k_{self,2} x_{acid}\left(a_{MEC}.a_{EtOH} - \frac{a_{DEC}.a_W}{K_{a,2}}\right)$$
$$+ k_{self,3} x_{acid}\left(a_{DEC}.a_{EtOH} - \frac{a_{TEC}.a_W}{K_{a,3}}\right) \qquad (6.12)$$

$$-\frac{dx_W}{dt} = k_{self,1} x_{acid}\left(\frac{a_{MEC}.a_W}{K_{a,1}} - a_{CA}.a_{EtOH}\right) + k_{self,2} x_{acid}\left(\frac{a_{DEC}.a_W}{K_{a,2}} - a_{MEC}.a_{EtOH}\right)$$
$$+ k_{self,3} x_{acid}\left(\frac{a_{TEC}.a_W}{K_{a,3}} - a_{DEC}.a_{EtOH}\right) \qquad ..(6.13)$$

where for the ith reaction $\qquad k_{self,i} = k^o_{self,i} . \exp\left(-\frac{E_{A,self\ i}}{RT}\right) \qquad ...(6.14)$

6.4.4. Determination of Rate Constants. To determine values of the six adjustable parameters for the self-catalyzed esterification (pre-exponential factors $k^o_{self,1}$, $k^o_{self,2}$ and $k^o_{self,3}$, and activation energies $E_{A,self\ 1}$, $E_{A,self\ 2}$ and $E_{A,self\ 3}$), the rate expressions were numerically integrated via a fourth order Runge-Kutta method using ordinary differential equation solver ode23 in Matlab 7.0. Starting with an initial set of estimated rate constants, the liquid phase mole fractions of all species over the course of reaction were calculated and compared with the experimental data collected in Runs 15 to 22. The rate constants were then sequentially incremented in order to minimize the sum of the mean square differences F_{min}^2, given by

$$F_{min}^2 = \frac{\sum_{samples}\left(x_{j,cal} - x_{j,expt}\right)^2}{n_{samples}} \qquad ...(6.15)$$

The values of the self-catalyzed kinetic parameters which best describe the data are reported in Table 6.3. Predicted mole fraction curves are shown as continuous lines in Figure 6.8 in the text; model fit for other self-catalyzed reactions are located in the supplementary material (Figures 6.S15 to 6.S22). The correlation between the experimental data and the calculated trend lines is reasonable.

After determining a final set of rate constants, the calculated mole fractions of each component were compared to the experimental values by calculating a mean deviation of all data points for an experiment, represented both on an absolute and on a relative (percentage) basis as shown below

$$F_{abs} = \frac{\sum\limits_{samples} \left| x_{j,cal} - x_{j,expt} \right|}{n_{samples}} \times 100\% \qquad \ldots(6.16)$$

$$F_{rel} = \frac{\sum\limits_{samples} \left| \dfrac{x_{j,cal} - x_{j,expt}}{x_{j,expt}} \right|}{n_{samples}} \times 100\% \qquad \ldots(6.17)$$

The values of the absolute mole fraction error F_{abs} and relative mole fraction error F_{rel} are reported as in Table 6.1 for the self-catalyzed reactions (Runs 15-22). Residual errors are highest for TEC at reaction times up to about 300 minutes; there are also some minor inconsistencies in the experimental concentrations for DEC, for reasons not clear at this time.

Table 6.3 Kinetic model parameters for self-catalyzed reactions

Parameters	Units	Values
$k^{o}_{self,1}$	s^{-1}	8.37E+6
$k^{o}_{self,2}$	s^{-1}	9.82E+6
$k^{o}_{self,3}$	s^{-1}	5.00E+6
$E_{A,self\ 1}$	kJ/kmol	70800
$E_{A,self\ 2}$	kJ/kmol	72000
$E_{A,self\ 3}$	kJ/kmol	72400
$K_{a,1}$		6.35
$K_{a,2}$		2.72
$K_{a,3}$		3.78

6.4.5. Kinetic Model for Combined Resin-Catalyzed and Self-Catalyzed Esterification. Kinetics of the ion exchange resin-catalyzed esterification of citric acid (Runs 1 – 14 in Table 6.1) has been described using a pseudo-homogeneous model that includes the self-catalyzed reactions and diethyl ether (DEE) formation. The inclusion of self-catalyzed reactions in esterification has also been previously presented by Omota et al.[28].

The rate of formation of each species in the reaction mixture is described by Equations (6.18) to (6.24) below:

$$-\frac{dx_{CA}}{dt} = \left(w_{cat}\ \mathrm{k}_{cat,1} + \mathrm{x}_{acid}\ \mathrm{k}_{self,1}\right)\left(a_{CA}.a_{EtOH} - \frac{a_{MEC}.a_W}{K_{a,1}}\right) \qquad \ldots(6.18)$$

$$-\frac{dx_{MEC}}{dt} = \left(w_{cat}\ \mathrm{k}_{cat,2} + \mathrm{x}_{acid}\ \mathrm{k}_{self,2}\right)\left(a_{MEC}.a_{EtOH} - \frac{a_{DEC}.a_W}{K_{a,2}}\right) +$$
$$\left(w_{cat}\ \mathrm{k}_{cat,1} + \mathrm{x}_{acid}\ \mathrm{k}_{self,1}\right)\left(\frac{a_{MEC}.a_W}{K_{a,1}} - a_{CA}.a_{EtOH}\right) \qquad \ldots(6.19)$$

$$-\frac{dx_{DEC}}{dt} = \left(w_{cat}\ \mathrm{k}_{cat,3} + \mathrm{x}_{acid}\ \mathrm{k}_{self,3}\right)\left(a_{DEC}.a_{EtOH} - \frac{a_{TEC}.a_W}{K_{a,3}}\right)$$
$$+ \left(w_{cat}\ \mathrm{k}_{cat,2} + \mathrm{x}_{acid}\ \mathrm{k}_{self,2}\right)\left(\frac{a_{DEC}.a_W}{K_{a,2}} - a_{MEC}.a_{EtOH}\right) \qquad \ldots(6.20)$$

$$-\frac{dx_{TEC}}{dt} = \left(w_{cat}\ \mathrm{k}_{cat,3} + \mathrm{x}_{acid}\ \mathrm{k}_{self,3}\right)\left(\frac{a_{TEC}.a_W}{K_{a,3}} - a_{DEC}.a_{EtOH}\right) \qquad \ldots(6.21)$$

$$-\frac{dx_{EtOH}}{dt} = \left(w_{cat}\ \mathrm{k}_{cat,1} + \mathrm{x}_{acid}\ \mathrm{k}_{self,1}\right)\left(a_{CA}.a_{EtOH} - \frac{a_{MEC}.a_W}{K_{a,1}}\right)$$
$$+ \left(w_{cat}\ \mathrm{k}_{cat,2} + \mathrm{x}_{acid}\ \mathrm{k}_{self,2}\right)\left(a_{MEC}.a_{EtOH} - \frac{a_{DEC}.a_W}{K_{a,2}}\right) \qquad \ldots(6.22)$$
$$+ \left(w_{cat}\ \mathrm{k}_{cat,3} + \mathrm{x}_{acid}\ \mathrm{k}_{self,3}\right)\left(a_{DEC}.a_{EtOH} - \frac{a_{TEC}.a_W}{K_{a,3}}\right) + 2\,w_{cat}\ k_{cat,4}$$

$$-\frac{dx_W}{dt} = \left(w_{cat}\ \mathrm{k}_{cat,1} + \mathrm{x}_{acid}\ \mathrm{k}_{self,1}\right)\left(\frac{a_{MEC}.a_W}{K_{a,1}} - a_{CA}.a_{EtOH}\right)$$
$$+ \left(w_{cat}\ \mathrm{k}_{cat,2} + \mathrm{x}_{acid}\ \mathrm{k}_{self,2}\right)\left(\frac{a_{DEC}.a_W}{K_{a,2}} - a_{MEC}.a_{EtOH}\right) \qquad \ldots(6.23)$$
$$+ \left(w_{cat}\ \mathrm{k}_{cat,3} + \mathrm{x}_{acid}\ \mathrm{k}_{self,3}\right)\left(\frac{a_{TEC}.a_W}{K_{a,3}} - a_{DEC}.a_{EtOH}\right) - w_{cat}.k_{cat4}$$

$$-\frac{dx_{DEE}}{dt} = - w_{cat}.k_{cat,4} \qquad \ldots(6.24)$$

where
$$\mathrm{x}_{acid} = \left(\mathrm{x}_{CA} + \frac{2}{3}\mathrm{x}_{MEC} + \frac{1}{3}\mathrm{x}_{DEC}\right) \qquad \ldots(6.25)$$

$$k_{cat,i} = \mathrm{k}^{\circ}_{cat,i}\ \exp\left(\frac{-\mathrm{E}_{A,cat\,i}}{RT}\right) \qquad \ldots(6.26)$$

$$k_{\text{self,i}} = k^{\text{o}}_{\text{self, i}} \ \exp\left(\frac{-E_{A,\text{self i}}}{RT}\right) \qquad \qquad \ldots(6.27)$$

Six adjustable parameters for the resin-catalyzed reactions (the pre-exponential factors $k^{\text{o}}_{\text{cat,1}}$, $k^{\text{o}}_{\text{cat,2}}$ and $k^{\text{o}}_{\text{cat,3}}$, and activation energies $E_{A,\text{cat 1}}$, $E_{A,\text{cat 2}}$ and $E_{A,\text{cat 3}}$) have been fitted to the experimental data of Runs 1 to 14 by minimizing F_{min}^2 for those runs. The constants for self-catalyzed reactions determined earlier were used without alteration in determining the kinetic constants. The final values of the kinetic parameters are shown in Table 6.4.

Table 6.4 Kinetic model parameters for resin-catalyzed reactions

Parameters	Units	Values
$k^{\text{o}}_{\text{cat,1}}$	kg sol kg_{cat}^{-1} s^{-1}	3.34E+8
$k^{\text{o}}_{\text{cat,2}}$	kg sol kg_{cat}^{-1} s^{-1}	1.87E+9
$k^{\text{o}}_{\text{cat,3}}$	kg sol kg_{cat}^{-1} s^{-1}	1.99E+7
$k^{\text{o}}_{\text{cat,4}}$	kg sol kg_{cat}^{-1} s^{-1}	3.35E+8
$E_{A,\text{cat 1}}$	kJ/kmol	76900
$E_{A,\text{cat 2}}$	kJ/kmol	83100
$E_{A,\text{cat 3}}$	kJ/kmol	73200
$E_{A,\text{cat 4}}$	kJ/kmol	102000
$K_{a,1}$		6.35
$K_{a,2}$		2.72
$K_{a,3}$		3.78

Representative predicted mole fractions are given as continuous lines in Figures 6.2 to 6.7; the full set of predicted mole fraction curves for resin-catalyzed (Runs 1 – 14) are reported in the supplementary material (Figures 6.S1 – 6.S14). It can be observed from Figures 6.2 to 6.7 that the correlation between the experimental data and the calculated trend lines is good. The residual errors, both absolute and relative (Eq. 6.16 and 6.17), are shown in Table 6.1. For citric acid, the error in mole fraction is highest in the region when the citric acid concentration is very low. Large errors are also observed for TEC in the initial reaction period (< 300 min), where its concentration is low.

The citrate esterification system under consideration never really achieves equilibrium in a true sense, since irreversible DEE formation (a zero order reaction at high ethanol concentration) continues to proceed by converting the ethanol to DEE even after other reactions approach equilibrium. If this reaction were allowed to proceed for very long reaction times, it would ultimately initiate hydrolysis of the various ethyl citrates, liberating ethanol which would further etherify to DEE as a terminal product.

Finally, fitting of the reaction kinetic data was performed using a mole fraction-based model to determine whether non-ideal solution behavior played a significant role. The mole fraction-based model did not describe the kinetic data as satisfactorily as an activity-based model. Figure 6.11 gives fits for the two models for reaction at 120°C, 5:1 initial mole ratio of citric acid:ethanol, and 5% ion exchange resin catalyst loading using the combined resin-catalyzed and self-catalyzed esterification kinetic model described in Section 6.4.5. The fit is clearly superior with the activity-based model.
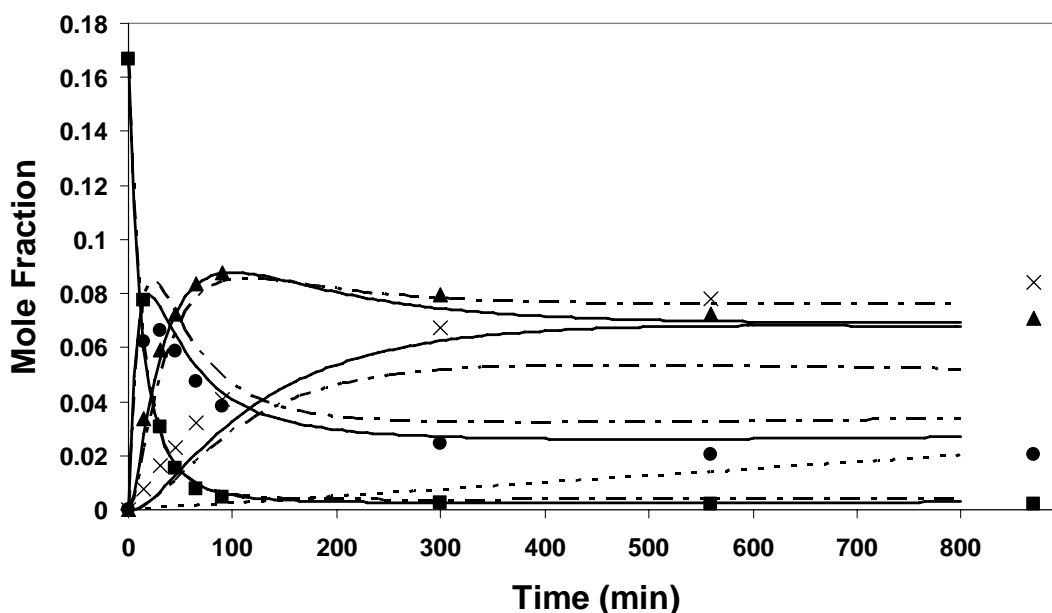
Figure 6.11 **Comparison of activity-based model and mole fraction-based model fits to experimental data. Data at right edge of graph represent liquid phase composition at end of reaction (t = 1600 minutes). Reaction Conditions: Mole Ratio Ethanol:Citric acid, 5:1; Catalyst Loading, 5 wt%; Reaction Temperature, 120°C. (■, CA; ●, MEC; ▲, DEC; ✕, TEC; ────── Calculated profiles using activity model; ─·─·─ Calculated profiles using mole fraction model)**

6.5. Conclusions

Experimental kinetic studies of citric acid esterification were performed at reaction temperature from 78°C to 120°C, initial mole ratio of ethanol:citric acid from 5:1 to 15:1, and Amberlyst-15 catalyst concentration up to 5 wt%. The kinetics of esterification reactions have been correlated using an activity-based pseudo-homogeneous model that includes both the resin-catalyzed and self-catalyzed esterification and diethyl ether formation. The rate expressions are applicable over a wide range of catalyst concentrations, molar ratios of reactants, and temperatures. The results constitute an accessible, reliable kinetic model that is useful in the design of reactive distillation and other esterification systems for citrate ester formation.

SECTION SEVEN

PROCESS FOR TRI-ETHYL CITRATE FORMATION

7.1. Background

Citric acid esterification with ethanol to form TEC proceeds sequentially through series reactions involving mono-ethyl citrate (MEC) and di-ethyl citrate (DEC), as described in section 6. A schematic of citric acid esterification is shown in Figure 6.1. Prior information on the kinetics of citric acid esterification with ethanol or n-butanol is confined to mainly the Chinese and German patent literature, and is detailed in section 6.

The esterification of citric acid is an equilibrium-limited reaction, and thus proceeds only to partial completion in a conventional reactor. To overcome this limitation, continuous removal of one of the products of the reaction mixture is required in order to drive the reaction to completion. We propose to do this using continuous reactive distillation.

7.1.1. Citric Acid Esterification via Reactive Distillation

Synthesis of organic acid esters by reactive distillation is well established, but in most applications the ester has either the highest volatility of the reagents present (e.g., methyl acetate) or the lowest volatility, with water as the most volatile component.[82] In these cases, recovery of 100% pure ester is straightforward via optimization of column operating conditions. Triethyl citrate (hereafter TEC) production via reactive distillation does not fit into either of these categories, since it has a volatility that is lower than ethanol and water but higher than citric acid (which is essentially non-volatile). Therefore, it is only possible to isolate the pure product if complete conversion of citric acid and the intermediate products MEC and DEC are achieved within the reactive distillation column. The primary challenge is therefore to achieve sufficiently rapid esterification kinetics so as to ensure complete conversion to the desired product TEC. Previous experimental work on similar esterification systems has been described by Bock et al.[103] for the synthesis of isopropyl myristate. Omota et al.[104] have described a reactive distillation system for synthesis of fatty esters where an immiscible two-phase water-alcohol mixture distills as the top product.

There has been no prior study on the application of reactive distillation for citrate esters formation other than our work. Therefore, the present work has been carried out to develop a favorable reactive distillation configuration for high citric acid conversion and high selectivity to TEC. Experimental results are presented from a continuous pilot-scale reactive distillation system for citric acid esterification experiments operating at 1 atm pressure. Simulation of the experimental pilot-scale reactive distillation column to obtain high yield of TEC has been performed using the ASPEN Plus process simulation software. Effect of important design variable has been studied for the pilot scale reactive distillation column. Three process configurations have been presented for the plant scale design of a reactive distillation column.

7.2. Experimental

7.2.1. Materials. Anhydrous citric acid crystals were obtained from Aldrich Chemicals. Absolute ethanol (99% purity) and HPLC grade water were obtained from J. T. Baker. The strong acid cation exchange resin catalyst Amberlyst-15 (Rohm and Haas, Philadelphia, PA) was obtained in H^+ form and was used without modification. Purity of all chemicals was checked by gas chromatography or HPLC.

7.2.2. Analysis. Analytical details have been provided in detail under section 6.2.2.

7.2.3. Reactive Distillation Column. Details of reactive distillation column and standard operating procedures have been provided in detail under sections 5.2.3 and 5.2.4.

7.3. Results and Discussion

7.3.1. Reactive Distillation Experiments. The reactive distillation column was configured such that 23 wt% citric acid in anhydrous ethanol (F1 in Figure 5.2) was fed near the top of the enriching zone (0.2 m from top of column), while preheated ethanol (F2 in Figure 5.2), either in liquid or vapor form, was fed 1 m above the reboiler at the bottom of the reactive zone. The reflux ratio (L/D) was set to zero, although a small amount of internal reflux was noted experimentally (L/D < 0.05). The reboiler duty was held constant for all experiments. The column operating pressure was limited to 1 atm.

The goal of column operation was to obtain TEC along with some quantity of ethanol as the bottom product. The presence of ethanol in the reboiler was required to control reboiler temperature and thus prevent formation of oligomeric byproducts and degradation products via secondary reactions of residual citric acid, MEC and DEC. We observed such by-products in early experiments under conditions where no water or ethanol were present in the reboiler and a high reboiler temperature (>200°C) was observed.

In batch kinetic experiments (Section 6), we observed that citric acid esterification was relatively slow at 80°C (the normal boiling point of ethanol). This kinetic limitation dictates that relatively low conversion of citric acid and low citrate yields can be expected in the glass column – a significant limitation in the reactive distillation experiments.

Four reactive distillation experiments are reported here for esterification of citric acid with ethanol. In an initial esterification experiment, the column was operated such that the reboiler temperature reached 235°C, indicating that there was neither ethanol nor water in the reboiler. Under these conditions, significant by-products were formed that included citraconic acid as shown by the HPLC analysis in Figure 7.1a. We thus concluded that a feasible reactive distillation process for TEC formation requires the presence of ethanol in the reboiler to maintain a low enough reboiler temperature such that secondary reactions are avoided. Ethanol in the bottoms stream can be easily distilled off under vacuum using a simple distillation column. Results from Run 1 are shown in Table 7.1.
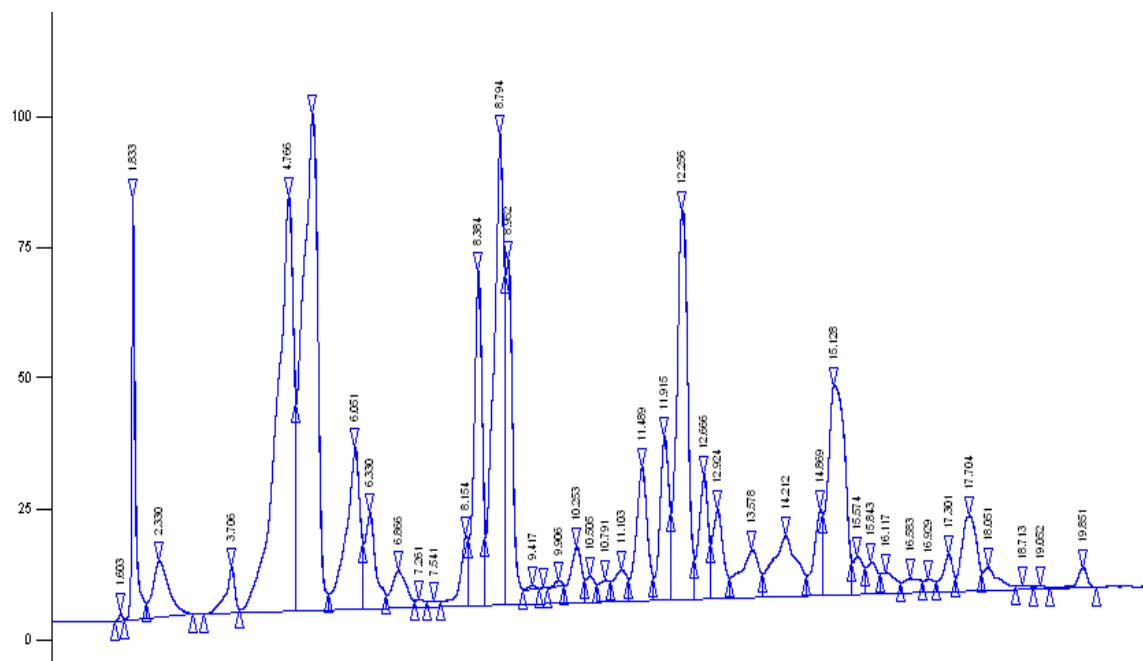
Figure 7.1a: HPLC analysis of reboiler composition from Run 1

In a second run, the reboiler heating rate was adjusted such that the reboiler liquid phase contained 29wt% ethanol at steady state and reboiler temperature was below 110°C. Figure 7.1b shows the HPLC analysis of the reboiler effluent - no products of secondary reactions are detected. Unfortunately, we could not verify that Run 2 achieved steady state even after 16 hr of operation, although it appears to be very close to steady state based on samples collected. Results from Run 2 are shown in Table 7.1. From this run, we conclude that it is desirable to design and operate citric acid esterification such that the reboiler effluent contains approximately 30% ethanol.

In Run 3, carried out at significantly higher feed rates than those in Run 2, steady state operation was achieved. HPLC analysis of the reboiler effluent is very similar to that obtained in Run 2 indicating that no secondary reaction products are detected. Experimental results from this run are shown in Table 7.1; a high concentration of ethanol is observed in the reboiler effluent along with a lower conversion of citric acid than observed in Run 2. Unfortunately, this experiment was not optimized and was not chosen as a basis for simulation.

Run 4 was carried out at similar feed conditions to Run 3, except that the ethanol feed was superheated to 84°C. Results from this run are shown in Table 7.1. Because the results show good conversion to citrate esters, steady state operation, and a reasonable quantity of ethanol in the bottoms stream, we have used it as a basis for column simulations and for determining catalyst efficiency parameters of the pilot-scale column.
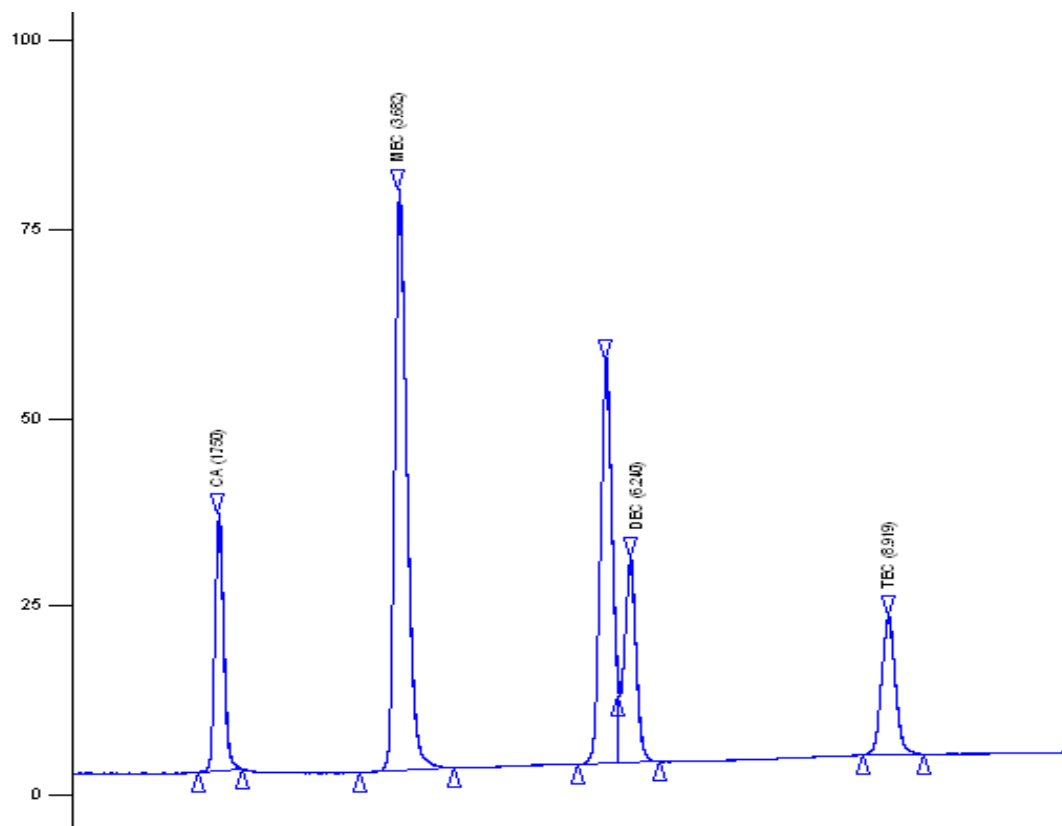
Figure 7.1b: HPLC analysis of reboiler composition from Run 2

7.3.2. Simulation of Pilot-scale Reactive Distillation. Run 4 of the reactive distillation experiments described in Section 7.3.1 was modeled using the RADFRAC module of the Aspen Plus simulation software. RADFRAC simulates reactive distillation by considering phase equilibrium simultaneously with chemical reaction, assuming either that chemical equilibrium is achieved on each stage or that reactions proceed via a specified kinetic rate. In the latter case, an estimate of liquid residence time or liquid holdup on each stage of the distillation column is required. Details of the RADFRAC algorithm are described by Venkataraman et al. (1990). Aspen Plus is further supported by a strong physical and chemical properties database, including hydrodynamics of a structure similar to the Katapak-S structured column packing used in our laboratory column.

Our experimental evaluation of citric acid esterification clearly showed that reaction is slow at column operating conditions, and that solution behavior is significantly non-ideal. Hence, we wrote and incorporated into the Aspen-Plus simulation a subroutine incorporating the activity-based kinetic model for citric acid esterification, based on UNIFAC that we developed in an earlier work[1]. In addition to both resin-catalyzed and self-catalyzed sequential esterification reactions, the kinetic model includes the formation of diethyl ether (DEE) as a byproduct of reaction. The design parameters used in the kinetic model are shown in Table 7.2.

Table 7.1 Results of Pilot-scale Reactive Distillation Experiments

Experiment No.	Run 1[a]	Run 2[b]	Run 3[c]	Run 4[d]
Citric Acid Feed				
Wt% Citric acid	23	23	23	23
Citric acid rate (mol/min)	0.0084	0.0084	0.023	0.023
Ethanol rate (mol/min)	0.11	0.11	0.34	0.34
Temp (^{o}C)	25	25	25	25
Ethanol Feed				
Rate (mol/min)	0.34	0.34	0.32	0.32
Temp (^{o}C)	85	78	78	84
Distillate Temp (^{o}C)	78	78	78	78
Bottoms Temp (^{o}C)	235	87	82	91
CA conversion (%)	-	85	41	61
Distillate composition (wt%)				
Ethanol	-	98.1	98.4	98.2
Water	-	1.2	0.8	1.0
DEE	-	-	-	-
Bottoms composition (wt%)				
Citric acid	-	9.6	13.5	18.2
MEC	-	30.2	9.8	24.6
DEC	-	30.8	2.7	14.0
TEC	-	8.0	0.3	2.2
Ethanol	-	29.0	73.6	40.4
Water	-	0.0	0.0	0.0

[a] Steady state was not reached in this run; high reboiler temperature gave degradation products

[b] Steady state was not verified by multiple samples; results are for sample at 16 hr of operation

[c] Steady state achieved; four samples collected between 6 and 10 hr of operation (10 hr shown)

[d] Steady state achieved; four samples collected between 6 and 16 hr of operation (16 hr shown)

Table 7.2 Design parameters used in Aspen Plus simulations

	Pilot scale experiment simulation	Pilot scale parametric study simulation (Base case)	Plant scale simulation (Scheme 1 – RD column only)
Feed ratio EtOH : Citric acid	53	53	14.6
Top feed - F1			
• Temperature (oC)	25	70	70
• Pressure (atm)	1.0	2.6	2.6
Bottom feed - F2			
• Temperature (oC)	78	78	78
• Pressure (atm)	1.1	2.7	2.7
Total number of stages (N)	10	60	120
Feed stages	Above 3 and On 8	Above 2 and On 58	Above 2 and On 118
Column operating pressure (atm)	1.0	2.5	2.5
Column pressure drop (atm)	0.05	0.1	0.1
Reactive stages	3 to 8	3 to 58	3 to 118
Reflux ratio	0.01	0.01	0.01
Reboil ratio	3.35	5.8	4.8
Murphree stage efficiency (Stages 2 to N)	0.5	0.5	0.5
Liquid holdup per stage from stage 2 to (N-1)	7% of stage volume	7% of stage volume	5.5% of stage volume
Catalytic packing			
• Type	Kerapak	Kerapak	Kerapak
• Height equivalent to theoretical stage (m)	0.6	0.6	0.6
• Fractional approach to maximum capacity	0.135	0.1	0.07
Heat of reactions	0	0	0

The Aspen Plus molecular library contains all species involved in this system except MEC and DEC, so these compounds were defined using the group contribution method. All necessary physicochemical properties used in the simulations are taken as the default values from Aspen-Plus.

The simulation of Run 4 in the pilot-scale column was carried out using the kinetic parameter values given in Tables 7.3a and 7.3b. In the simulation, the citric acid conversion was fitted by a single parameter representing catalyst efficiency (η_{cat}). This parameter was multiplied by the kinetic parameters determined in batch studies[1] to give an effective rate constant for the catalyst in the column. A value of $\eta_{cat} = 75\%$ was found to best fit the experimental results, the calculations for which are shown in the supplementary information. Using this value, the results from the Aspen Plus simulation are in reasonable agreement with the experimental data from Run 4 (Figure 7.2).

Stream 1
Flow 21.7 ml/min

	Wt %
CA	45.05
EtOH	74.95
Water	0.0

Above 3

Stream 2
Flow 18.9 ml/min

	Wt %
EtOH	100

On 8

Stream 3
Flow 28.8 ml/min

	Wt %	Expt
EtOH	98.82	98.24
Water		0.96

Stream 4
Flow 7.2 ml/min

	Wt %	Expt
CA	16.45	18.27
MEC	28.62	24.60
DEC	12.71	13.94
TEC	1.20	2.30
EtOH	40.19	40.37
Water	0.00	0.00
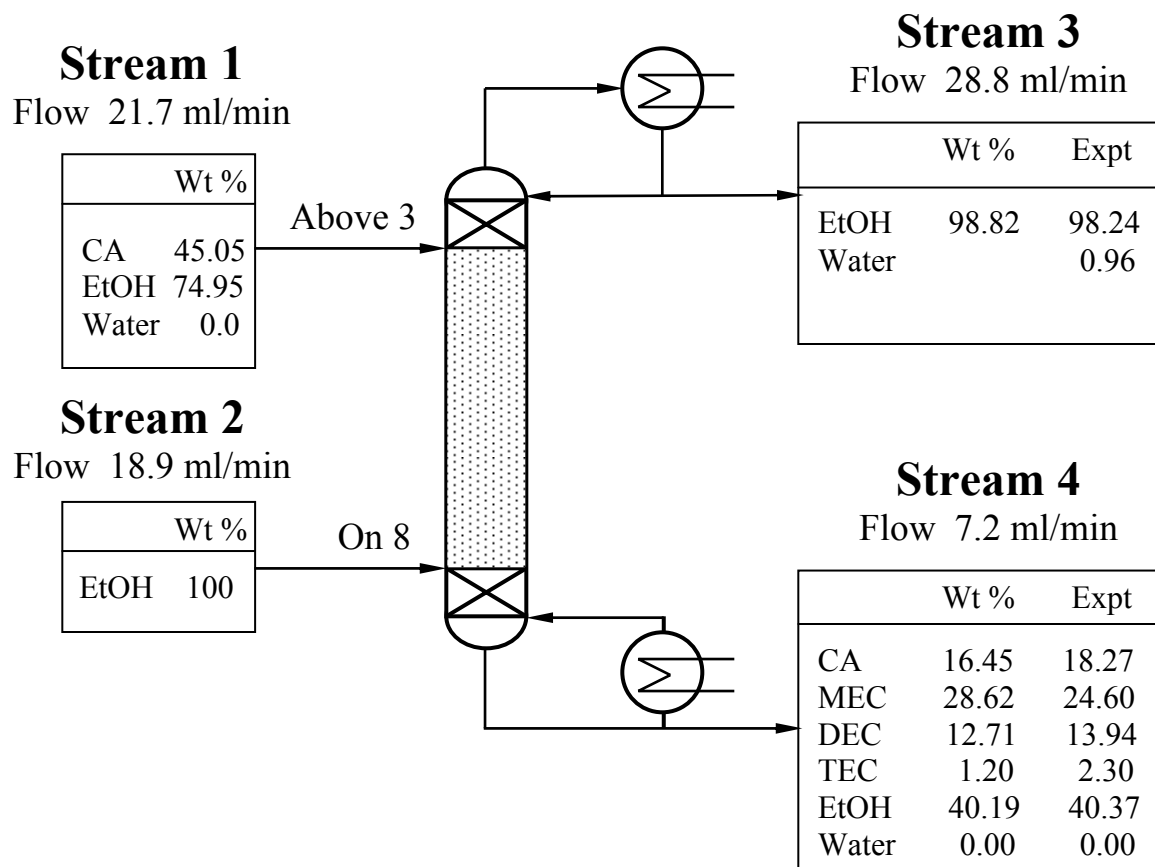
Figure 7.2: Simulation of pilot scale reactive distillation column (Run 4)

Table 7.3a Values of pre-exponential factor and energy of activation for Aspen simulation for the catalyzed reaction

Reaction	k Preexponential factor per gm catalyst basis (kmol i/kgmol n/min)	E Energy of Activation
CA + EtOH ⟷ MEC + W	2.76E+8	76925
MEC + W ⟷ CA + EtOH	4.34E+7	76925
MEC + EtOH ⟷ DEC + W	1.54E+9	83130
DEC + W ⟷ MEC + EtOH	5.67 E+8	83130
DEC + EtOH ⟷ TEC + W	1.64E+7	73210
TEC + W ⟷ DEC + EtOH	4.34E+6	73210
2 EtOH → DEE + Water	2.76E+8	102313

Table 7.3b Values of pre-exponential factor and energy of activation for Aspen simulation for the self-catalyzed reaction

Reaction	k Preexponential factor per gm catalyst basis (kmol i/kgmol n/min)	E Energy of Activation
CA + EtOH ⟷ MEC + W	8.37E+6	70784
MEC + W ⟷ CA + EtOH	1.32E+6	70784
MEC + EtOH ⟷ DEC + W	9.82E+6	72011
DEC + W ⟷ MEC + EtOH	3.61E+6	72011
DEC + EtOH ⟷ TEC + W	5.00E+6	72355
TEC + W ⟷ DEC + EtOH	1.32E+6	72355

The average deviation in species composition for citric acid and its esterification products is about 13%, an acceptable result considering the complexities of the reactive distillation process and the analytical challenges associated with the lack of a pure chemical standard for MEC and DEC. The validity of the simulation is further supported by good agreement between experimental and predicted reboiler and condenser temperatures.

7.4. Extended Pilot-scale Column Simulation

Simulation of the experimental results from Run 4 gave a catalyst efficiency of 75% for the pilot-scale RD column. Using this value, the effect of various column designs and operating parameters such as number of reactive stages, ethanol feed position, column pressure, reflux ratio, and boilup ratio on the performance of a pilot-scale reactive distillation column was investigated. Parameters for the base case simulation of this parametric study are given in the second column of Table 7.2. These parameters are different from those used for simulating the experimental results in two aspects: a 50% citric acid in ethanol solution was used (vs. 24% in Run 4) and the column pressure was taken as 2.5 bar to increase overall column temperature and thus esterification rate to the highest possible values while still avoiding secondary degradation reactions.

Figure 7.3 shows the liquid phase mass fraction profile inside the column for the base case simulation. The ethanol concentration is high everywhere in the column because of the high molar excess of ethanol used; the increase in ethanol concentration at Stage 58 reflects the ethanol feed location. Citric acid concentration decreases quit rapidly within the first few stages below its point of introduction, followed by a decline in MEC concentration. DEC concentration decreases very slowly, indicating that the conversion of DEC to TEC is the slowest reaction and is responsible for the large number of stages required to achieve high TEC yields. The temperature profile of the column is shown in Figure 7.4, a slight exothermic profile is observed as reaction proceeds down the column.
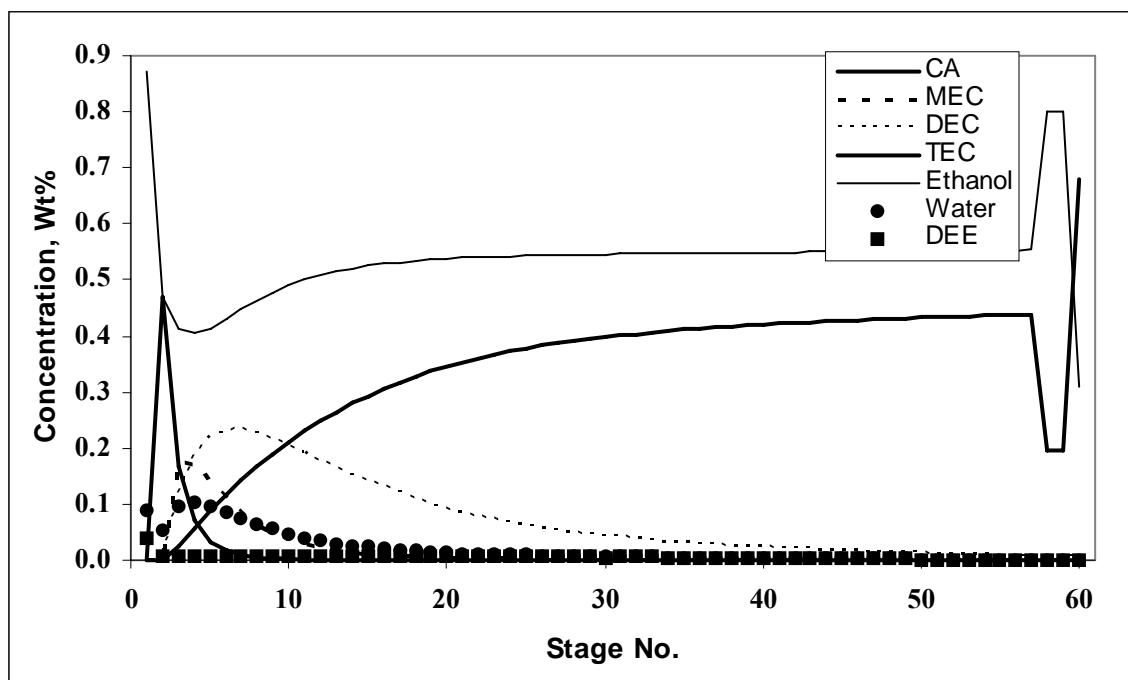
Figure 7.3 Liquid phase composition profile for base case simulation of pilot scale reactive distillation column
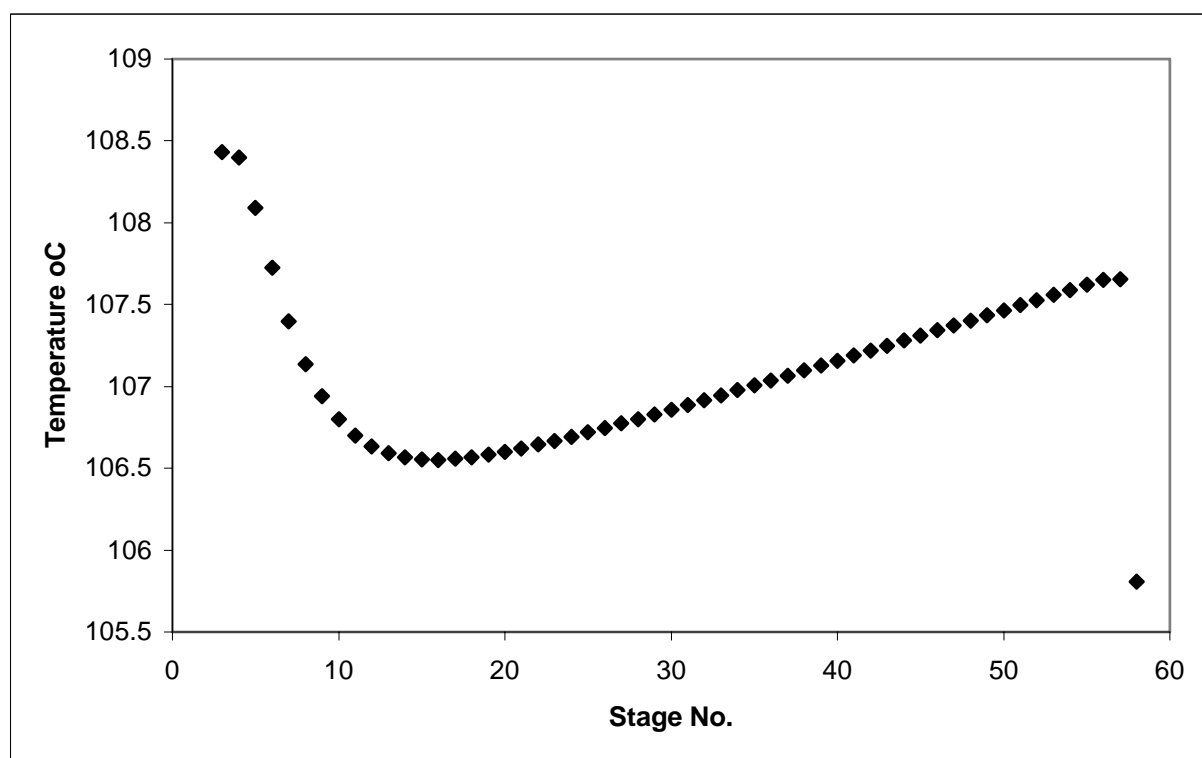
Figure 7.4 Temperature profile for base case simulation of pilot scale reactive distillation column

7.4.1. Effect of Number of Reactive Stages. The number of reactive stages for the parametric simulation is assumed to start from stage 3 up to stage N-2, where N is the

total number of stages in the column. Figure 7.5 shows the effect of increasing the number of reactive stages from 16 (in a 20 stage column) to 116 (in a 120 stage column) on the yield of TEC when the column is operated at 2.5 atm with a reflux ratio of 0.01 and a boilup ratio of 5.8. The reactive stages from 2 up to reboiler (N) have been assumed to have a Murphy stage efficiency of 0.5. There is a rapid increase in TEC yield as the number of stages is increased from 16 to 56 (in a 60 stage column), followed by a further marginal increase in yield as the number of stages is increased to 116 (in a 120 stage column).
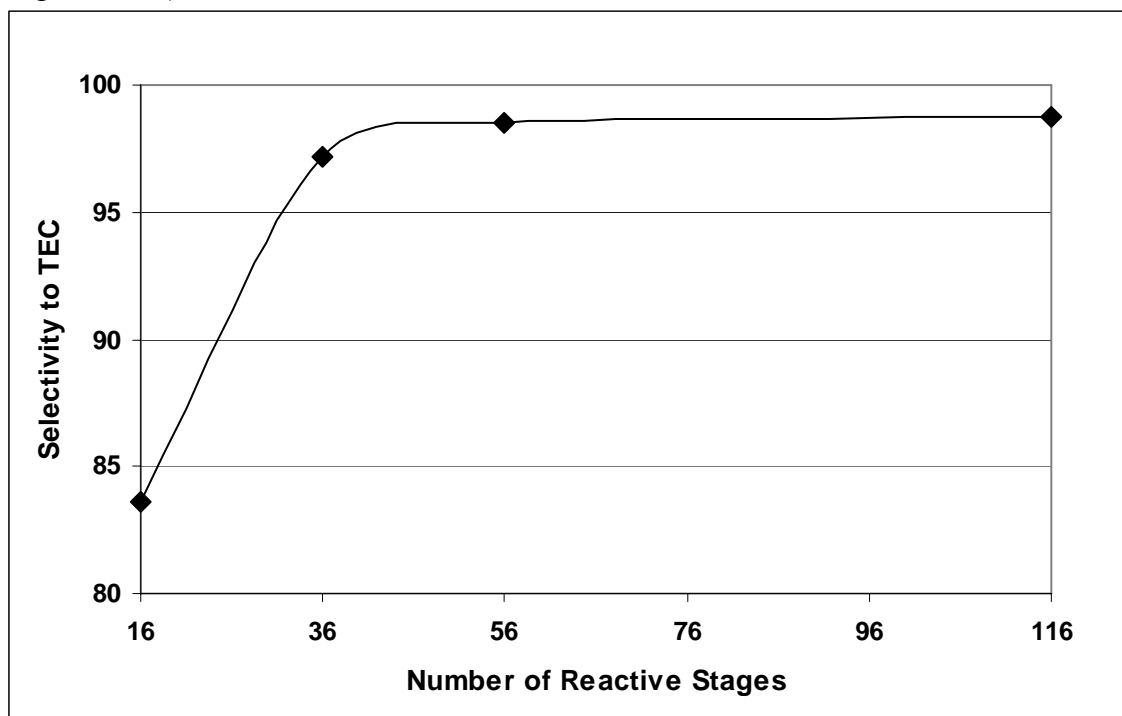
Figure 7.5 Effect of number of reactive stages on selectivity to TEC.
Column conditions : Reflux ratio – 0.01, Boilup ratio – 5.8, Column pressure – 2.5 atm

7.4.2. Effect of Ethanol Feed Position. Figure 7.6 shows the effect of changing ethanol feed position from stage 40 to 58 in a 60 stage reactive distillation column having reactive stages from 3 to 58, operating at 2.5 atm, reflux ratio of 0.01 and boilup ratio of 5.8. Since citric acid is not volatile, its feed position is kept at Stage 2. As the ethanol feed position is lowered from 40 to 58, it is observed that TEC selectivity increases from 96.5% to 98.5% with little change in the reboiler ethanol concentration. This leads to the conclusion that in order to obtain optimum performance for citrate ester formation, the ethanol feed position should be right at the bottom of the reactive zone.
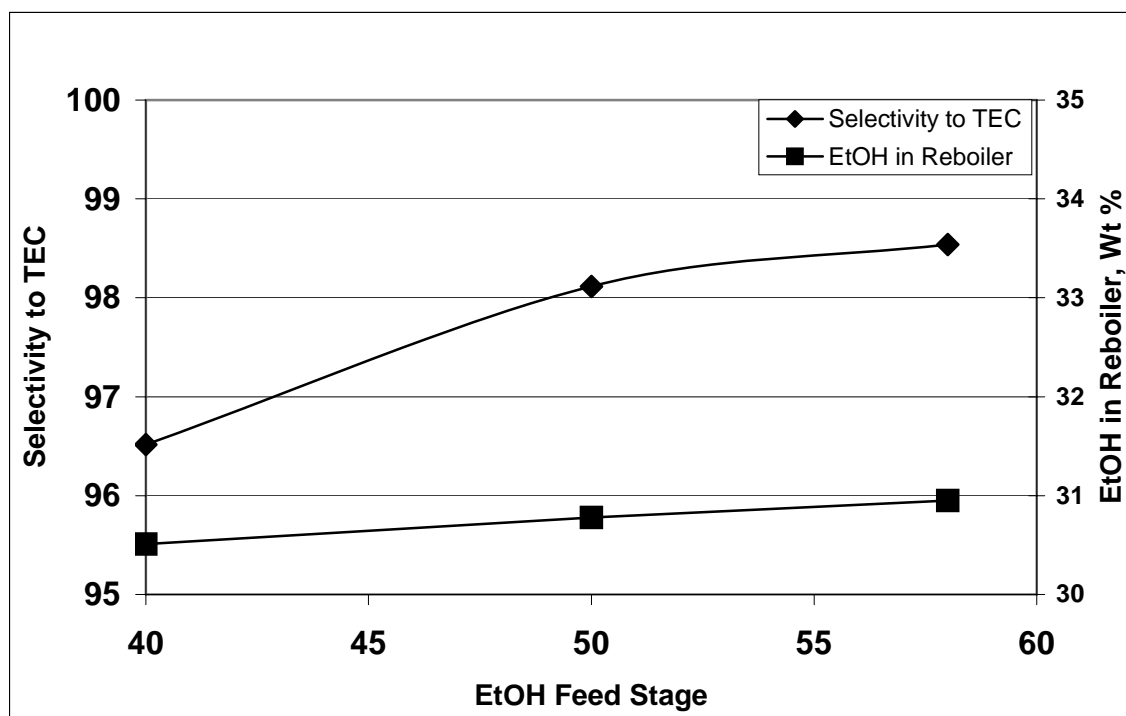
Figure 7.6 Effect of ethanol feed stage position on selectivity to TEC and ethanol in reboiler. Column conditions: 60 stage column having 56 reactive stages, Reflux ratio – 0.01, Boilup ratio – 5.8, Column pressure – 2.5

7.4.3. Influence of Column Operating Pressure. The effect of pressure on the performance of the reactive distillation column has been studied in the pressure range of 1 to 4 bar absolute for a 60 stage column containing 56 reactive stages, operating at a reflux ratio of 0.01 and boilup ratio of 5.8. As pressure increases, so does the reactive zone temperature and therefore the reaction kinetics. As shown in Figure 7.7, the yield of TEC improves up to a pressure of 2.5 bar, above which higher DEE concentrations are seen in the column. These higher DEE concentrations lead to reverse reaction (hydrolysis) that reduces TEC yield; the maximum achievable TEC yield is 98.5% at 2.5 bar.

7.4.4. Effect of Reflux Ratio. The influence of reflux ratio (L/D) over the range 0.01 to 0.5 on TEC yield and ethanol concentration in the reboiler was investigated for the otherwise base-case column. It is seen in Figure 7.8 that TEC yield is highest at the lowest reflux ratio of 0.01 and decreases sharply for L/D > 0.2. A reflux ratio close to zero suggests that water removal out the top of the column is critical for effective column performance; in this mode the column is essentially operating as a reactive stripping column. This mode of operation is feasible because the citric acid feed point is above Stage 2, essentially at the top of the distillation column. The ethanol concentration in the reboiler increases nearly linearly with reflux ratio increasing 0.01 to 0.5, as shown in Figure 7.8.
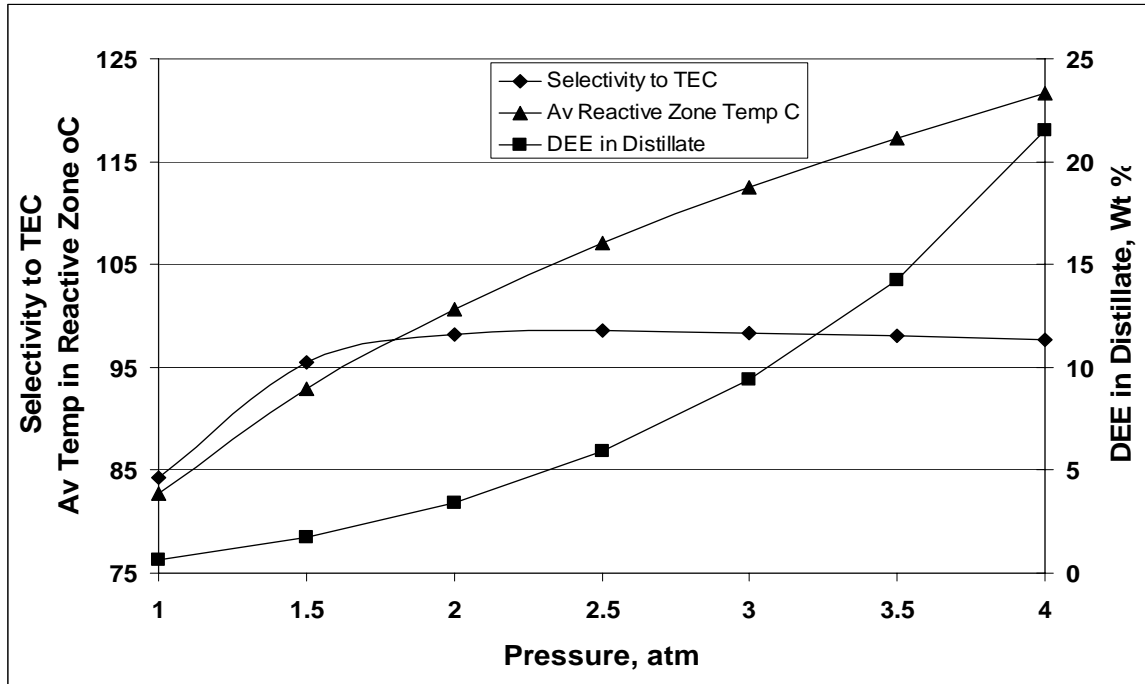
Figure 7.7 Effect of column operating pressure on selectivity to TEC, DEE in distillate and average reactive zone temp °C. Column conditions – 60 stage column having 56 reactive stages, Reflux ratio – 0.01, Boilup ratio – 5.8
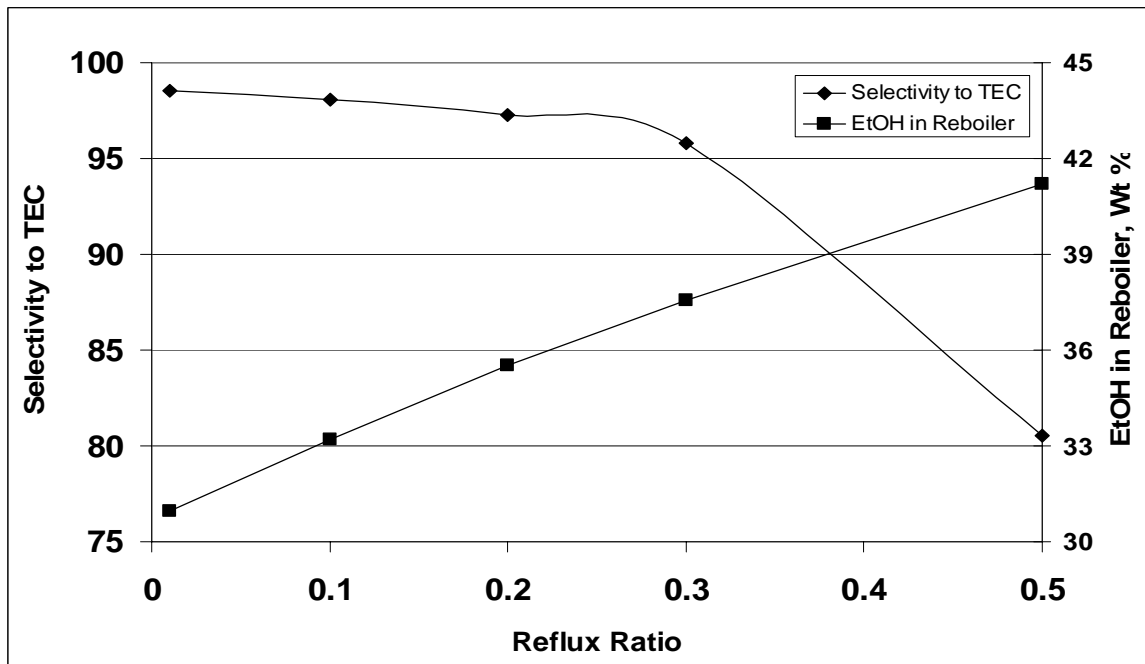
Figure 7.8 Effect of reflux ratio on selectivity to TEC and ethanol in reboiler. Column conditions – 60 stage column having 56 reactive stages, Boilup ratio – 5.8, Column pressure – 2.5 atm

7.4.5. Influence of Boilup Ratio. The effect of changing boilup ratio is given in Figure 7.9 for the base case column. The yield of TEC is practically unchanged above a

boilup ratio of 3, and as expected, the ethanol concentration in the reboiler decreases from 55.2 to 17.3% as boilup ratio increases from 2 to 10. Diethyl ether (DEE) in the distillate decreases from 7.4 to 3.5 wt% with boilup ratio increasing from 2 to 10; increasing boilup ratio increases vapor velocity and thus decreases vapor residence time in the column, therefore reducing the extent of formation of DEE.
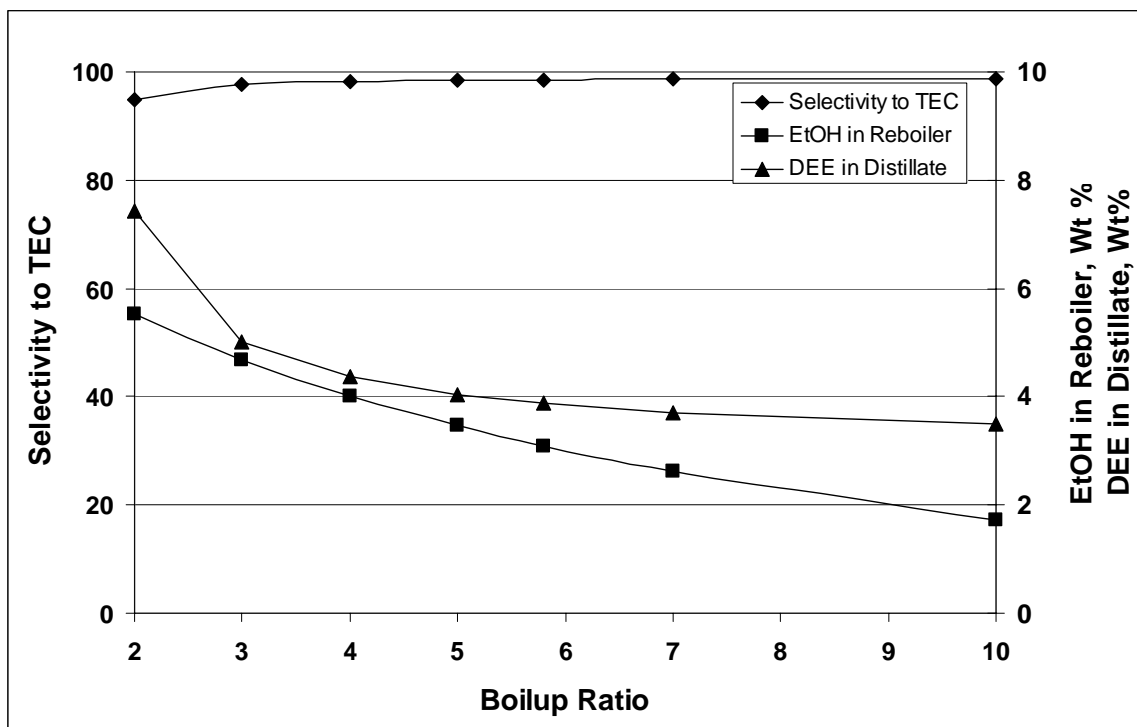
Figure 7.9 Effect of boilup ratio on selectivity to TEC, ethanol in reboiler and DEE in distillate. Column conditions – 60 stage column having 56 reactive stages, Reflux ratio – 0.01, Column pressure – 2.5 atm

7.5. Simulation of Commercial Scale TEC Production

Three process flow schemes have been analyzed to evaluate the feasibility of commercial scale production of 25 million lb/yr of TEC. The three schemes are illustrated in Figure 7.10 and described in some detail below.

In all cases, the feed to the reactive distillation column is a 50 wt% solution of citric acid in ethanol. The citric acid flow is fixed at 4.7 kmol/hr at feed point F1. The solubility of citric acid in ethanol is taken at 50 wt% at 70°C, the ethanol flow rate at F1 being 19.6 kmol/hr. The ethanol flow at F2 is taken at 49.04 kmol/hr. We have not included the premixing and heating tank for citric acid dissolution in ethanol in the proposed process scheme. A Katapak Y170 packing has been considered for the reactive distillation column. It has been attempted to obtain a TEC selectivity of >98.5% wherever possible using all the three process flow schemes.
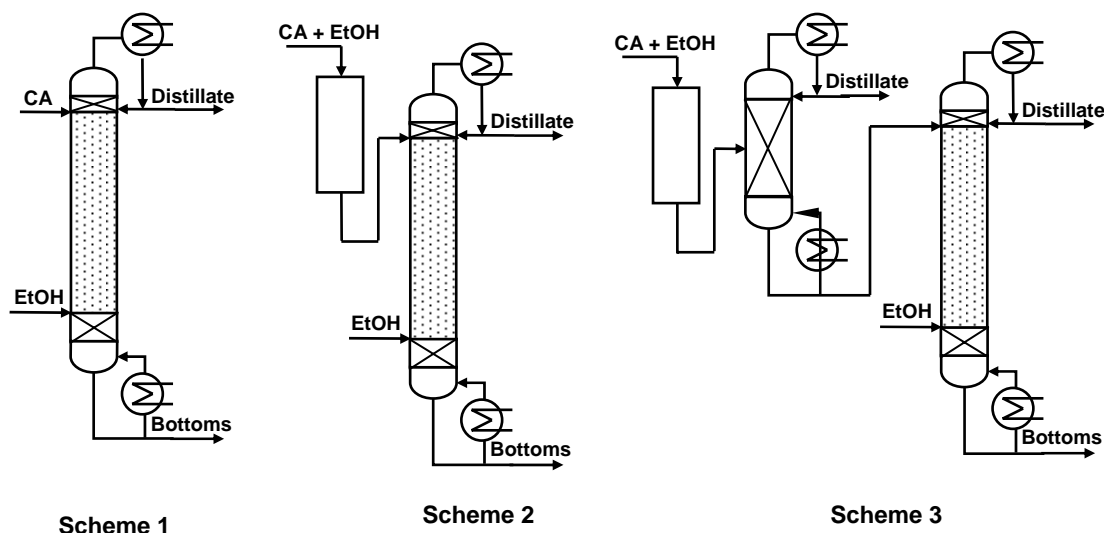
Figure 7.10 **Different reactive distillation configurations for ASPEN simulations: 1) reactive distillation column with non-reactive rectifying, non-reactive stripping and reactive middle section; 2) plug flow pre-reactor followed by reactive distillation column; 3) plug flow pre-reactor followed by a simple distillation column and reactive distillation column. The reactive section is distinguished by the shaded areas**.

Scheme 1: This process consists of a stand-alone reactive distillation column for TEC formation.

Scheme 2: This process consists of a fixed-bed prereactor for initial conversion of citric acid and ethanol to TEC, followed by a reactive distillation column for completion of TEC formation.

Scheme 3: This process consists of the same two unit operations as Scheme 2, with the addition of a regular distillation column following the prereactor to remove product water as its azeotrope with ethanol. The bottom of this distillation column is then fed to the reactive distillation column for completion of TEC formation.

Table 7.2, column 3 gives the important design results and compositions of the product streams from simulations of the three processes.

For Scheme 1, using the above mentioned process flow rates, achieving a TEC yield greater than 98.5%, is not achieved even by using 120 actual stages in the reactive distillation column and operation at 2.5 atm total pressure. The results obtained using a 120 stage column is shown in configuration 1 using scheme 1. If the ethanol flow at feed F2 is increased to 71 kmol/hr it is possible to realize a >98.5% selectivity to TEC, results of which are showed under configuration 2 of scheme 1.

The bottom stream from the reactive distillation column from configuration 2 of scheme 1, which contains mainly ethanol and TEC, is fed to a simple distillation column (not shown in Figure 7.10) containing 14 stages and operating at 0.2 atm total pressure. The bottom stream from this TEC purification column contains 1.1 wt% DEC and 98.9 wt% of TEC; ethanol in the distillate is recycled to the process. The distillate stream from the reactive distillation column can be fed to a simple distillation column (not

shown in Figure 7.10) containing 15 stages in order to separate the DEE from the ethanol-water mixture. The distillate from this column is rich in DEE and contains 0.42 wt % ethanol and 0.85 wt % water. The bottoms stream from this distillation column contains 2.94 wt % DEE in ethanol; this stream can be sent to the ethanol purification train for recycling.

In process Scheme 2, the citric acid – ethanol feed mixture is fed to a fixed-bed, plug flow pre-reactor. The goal of adding such a pre-reactor is to approach equilibrium in the esterification reactions prior to the reactive distillation column, thus reducing column size. The pre-reactor in the simulation operated at $100^{o}C$ and 2.3 atm total pressure: at these conditions, a conversion close to the equilibrium value is obtained for a reactor space time of approximately 27 hours – an admittedly large value that could be substantially reduced by increasing reactor temperature. The outlet from the pre-reactor is directed to the reactive distillation column operating at 2.5 atm pressure. As seen in Table 7.6, the number of stages required in the reactive distillation column for Scheme 2 is 120, essentially the same value required for Scheme 1. This is because the reactions of citric acid and MEC are rapid relative to the conversion of DEC to TEC; therefore column size is almost entirely dictated by the kinetics of TEC formation from DEC.

The bottom stream from the RD column is fed to a simple distillation column in order to purify the formed TEC. A purified stream containing 1.57 wt% DEC and 98.43 wt% TEC was obtained.

A comparison of schemes 1 to 2 shows that the ethanol to citric acid ratio used in scheme 1 is higher compared to that in scheme 2 and 3.

For Scheme 3, a pre-reactor was used at the same conditions as in Scheme 2, but the effluent from per-reactor was fed to a simple distillation column of 10 stages operating at atmospheric pressure. In this column, about 90% of the water produced in reaction is removed as its azeotrope with ethanol in the distillate stream. The bottom stream from this column is then fed to a reactive distillation column having 60 stages and operating at 1.6 atm pressure. The bottom stream from the reactive distillation column is fed to a simple distillation column having 14 stages operating under 0.2 atm pressure in order to separate the ethanol from the TEC. The bottom stream from this TEC purification column contains 1.40 wt% DEC and 98.60 wt% TEC. Results from this simulation are shown under configuration 1 of scheme 3.

In another variation of scheme 3, azeotropic ethanol is used. Using an 80 stage reactive distillation column good conversion results are obtained as shown under configuration 2 of scheme 3.

Analysis of these three commercial scale configurations indicates that a large reactive distillation column (up to 120 stages) is required to achieve high TEC yields from citric acid. The addition of a pre-reactor and an intermediate distillation column to remove some of the product water considerably reduces the required size of the reactive distillation column, although the addition of just a pre-reactor has little or no effect on the subsequent column size.

7.6. Conclusions

It has been confirmed using experimental results and mathematical simulation that it is viable to produce TEC in high purity using reactive distillation. Using the limited conversion results obtained in the glass reactive distillation column, arising from pressure and height limitation of the reactive zone, catalyst efficiency is determined and the same is used to simulate a pilot scale column to obtain high selectivity of TEC. Parameter simulation studies were performed.

It was observed that about 60 stages are required in order to obtain high selectivity of TEC. The operating pressure of the column is limited by the maximum operating temperature of the Amberlyst-15 catalyst which is 120°C. Moreover as the operating temperature increases the DEE in distillate increases rather rapidly. The reactive distillation column is best operated at very low reflux ratios.

Simulation of a commercial scale process to produce 25 million lb of TEC per annum has been presented using three different schemes. The reactive distillation column required is large (120 stages); the size of the column is somewhat reduced by introduction of a pre-reactor followed by distillation to remove product water prior to introduction into the reactive distillation column.

SECTION EIGHT

KINETICS OF SUCCINIC ACID ESTERIFICATION

8.1. Background

Synthesis and use of bio-based chemicals has been attracting increased attention, due to rising global crude oil prices and the increasing desire to reduce dependence on petroleum. Bio-based chemicals are prime candidates for replacement of petroleum-based products since they are environmentally friendly, have low toxicity and high degradability. The esters of bio-based organic acids fall into the category of benign or green solvents, and are promising replacements for halogenated petroleum-based solvents in a wide variety of applications.

Succinic acid is a di-basic acid having two carboxylic acid functional groups and one hydroxyl group. Succinic acid can be esterified with alcohols such as ethanol and n-butanol through a series of reactions to yield di-ethyl succinate (DES) and di-n-butyl succinate. A schematic reaction scheme for esterification of succinic acid with an alcohol is shown in Figure 8.1.
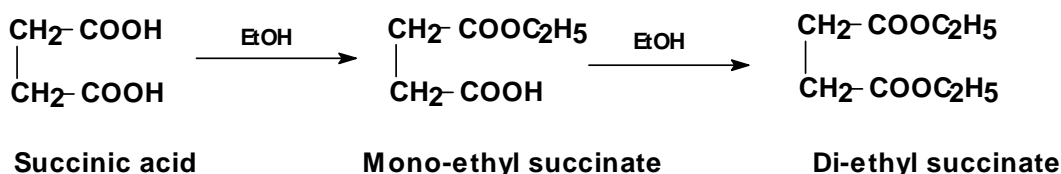
Figure 8.1 Schematic Diagram for Esterification of Succinic Acid
with Ethanol

A conventional process to synthesize DES typically would use a stream of succinic acid and ethanol which are esterified in a batch or CSTR using sulfuric acid as a homogeneous catalyst. Many of the difficulties associated with use of homogeneous catalysts can be eliminated through use of heterogeneous catalysts like ion exchange resins or supported clays. The heterogeneous catalyst allows easy mechanical separation of the catalyst from reaction media by decantation or filtration, reduces or eliminates corrosion problems, and facilitates continuous process operation.

Prior information on the kinetics of succinic acid esterification with ethanol or n-butanol is scarce in the literature. Saigo et al.[105] have synthesized succinic acid esters using phosphinechalcogenide as a catalyst. Recently Benedict et al.[106] have described a process for the pervaporation assisted esterification of lactic and succinic acids with downstream ester recovery using Amberlyst XN-1010 and Nafion NR50 as catalyst.

Succinate esters are of low toxicity and low vapor pressure and have exceptional solvent properties, making them attractive candidates as replacements for petroleum based solvents. Succinate esters are intermediates in the production of poly-butylene succinate (PBS) polymers, a polyester composed of succinic acid and 1,4-butanediol. The butanediol is produced by hydrogenation of succinate diester via the same technology in which maleic anhydride is commercially hydrogenated to 1,4-butanediol.[107,108] Hence the entire PBS polymer is a succinate based, bio-renewable

material. These PBS polymers have many potential applications in automobile parts and consumer goods and could ultimately approach the commodity status of petroleum based polyethylene and polypropylene. Esters of succinic acid mainly the dimethyl esters are being investigated for their insulinotropic potential in rats.[109-113]

At present no information available in the open literature describing the kinetics of succinic acid esterification with ethanol in presence of ion exchange resin catalysts. In order to fill this gap, we have conducted isothermal experimental batch studies on the esterification of succinic acid with ethanol in presence of Amberlyst-15 ion exchange resin as catalyst. A pseudo-homogeneous mole fraction based kinetic model is presented for correlation of the experimental data.

This kinetic model is useful for process design of continuous succinic acid esterification system using reactive distillation as an example.

8.2. Experimental

8.2.1. Materials. For the kinetic experiments, anhydrous succinic acid crystals were obtained from Sigma-Aldrich. Absolute ethanol (99% purity) and HPLC grade water were obtained from J. T. Baker Inc. The strong acid cation exchange resin catalyst Amberlyst-15 (Rohm and Haas, Philadelphia, PA) was obtained in H^+ form and was used without modification. Purity of all chemicals was checked by gas chromatography or HPLC.

8.2.2. Analysis. The presence of succinic acid, mono-ethyl succinate (MES) and diethyl-succinate (DES) was first confirmed by GC-MS analysis of their trimethylsilyl (TMS) derivatives. For reaction samples, succinic acid and its ethyl esters (MES and DES) were quantitatively analyzed on a Hewlett-Packard 1090 HPLC using a reversed phase C18 column (Novapak, 3.9 mm x 150 mm) held at 40^oC. Water/acetonitrile (ACN) mixtures, buffered at pH=1.3, were used as mobile phase (0.8 ml/min) in a gradient mode (0% ACN (t=0) to 60% ACN (t=20 min) to 90% ACN (t=25 min) to 0% ACN (t=28 min)), and species were quantified by UV detection (Hitachi L400H) at a wavelength of 210 nm. Succinic acid and DES were identified and quantified by comparing HPLC retention time and peak area with their respective calibration standards. Pure standard for MES could not be obtained commercially. On a mass basis, the response factor for DES was found to be 1.11 times higher than that for succinic acid; therefore response factor for MES was calculated as an average of response factors for succinic acid and DES. Using this response factor for MES, the carbon balance for each reaction sample, based on succinic acid and its esters, was in the range of ±10%.

Reaction samples were analyzed for water content using a Varian 3700 gas chromatograph equipped with thermal conductivity detector (TCD) and a Stainless Steel column (4 m x 3.25 mm) packed with a liquid stationary phase of Porapak Q. The column oven was subject to a temperature program involving heating from 413 K (after a 2-min hold) to 493 K (and held for 6 min) at a rate of 20 K min^{-1}. n-Butanol was used as an internal standard. High purity helium (99.999 % pure) was used as carrier gas at a flow rate of 20 ml/min. The injector and detectors were maintained at 493 K.

Samples were analyzed for ethanol and DEE using a Perkin-Elmer Sigma-2000 gas chromatograph equipped with flame ionization detector (FID) and a bonded-phase

fused-silica capillary column (SPB-5, 30 m x 0.53 mm). The column oven was subject to a temperature program involving heating from 313 K (after a 7-min hold) to 473 K (and held for 5 min) at a rate of 2 K min^{-1}. Anhydrous toluene was used as an internal standard. High purity helium (99.999 % pure) was used as carrier gas at a flow rate of 10 ml/min. The injector and detectors were maintained at 493 K.

8.2.3. Batch Kinetic Experiments. Esterification reactions at 78°C were performed in a 2 x 10^{-4} m^3 jacketed glass reactor equipped with a re-circulating constant temperature oil bath. The reaction volume was maintained between 100 to 110 ml. A spiral coil condenser, open to the atmosphere, was placed on top of the reactor. The glass reactor was equipped with temperature and stirrer speed monitoring devices and a sampling port. In operation, measured quantities of ethanol and succinic acid were added to the reactor, and heating and stirring were started simultaneously. Once the desired temperature was achieved, usually in about 15 minutes, catalyst (Amberlyst-15 ion exchange resin) was added for the case of resin catalyzed reactions and stirring speed was increased to 800 rpm. This point in time was considered as the zero reaction time. Samples were withdrawn at specific time intervals and immediately transferred to an ice bath (prior to analysis) in order to ensure that no further reaction took place.

For reaction temperatures of 90°C and above, esterification was performed in a 1 x 10^{-4} m^3 stainless steel autoclave (5000 Multi-reactor System, Parr Instrument Co.) equipped with temperature and stirrer speed monitors and a sampling port. In operation, measured quantities of ethanol, succinic acid and catalyst for the resin catalyzed reaction cases were added to the reactor and heating was started with slow stirring. The total reaction volume was maintained between 55 to 60 ml. The desired temperature was achieved in about 15 minutes, at which time the stirring rate was increased to 740 rpm. This time was considered as the zero reaction time. Samples were withdrawn at specific time intervals through a cooled metal tube and immediately transferred to an ice bath in order to ensure no further reaction took place before analysis. All samples were analyzed using the method described under section 8.2.2.

8.3. Results and Discussion

Several batch kinetic experiments were carried out to study the effects of reaction temperature, catalyst loading, and initial reactant molar ratio on the heterogeneously catalyzed esterification of succinic acid with ethanol. It was observed from initial experimentation that the external mass-transfer resistances were negligible at a stirring speed of above 500 rpm. Hence all kinetic experiments were performed at 800 rpm. The influence of internal mass transfer resistances were neglected for reactions catalyzed by Amberlyst-15 (**discussed in detail in Section 2**).   Table 8.1 shows the reaction conditions for all of the experimental studies performed in this work.

8.3.1. Effect of Reaction Temperature. Effect of increasing reaction temperature from 78° to 120°C on the esterification of succinic acid with ethanol at a catalyst loading of 2 wt% and an initial mole ratio of ethanol to succinic acid of 10:1 was studied in the present work. Figures 8.2 to 8.6 show the effect of reaction temperature at 78°C, 90°C,

Table 8.1 Summary of Kinetic Studies and Average Prediction Errors

Run No.	Figure No.	Mole Ratio EtOH:CA	Catalyst Loading (wt%)	Temp (°C)	Average % Error over experiment (Eq 8.4)					Absolute Error in mole fraction				
					SA	MES	DES	EtOH	Water	SA	MES	DES	EtOH	Water
1	2	10:1	2	78	44.3	14.8	21.5	2.23	8.62	0.55	0.60	0.29	1.74	0.64
2	3	10 : 1	2	90	41.6	12.8	30.5	1.7	14.4	0.52	0.41	0.54	1.37	0.99
3	4	10 : 1	2	100	38.5	9.3	22.0	1.5	10.7	0.37	0.29	0.49	1.19	0.89
4	5	10 : 1	2	110	30.3	6.5	16.9	1.5	8.9	0.24	0.21	0.49	1.21	0.90
5	6	10 : 1	2	120	33.6	9.0	11.3	1.0	6.1	0.22	0.22	0.38	0.81	0.65
6	7	10 : 1	1	90	30.2	12.9	41.7	1.8	21.3	0.56	0.38	0.49	1.51	1.12
7	8	10 : 1	3	90	41.2	9.1	19.2	1.3	7.3	0.31	0.27	0.37	1.00	0.60
8	9	10 : 1	5	90	49.3	12.4	15.3	1.0	6.2	0.34	0.33	0.44	0.80	0.58
9	10	10 : 1	1	78	23.4	11.6	43.1	3.8	21.2	0.35	0.42	0.69	2.97	1.70
10	11	10 : 1	5	78	23.5	10.9	18.8	1.8	8.3	0.16	0.37	0.64	1.38	1.02
11	12	15 : 1	2	90	42.7	15.0	26.4	0.5	8.9	0.25	0.29	0.31	0.46	0.37
12	13	20 : 1	2	90	41.1	14.2	28.0	0.8	13.1	0.19	0.20	0.26	0.71	0.49

100 °C, 110 °C and 120 °C respectively. It can be observed from these Figures that the rate of conversion of succinic acid and MES clearly increases with increasing reaction temperature.
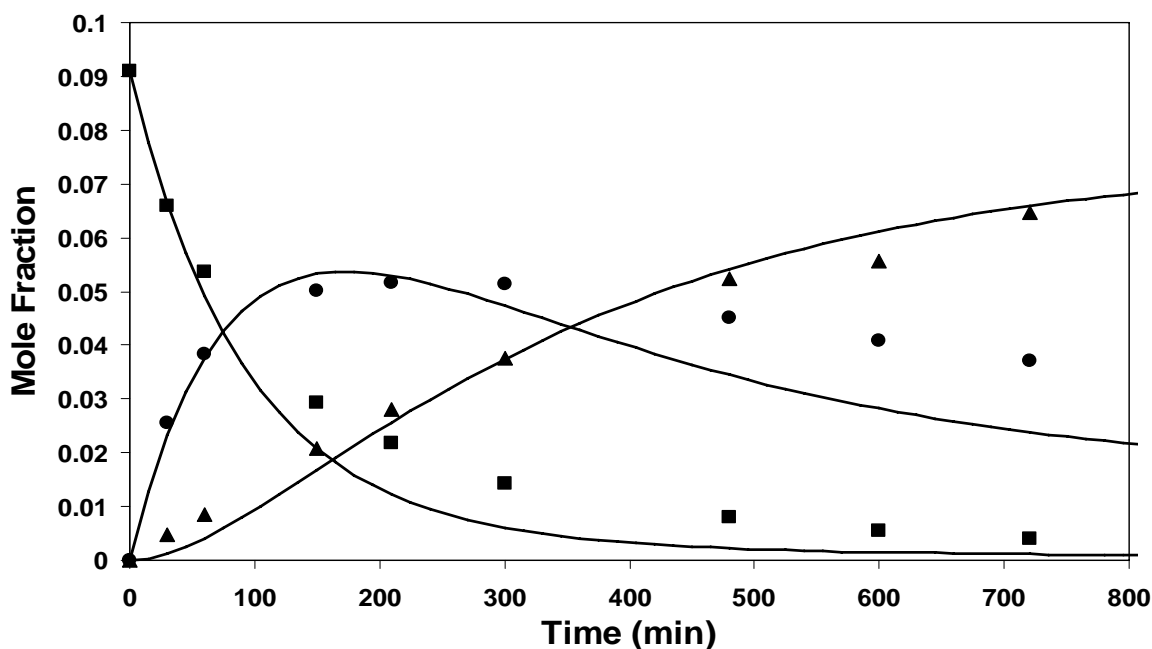
Figure 8.2 Esterification of Succinic acid Solution Catalyzed by Ion-Exchange Resin. Reaction Conditions: Mole Ratio of Ethanol to Succinic acid, 10:1; Catalyst Loading, 2 wt%; Reaction Temperature, 78°C. (■, SA; ●, MES; ▲, DES)
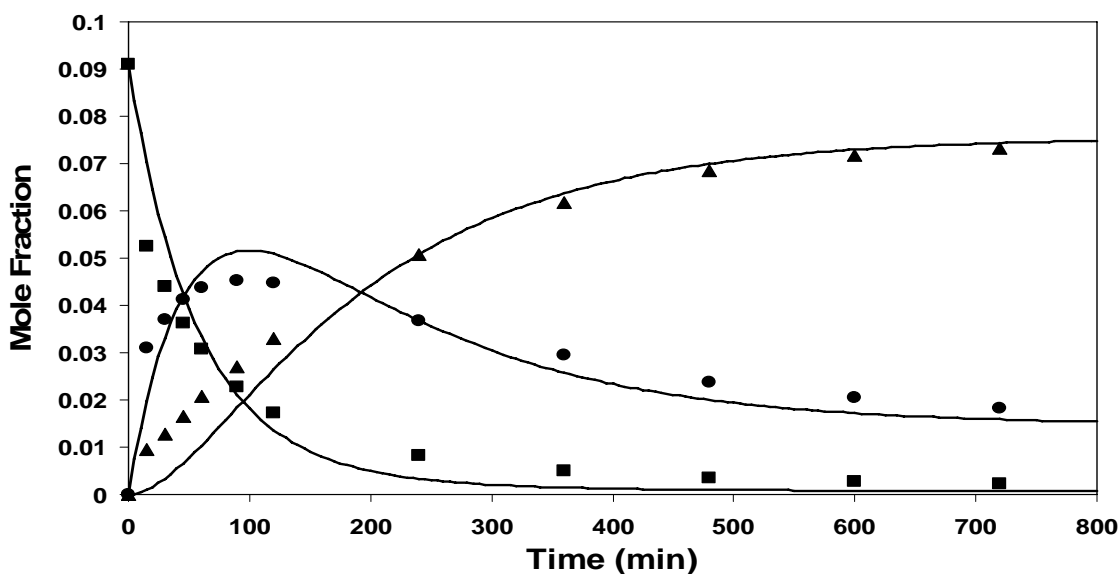
Figure 8.3 Esterification of Succinic acid Solution Catalyzed by Ion-Exchange Resin. Reaction Conditions: Mole Ratio of Ethanol to Succinic acid, 10:1; Catalyst Loading, 2 wt%; Reaction Temperature, 90°C. (■, SA; ● , MES; ▲, DES)
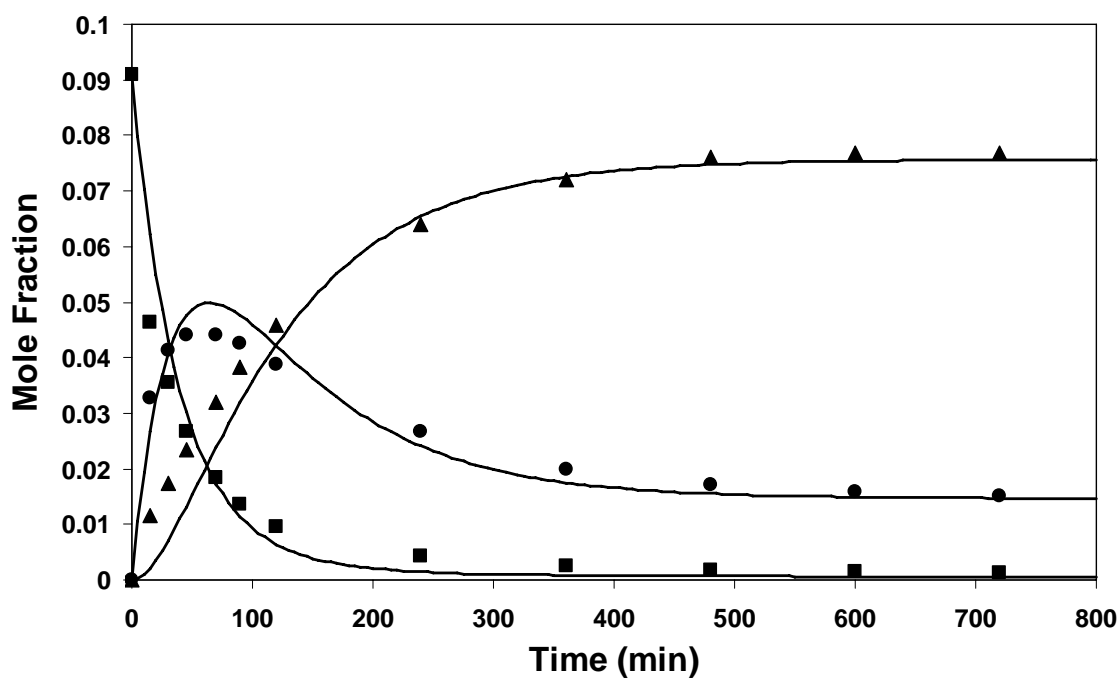
Figure 8.4 Esterification of Succinic acid Solution Catalyzed by Ion-Exchange Resin. Reaction Conditions: Mole Ratio of Ethanol to Succinic acid, 10:1; Catalyst Loading, 2 wt%; Reaction Temperature, 100°C. (■, SA; ●, MES; ▲, DES)

Figure 8.5 Esterification of Succinic acid Solution Catalyzed by Ion-Exchange Resin. Reaction Conditions: Mole Ratio of Ethanol to Succinic acid, 10:1; Catalyst Loading, 2 wt%; Reaction Temperature, 110°C. (■, SA; ●, MES; ▲, DES)

Figure 8.6 Esterification of Succinic acid Solution Catalyzed by Ion-Exchange Resin. Reaction Conditions: Mole Ratio of Ethanol to Succinic acid, 10:1; Catalyst Loading, 2 wt%; Reaction Temperature, 120°C. (■, SA; ●, MES; ▲ , DES)

8.3.2. Effect of Catalyst Loading. The effect of varying catalyst loading from 1 to 5% on the esterification of succinic acid with ethanol at 90°C and an initial mole ratio of ethanol to succinic acid of 10:1 was studied in the present work. Figures 8.3 and 8.7 to 8.9 show the effect of 2%, 1%, 3% and 5% catalyst loading on the rate of reaction at 90°C. It can be observed from these figures that the reaction rate increases with increase in catalyst loading which is an expected observation for ion exchange resin catalyzed reactions.

Additional data for effect of catalyst loading has been studied for reaction temperature of 78 C and initial mole ratio of ethanol to succinic aicd of 10:1. Figures 8.2, 8.10 and 8.11 show the effect of catalyst loading of 2%, 1% and 5% on the reaction kinetics respectively.

8.3.3. Effect of Initial Reactant Mole Ratio of ethanol to succinic acid. The effect of reactant mole has been studied at reaction temperature of 90 C and 2% catalyst loading. Figures 8.3, 8.12 and 8.13 show the effect of initial reactant mole ratio of ethanol to succinic acid at 10:1, 15:1 and 20:1 respectively.
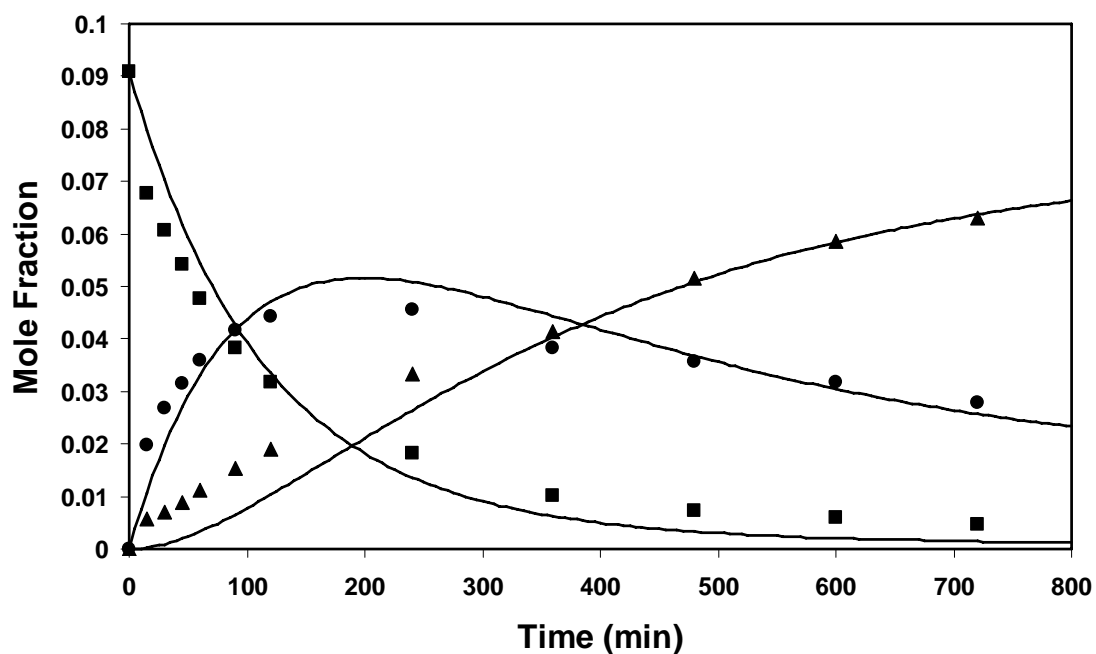
Figure 8.7 Esterification of Succinic acid Solution Catalyzed by Ion-Exchange Resin. Reaction Conditions: Mole Ratio of Ethanol to Succinic acid, 10:1; Catalyst Loading, 1 wt%; Reaction Temperature, 90°C. (■ , SA; ● , MES; ▲ , DES)
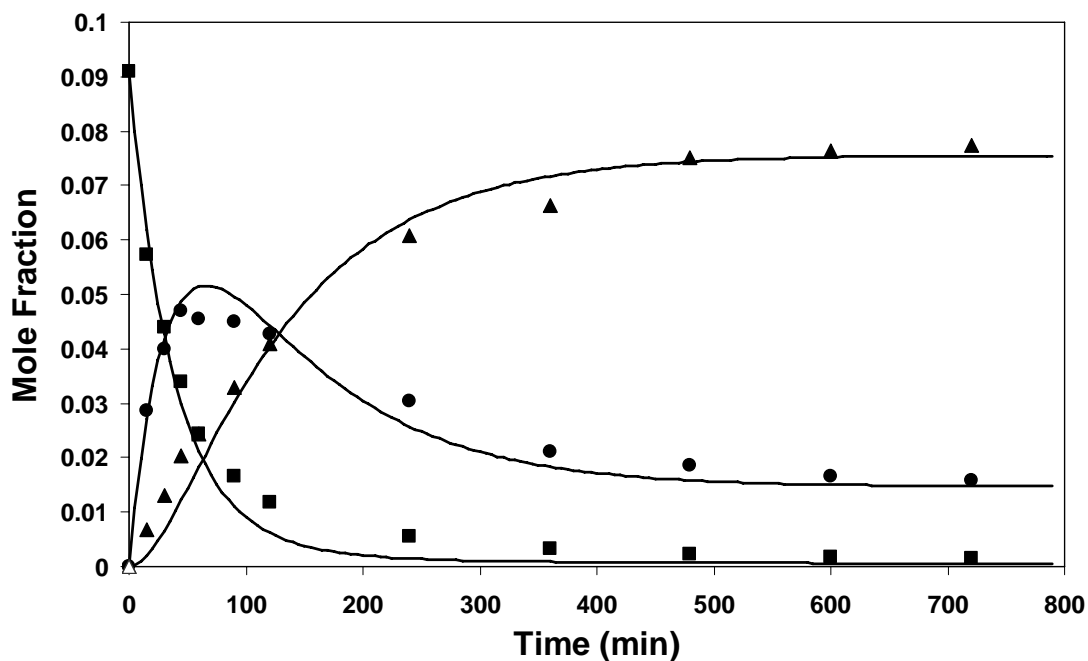
Figure 8.8 Esterification of Succinic acid Solution Catalyzed by Ion-Exchange Resin. Reaction Conditions: Mole Ratio of Ethanol to Succinic acid, 10:1; Catalyst Loading, 3 wt%; Reaction Temperature, 90°C. (■ , SA; ● , MES; ▲ , DES)
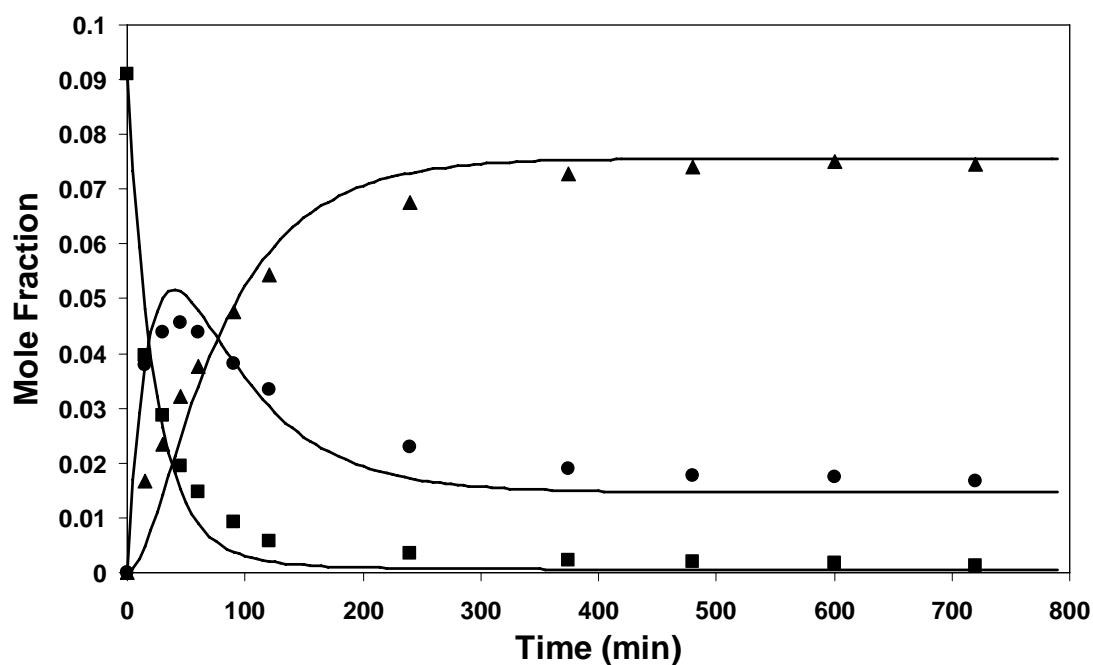
Figure 8.9 Esterification of Succinic acid Solution Catalyzed by Ion-Exchange Resin. Reaction Conditions: Mole Ratio of Ethanol to Succinic acid, 10:1; Catalyst Loading, 5 wt%; Reaction Temperature, 90°C. (■ , SA; ● , MES; ▲ , DES)
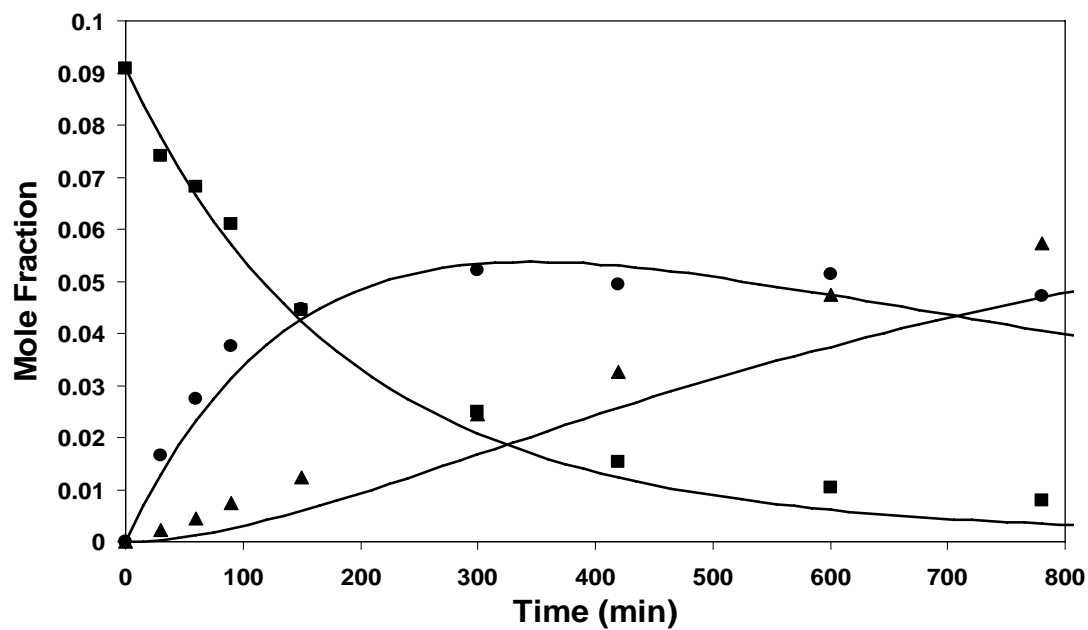
Figure 8.10 Esterification of Succinic acid Solution Catalyzed by Ion-Exchange Resin. Reaction Conditions: Mole Ratio of Ethanol to Succinic acid, 10:1; Catalyst Loading, 1 wt%; Reaction Temperature, 78°C. (■ , SA; ● , MES; ▲ , DES)
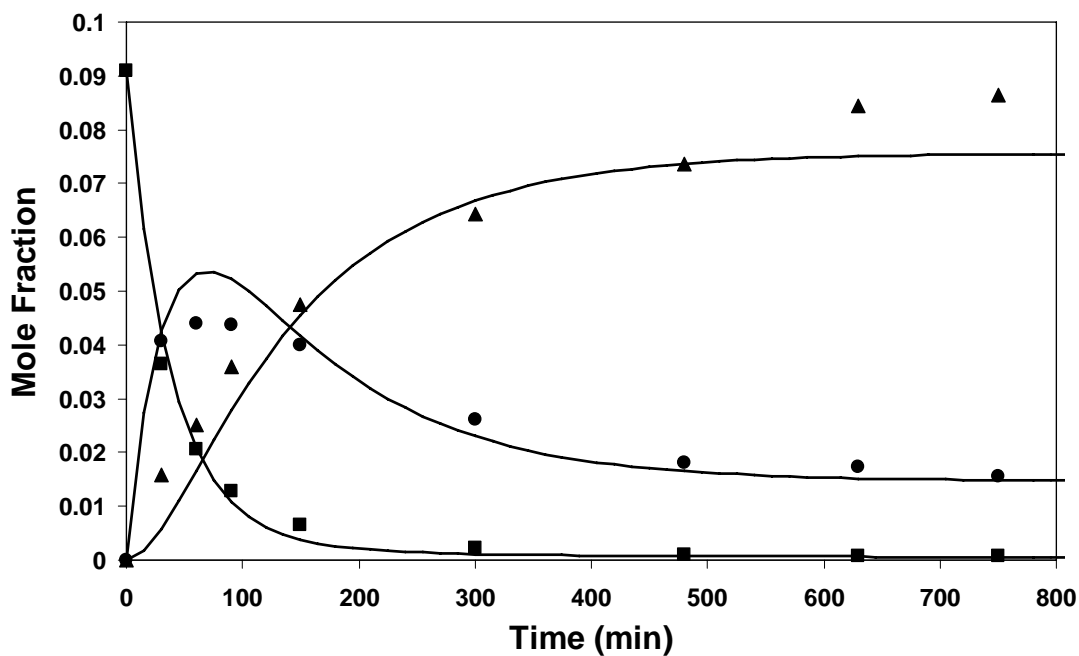
Figure 8.11 Esterification of Succinic acid Solution Catalyzed by Ion-Exchange Resin. Reaction Conditions: Mole Ratio of Ethanol to Succinic acid, 10:1; Catalyst Loading, 5 wt%; Reaction Temperature, 78°C. (■ , SA; ● , MES; ▲ , DES)
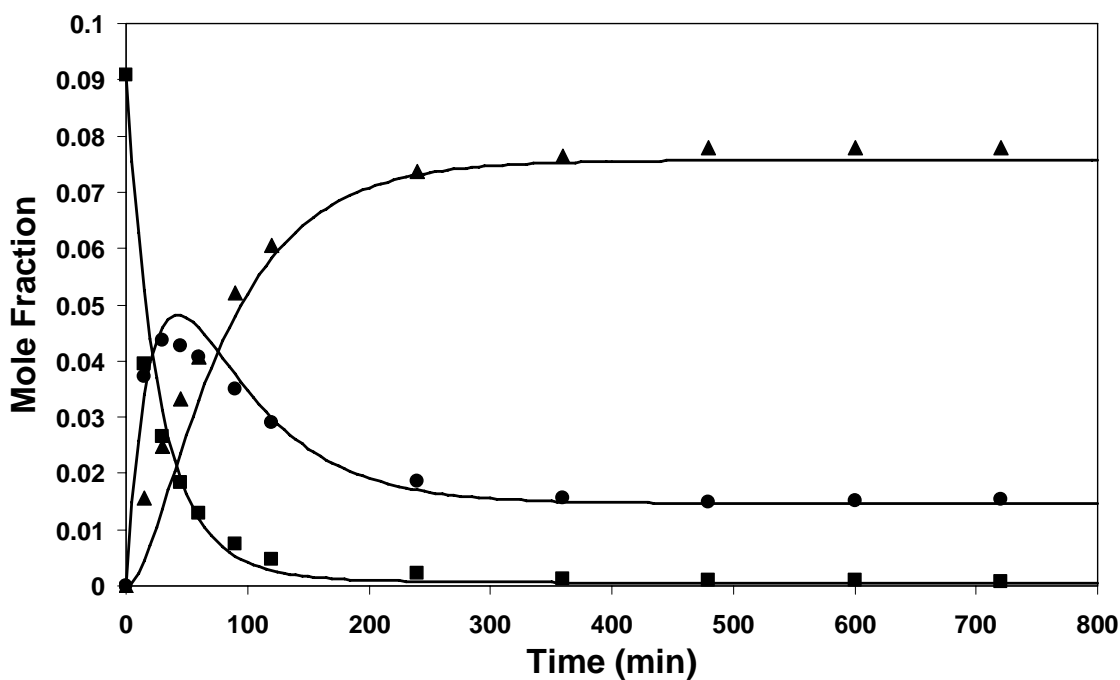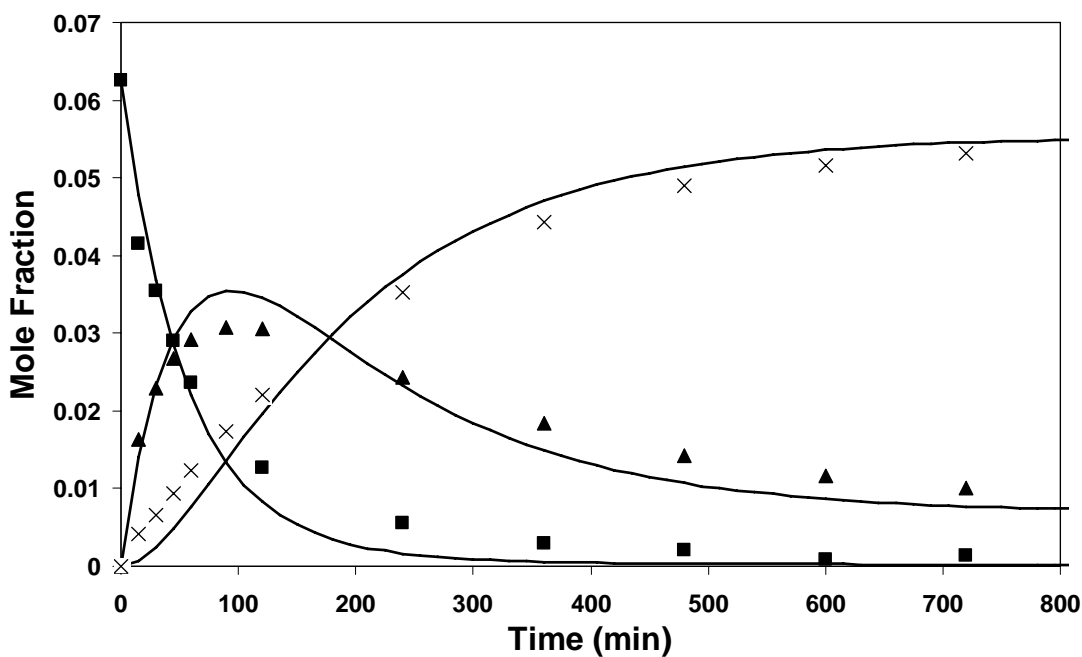

Figure 8.12 Esterification of Succinic acid Solution Catalyzed by Ion-Exchange Resin. Reaction Conditions: Mole Ratio of Ethanol to Succinic acid, 15:1; Catalyst Loading, 2 wt%; Reaction Temperature, 90°C. (■ , SA; ● , MES; ▲ , DES)
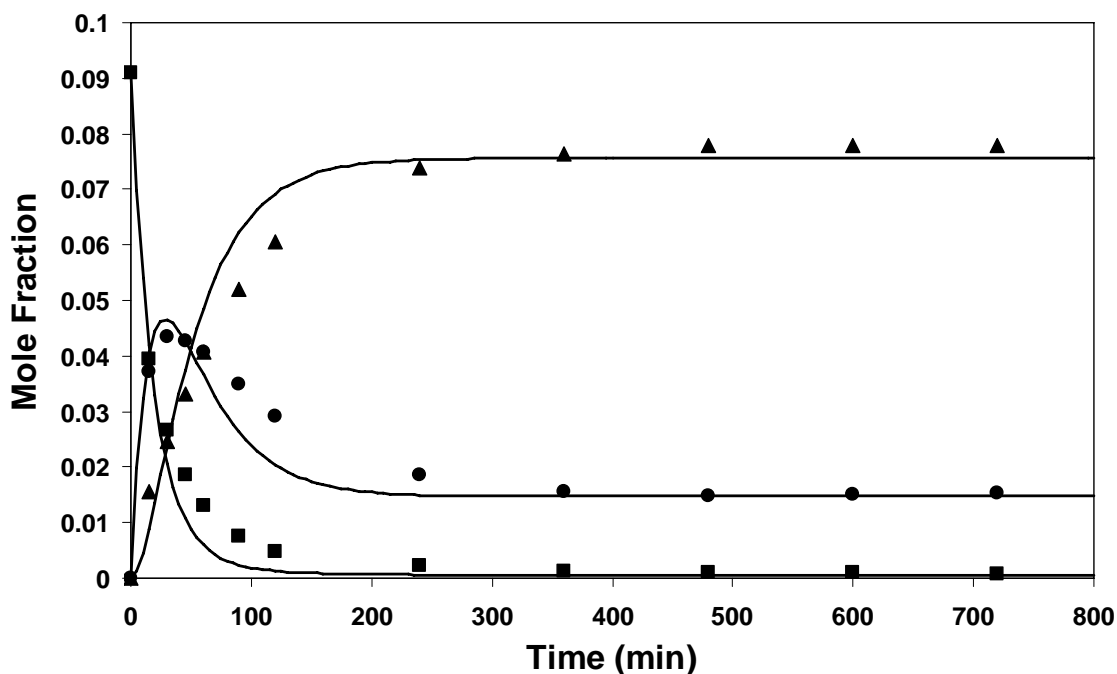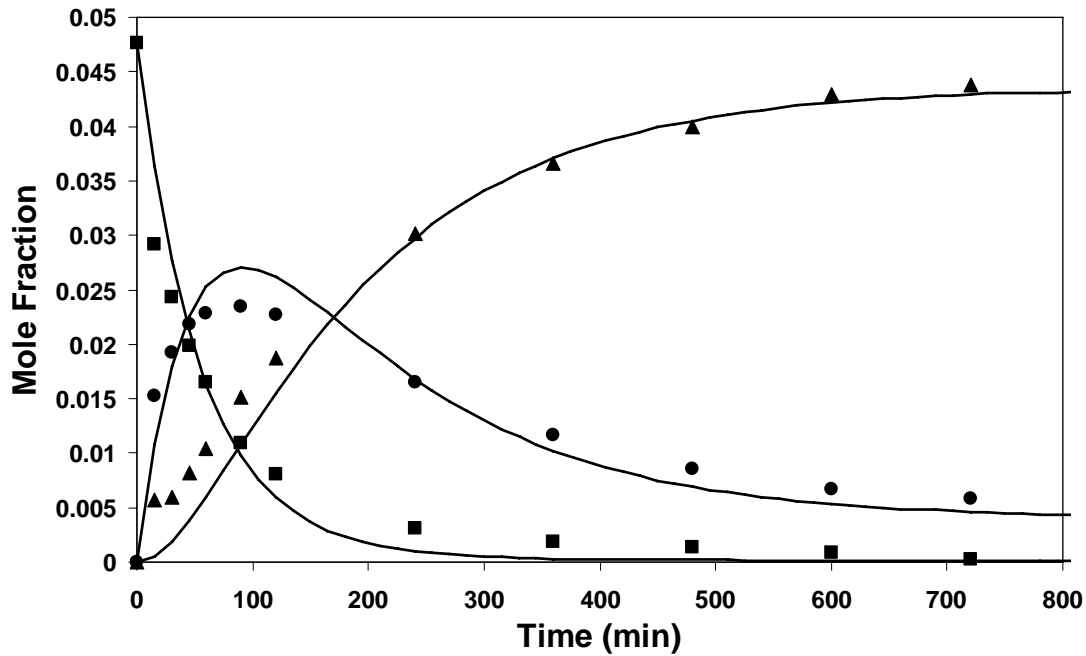
Figure 8.13 **Esterification of Succinic acid Solution Catalyzed by Ion-Exchange Resin. Reaction Conditions: Mole Ratio of Ethanol to Succinic acid, 20:1; Catalyst Loading, 2 wt%; Reaction Temperature, 90°C. (■, SA; ●, MES; ▲ , DES)**

8.4. Kinetic Model

8.4.1. Kinetic Pathways. Reaction 8.1 and 8.2 below describe the pathways involved in the esterification of succnic acid with ethanol

$$SA + EtOH \underset{k_1/Keq_{a,1}}{\overset{k_1}{\rightleftharpoons}} MES + W \qquad \text{...(8.1)}$$

$$MES + EtOH \underset{k_2/Keq_{a,2}}{\overset{k_2}{\rightleftharpoons}} DES + W \qquad \text{...(8.2)}$$

Reactions 1 and 2 are the series reactions to form DES from sucicnic acid by sequential formation of MES (Equation 8.1).

Based on the above reactions, a pseudo-homogeneous, mole fraction based model has been developed.

8.4.2. Chemical equilibrium constant. The chemical equilibrium constants are given by

$$Keq_{x,i} = \prod x_i^{v_i} \qquad \text{...(8.3)}$$

The value of mole fraction equilibrium constants $Keq_{x,i}$ for reactions under consideration were determined by analysis of the experimental data at long reaction times (e.g. approaching equilibrium) and were found to be 5.27 and 1.15 for the formation of

MES and DES respectively. These constants were taken to be independent of temperature.

8.4.3. Determination of Rate Constants. The kinetic equations were numerically integrated via a fourth order Runge-Kutta method using ordinary differential equation solver ode23 in Matlab 7.0. Using an initial set of rate constants the liquid phase mole fractions for all species over the course of reaction were calculated and compared with the experimental values. The rate constants were then incremented sequentially in order to minimize the sum of the mean square differences given by

$$F_{min}{}^2 = \frac{\sum\limits_{samples} \left(x_{j,cal} - x_{j,expt} \right)^2}{n_{samples}} \qquad \ldots(8.4)$$

After this optimization, the calculated mole fractions of the components involved in the reaction were compared to the experimental ones, giving the mean relative deviation, represented both absolutely and as on % basis as shown below

$$F_{abs} = \frac{\sum\limits_{samples} \left| x_{j,cal} - x_{j,expt} \right|}{n_{samples}} \times 100\,\% \qquad \ldots(8.5)$$

$$F_{rel} = \frac{\sum\limits_{samples} \left| \dfrac{x_{j,cal} - x_{j,expt}}{x_{j,expt}} \right|}{n_{samples}} \times 100\,\% \qquad \ldots(8.6)$$

The values of the absolute mole fraction error F_{abs} and relative mole fraction error F_{rel} are reported as in Table 8.1.

8.4.4. Mole Fraction based Kinetic Model. Kinetics of the ion exchange resin-catalyzed esterification of succinic acid, data for which were determined from Runs 1 to 12 has been described using a pseudo-homogeneous model.

The rate of formation of each species in the reaction mixture is described by Equations (7) to (12) given below:

$$-\frac{dx_{SA}}{dt} = w_{cat}\, K_1 \cdot \left(x_{SA} \cdot x_{EtOH} - \frac{x_{MES} \cdot x_W}{Keq_{x,1}} \right) \qquad \ldots(8.7)$$

$$-\frac{dx_{MES}}{dt} = w_{cat}\, K_2 \left(x_{MES} \cdot x_{EtOH} - \frac{x_{DES} \cdot a_W}{Keq_{x,2}} \right) + w_{cat}\, K_1 \left(\frac{x_{MES} \cdot x_W}{Keq_{x,1}} - x_{SA} \cdot x_{EtOH} \right) \qquad \ldots(8.8)$$

$$-\frac{dx_{DES}}{dt} = w_{cat}\, K_2 \left(\frac{x_{DES} \cdot x_W}{Keq_{x,2}} - x_{MES} \cdot x_{EtOH} \right) \qquad \ldots(8.9)$$

$$-\frac{dx_{EtOH}}{dt} = w_{cat}\, K_1 \left(x_{SA} \cdot x_{EtOH} - \frac{x_{MES} \cdot x_W}{Keq_{x,1}} \right) + w_{cat}\, K_2 \left(x_{MES} \cdot x_{EtOH} - \frac{x_{DES} \cdot x_W}{Keq_{x,2}} \right) \qquad \ldots(8.10)$$

$$-\frac{dx_W}{dt} = w_{cat}\,K_1\left(\frac{x_{MES}.x_W}{Keq_{x,1}} - x_{SA}.x_{EtOH}\right) + w_{cat}\,K_2\left(\frac{x_{DES}.x_W}{Keq_{x,2}} - x_{MES}.x_{EtOH}\right) \quad ...(8.11)$$

where
$$K_i = k_i^o\,\exp\left(\frac{-E_{A,i}}{RT}\right) \qquad ...(8.12)$$

Six adjustable parameters for the resin-catalyzed reactions, the pre-exponential factors k_1^o and k_2^o, and the energies of activation $E_{A,1}$ and $E_{A,2}$ have been fitted to the experimental data of Runs 1 to 12. The values of the kinetic parameters are shown in Table 8.2. Predicted mole fractions are given as continuous lines in Figures 8.2 to 8.13. It can be observed from Figures 8.2 to 8.13 that the correlation between the experimental data and the calculated trend lines is satisfactory. The residual errors are shown in Table 8.1.

Table 8.2 Parameters for resin-catalyzed reactions

Parameters	Units	Values
k_1^o	(total moles) kg sol (mole i)$^{-1}$ kg$_{cat}^{-1}$ s^{-1}	37
k_2^o	(total moles) kg sol (mole i)$^{-1}$ kg$_{cat}^{-1}$ s^{-1}	624
$E_{A,1}$	kJ/kmol	44287
$E_{A,2}$	kJ/kmol	749370
$Keq_{x,1}$		5.27
$Keq_{x,2}$		1.15

For succinic acid the average % error in mole fraction is highest in the region when the succinic acid concentration falls very low. Large errors are also observed in the case of DES in the initial reaction period up to about 300 minutes where its concentration is low.

For the reaction system under consideration the formation of di-ethyl ether, from the etherification reaction of two molecules of ethanol has not been considered, since the esterification reaction is very fast in comparison to the kinetics of di-ethyl ether formation. The kinetics of di-ethyl ether formation has been described under section 6.4.5.

8.5. Conclusions

Experimental reaction kinetic studies were performed in order to study the effect of reaction temperature from 78 to 120°C initial mole ratio of ethanol to succinic acid varying from 10:1 to 20:1 and catalyst concentration varying from 1% to 5% heterogeneously catalyzed using Amberlyst-15, an ion exchange resin. The kinetics of esterification reaction has been correlated using a mole fraction based pseudo homogeneous model. The rate expressions are applicable over a wide range of catalyst concentration, molar ratios of reactants and temperature. The model presented in this

paper can be conveniently used for design and scale up of integrated processes like reactive distillation for synthesis of DES.

8.6. Nomenclature and Units

DES	di-ethyl succinate
E_A	energy of activation, kJ kmol^{-1}
EtOH	ethanol
K_1	rate constant for catalyzed reaction, (total moles) kg sol (mole i)$^{-1}$ kg$_{cat}^{-1}$ s$^-$
k_{cat}	pre-exponential factor for catalyzed reaction, (total moles) kg sol (mole i)$^{-1}$ kg$_{cat}^{-1}$ s^{-1}
K_x	mole fraction based reaction equilibrium constant
MES	mono-ethyl succinate
R	Gas constant; kJ/kmol.K
SA	succinic acid
T	Temperature
W	water
w_{cat}	Catalyst concentration (kg$_{cat}$/kg$_{soln}$)
x_j;	Mole fraction of jth component in liquid phase solution

Subscripts

i	reaction index
j	component in solution

Greek letters

γ	liquid phase activity coefficient

PROPIONIC ACID ESTERIFICATION

9.1. Experimental

9.1.1. Materials. For the kinetic experiments, propionic acid and ethyl propionate were purchased from Sigma-Aldrich. Absolute ethanol (99% purity) and HPLC grade water were obtained from J. T. Baker Inc. The strong acid cation exchange resin catalyst Amberlyst-15 (Rohm and Haas, Philadelphia, PA) was obtained in H^+ form and was used without modification. Purity of all chemicals was checked by gas chromatography or HPLC.

9.1.2. Analysis. Reaction samples were analyzed for water, ethanol, propionic acid and ethyl propionate, using a Varian 3700 gas chromatograph equipped with thermal conductivity detector (TCD) and a Stainless Steel column (4 m x 3.25 mm) packed with a liquid stationary phase of Porapak Q. The column oven was subject to a temperature program involving heating from 413 K (after a 2-min hold) to 493 K (and held for 6 min) at a rate of 20 K min^{-1}. n-Butanol was used as an internal standard. High purity helium (99.999 % pure) was used as carrier gas at a flow rate of 20 ml/min. The injector and detectors were maintained at 493 K. The material carbon balance for each reaction sample, based on propionic acid, ethyl propionate, water and ethanol, was in the range of ±10%.

9.1.3. Batch Kinetic Experiments. Esterification reactions were performed in a 1 x 10^{-4} m^3 stainless steel autoclave (5000 Multi-reactor System, Parr Instrument Co.) equipped with temperature and stirrer speed monitors and a sampling port. In operation, measured quantities of ethanol, propionic acid and catalyst for the resin catalyzed reaction cases were added to the reactor and heating was started with slow stirring. The total reaction volume was maintained between 55 to 60 ml. The desired temperature was achieved in about 15 minutes, at which time the stirring rate was increased to 740 rpm. This time was considered as the zero reaction time. Samples were withdrawn at specific time intervals through a cooled metal tube and immediately transferred to an ice bath in order to ensure no further reaction took place before analysis. All samples were analyzed using the method described under Section 9.1.2.

9.2. Results and Discussion

Several batch kinetic experiments were carried out to study the effects of reaction temperature, catalyst loading, and initial reactant molar ratio on the heterogeneously catalyzed esterification of propionic acid with ethanol. Table 9.1 shows the reaction conditions for all of the experimental studies performed in this work.

Table 9.1 Summary of Kinetic Studies

Run No.	Figure No.	Mole Ratio EtOH:PA	Catalyst Loading (wt%)	Temp (^{o}C)
1	1	3	3	60
2	2	3	3	70
3	3	3	3	80
4	4	3	3	90
5	5	3	1	70
6	6	1	1	70
7	7	1	2	70
8	8	1	3	70

9.2.1. Effect of Reaction Temperature. Effect of increasing reaction temperature from 60° to 90°C on the esterification of propionic acid with ethanol at a catalyst loading of 3 wt% and an initial mole ratio of ethanol to propionic acid of 3:1 was studied in the present work. Figures 9.1 to 9.4 show the effect of reaction temperature at 60°C, 70°C, 80°C and 90°C respectively. It can be observed from these Figures that the rate of conversion of propionic acid clearly increases with increasing reaction temperature.
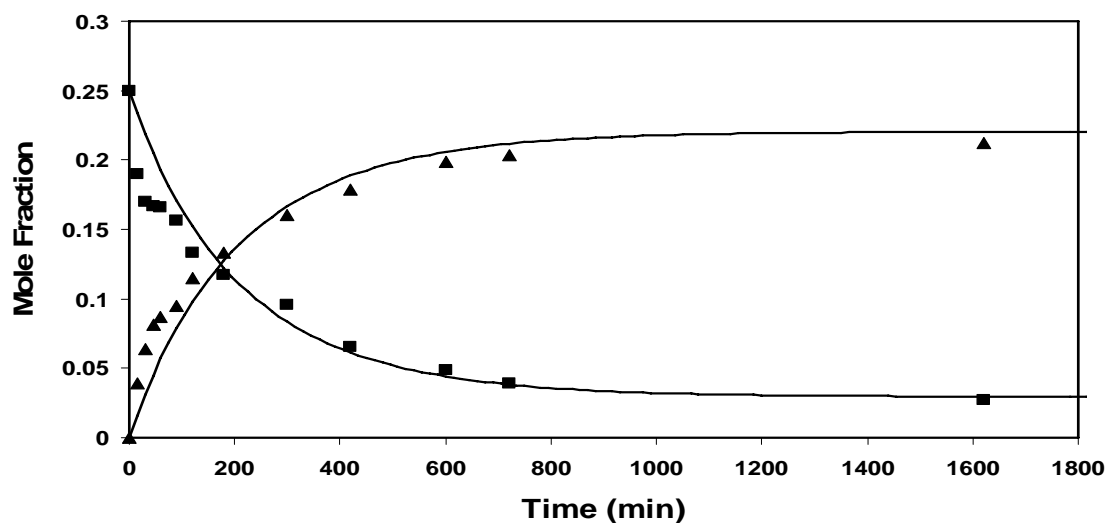
Figure 9.1 **Esterification Reaction Catalyzed by Ion-Exchange Resin. Reaction Conditions: Mole Ratio of Ethanol to Propionic acid, 3:1; Catalyst Loading, 3 wt%; Reaction Temperature, 60°C. (■, PA; ▲, EP)**

9.2.2. Effect of Catalyst Loading. The effect of varying catalyst loading from 1 to 3% on the esterification of propionic acid with ethanol at 70°C and an initial mole ratio of ethanol to propionic acid of 3:1 and 1:1 was studied in the present work. Figures 9.2 and 9.5 show the effect of 3% and 1% catalyst loading on the rate of reaction at 70°C and initial ethanol to propionic acid ratio of 3:1. Figures 9.6 to 9.8 show the effect of 1%, 2% and 3% catalyst loading on the reaction rate at 70°C and initial ethanol to propionic acid ratio of 1:1. It can be observed from these figures that the reaction rate clearly increases with increase in catalyst loading which is an expected observation for ion exchange resin catalyzed reactions.

9.3.3. Effect of Initial Reactant Mole Ratio of ethanol to propionic acid. The effect of reactant mole has been studied at reaction temperature of 70°C and 3% catalyst loading. Figures 9.2 and 9.8 show the effect of initial reactant mole ratio of ethanol to propionic acid at 3:1 and 1:1 respectively.
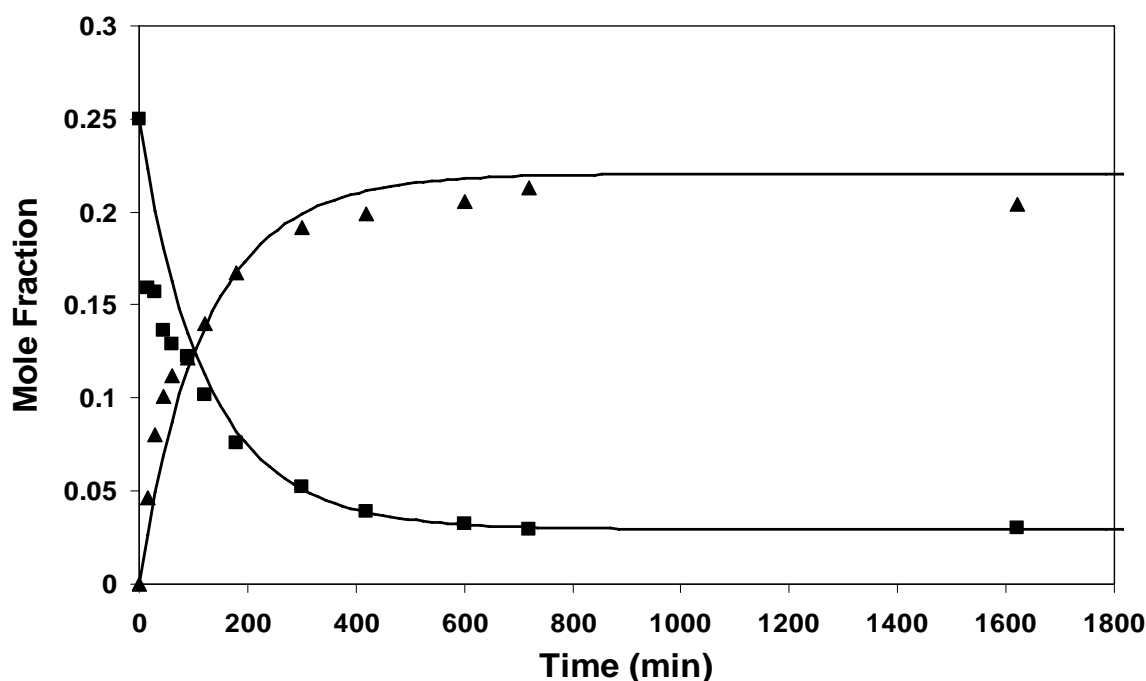
Figure 9.2 Esterification Reaction Catalyzed by Ion-Exchange Resin. Reaction Conditions: Mole Ratio of Ethanol to Propionic acid, 3:1; Catalyst Loading, 3 wt%; Reaction Temperature, 70°C. (■, PA; ▲, EP)
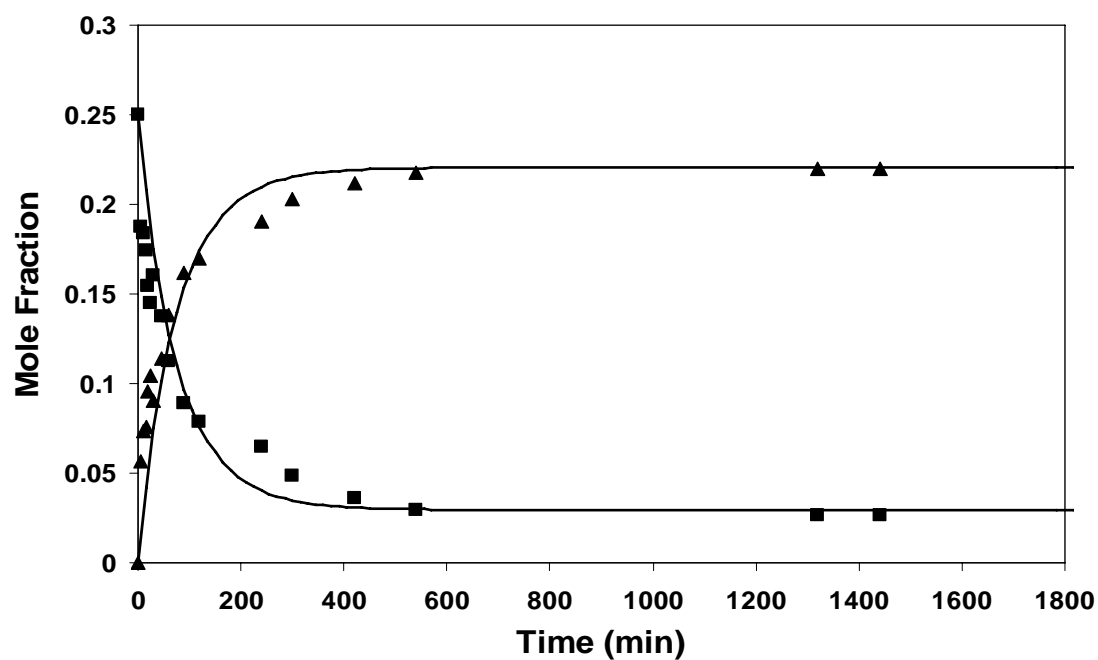
Figure 9.3 Esterification Reaction Catalyzed by Ion-Exchange Resin. Reaction Conditions: Mole Ratio of Ethanol to Propionic acid, 3:1; Catalyst Loading, 3 wt%; Reaction Temperature, 80°C. (■ , PA; ▲ , EP)
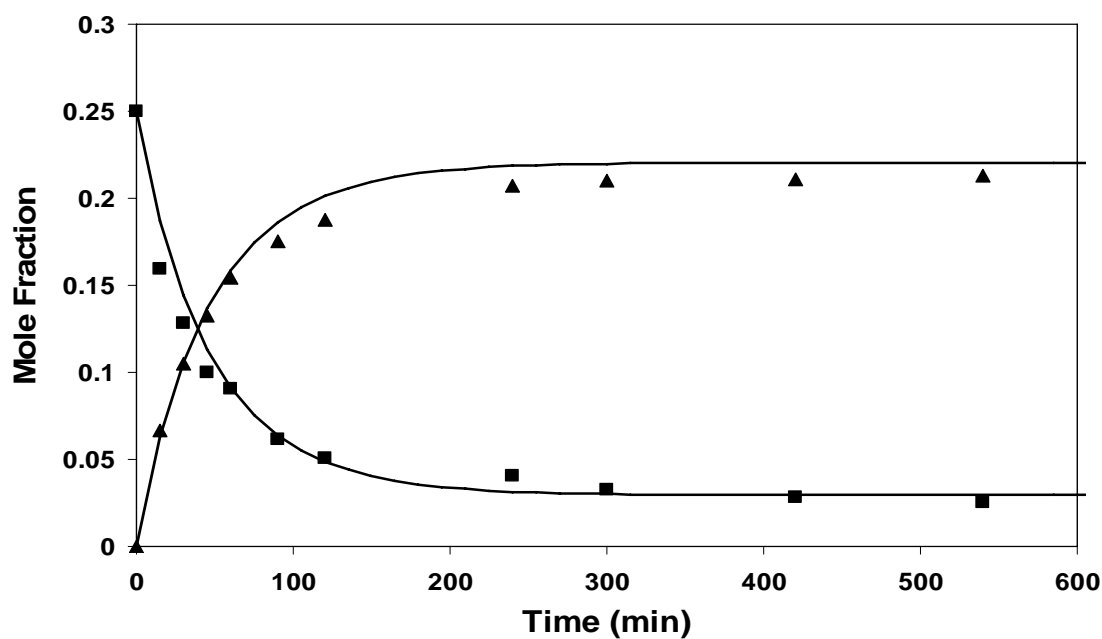
Figure 9.4 Esterification Reaction Catalyzed by Ion-Exchange Resin. Reaction Conditions: Mole Ratio of Ethanol to Propionic acid, 3:1; Catalyst Loading, 3 wt%; Reaction Temperature, 90°C. (■ , PA; ▲ , EP)
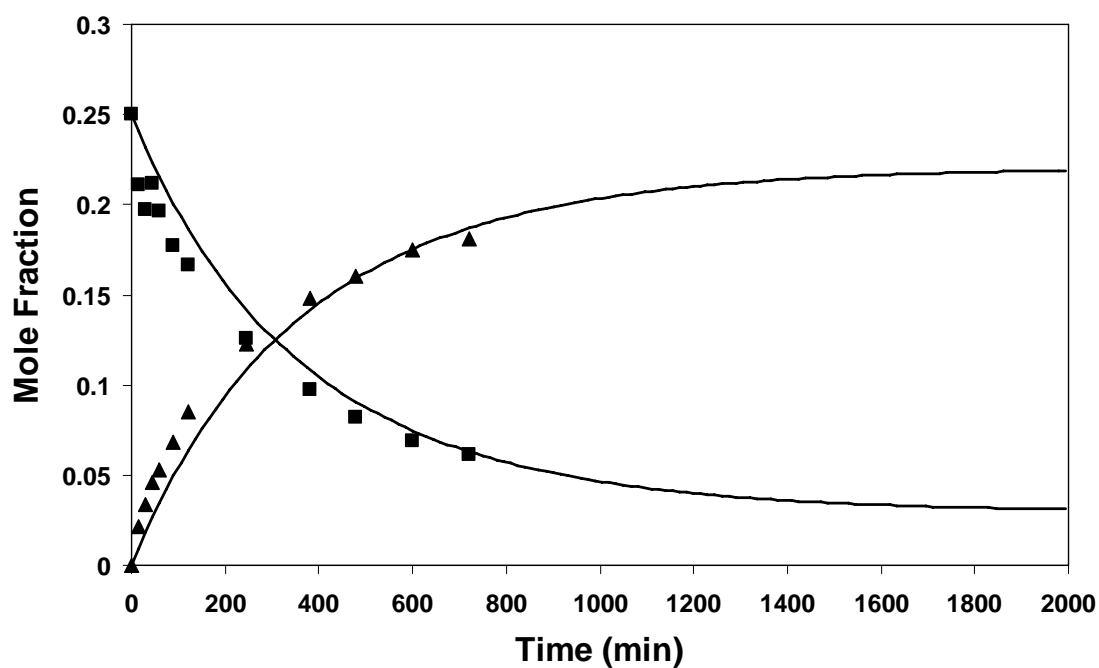
Figure 9.5 Esterification Reaction Catalyzed by Ion-Exchange Resin. Reaction Conditions: Mole Ratio of Ethanol to Propionic acid, 3:1; Catalyst Loading, 1 wt%; Reaction Temperature, 70°C. (■ , PA; ▲ , EP)
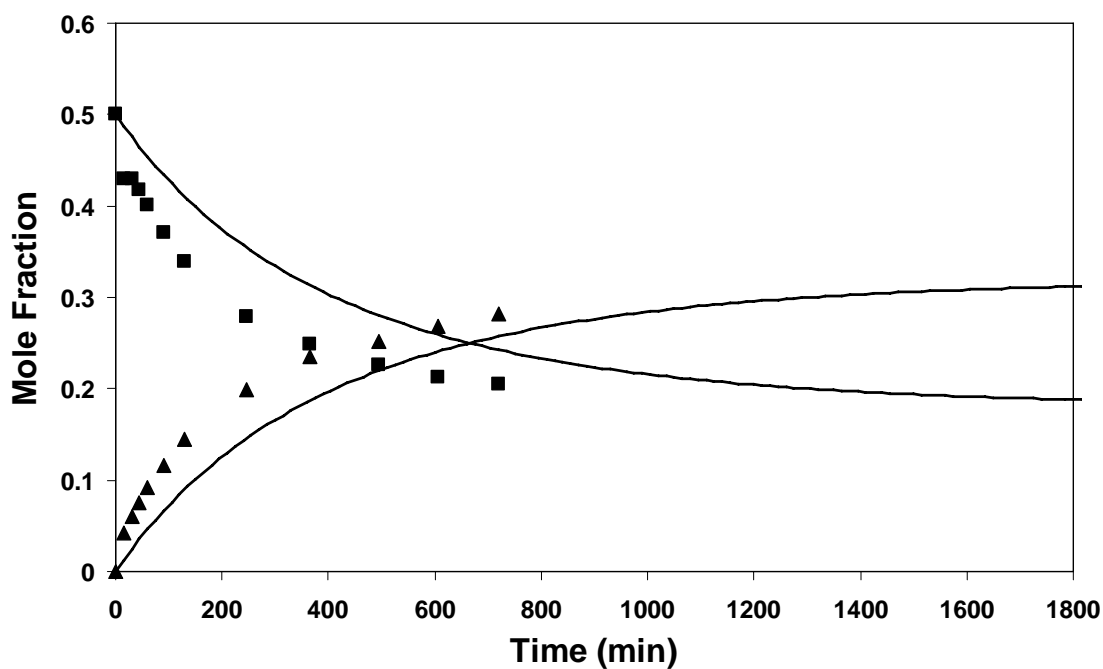
Figure 9.6 Esterification Reaction Catalyzed by Ion-Exchange Resin. Reaction Conditions: Mole Ratio of Ethanol to Propionic acid, 1:1; Catalyst Loading, 1 wt%; Reaction Temperature, 70°C. (■ , PA; ▲ , EP)
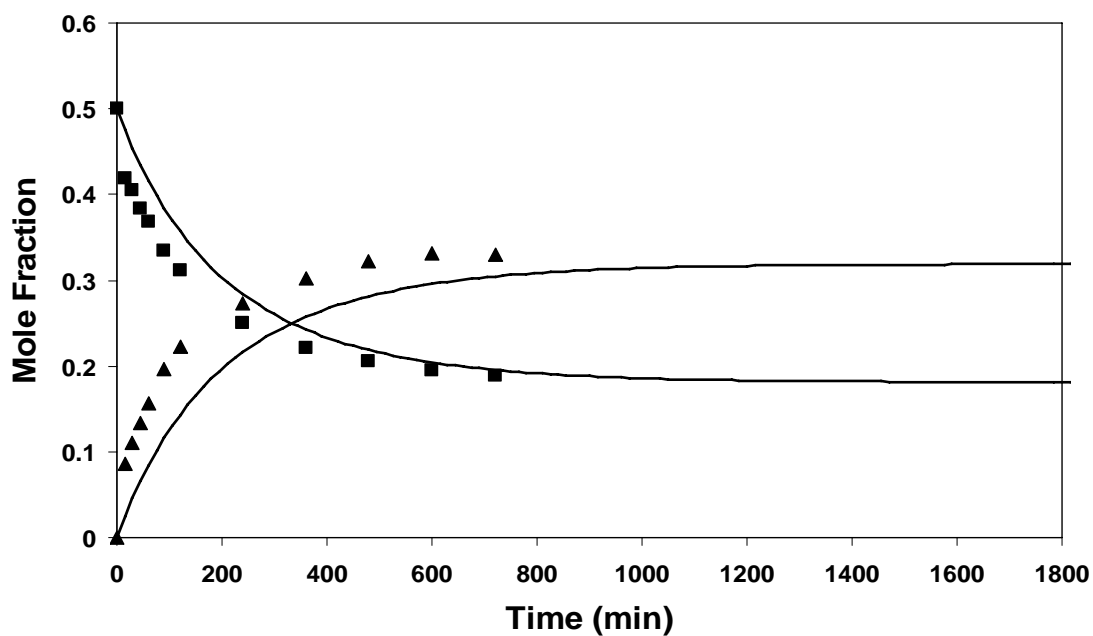
Figure 9.7 Esterification Reaction Catalyzed by Ion-Exchange Resin. Reaction Conditions: Mole Ratio of Ethanol to Propionic acid, 1:1; Catalyst Loading, 2 wt%; Reaction Temperature, 70°C. (■ , PA;   ▲   , EP)
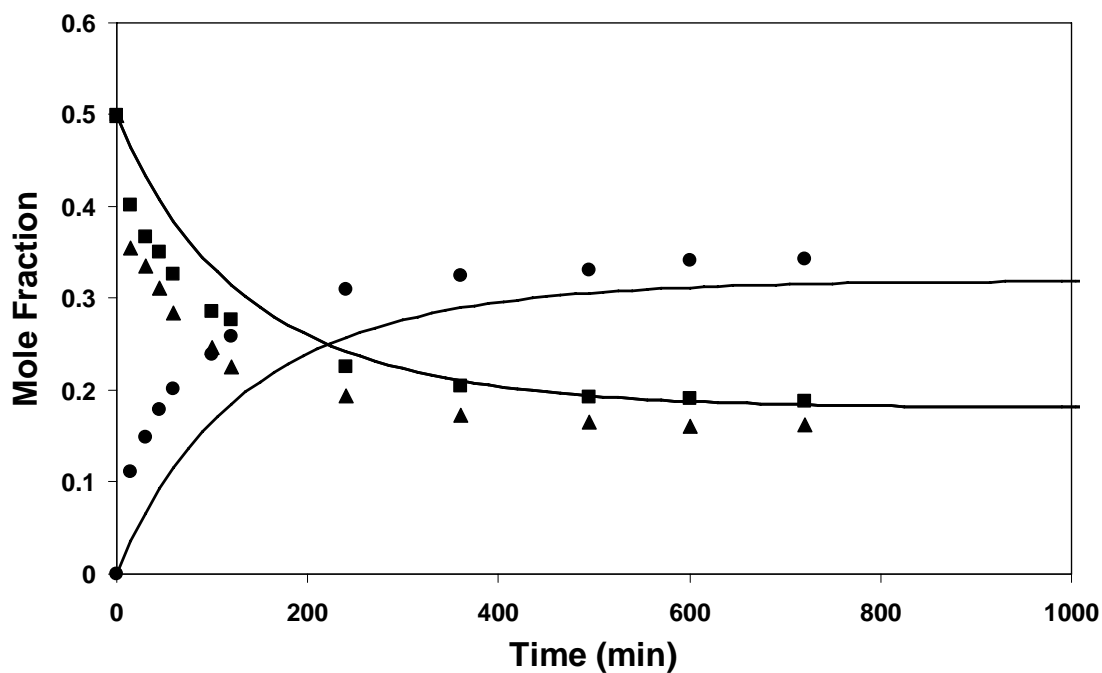
Figure 9.8 Esterification Reaction Catalyzed by Ion-Exchange Resin. Reaction Conditions: Mole Ratio of Ethanol to Propionic acid, 1:1; Catalyst Loading, 3 wt%; Reaction Temperature, 70°C. (■ , PA;▲, EtOH; •, EP)

9.3. Kinetic Model

9.3.1. Kinetic Pathways. Reaction 9.1 describes the pathways involved in the esterification of propionic acid with ethanol

$$PA + EtOH \; \underset{k_1/Keq_{a,1}}{\overset{k_1}{\rightleftarrows}} \; EP + W \qquad \qquad \dots(9.1)$$
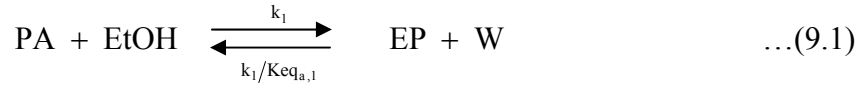
Based on the above reaction, a pseudo-homogeneous, mole fraction based model has been developed.

Chemical equilibrium constant
The chemical equilibrium constants are given by

$$Keq_x = \prod x^{v_i} \qquad \qquad \dots(9.2)$$

The value of mole fraction equilibrium constants Keq_x for reactions under consideration were determined by analysis of the experimental data at long reaction times (e.g. approaching equilibrium) and was found to be 3.1. This constant was found to be independent of temperature.

9.3.2. Determination of Rate Constants. The kinetic equations were numerically integrated via a fourth order Runge-Kutta method using ordinary differential equation solver ode23 in Matlab 7.0. Using an initial set of rate constants the liquid phase mole fractions for all species over the course of reaction were calculated and compared with the experimental values. The rate constants were then incremented sequentially in order to minimize the sum of the mean square differences given by

$$F_{min}^2 = \frac{\sum\limits_{samples} \left(x_{j,cal} - x_{j,expt} \right)^2}{n_{samples}} \qquad \qquad \dots(9.3)$$

After this optimization, the calculated mole fractions of the components involved in the reaction were compared to the experimental ones, giving the mean relative deviation, represented both absolutely and as on % basis as shown below

$$F_{abs} = \frac{\sum\limits_{samples} \left| x_{j,cal} - x_{j,expt} \right|}{n_{samples}} \text{ x } 100\% \qquad \qquad \dots(9.4)$$

$$F_{rel} = \frac{\sum\limits_{samples} \left| \frac{x_{j,cal} - x_{j,expt}}{x_{j,expt}} \right|}{n_{samples}} \text{ x } 100\% \qquad \qquad \dots(9.5)$$

9.3.3. Mole Fraction based Kinetic Model. Kinetics of the ion exchange resin-catalyzed esterification of propionic acid, data for which were determined from Runs 1 to 8 has been described using a pseudo-homogeneous model. The rate of formation of each species in the reaction mixture is described by Equations (9.6) to (9.9) given below:

$$-\frac{dx_{PA}}{dt} = w_{cat} \, K. \left(x_{PA}.x_{EtOH} - \frac{x_{EP}.x_W}{Keq_x} \right) \qquad \ldots(9.6)$$

$$-\frac{dx_{EP}}{dt} = w_{cat} \, K \left(\frac{x_{EP}.x_W}{Keq_x} - x_{PA}.x_{EtOH} \right) \qquad \ldots(9.7)$$

$$-\frac{dx_{EtOH}}{dt} = w_{cat} \, K \left(x_{PA}.x_{EtOH} - \frac{x_{EP}.x_W}{Keq_x} \right) \qquad \ldots(9.8)$$

$$-\frac{dx_W}{dt} = w_{cat} \, K \left(\frac{x_{EP}.x_W}{Keq_x} - x_{PA}.x_{EtOH} \right) \qquad \ldots(9.9)$$

where
$$K = k^\circ \, \exp\left(\frac{-E_A}{RT} \right) \qquad \ldots(9.10)$$

Two adjustable parameters for the resin-catalyzed reactions, the pre-exponential factors k° and the energies of activation E_A have been fitted to the experimental data of Runs 1 to 8. The values of the parameters determined are

$k^\circ = 2.55 \, E+05 \;$ kg sol $kg_{cat}^{-1} \, s^{-1}$

$E_A = 50254 \;$ kJ/kmol

9.4. Reactive Distillation Experiments

The reactive distillation column was configured such that propionic acid (F1 in Figure 5.2) was fed near the top of the enriching zone (0.2 m from top of column), while ethanol (F2 in Figure 5.2), either in liquid or vapor form, was fed 1 m above the reboiler at the bottom of the reactive zone. The reflux ratio (L/D) was set to zero, although a small amount of internal reflux was noted experimentally (L/D < 0.05). The reboiler duty was held constant for all experiments. The column operating pressure was limited to 1 atm.

There are two binary azeotropes (water-ethanol and water-ethyl propionate) and one ternary azeotrope (water-ethanol-ethyl propionate) associated with this system. Besides, boiling point for water and ethyl propionate is 100 and 99.3°C. This complicates the separation of ethyl propionate from water. Review of ethyl acetate system (which resembles closely to ethyl propionate) and preliminary ASPEN modeling showed that it is feasible to make pure ethyl-propionate using an azeotropic distillation column similar in principle to that reported for the ethyl-acetate system. The goal of column operation was to obtain complete conversion of propionic acid to ethyl propionate. Since the reaction was observed to be exothermic, ethanol feeding temperature was maintained at 25°C. We conducted several reactive distillation experiments to study the feasibility of this system and two representative results are presented herein.

9.4.1. Run 1. In this particular experiment, the molar feed ratio of ethanol to propionic acid was maintained at 3. At steady state, 72% propionic acid is converted to ethyl propionate. Even though the boiling point of propionic acid is 144°C, we observed that the distillate stream consisted of 31 mol% of propionic acid along-with water, ethanol and ethyl propionate. The exothermicity of this reaction is evident form the temperature profile given in figure 9.9.
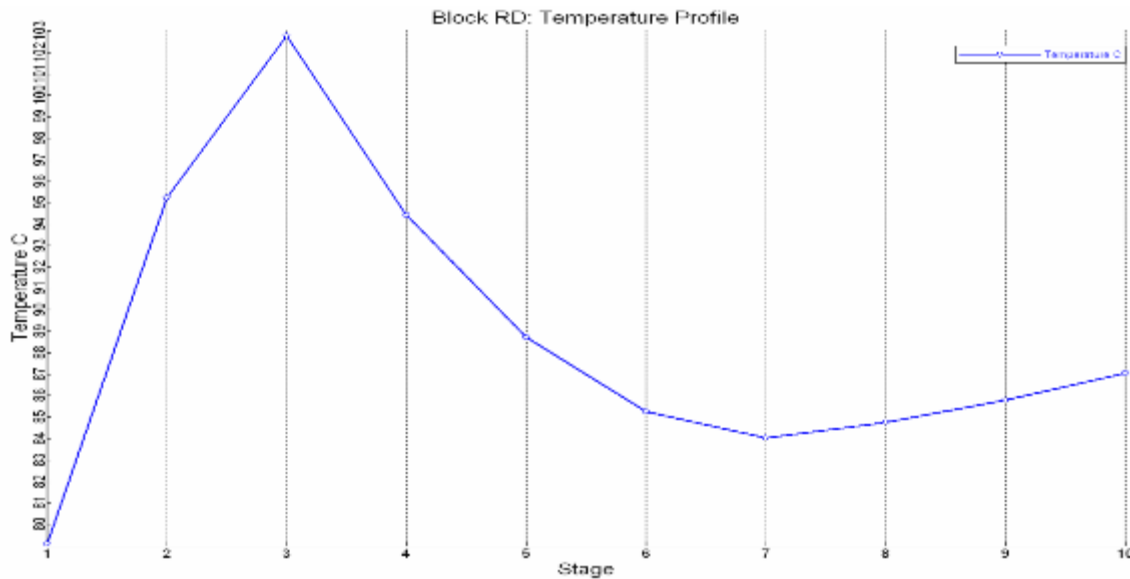
Figure 9.9 Temperature profile for Pilot scale Run 1

This run was modeled in ASPEN according to parameters given below and the results are shown in Figure 9.10.

Parameters used in Aspen simulation of pilot scale Run 1
- Total number of stages – 10
- Feed points – above stage 3 and on stage 8
- Reactive stages – 3 to 8
- Reflux ratio – 0.02
- Boilup ratio – 1.5
- HETP – 0.6 m
- Murphree efficiency from stages 2 to 10 – 0.5
- Liquid holdup per stage – 0.07 lit

Fractional approach to maximum capacity – 0.07

Stream 1
Flow   0.45 kg/hr

Wt %	
PA	100.0

On 3

Stream 2
Flow   0.916 kg/hr

Wt %	
EtOH	100.0

On 8

RR : 0.02
BR : 1.5

Pressure : 1 atm

10

Stream 3
Flow   0.824 kg/hr

	Mole %	Expt mole%
PA	9.64	9.93
EtPA	29.47	31.20
EtOH	30.98	29.21
Water	29.92	29.66

Stream 4
Flow   0.546 kg/hr

	Mole %	Expt mole %
PA	1.46	2.37
EtPA	2.58	2.23
EtOH	93.93	93.48
Water	2.02	1.90
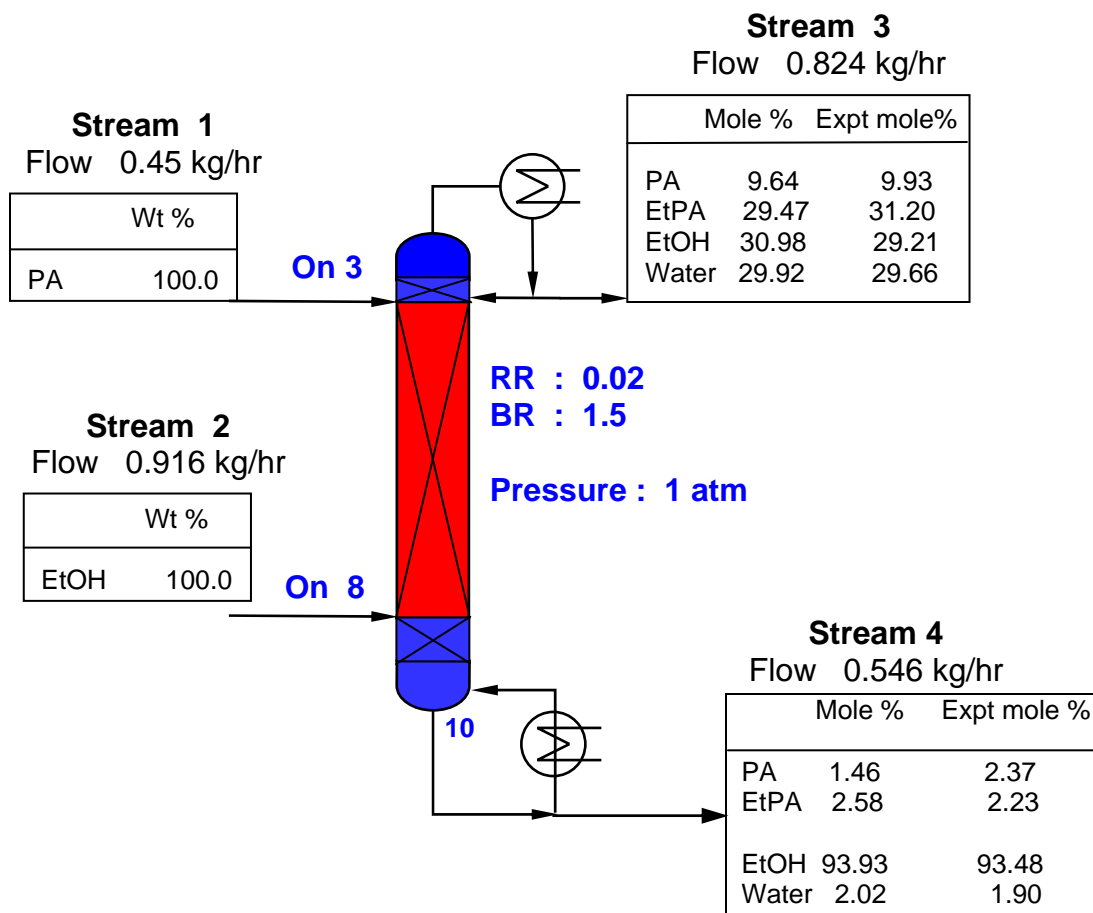
Figure 9.10 Experimental and ASPEN simulation results from Pilot Scale Run 1
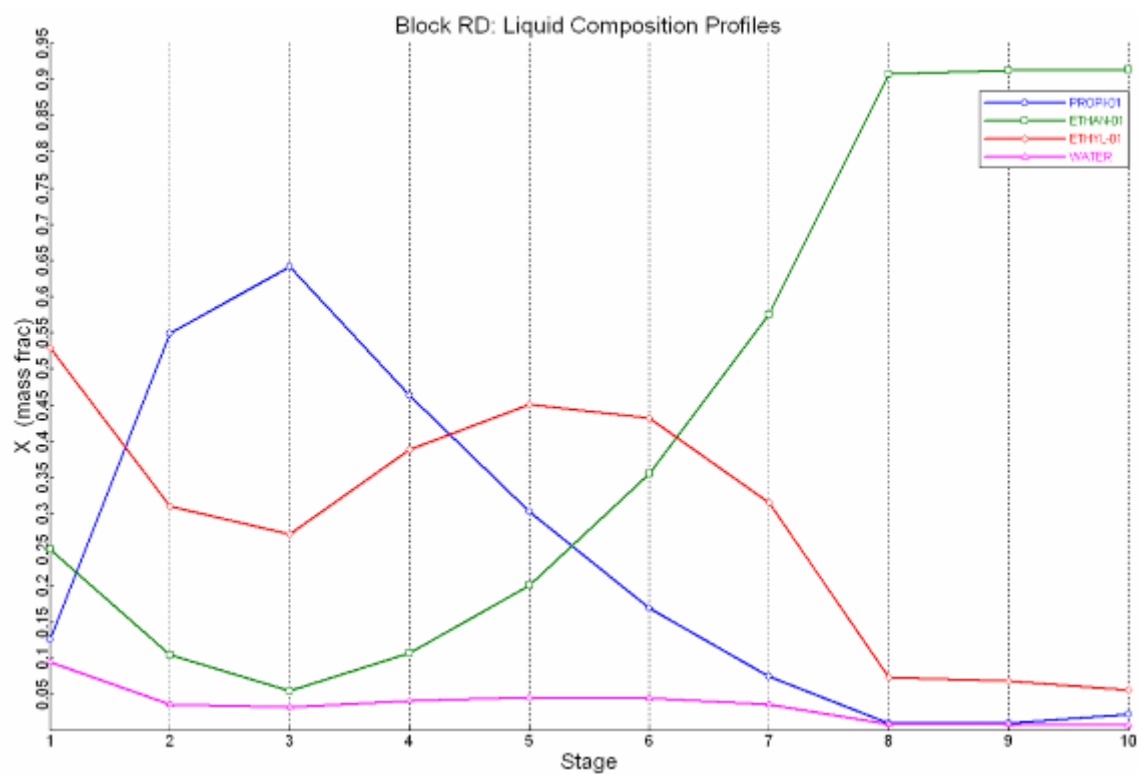
Figure 9.11 Liquid phase composition profile in wt% for Pilot scale Run 1
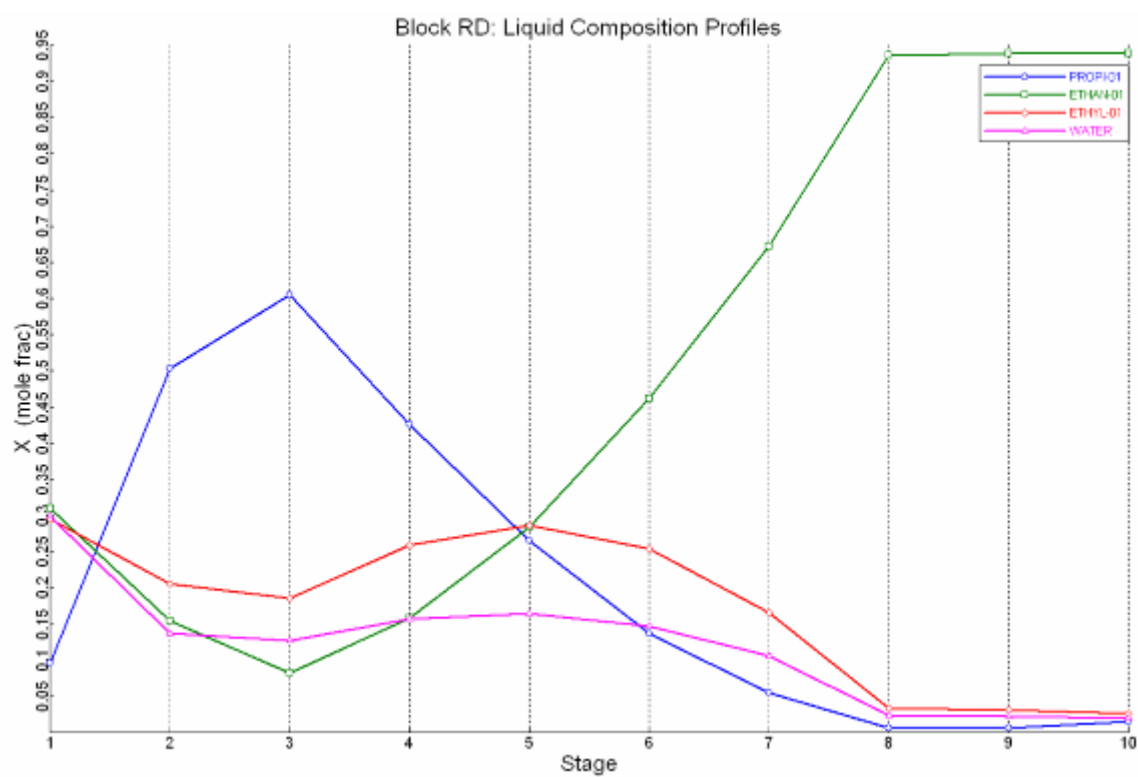
Figure 9.12 Liquid phase composition profile in mole % for Pilot scale Run 1

9.4.2. Run 2. In this particular experiment, the molar feed ratio of ethanol to propionic acid was maintained at 1. At steady state, 50% propionic acid is converted to ethyl propionate. We also observed two distinct phases in distillate stream. A comparison between experimental and ASPEN simulation is shown below in Figure 9.5.

Stream 3 (Org)
Expt Flow   0.078 mol/min
Calc Flow   0.128 mol/min

	Mole %	Expt mole%
PA	21.99	1.55
EtPA	29.88	48.13
EtOH	9.93	21.68
Water	38.19	28.65

Stream 1
Flow   0.1254 mol/min

	Wt %
PA	100.0

On 3

Stream 3 (Aq)
Expt Flow   0.0358 mol/min
Calc Flow   0.0007 mol/min

	Mole %	Expt mole%
PA	4.63	0.28
EtPA	0.81	1.12
EtOH	3.12	11.45
Water	91.44	87.15

Stream 2
Flow   0.1565 mol/min

	Wt %
EtOH	100.0

On 8

RR : 0.02
BR : 1.5

Pressure : 1 atm

10

Stream 4
Expt Flow   0.1544 mol/min
Calc Flow   0.1544 mol/min

	Mole %	Expt mole %
PA	20.87	35.05
EtPA	17.42	16.19
EtOH	51.00	41.87
Water	10.72	6.88

Figure 9.13 Experimental and ASPEN simulation results from Pilot Scale Run 2

SPEAD MODELING FOR ORGANIC ACID AND ESTERS
VAPOR PRESSURE

10.1. Background

The Step Potential Equilibria and Dynamics (SPEAD) molecular simulation was recognized as the best method for prediction of vapor pressure and heat vaporization at the contest held by Case Scientific in 2004.[114] It is in development by Elliott et al. and is being implemented by ChemStations, Inc. as a physical properties standard model in chemical process simulation.[115,116]

The SPEAD estimates vapor pressures of hydrocarbons including aromatic hydrocarbons, the low molecular ethers and alcohols, and simple esters with error of less than 10 % of the experimental values.[115] However, the application of SPEAD has not been extended to high molecular and/or multifunctional group molecules. As a part of our work on VLE, we worked closely with SPEAD developers to optimize parameters for prediction of Psat of ethyl lactate oligomers and acetals of glycerols.

10.2. Approaches in SPEAD Modeling

10.2.1. Pair Interaction Sites of Ethyl Lactate Oligomers and Acetals of Glycerols. The SPEAD interaction sites of ethyl lactate oligomers and acetals are designated as described in Figure 10.1. Each interaction site is specified by a three or four digit index, identifying the main and sub groups. For example, the site 1602 is made of the main group16 and the sub group 2.

Ethyl Lactate Oligomers

4-hydroxymethyl-2-methyl-1,3-dioxolane   5-hydroxy-2-methyl-1,3-dioxane
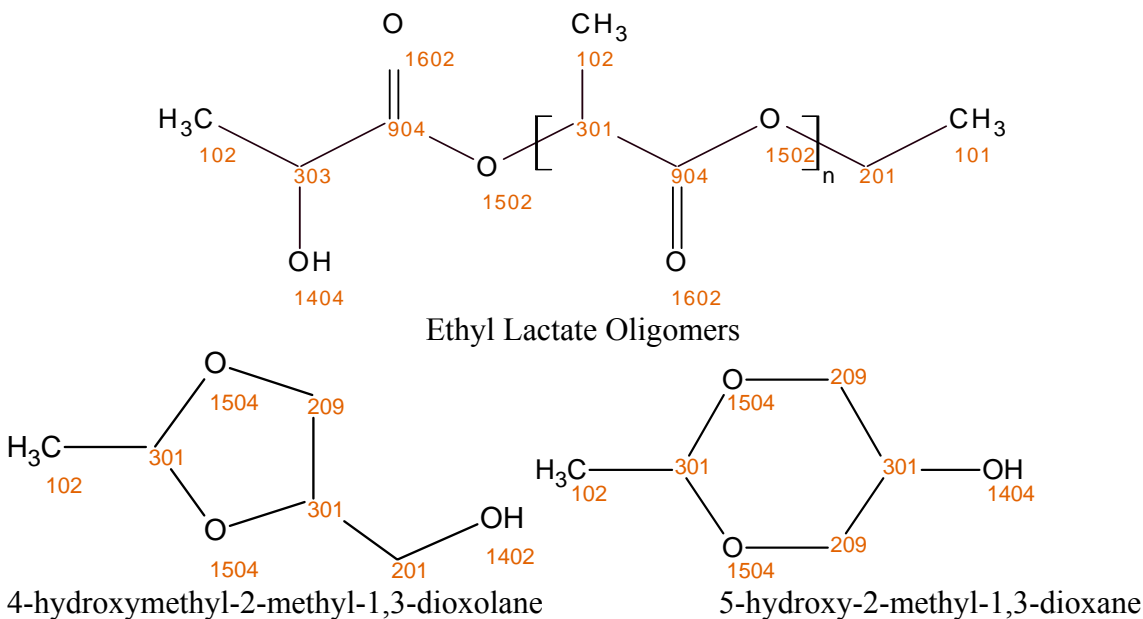
Figure 10.1 **The Interaction Sites of Ethyl Lactate Oligomers and Acetals**

At present, SPEAD has not been fully developed for the multi-oxygen-containing molecules such as ethyl lactate or acetals. Therefore, the site 1404 for secondary –OH groups and sites 904, 1502, 1602 for ester groups in Figure 10.1 are not yet parametized. Finding the optimal parameters for these sites is crucial for reliably predicting vapor pressures of acetals and oligomers.

10.2.2. Approach of Optimizing Secondary -OH and -COO- groups. SPEAD has been developed with the premise that parameters are transferable within the homologous compounds. Therefore, the best parameters for secondary –OH and –COO– groups (shown in Figure 10.2) can be obtained from fitting the good experimental P^{sat} data available in the DIPPR database for 2-alkanols and esters. A datum is considered good if it has the DIPPR notation "*acceptance*" and the DIPPR "*deviation*" of less than 5 %.
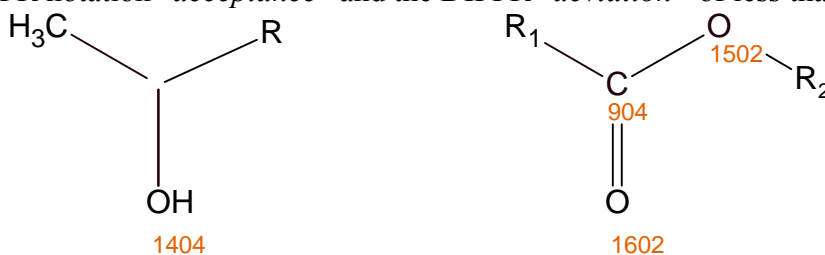
Figure10.2 Group Indices in 2-Alkanols and Base Esters used in Optimization

10.2.3. Mathematical Methodology. The wells for each group 904, 1404, 1502, and 1602 are characterized by two parameters which are the inner (ε_1) and outer (ε_4) potential well depths. In addition, group 1404 (-OH) and 1602 (>CO=) can form hydrogen bonds, which are described by the three parameters: the energy (*eHb*), the volume (*BondVol*), and the rate (*BondRate*) of the bonds. As a result, the optimization of secondary -OH and ester groups involves either five or nine parameters, respectively.

As it has been stated by Korsten[117] and also is observed that logarithm of vapor pressure of any compound is linear to $T^{-1.3}$. Therefore, a good prediction of P^{sat} for a series of homologous compounds must have a minimum error in both P^{sat} and slope of the $\ln(P^{sat})$ with respect to $T^{-1.3}$. Figure 10.3 below illustrates the possible errors in prediction.
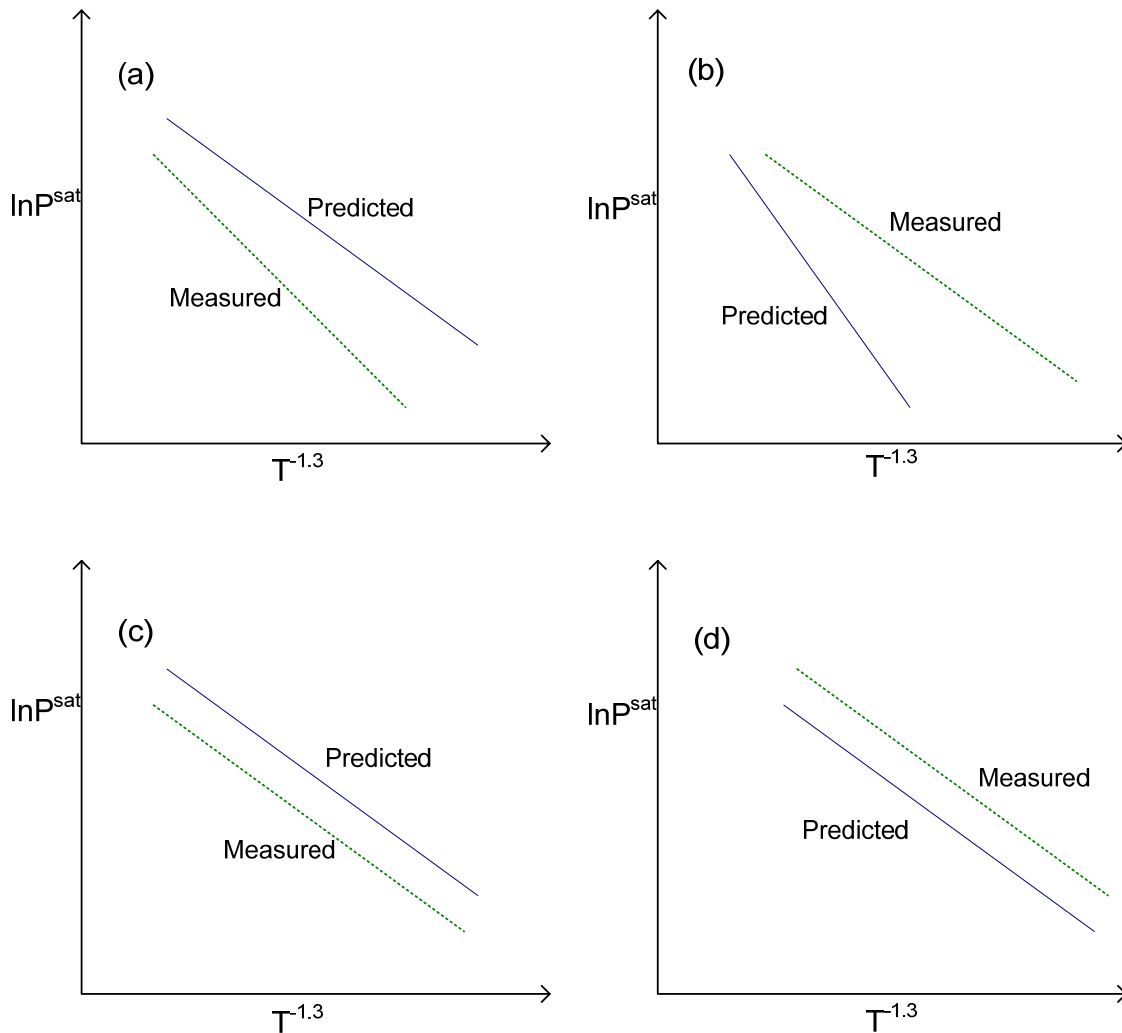
Figure 10.3 Illustration of Error in Prediction of Psat

SPEAD developers have used grid search, simplex and recursive random search[118] algorithms for parameterization of hydrocarbons and series of simple homologous compounds. But, these methods have not been successful in finding a global optimum for a system with hydrogen bonding.

A FORTRAN program was written using the routine DBCONF from the International Mathematical and Statistical Library (IMSL) to optimize the five and nine parameters of secondary -OH and ester groups.

To minimize the errors described in Figure 10.3, the objective function $(f \rightarrow \min)$ is defined as follows:

$$f = f_1 * f_2 \tag{10.1}$$

$$f_1 = \left[\sum_{i=1}^{i=n} abs\left(\ln P_{i,pre}^{sat} - \ln P_{i,\exp}^{sat} \right) \right] \tag{10.2}$$

$$f_2 = \left[\frac{1}{n-1} \sum_{i=1}^{i=n} abs \left(\frac{\left(\ln P_{i+1,pre}^{sat} - \ln P_{i,pre}^{sat} \right)}{\left(T_{i+1}^{-1.3} - T_i^{-1.3} \right)} - \frac{\left(\ln P_{i+1,\exp}^{sat} - \ln P_{i,\exp}^{sat} \right)}{\left(T_{i+1}^{-1.3} - T_i^{-1.3} \right)} \right) \right] \qquad (10.3)$$

where n is number of data points, $P_{i,pre}^{sat}$ and $P_{i,\exp}^{sat}$ are predicted and experimental vapor pressures for datum point i.

10.2.4. The DBCONF routine algorithm. DBCONF uses a popular variant of the Quasi-Newton method, which is called the BFGS (Broyden-Fletcher-Goldfarb-Shanno) method and an active set strategy to solve a nonlinear optimization problem subject to simple bounds on the variables.[119-122] The algorithm can be summarized as follows:

An active set **A** containing the indices of the variables at their bounds is built from a given starting point $x^{(0)}$ and an estimate of Hessian matrix $H_0 = \nabla^2 f\left(x^{(0)}\right)$. The routine then computes the search direction for the "free variables", which is not in the active set according to the formula:

$$x^{(k+1)} = x^{(k)} - H_k^{-1} \nabla f\left(x^{(k)}\right) \qquad (10.4)$$

$$s^{(k)} = x^{(k+1)} - x^{(k)} \qquad (10.5)$$

$$y^{(k)} = \nabla f\left(x^{(k=1)}\right) - \nabla f\left(x^{(k)}\right) \qquad (10.6)$$

$$H_{k+1} = H_k - \frac{H_k s^{(k)} \left(s^{(k)}\right)^T H_k}{s^{(k)} \bullet H_k s^{(k)}} + \frac{y^{(k)} \left(y^{(k)}\right)^T}{y^{(k)} \bullet s^{(k)}} \qquad (10.7)$$

The active set is changed only when a free variable hits its bounds during an iteration or the optimality condition is met for the free variables but not for all variables in **A**, the active set. In the latter case, a variable that violates the optimality condition will be dropped out of **A**.

More details on the DBCONF algorithm can be found in the IMSL documentation. The quasi-Newton method and line search are explained by Dennis and Schnabel,[123] and the active set strategy is explained by Gill and Murray.[124] A copy of FORTRAN code to call DBCONF and sample of input and output data files are included in Appendix C.

10.3. Results of Optimization of the 2nd -OH and -COO- groups

Existing data were divided into two sets. Some were used for parameter fitting and make up the training set. The other data are used for evaluation of predictive capability and make up the validation set. The training sets and results of optimization to obtain parameters for the secondary -OH and –COO- interaction sites are summarized in Table 10.1. More details of the output files containing experimental and predicted vapor pressures, generated by FORTRAN program are in Appendix III.

The secondary -OH group – All secondary alcohol data from DIPPR is used in optimization (2-alkanols (C2-C9)). The 2-heptanol was not included in the training set,

because its vapor pressures in DIPPR database are not experimental but smoothed data. The average error ( ) in fitting 160 data points of the training set is 6 %. P^{sat} are from 0.01 kPa to 1 MPa.

Parameters obtained from optimization of 2-alkanols are used for prediction of vapor pressure for 3-alkanols and 2-heptanol. As shown in Table 10.1 predictions are in good agreement with the reported values in literature. The errors are large for the 3-pentanol and 3-hexanol, but P^{sat} data of these compounds are measured at low temperature (P^{sat} < 0.01 kPa), and they are not in the same range with data used in the training set.

The parameters of 1404 group from 2-alkanols are also tested with cyclohexanol and cyclomethylhexanol to verify if they can be transferable to the secondary OH group, which bonded to a non-aromatic ring. As expected, the predictions are overestimated, because cyclic alcohols have higher boiling points than the straight chain alcohols, affected by their stronger intermolecular hydrogen bonds.

Table 10.1 Compounds used in Optimization and Validation of –OH and –COO– site

Compound Name	Notation	# data points	Deviation in Prediction			References
				Bias	Max	
Training -OH site						
2-propanol	2olC3	33	6	4.1	15.7	[12-14]
2-butanol	2olC4	32	11.3	-11.3	-14.4	[15, 16]
2-pentanol	2olC5	33	3.3	-2	-6.7	[17, 18]
2-hexanol	2olC6	27	5.5	4.6	15.6	[18, 19]
2-octanol	2olC8	33	5.3	3.9	16.6	[18, 20]
2-nonanol	2olC9	2	3	2.7	5.7	[21, 22]
Testing -OH site						
2-heptanol	2olC7	9	4.9	-4.9	-7	[23]
3-pentanol	3olC5	24	24.1	-24.1	-29.8	[18, 24]
3-hexanol	3olC6	22	12	-11.7	-32.2	[18, 23, 24]
3-heptanol	3olC7	6	8	-8	-9.9	[25, 26]
cyclohexanol	c2olC6	33	29.4	29.4	49.9	[13, 27]
cis 2-methylcyclohexanol	c2ol_2_C1C6	3	21.9	21.9	30.9	[28, 29]
cis 4-methylcyclohexanol	c2ol_4_C1C6	2	28.4	28.4	41.7	[30, 31]
2,3-butanediol	diolC4	22	79.4	-79.4	-90.9	[32]
Training -COO- site						
ethyl propionate	C3ateC2	28	5.2	3.3	9	[33]
n-butyl propionate	C3ateC4	32	2.1	0.7	-8.2	[17]
methyl n-butyrate	C4ateC1	30	15.3	-14.9	-38.4	[17, 34]
ethyl n-butyrate	C4ateC2	9	6	-4.7	-24.1	[28]
n-propyl n-butyrate	C4ateC3	28	1.5	-1.4	-3.5	[35, 36]
isobutyl isobutyrate	iC4ateIC4	17	16.7	16.7	22.2	[13, 37]
methyl decanoate	C10ateC1	18	6.3	-6	-13.1	[38, 39]
Testing -COO- site						
n-propyl propionate	C3ateC3	3	5.2	-0.3	-8.2	[33]
n-butyl n-butyrate	C4ateC4	2	13	-4.6	-17.6	[28]
n-propyl isobutyrate	iC4ateC3	1	16	16	16	[40]
n-butyl valerate	C5ateC4	2	5.2	2.5	7.7	[40, 41]
ethyl isovalerate	iC5ateC2	1	18.3	-18.3	-18.3	[28]
methyl laurate	C12ateC1	14	8.7	-1.9	-16.7	[42]
isopropyl laurate	C12ateIC3	7	4.9	3.7	11	[42]
isobutyl laurate	C12ateIC4	11	7	-3.5	-10.9	[42]
2-ethyl hexyl laurate	C12ate2C2C6	9	26.1	-26.1	-36.4	[42]
methyl tetracosanoate	C24ateC1	6	26.7	-26.7	-41.8	[42]

Table 10.2 Parameters used in computing P^{sat} for Compounds listed in Table 10.1

Site	Description	Potential Well Depth		Hydrogen Bonding		
		ε_1	ε_4	BondVol	Bond Rate	Bond Energy
101	–CH3a	91.871	16.445			
102	–CH3b	55.100	32.400			
106	–CH3f	108.000	11.000			
201	–CH2–	26.558	21.827			
209	–CH2– in a ring	30.000	21.000			
301	>CH– to a Carbon	7.100	6.946			
303	>CH– to the 2nd –OH	31.500	4.400			
*1504	Cyclic ether –O–	140.25	23.65			
*904	=C–	10.209	1.698			
*1404	2nd –OH	142.743	41.760	0.00003587	140.00	4.247
*1502	Ester –O–	100.198	4.087			
*1602	=O	152.632	44.705	0.002	104.65	0.682

Sites with * are optimized in this study.

The ester -COO- group – Optimization of the ester groups uses 162 data points as summarized in Table 10.1, Deviation of the fitting data is ~ 8 % of the measured values. Experimental P^{sat} are limited, therefore the validation to check for transferability of the obtainable parameters only includes 56 data points. Results show that vapor pressure of esters containing up to 30 carbons can be predicted within 27 % of the measured values, using parameters listed in Table 10.2.

10.4. Prediction of Psat for Ethyl lactate Oligomers

First, vapor pressure of methyl lactate and ethyl lactate are predicted to compare with experimental values. Result shows that SPEAD could not provide an adequate prediction for ethyl and methyl lactates using the above-optimized parameters.

Table 10.3   SPEAD Prediction Using Parameters Listed in Table 10.2 Compared to the other P^{sat} of Methyl Lactate and Ethyl Lactate

Method	Methyl lactate					
	T =313.15 K P=0.0012 MPa		T= 333.25 K P=0.0036 MPa		T =353.35 K P=0.0094 MPa	
	Value	% Dev	Value	% Dev	Value	% Dev
Riedel	0.00057	-52%	0.00213	-41%	0.00662	-41%
Othmer-Yu	0.00945	689%	0.02998	731%	0.08191	731%
Gomez-Thodos	0.00027	-78%	0.00129	-64%	0.00483	-64%
Lee-Kesler	0.00054	-55%	0.00204	-43%	0.00644	-43%
Maxwell-Bonnell	0.00182	52%	0.00501	39%	0.01197	39%
SPEAD	0.00003	-97%	0.00015	-96%	0.00058	-94%

Method	Ethyl lactate					
	T =313.15 K P=0.0012 MPa		T= 333.25 K P=0.0031 MPa		T =353.35 K P=0.0076 MPa	
	Value	% Dev	Value	% Dev	Value	% Dev
Riedel	0.00034	-71%	0.00133	-57%	0.00431	-43%
Othmer-Yu	0.00610	430%	0.01997	538%	0.05607	638%
Gomez-Thodos	0.00012	-89%	0.00067	-79%	0.00277	-64%
Lee-Kesler	0.00032	-73%	0.00127	-60%	0.00417	-45%
Maxwell-Bonnell	0.00098	-15%	0.00295	-6%	0.00761	0.2%
SPEAD	0.00003	-97%	0.00015	-95%	0.00060	-92%

10.4.1. Effect of intramolecular H-bonds in Lactates. As shown, other methods of predicting vapor pressure used in DIPPR also underestimated the lactates. These compounds containing both a secondary hydroxyl and an ester group in their molecules, can form intramolecular hydrogen bonds (–OH….O=C<). To verify whether the intramolecular hydrogen bonding could be the cause of underestimation in SPEAD, full atom liquid simulations of 50 ns were conducted using COMPASS potentials in the NVT ensemble with the Anderson thermostat, provided by Accelrys MS Modeling 4.0. Vibrational and torsional energies are included. Results indicated that twenty percent of the liquid phase hydrogen bonds are intramolecular.

Adjusting for the effect of intramolecular H-bonds in calculating the Helmholtz energy in SPEAD is beyond the scope of this study. However, it is found that SPEAD gives a good prediction for the lactates (still a small underestimation) if all parameters of H-bond in 1404 group are set to be zero. Below is an example of P^{sat} prediction for ethyl lactate using the described settings.

Table 10.4 Prediction of Psat for Ethyl Lactate Using Parameters Listed in Table 10.2 (except for H-bonding)

T (K)	P (MPa) Measured	P (MPa) SPEAD	T (K)	P (MPa) Measured	P (MPa) SPEAD
353.15	0.0077	0.0065	317.45	0.0013	0.0010
351.15	0.0072	0.0059	314.65	0.0010	0.0008
349.55	0.0067	0.0055	313.25	0.0011	0.0008
347.15	0.0062	0.0049	312.85	0.0010	0.0007
343.55	0.0053	0.0041	310.45	0.0008	0.0006
341.65	0.0047	0.0037	309.15	0.0007	0.0006
337.45	0.0040	0.0030	308.15	0.0007	0.0006
333.15	0.0031	0.0024	305.65	0.0005	0.0005
330.65	0.0028	0.0021	304.05	0.0005	0.0004
327.35	0.0023	0.0017	303.15	0.0005	0.0004
325.05	0.0021	0.0015	300.05	0.0004	0.0003

The normal boiling point for ethyl lactate is 427.15K, and the predicted value is 428.02 K. Same results are obtained for methyl lactate (Tb = 417.95 K, predicted value = 418.45 Tb). For the methyl 3-hydroxy butanoate (at P = 0.00132 MPa, T = 336.2 K, and predicted T= 330.2 K).

10.4.2. A common point for Ethyl Lactate Oligomers. Another evaluation of SPEAD prediction for oligomers is the use of Eqn A, which was described by Korsten. Vapor pressures are generated for each lactate ester (E_1LA, E_2LA, E_3LA, E_4LA, E_5LA) at temperatures between 300–700 °K (increment of 20 °K) using the parameters listed in Table 10.2 (all parameters for H-bonds are zero). Results show that the SPEAD-predicted vapor pressure curves of lactate oligomers are not completely linear. But, fitting the predictions with linear equations, the extrapolated vapor pressures for E_2LA, E_3LA, E_4LA, and E_5LA merge at the common point α (T_α = 4947.K, P_α = 2643.3 MPa) as illustrated in Figure 10.3. Therefore, the predictions are generally consistent with the empirical common point analysis of Korsten. The coefficients shown in Eqns 10.1 and 10.2 for slopes of these vapor pressure curves are obtained from regression using the least square method.
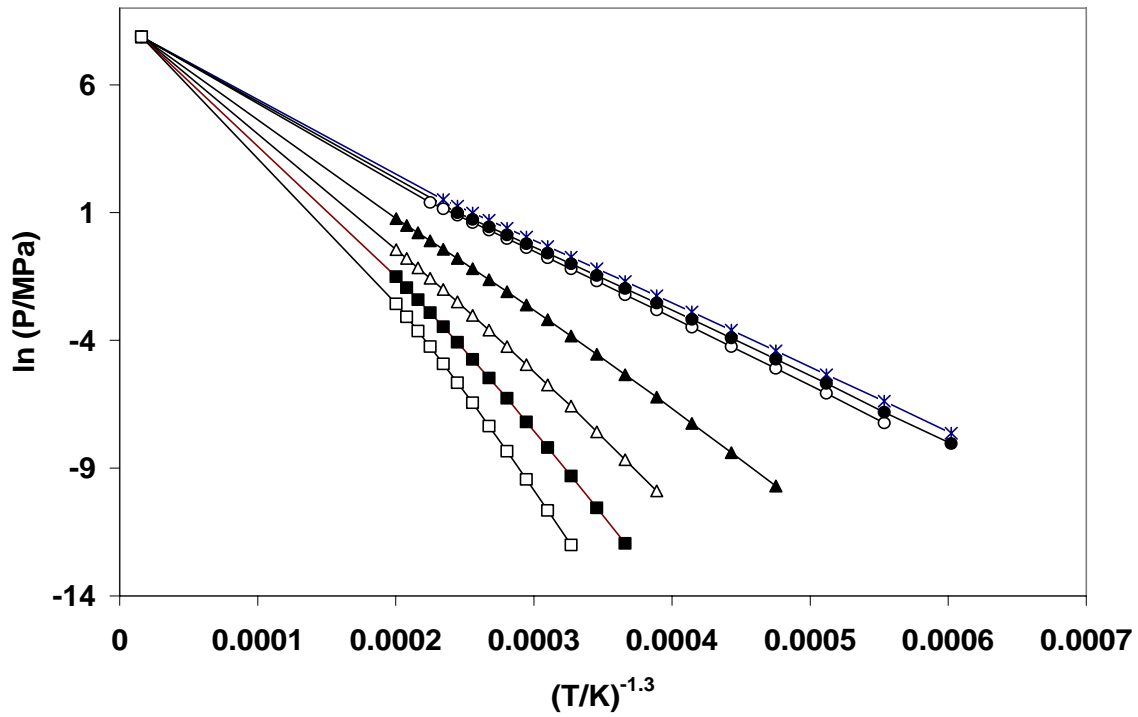
Figure 10.4 **Trend of Predicted Vapor Pressure of Ethyl Lactate Oligomers**

*: methyl lactate, ○: methyl 3-hydroxy-butyrate, ●: L_1E, ▲: L_2E, Δ: L_3E, ■: L_4E, ◊: L_5E

$$\ln P = \ln P_\alpha + B\left(\frac{1}{T^{1.30}} - \frac{1}{T_\alpha^{1.30}}\right) \qquad \text{(Eqn. A)}$$

$$B = B_0(\theta_B) + B_1 M^{0.65} = 4669.09 - 321.42\theta_B - 1162.8M^{0.65} \qquad (10.8)$$

$$\left(T_\alpha = 4947.5 \text{ K}, \ P_\alpha = 2643.3 \text{ MPa}\right), \text{ and } \theta_B = 22.596$$

The above equations can be combined as:

$$\ln P = 7.88 - \left(2593.72 + 1162.8M^{0.65}\right)\left(\frac{1}{T^{1.30}} - \frac{1}{4947.5^{1.30}}\right) \qquad (10.9)$$

where M is molecular weight of the corresponding ethyl lactate oligomer, T is in K, and P is in MPa.

Using Eqn 10.9 to check for the total vapor pressure of mixture in Table 10.3,
At T =322.27 K, $E_1LA = 0.162$, $E_2LA = 0.774$, $E_3LA = 0.054$, $E_4LA = 0.01$

$$P_{monomer} = \exp\left[7.88 - \left(2593.72 + 1162.8 * 118.13^{0.65}\right)\left(\frac{1}{322.27^{1.30}} - \frac{1}{4947.5^{1.30}}\right)\right]$$

$$= 0.000707 \text{ MPa}$$

$P_{2\text{-mer}} = 4.81 \times 10^{-06}$ MPa, $P_{3\text{-mer}} = 6.19 \times 10^{-06}$ MPa, $P_{4\text{-mer}} = 1.19 \times 10^{-06}$ MPa

If mixture is an ideal solution, then

$P_{mixture} = 0.162(0.000707) + 0.774(4.81 \times 10^{-06}) + 0.054(6.19 \times 10^{-06}) + 0.01(1.19 \times 10^{-06})$

$= 0.000118$ MPa $= 0.118$ kPa.

Result is in the same order with the value from measurement.

10.5. Prediction of P^{sat} for Acetals

Acetals of interests are the 4-hydroxymethyl-2-methyl-1,3-dioxolane (4HMD) and 5-hydroxy-2-methyl-1,3-dioxane (5HMD). These compounds contain two ether -O- groups in a molecule. Different from alcohols and esters, the oxygen atom does not form intramolecular H-bonds in ethers; therefore vapor pressures of mono-oxides (each molecular containing a single -O- group), such as tetrahydrofuran, are much higher than vapor pressures of alcohols, esters, di-ethers, and the above acetals 4HMD and 5HMD.
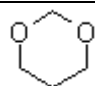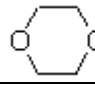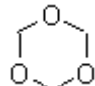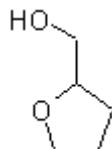
The existing SPEAD parameters (ε_i = 287.4, ε = 26.7) for the cyclic-ether oxygen (group 1504) provide an excellent P^{sat} prediction for tetrahydrofuran. But, using these existing parameters for 1,3-dioxane and 1,4-dioxane, SPEAD underestimates vapor pressures by at least 85 %. In addition to ether oxygens, the 4HMD and 5HMD also contain a hydroxyl group in their structures; therefore if the existing SPEAD parameters are not sufficient for use in 1,3-dioxane and 1,4-dioxane, then they are obviously not suitable for the 4HMD and 5HMD. Thus, optimization is needed for group 1504 assuming the methylene site in a ring (group 209) is already parametized.

Experimental P^{sat} data are very limited for acetals. Table 10.5 lists the compounds found in the DIPPR data bank that have the most similar structure to the 4HMD and 5HMD,. The 1,3-dioxane and 1,-4 dioxane are used in optimization; the trioxane and tetrafurfural alcohol are used in validation.

Since the ether group does not associate with H-bond, optimization of 1504 group only involves two variables, the inner and outer well depths of the site. A minor modification is made in the FORTRAN program for fitting. As discussed in the previous sections, this program was written to optimize either five or nine parameters in alcohol and ester groups. The best parameters for group 1504 are found to be ε_i = 140.25, and ε = 23.65. Using these parameters, vapor pressures of trioxane and tetrahydrofurfuryl (testing compounds) are respectively predicted within 4 and 16 % of the reported values in literature.

Table 10.6 summarized the prediction of P^{sat} for acetals 4HMD and 5HMD using the new well depths for group 1504. There is currently no convergence in the smoothed SPEAD calculation of compressibility factor Z at below 300 K and above 500 K for both 4HMD and 5HMD, so the vapor pressures are evaluated only between these temperatures.

Table 10.5 Compounds used in Optimization and Validation of the –O– Site

Compound Name	Structure	# data points	Deviation in Prediction σ	Bias	Max	References
			Training –O– site			
1,3-dioxane		15	4.7	4.7	11.7	[43-45]
1,4-dioxane		33	2	0	4.1	[37, 46, 47]
			Testing –O– site			
Trioxane (or trioxymethylene)		11	3.7	3	6.8	[17, 48]
Tetrahydrofurfuryl alcohol		20	15.4	-15.4	46.1	[49-51]

As shown in Table 10.6, SPEAD predicted values are very close to the reported boiling points, which are the only VLE data available in literature for 4HMD and 5HMD.[125] The linear trend of predicted vapor pressure curves follows the Korsten correlation. In addition, regression using the least square method shows vapor pressure curves of these homologous isomers 4HMD and 5HMD (same molecular weight and same functionality) merge at a common point α (T_α = 1024 K, P_α = 126.7 MPa) and the value of B is 33.49 in Eqn 10.9.

Table 10.6   Prediction of P^{sat} for Acetals using SPEAD. $T_{b(dioxane)}$ = 449.15 K, SPEAD value = 453.15 K. $T_{b(dioxolane)}$ = 460.15 K, SPEAD value = 467.96 K.[125]

T (K)	P (kPa) 5HMD	P (kPa) 4HMD	T (K)	P (kPa) 5HMD	P (kPa) 4HMD
300	0.038	0.017			
310	0.085	0.040	410	22.9	13.7
320	0.181	0.088	420	33.5	20.3
330	0.365	0.183	430	47.9	29.6
340	0.699	0.360	440	67.0	42.0
350	1.30	0.68	450	92.0	58.5
360	2.30	1.20	460	124.1	80.0
370	3.80	2.10	470	164.6	107.4
380	6.20	3.50	480	214.9	142.0
390	9.90	5.70	490	276.7	185.0
400	5.30	9.00	500	351.6	237.6
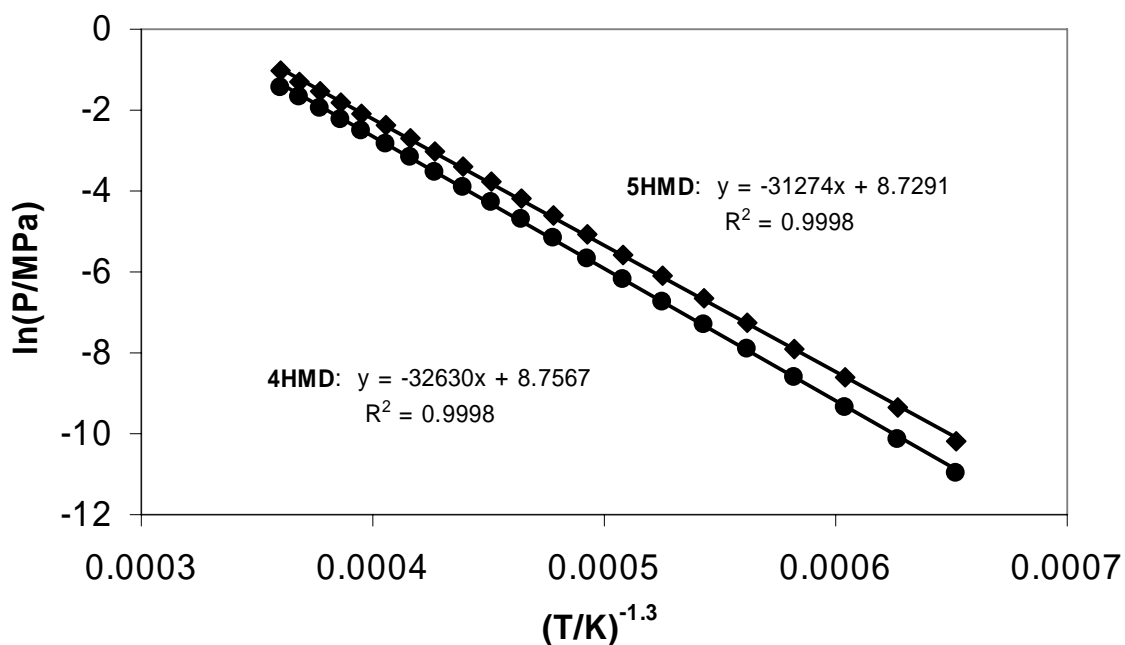
Figure 10.5 SPEAD Predicted Vapor Pressure of Acetals

●: 5HMD, ■: 4HMD. Lines: linear regression

Table 10.7 and Figure 10.5 are predicted VLE of 4HMD and 5HMD mixtures at 373.15 K. As expected, SPEAD predicts 4HMD and 5HMD form ideal solutions. It will be difficult to separate these acetals using distillation due to their small relative volatility.

Table 10.7 SPEAD Prediction of *T-P-x-y* for 4HMD (1) + 5HMD (2) at 373.15 K

x_1	y_1	P (MPa)	x_1	y_1	P (MPa)
0.0	0.000	0.0025			
0.1	0.167	0.0027	0.6	0.729	0.0037
0.2	0.310	0.0029	0.7	0.807	0.0039
0.3	0.435	0.0031	0.8	0.878	0.0041
0.4	0.545	0.0033	0.9	0.942	0.0043
0.5	0.642	0.0035	1.0	1.000	0.0045
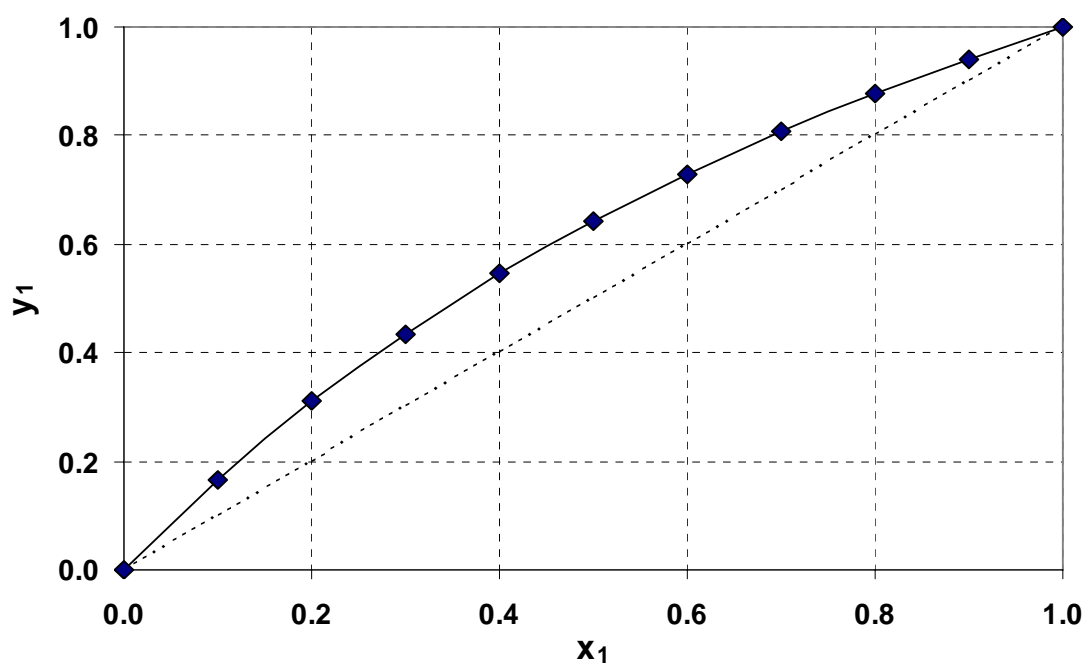
Figure 10.6 VLE of 5HMD (1) + 4HMD (2) Mixtures at 373 K.

x, y: liquid and molar compositions.

APPENDIX

Project Tasks as Stated in SOW submitted to DOE

Task 1) Project Management and Process Economics
   a) Project Management
   b) Evaluation of Process Economics

NCGA has managed the project with its subcontractors Michigan State University and MECS, Inc. Detailed process economic analysis has been carried out for the key organic acid esters developed on the project. Task completed.

Task 2) Market Assessment & Identification of Compounds
   a) Assessment of Potential Products and Markets
   b) Prioritization of Candidate Esters

NCGA commissioned Nexant, Inc. to carry out a market assessment of biomass derived chemicals including organic acid esters derived from biomass. Nexant completed the study in 2006.

Task 3) Feasibility Studies
   a) Conduct Preliminary Batch Experiments
   b) Conduct Preliminary Continuous Reactive Distillation Experiments (Go / No Go Decision Point based on Initial Results and Process Economics

Laboratory feasibility studies were completed on four organic acid systems in both batch experiments and in preliminary reactive distillation experiments. Task completed.

Task 4) Physical Property and Thermodynamic Data
   a) Collect Data
   b) Develop ability to fit data for Use in Process Simulations

Physical property data on lactate, citrate, succinate, and propionate systems were collected in batch reactions, in T-x-y, and in P-x-y phase equilibrium systems. Modeling data included UNIQUAC for Aspen simulations and SPEAD for general properties measurements. Task completed.

Task 5) Assessment of Pilot-Scale Performance
   a) Pilot Scale Simulation
   b) Corroboration of Pilot Scale Simulations and Experiments
   c) Optimize Ester Yield at Pilot Scale

Pilot-scale reactive distillation experiments were carried out on the key organic acid ester systems studied. Yields were optimized in the pilot-scale apparatus. Pilot-scale simulations were developed using AspenPlus process simulation software, and the simulations were corroborated with experiment to give actual column performance parameters. Task completed.

Task 6) Design and Analysis of Commercial Process
   a)   Commercial Scale Simulation
   b)   Final Optimization and Assessment based on Economics of the Commercial
        Facility

*Based on the column performance parameters determined in Task 5), commercial scale
processes were designed for the key organic acid esters investigated. These processes
included multiple unit operations and were designed to integrate into existing corn
processing facilities. The processes were optimized and a complete economic evaluation
of each process was carried out by MECS (Task 1). Task Complete.*

Task 7) Exploratory Studies

*Very limited effort was expended on peripheral studies exploring different avenues for
esterification and reactive distillation. We conducted a few experiments on amino acid
esters, but with limited success. Task completed.*

SECTION ELEVEN

REFERENCES

1. Malone, M.; Doherty, M. "Reactive Distillation." *Ind. Eng. Chem. Res.* **39**, 3953-3957 (2000)
2. Taylor, R.; Krishna, R. "Modeling Reactive Distillation." *Chem. Eng. Sci.* **55**, 5183-5229 (2000)
3. Agreda V. H. and Partin, L. R. Reactive distillation process for the production of methyl acetate. US Patent 4435595, (1984).
4. Feng, X.; Huang, Y.M. "Studies of a Membrane Reactor: Esterification Facilitated by Pervaporation." *Chem. Eng. Sci.* **51**(20), 4673-4679 (1996).
5. Popken, T.;Steinigeweg, S. and Gmehling, J. "Synthesis and Hydrolysis of Methyl Acetate by Reactive Distillation Using Structured Catalytic Packings: Experiments and Simulation." *Ind. Eng. Chem. Res.* **40**: 1566-1574 (2001).
6. Peng, J.;Lextrait, S.;Edgar, T. F. and Eldridge, R. B. "A Comparison of Steady-State Equilibrium and Rate-Based Models for Packed Reactive Distillation." *Ind. Eng. Chem. Res.* **41**: 2735-2744 (2002).
7. Hanika, J.;Kolena, J. and Smejkal, Q. "Butyl acetate via reactive distillation - modelling and experiment." *Chem. Eng. Sci.* **54**: 5205-5209 (1999).
8. Steinigeweg, S. and Gmehling, J. "n-Butyl Acetate Synthesis via Reactive Distillation: Thermodynamic Aspects, Reaction Kinetics, Pilot-Plant Experiments, and Simulation Studies." *Ind. Eng. Chem. Res.* **41**: 5483-5490 (2002).
9. Benedict, D.J.; Parulekar, S.J.; Tsai, S.P. "Esterification of Lactic Acid and Ethanol With/Without Pervaporation." *Ind. Eng. Chem. Res.* **42** (2003).
10. Jafar, J.J.; Budd, P.M.; Hughes, R. "Enhancement of Esterification Reaction Yield Using Zeolite A Vapour Permeation Membrane." *J. Membrane Science* **199**, 117-123 (2002).
11. Walsh, K.; "Solvents - ADM and NETC Launch Ethyl Lactate for Industrial Applications." *Chemical Week* **161**(40), 23 (1999).
12. Font, A.;Asensi, J. C.;Ruiz, F. and Gomis, V. "Application of Isooctane to the Dehydration of Ethanol. Design of a Column Sequence to Obtain Absolute Enthanol by Heterogeneous Azeotropic Distillation." *Ind. Eng. Chem. Res.* **42**: 140-144 (2003).
13. Tao, L.;Malone, M. F. and Doherty, M. F. "Synthesis of Azeotropic Distillation Systems with Recycles." *Ind. Eng. Chem. Res.* **preprint** (2003).
14. Barbosa, D. and Doherty, M. F. "The Influence of Equilibrium Chemical Reactions on Vapor-Liquid Phase Diagrams." *Chem. Eng. Sci.* **43**: 529-540 (1988).
15. Vu, D.T.; Kolah, A.K.; Asthana, N.S.; Peereboom, L; Lira, C.T.; Miller, D.J. Oligomer Distribution in Concentrated Lactic acid Solutions. *Fluid Phase Equilibria* **2005**, *236*, 39.
16. Holten, C.H. *Lactic acid: Properties and Chemistry of Lactic acid and Derivatives*; Verlag Chemie: Copenhagen, 1971.

17. Dhale, A.D.; Myrant, L.K.; Chopade, S.P., Jackson, J.E.; Miller, D.J. Propylene Glycol and Ethylene Glycol Recovery from Aqueous Solutions via Reactive Distillation. *Chem. Eng. Sci.* **2004**, *59*, 2881.

18. Beckmann, A.; Nierlich, F.; Popeken, T.; Reusch, D.; von Scala, C.; Tuchlenski, A. Industrial Experience in Scale-up of Reactive Distillation with Examples from C_4-Chemistry. *Chem. Eng. Sci.* **2002**, *57*, 1525.

19. Sanz, M.T.; Murga, R.; Beltran, S.; Cabezas, J.L.; Coca, J. Autocatalyzed and Ion-Exchanged-Resin-Catalyzed Esterification Kinetics of Lactic acid with Methanol. *Ind. Eng. Chem. Res.* **2002**, *41*, 512.

20. Sanz, M.T.; Murga, R.; Beltran, S.; Cabezas, J.L.; Coca, J. Kinetic Study for Reactive System of Lactic Acid Esterification with Methanol: Methyl Lactate Hydrolysis Reaction. *Ind. Eng. Chem. Res.* **2004**, *43*, 2049.

21. Choi, J.I.; Hong, W.H.; Chang, H.N. Reaction Kinetics of Lactic acid with Methanol Catalyzed by Acid Resins. *Int. J. Chem. Kinet.* **1996**, *28*, 37.

22. See, Y.; Hong, W.H.; Hong, T.H. Effects of Operation Variables on the Recovery of Lactic acid in a Batch Distillation Process with Chemical Reactions. *Korean J. Chem. Eng.* **1999**, *16*, 556.

23. Yadav, G.D.; Kulkarni, H.B. Ion-Exchange Resin Catalysis in Synthesis of Isopropyl Lactate. *React. Funct. Polym.* **2000**, *44*, 153.

24. Tanaka, K.; Yoshikawa, R.; Ying, C.; Kita, H.; Okamoto, K. Application of Zeolite T Membrane to Vapor-Permeation-Aided Esterification of Lactic Acid with Ethanol. *Chem. Eng. Sci.* **2002**, *57*, 1577.

25. Engin, A.; Haluk, H.; Gurkan, K. Production of Lactic Acid Esters Catalyzed by Heteropolyacid Supported Over Ion-Exchange Resins. *Green Chem.* **2003**, *5*, 460.

26. Zhang, Y.; Ma, L.; Yang, J. Kinetics of Esterification of Lactic Acid with Ethanol Catalyzed by Cation-Exchange Resin. *React. Funct. Polym.* **2004**, *61*, 101.

27. Reid, R.C.; Prausnitz, M.J.; Sherwood, T. K. *The Properties of Gases and Liquids*; McGraw-Hill Book Company: New York, 1987.

28. Chakrabarti, A; Sharma, M.M. Cationic Ion-Exchange Resin as Catalyst. *React. Polym.* **1993**, *20*, 1.

29. Gangadwala, J.; Mankar, S.; Mahajani, S.; Kienle, A.; Stein, E. Esterification of Acetic Acid with Butanol in the Presence of Ion-Exchange Resins as Catalysts. *Ind. Eng. Chem. Res.* **2003**, *42*, 2146.

30. Vu, D.T.; Kolah, A.K.; Asthana, N.S.; Peereboom, L; Lira, C.T.; Miller, D.J. Oligomer Distribution in Concentrated Lactic acid Solutions. *Fluid Phase Equilibria* **2005**, *236*, 39.

31. Mazzotti, M.; Neri, B.; Gelosa, D.; Kruglov, A.; Morbidelli, M. Kinetics of Liquid-Phase Esterification Catalyzed by Acidic Resins. *Ind. Eng. Chem. Res.* **1997**, *36*, 3.

32. Scheele, C.H.; Mjolk, O.: Kgl. Vetenskaps-Academiens nya Handlingar, 1 Stockholm (1780) 116-124.

33. Hartmann, M.H. in: Kaplan, D.L. (Ed.), Biopolymers from Renewal Resources, Springer-Verlag, Berlin, 1998, pp. 367-411.

34. Ritter, S.K. Chem. & Eng. News, 82:22 (2004) 31-34.

35. Robert, W. Chem. Week. April 10 (2002) 31.

36. Garlotta, D. J. Polym. Environment. 9 (2002) 63-84.

37. Montgomery, R. J. Am. Chem. Soc. 74 (1952) 1466-1468.
38. Ueda, R.; Terashima, T. Hakko Kogaku Zaashi. 36 (1958) 371-374.
39. Watson, P.D. Ind. Eng. Chem. 32 (1940) 399-401.
40. Holten, *ibid*, pp 200.
41. Maurer, G. AIChE J. 32 (1986) 932-948.
42. Kogan, L.V. Zhur. Prikl. Khim. 52 (1979) 2149.
43. Kogan, L.V. and Ogorodnikov, S.K. J. Appl. Chem. USSR. 53 (1980) 98-101.
44. Kogan, L.V. and Ogorodnikov, S.K. J. Appl. Chem. USSR., 53, (1980) 102.
45. Brandani, V.; Giacomo,G.Di.; Foscolo, P.U. Ind. Eng. Chem. Process. Des. Dev. 19 (1980) 179-185.
46. Masamto, J. and Matsuzaki, K. Chem. Eng. Japan. 27 (1994) 6-11.
47. Hahnenstein, I.; Hasse, M.; Liu, Y-Q.; Maurer, G. AIChE. Symp. Ser. 298 (1994) 141-157.
48. Brandani, S.; Brandani, V.; Giacomo, G.D. Ind. Eng. Chem. Res. 30 (1991) 414-420.
49. Brandani, S.; Brandani, V.; Giacomo, G.D. Fluid Phase Equil. 63 (1991) 27-41.
50. Brandani, S.; Brandani, V.; Giacomo, G.D. Ind. Eng. Chem. Res. 31 (1992) 1792-1798.
51. S. Bezzi, L. Riccoboni, C. Sullam, Mem. cl. sci. fis. mat. nat. 8 (1937) 181-200.
52. Sanz, M. T.; Calvo, B.; Beltran, S.; Cabezas, J. L. *J. Chem. Eng. Data* **2002**, *47*, 1003-1006.
53. Sanz, M. T.; Beltran, S.; Calvo, B.; Cabezas, J. L. *J. Chem. Eng. Data* **2003**, *48*, 1446-1452.
54. Pathare, S.; Bhethanabotla, V. R.; Campbell, S. W. *Ind. Eng. Chem. Res.* **2004**, *49*, 510-513.
55. Van Ness, H. C.; Abbott, M. M. *Ind. Eng. Chem. Fundam.* **1978**, *17*, 66-67.
56. Campbell, S. W.; Bhethanabotla, V. R. *Chemical Engineering Education* **1997**, 34-39.
57. Redlich, O.; Kister, A. T. *Ind. Eng. Chem* **1948**, *40*, 345.
58. Van Ness, H. C.; Byer, S. M.; Gibbs, R. E. *AIChE J.* **1973**, *19*, 238-244.
59. Fredenslund, A.; Gmehling, J.; Rasmussen, P. *Vapor-Liquid Equilibria using UNIFAC*; Elsevier, 1971.
60. Udovenko, V. V.; Fatkulina, L. G. *Zhurnal Fizicheskoi Khimii* **1952**, *26*, 1438.
61. Mertl, I. *Collection of Czechoslovak Chemical Communications* **1972**, *37*, 366.
62. Peña-Tejedor, S.; Murga, R.; Sanz, M. T.; Beltrán, S. *Fluid Phase Equilibria* **2005**, *230*, 197-203.
63. Prausnitz, J. M.; Lichtenthaler, R. N.; Azevedo, E. G. d. *Molecular Thermodynamics of Fluid-Phase Equilibria*; 3rd ed.; Prentice-Hall, Inc., 1999.
64. Mahajani S. M.; Chopade S. P. *Encyclopedia of Separation Science.* Edited by Wilson I. D.; Edlard T. R.; Poole C. A.; Cooke, M. Academic Press, London UK, **2001**, 4075.
65. Sharma M. M.; Mahajani S. M. Industrial Application of Reactive Distillation in *Reactive Distillation* Edited by Sundmacher K.and Kienle A., Wiley VCH, Germany, **2003**, 1.
66. Hiwale R. S.; Mahajan Y. S.; Bhate, N. V.; Mahajani S. M. *Int. J. of Chem. React. Eng.*, **2004**, *2*, Review R1.

67. Seo Y.; Hong W. H.; Hong T. H. *Korean Journal of Chemical Engineering*, **1999**, *16 (5)*, 556.
68. Choi J.; Hong W. H. *Journal of Chemical Engineering of Japan.* **1999**, *32(2)*, 184.
69. Filachione E. M.; Costello E. J.; Fisher C. H. *J. Am. Chem. Soc.* **1951**, *73(11)*, 5265.
70. Halpern Y. US Patent 6583310, 2003.
71. Chahal S. P. Lactic acid in *Ullmann Encyclopedia of Industrial Chemistry*, Wiley-VCH, Verlag, GmbH & Co., **2002**.
72. Rehberg C. E.; Dixon M. B. *J. Am. Chem. Soc.*, **1950**, 5757.
73. Olahorn H. V. US Patent 2371281, 1945.
74. Fein M. L. *J. Am. Chem. Soc.*, **1951**, *73*, 5870.
75. Rehberg C. E.; Dixon M. B. *J. Am. Chem. Soc.* **1952**, *74*, 1609.
76. Cockrem M.C.M. US Patent 6664413, 1998.
77. Kaimal T. N. B.; Vijayalaxmi P.; Ramalinga B.; Laxmi A. A. US Patent 6342626, 2002.
78. Tretjak S., Teissier R., WO 2004/052825 A2, 2004.
79. Datta R.; Tsai S. US Patent 5723639, 1998.
80. Budd P. M.; Ricardo N. P. S.; Jafar J. J.; Stephenson B.; Houghes R. *Ind. Eng. Chem. Res.*, **2004**, *43*, 1863.
81. Steffens J. A. US Patent 1421604, 1922.
82. Schmitt M.; Hasse H.; Althaus K.; Schoenmakers H.; Gotze L.; Moritz P. *Chemical Engineering and Processing*, **2004**, *43*, 397.
83. Steinigeweg S.; Gmehling J. *Ind. Eng. Chem. Res.*, **2003**, *42 (3)*, 3612.
84. Smejkal Q. Hanika J.; Kolena J. *Chem. Eng. Sci.* **2001**, *56*, 365.
85. Schröter, J.; Konetzke, G.; Weidemann, F.; Klein, T.; Bohnen, H.; Bergrath, K.; Schmidt, K. Method for producing citric acid esters. WO 2003008369 A1, **2003**.
86. Tao, X. Optimization of conditions for tri-ethyl citrate synthesis. *Huazue Shijie*, **1998**, *39*(6), 302.
87. Frappier, E.P.; Davis, J.E.; Grendze, M.; Scriven, E.F.V.; Wyeth, J.T.; Chiu, K.W. World Patent WO. 9851657, **1998**.
88. Nong, L. Synthesis of tri-butyl citrate with aluminium phosphotungstate supported on activated carbon. *Jingxi Huagong Zhongjianti*. **2004**, *34*, 50.
89. Shi, L.; Ding, X.; Zhang, H.; Wu, D. Synthesis of tri-butyl citrate catalyzed by solid superacid $S_2O_8^{-2}/TiO_2$-SiO_2. *Yingyong Huagong* **2004**, *33*, 41.
90. Zheng, Y.; Wang, J.; Tan, M.; Zheng, S. Synthesis of tri-butyl citrate catalyzed by tetra-butyl titanate. *Jingxi Huagong Zhongjianti*. **2004**, *34*, 28.
91. Deng, B.; Huang, H.; Liu, G. The synthesis of tri-butyl citrate catalyzed by sodium hydrogen sulfate. *Jingxi Huagong Zhongjianti*, **2003**, *33*, 49.
92. Song, Y.; Wang, H.; Huang, S.; Gao, W.; Zhang, H.; Lian, P. Catalytic synthesis of tri-*n*-butyl citrate with aluminophosphate solid acid catalyst. *Huagong Keji*. **2003**, *11*, 6.
93. Liu, H.; Tan, F.; Yin, D. Catalytic synthesis of tri-butyl citrate with dealuminated USY zeolite. *Hecheng Huaxue*. **2003**, *11*, 175.

94. Meng, X.; Wang, M.; Liu, B.; An, Y.; Kang, Y. Synthesis of tri-butyl citrate catalyzed by the nanosolid superacid SO_4^{2-}/Fe_2O_3. *Hebei Shifan Daxue Xuebao, Ziran Kexueban.* **2003**, *27*, 64.

95. Zhao, J.; Cheng, Z.; Xing, C. Synthesis of tri-butyl citrate catalyzed by complex solid superacid WO_3-TiO_2-SO_4^{2-}. *Huagong Keji.* **2002**, *10(5)*, 11.

96. Meng, P.; Li, L.; Yang, C.; Zhou, C.; Jia, S. Synthesis of tri-butyl citrate with *p*-toluene sulfonic acid catalyst. *Hecheng Shuzhi Ji Suliao.* **2002**, *19(2)*, 16.

97. Fu, L.; Guo, X.; Lin, Q.; Li, J. Synthesis of tri-butyl citrate catalyzed by SO_4^{2-} modified zirconium crosslinked solid clay. *Jingzi Huagong.* **2002**, *19(1)*, 28.

98. Sundmacher, K.; Qi, Z. Importance of Reaction Kinetics for Catalytic Distillation Processes. in *Reactive Distillation – Status and Future Directions*, Sundmacher, K; Kienle, A. eds., Wiley-VCH, Weinheim, Germany, **2003**, 97-142.

99. Rehfinger, A.; Hoffmann, U. Kinetics of methyl tertiary butyl ether liquid-phase synthesized by ion exchange resin- I. Intrinsic rate expression in liquid-phase activities. *Chem. Eng. Sci.* **1990**, *45*, 1605.

100.   Sundmacher, K.; Hoffmann, U. Macrokinetic analysis of MTBE-synthesis in chemical potentials. *Chem. Eng. Sci.* **1994**, *49*, 3077.

101.   Venimadhavan, G.; Buzard, G.; Doherty, M.F.; Malone, M.F. Effect of kinetics on residue curve maps for reactive distillation. *AIChE J.* **1995**, *41*, 2613.

102.   Song, W.; Venimadhavan, G.; Manning, J.M.; Malone, M.F.; Doherty, M.F. Measurement of residue curve maps and heterogeneous kinetics in methyl acetate synthesis. *Ind. Eng. Chem. Res.* **1998,** *37*, 1917-1928.

103.   Bock H., Wozny G. and Gutsche B. Design and Control of a Reactive Distillation Column including the Recovery System. *Chem. Eng .Prog.*, **1997**, *36*, 101-109.

104.   Omata F., Dimian A.C. and Bliek A. Fatty acid Esterification by Reactive Distillation. Part 1: Equilibrium-based design. *Chem. Eng. Sci.*, **2003**, *58*, 3159-3174.

105.   Saigo K.; Hashimoto Y.; Hayashi M.   Catalysts for bisalkoxycarbonylation of olefins and manufacture of succinic acid esters. *Jpn. Kokai Tokkyo Koho*, **2000**, 200271485.

106.   Benedict D. J.; Parulekar S.J.; Tsai S.-P. Pervaporation-assisted esterification of lactic and succinic acids with downstream recovery. *J. Mem. Sci.* **2006**, *281,* 435-445.

107.   Turek T.; Trimm D.L. The catalytic hydrogenolysis of esters to alcohols. *Catal. Rev. Sci. Eng.* **1994**, *36(4)*, 645.

108.   Attig T.G.; Graham A.M. Process and catalysts for the manufacture of gamma-butyrolactone and 1,4-butanediol by hydrogenation of maleic acid. U.S. Patent 4827001, **1989**.

109.   Mukala-Nsengu A.; Fernández-Pascual S.; Martín F.; Martín-del-Río R.; Tamarit-Rodriguez J. Similar effects of succinic acid dimethyl ester and glucose on islet calcium oscillations and insulin release. *Biochem. Pharmacology.* **2004**, *67*, 981-988.

110.   Laghmich A.; Ladrière L.; Dannacher H.; Björjling F.; Malaisse W.J. New esters of succinic acid and mixed molecules forrmed by such esters and a

meglitinide analog. Study of their insulinotropic potential. *Pharmacological Res.* **2000**, *41*, 543-554.

111.   Kadiata M.N.; Malaisse W.J. Opposite effects of d-glucose pentaacetate and d-galactose pentaacetate anomers on insulin release evoked by succinic acid dimethyl ester in rat pancreatic islets. *Life Sci.*, **1999**, *64*, 751-754.

112.   Ladrière L.; Malaisse-Lagae F.; Verbruggen I.; Willem R.; Malaisse W.J. Effects of starvation and diabetes on the metabolism of [2,3-^{13}C] succinic acid dimethyl ester in rat hepatocytes. *Metabolism*, **1999**, *48*, 102-106.

113.   Leclercq-Meyer V.; Malaisse W.J. Potentiation of glucagon-like peptide 1 insulinotropic action by succinic aicd dimethyl ester. *Life Sci.***, 1996**, *58*, 1195-1199.

114.   Fiona Case, et al., *The second industrial fluid properties simulation challenge.* Fluid Phase Equilibria, 2005. **236**: p. 1-14.

115.   Elliott, J.R., *SPEAD 1.03. 1.04, Intro and Help.*

116.   J. R. Elliott, *SPEAD Progress Report, June 2003*. 2003.

117.   Korsten, H., *Internally Consistent Prediction of Vapor Pressure and Related Properties.* Ind. Eng. Chem, 2000. **39**: p. 813-820.

118.   Ye, T. and S. Kalyanaraman. *A Recursive Random Search Algorithm for Large-Scale Network Parameter Configuration.* in *ACM SIGMETRICS International Conference on Measurement and Modeling of Computer Systems.* 2003. San Diego, CA, USA.

119.   Broyden, G., *The Convergence of a Class of Double-Rank Minimization Algorithms, Parts I and II.* J. Inst. Math. Appl., 1970. **6**: p. 76-90 and 222-231.

120.   Shanno, D.F., *Conditioning of Quasi-Newton Methods for Function Minimization.* Mathematics of Computation, 1970. **24**: p. 647-656.

121.   Goldfrab, D., *A Family of Variable Metric Methods Derived by Variational Means.* Mathematics of Computation, 1970. **24**: p. 23-26.

122.   Fletcher, R., *A New Approach to Variable Metric Algorithms.* Computer Journal, 1970. **13**: p. 317-322.

123.   Dennis, J.E. and R.B. Schnabel, *Numerical Methods for Unconstrained Optimization and Nonlinear Equations*. Computational Mathematics. 1983: Prentice-Hall. 378.

124.   Gill, P.E., W. Murray, and M.H. Wright, *Practical Optimization*. 1981: Academic Press. 401.

125.   *CRC Handbook of Chemistry and Physics*. 63 ed, ed. M.J.A. Robert C. Weast. 1982-1983: CRC Press.